Incorporation of Oxyanionic B, Cr, Mo, and Se into Hydrocalumite and Ettringite: Application to Cementitious Systems

By

Min Zhang

A thesis
presented to the University of Waterloo
in fulfillment of the
thesis requirement for the degree of
Doctor of Philosophy
in
Earth Sciences

Waterloo, Ontario, Canada, 2000

The University of Waterloo requires the signatures of all persons using or photocopying this thesis. Please sign below, and give address and date.

Incorporation of Oxyanionic B, Cr, Mo, and Se into Hydrocalumite and Ettringite: Application to Cementitious Systems

Abstract

B, Cr, Mo, and Se are often enriched in solid wastes such as fly ash and spent oil shale, and occur at high concentrations in their leachates. These elements are usually present as oxyanions, and are mobile at the near neutral to alkaline pH values of most natural waters. Therefore, mechanisms for removing these oxyanions from wastewaters are of great importance. Hydrocalumite ($Ca_4Al_2(OH)_{12}X{\cdot}6H_2O$) and ettringite ($Ca_6Al_2(OH)_{12}X_3{\cdot}26H_2O$) are commonly formed as secondary phases during the hydration of fly ash in alkaline solutions. They also comprise 10 to 20 % of the hydration phases formed in Portland cement. Previous research has shown that these phases incorporate substantial amounts of a wide variety of anions from solution. Precipitation of these mineral phases could be an effective mechanism for removing oxyanions from wastewaters.

Secondary phases formed from the interaction of fly ash and lime water were characterized as a function of reaction time by direct examination of the solid phases using optical microscopy, X-ray diffraction analysis (XRD) and scanning electron microscopy (SEM). Solution compositions were also monitored during leaching, to establish the correlation between the solution composition and the development of secondary phases. Ettringite formed at early reaction times in all the fly ashes examined (two Class F and one Class C fly ash). The ettringite crystals contained a high percentage of Si, indicating that they are solid solutions between ettringite ($Ca_6Al_2(OH)_{12}(SO_4)_3{\cdot}26H_2O$) and thaumasite ($Ca_6Si_2(OH)_{12}(SO_4)_2(CO_3)_2{\cdot}24H_2O$). With increasing reaction time, ettringite transformed to hydrocalumite in the Class F fly ashes, and to strätlingite ($Ca_2Al(OH)_6[AlSiO_3(OH)_2]{\cdot}4H_2O$) in the Class C fly ash. This is the first time that the transformation of ettringite to hydrocalumite has been directly observed by examination of the minerals. The observations suggest that under the experimental conditions, this transformation is a through-solution process. However, solid-state conversion from ettringite to hydrocalumite may also occur locally within a hydrocalumite crystal.

A substantial decrease in the solution concentrations of SO_4, B, Mo, and Se occurred when lime was added to the fly ashes. At early reaction times, ettringite incorporated these

anions into its structure. With increased reaction time, ettringite converted to hydrocalumite, and a further reduction in the concentrations of the anions was observed. This implies that incorporation of these anions by hydrocalumite could lead to lower residual solution concentrations than incorporation by ettringite. However, in the Class C fly ash, the lowest B concentration was coincident with the maximum formation of ettringite. The increase in the B solution concentrations observed at later reaction times is likely related to the transformation of ettringite to strätlingite, and indicates that ettringite incorporates more B than strätlingite.

The uptake behavior of B, Cr, Mo, and Se in pure ettringite-water and hydrocalumite-water systems was studied in order to clarify the relationship between the decrease in anion concentration and the precipitation of these phases in the lime-leached fly ashes. Hydrocalumite and ettringite were precipitated from solutions containing 10 ppm B, Cr, Mo, and Se. The residual solution concentrations of Cr, Mo, and Se were below detection after incorporation into hydrocalumite, and the B concentrations were below detection after incorporation into ettringite. The anion preference by ettringite was in the order: $B(OH)_4^-$> SeO_4^{2-} > CrO_4^{2-} > MoO_4^{2-}. In ettringite, anion size and electronic configuration are the key factors that influence the extent of anion uptake. It was not possible to establish an order of preference of hydrocalumite for these anions, except that borate was least preferred. The low uptake of B appears to be caused by a change in its coordination from $B(OH)_4^-$ to HBO_3^{2-} during incorporation.

The stability and solubility of the hydrocalumite phases were determined by synthesizing solid solutions with OH as one endmember and B, Cr, Mo, Se and SO_4 as the other endmembers. After 9 to 18 months of reaction, the solid phases were characterized and the solution compositions determined. In the ternary CaO-Al_2O_3-H_2O system, hydrogarnet was the dominant mineral phase. OH-hydrocalumite was also present, and a free energy of formation ($\Delta G°_{f,\,298}$) of -7336.14 ± 1.14 kJ·mol^{-1} was calculated for this phase. At oxyanion contents greater than 10%, hydrocalumite became the dominant phase in all the quaternary systems CaO-Al_2O_3-XO_3/Y_2O_3-H_2O (X = Cr^{6+}, Mo^{6+}, Se^{6+}, and S^{6+}; Y = B^{3+}). With an increase in the molar percentage of the anion, three different phase assemblages were generally observed: 1) hydrocalumite, hydrogarnet, and portlandite; 2) hydrocalumite and hydrogarnet; and 3) hydrocalumite and ettringite at the high end. However, ettringite was not observed in either the chromate or molybdate solid solution series. A free energy of formation of -17408.22 ± 4.34 kJ·mol^{-1} was calculated for the borate ettringite ($Ca_6Al_2(OH)_{12}[B(OH)_4]_4[OH]_2 \cdot 24H_2O$).

Extensive solid solutions were formed between borate and hydroxyl hydrocalumite endmembers. The trigonal planar geometry of borate fits well between the principal layers

and is compatible with hydroxyl in the structure. Immiscible solid solution phases were formed between tetrahedral anions and hydroxyl hydrocalumite. For example, sulfate occurs in tetrahedral coordination, a structural balance could not be easily achieved with linear hydroxyl. Consequently, the solid solution between sulfate and hydroxyl is limited to the region near the hydroxyl and sulfate endmembers. For the borate hydrocalumite endmember ($Ca_4Al_2(OH)_{12}(HBO_3)\cdot 5.5H_2O$), the $\Delta G°_{f,\,298}$ was determined to be -7750.42 ± 1.20 kJ·mol^{-1}. Determination of the free energies of the hydrocalumites containing other oxyanions, however, was not applicable due to the presence of immiscible solid solutions.

The maximum uptake capacity of B, Cr, Mo, and Se in hydrocalumite was determined based on the mass of $CaAl_2O_4$ (starting material). At a $H_2O/(CaAl_2O_4+CaO)$ ratio of approximately 75:1, the maximum capacity was calculated to be in the range 100,000 mg of anion per kg of $CaAl_2O_4$. Hydrocalumite was the major host mineral for the oxyanions under the experimental conditions used in this study, however, ettringite incorporated a moderate amount of oxyanion in the borate and selenate solid solution series. In the CaO-Al_2O_3-MoO_3-H_2O system, powellite ($CaMoO_4$) also accommodated molybdate. The results of these experiments demonstrate that the system CaO-Al_2O_3-XO_3/Y_2O_3-H_2O not only has a high uptake capacity for anions, but also has the capability to reduce their solution concentrations to acceptable levels.

The capability of Portland cement to incorporate anions was evaluated by reacting cement with a solution containing 200 ppm B and 100 ppm Cr, Mo, and Se for 30 days. The concentrations of B, Cr, Mo, and Se were reduced by 115 to 6 times at a w/s ratio 20:1, and by 4 to 1.5 times at a w/s ratio of 40:1. Portland cement showed an uptake preference of $B(OH)_4^- > CrO_4^{2-} > MoO_4^{2-} > SeO_4^{2-}$. Portlandite, ettringite, and CSH were the main hydration products generated. Ettringite was likely the major sink for these oxyanions, although CSH probably also removed some portion of the oxyanions from solution. A comparison on the order of preference by ettringite and by Portland cement suggests that selenate is least preferred by CSH.

Acknowledgements

I wish to express my acknowledgement to my supervisor, Dr. E. Reardon, who introduced me to aqueous geochemistry. I am grateful for his willingness to share his knowledge on thermodynamics and geochemical modeling, and for his encouragement of high standard research. I am especially benefited from his approach using experiment to answer questions, which significantly influenced my own thinking on the course of the research. He is also thanked for providing financial support through Research Assistantship.

I would like to extend my thanks to the members of my supervisory committee: Dr. H. Peemoeller and Dr. R. Nicholson. Their insightful criticism at the different stages has no doubt helped me understand the fundamentals on the various areas of the research. I would also like to thank my external examiner Dr. C. Palmer for his helpful discussion and his generosity for letting me share his thoughts on his manuscripts. I am indebted to Dr. S. Frape for his enthusiasm and understanding, and for his valuable inputs in the areas of rock-water interaction and phase diagrams.

My particular acknowledgment goes to M. Hobbs, Ph.D. candidate at the University of Waterloo. She has spent tremendous amount of her precious time on helping me gain laboratory skills in the early years of the study, on countless discussions of various topics from which I have benefited much, and on reviewing and correcting the manuscript during the preparation of the dissertation. Her comments and criticism helped shape the end product of the dissertation. I would also gratefully acknowledge her understanding and generosity, which made my stay at the University of Waterloo much enjoyable.

I am grateful to K. Lau for her substantial assistance in conducting experiments, collecting literature information, and constructing diagrams. Her excellent lab skills and strong sense of responsibility make it possible to provide highly reliable experimental results. I am also grateful to R. Fagan and J. Page for their assistance in the experiments. I wish to acknowledge Dr. K. H. Yang of University of Toronto, and J. Wang of University of Waterloo for their assistance on SEM. T. Fowler and L. Zhang are thanked for conducting the chemical analysis.

Finally, my thanks go to my parents, my husband Dr. J. He, and my daughter Shuyin, who each were so understanding and supportive, and were so tolerant of this seemingly endless special journal of my life. My husband helped finalize all the figures with his expert level of skills.

TABLE OF CONTENTS

LIST OF TABLES

LIST OF FIGURES

Chapter 1

Overview

1.1 Boron, chromium, molybdenum, and selenium

1.1.1 Geochemistry

The chemical properties of boron, chromium, molybdenum, and selenium are summarized in Table 1.1. Boron is the only non-metal in Group III of the periodic table and shows many similarities to carbon and silicon. Boron shares with C and Si the marked propensity to form covalent, molecular frameworks by bonding to itself (Greenwood and Earshaw, 1984). Chromium and molybdenum are Group VIA elements. In their zero-valent state, both elements have typical metallic body-centered cubic structures (Greenwood and Earshaw, 1984). In their highest oxidation state (6+), Cr and Mo show similarities in chemical behavior. Each has an acidic oxide (CrO_3, MoO_3) from which salts of the ion (CrO_4^{2-}, MoO_4^{2-}) are derived. In this respect Cr^{6+} and Mo^{6+} resemble S^{6+} (Rollinson, 1973). Except for the stoichiometric similarities, however, other chemical properties of these elements are quite different from the sulfur group (VI) (Cotton *et al.*, 1999). Selenium is a non-metallic element of the sulfur group. H_2SeO_4 is very similar to H_2SO_4 in its formation of hydrates, in acid strength, and in the properties of its salts, most of which are isomorphous with the corresponding sulfates (Cotton *et al.*, 1999).

Boron, chromium, molybdenum, and selenium are not abundant elements in the earth's crust (Table 1.2). Boron has an abundance of 9 ppm (Fyfe, 1974). The abundance of chromium is comparable with vanadium (136 ppm) and chlorine (126 ppm), whereas molybdenum is much rarer (1.2 ppm). Selenium comprises only 0.05 ppm of the earth's crust thus ranking in similar abundance to Ag and Hg. Relative to the concentrations in the earth's

crust, boron and selenium are enriched in soil (Bowen, 1979). The concentrations of all four elements are usually low in stream water, ranging from 10^{-4} to 10^{-2} ppm (Drever, 1998). In seawater, the concentrations are similarly low for chromium and selenium but higher for molybdenum and boron (Brownlow, 1996).

Table 1.1: Chemical properties of B, Cr, Mo, and Se, after Faure (1991).

Element	Z	Atomic Mass	Electronic Configuration	First Ionization Potential (eV)	Electronegativity
B	5	10.81	[He] $2s^2 2p^1$	8.298	2.0
Cr	24	52.00	[Ar] $3d^5 4s^1$	6.766	1.6
Mo	42	95.94	[Kr] $4d^5 4s^1$	7.099	1.8
Se	34	78.96	[Ar] $3d^{10} 4s^2 4p^4$	9.752	2.4

Table 1.2: Average chemical composition of B, Cr, Mo, and Se in the earth's crust, soil, seawater, and stream water (ppm).

Distribution	B	Cr	Mo	Se	Reference
Earth's Crust	9	122	1.2	0.05	Fyfe (1974)
Soil	20	70	1.2	0.4	Bowen (1979)
Seawater	4.45	$2x10^{-4}$	$1x10^{-2}$	$9x10^{-5}$	Brownlow (1996)
Streams	$2x10^{-2}$	$1x10^{-3}$	$5x10^{-4}$	$2x10^{-4}$	Drever (1998)

Although these elements have low crustal concentrations, they can be concentrated in specific geological settings and, therefore, be of commercial importance. Boron-bearing minerals are mainly grouped into two broad categories: borates and borosilicates (Grew and Anovitz, 1996). Borax ($Na_2B_4O_5(OH)_4 \cdot 8H_2O$) is most commonly mined boron mineral (Klein and Hurlbut, 1999). The chief ore of chromium is chromite ($FeCr_2O_4$). Crocoite ($PbCrO_4$) and chrome ochre (Cr_2O_3) are less important sources. Molybdenite (MoS_2) is a primary ore of molybdenum. Molybdate minerals, such as wulfenite ($PbMoO_4$) and powellite ($CaMoO_4$), are of minor importance. Selenium mainly occurs as selenides or substitute for sulfur in sulfide minerals (Wedepohl, 1969).

Table 1.3 shows the potential oxidation states of these elements and the corresponding radii of their ions in different coordinations (Faure, 1991). Boron has an oxidation number of +3. Various oxidation states, however, are associated with chromium, molybdenum, and selenium. In nature, chromium is known to occur only in the hexavalent and trivalent oxidation states (Wedepohl, 1969). Molybdenum is almost exclusively hexavalent in oxygen compounds, or tetravalent in molybdenite (Wedepohl, 1969). Many valence forms of selenium such as selenites (Se^{IV}), selenates (Se^{VI}), and elemental selenium (Se°) can occur in soils (Siler and Sigel, 1998). In near-surface natural waters, both trivalent and hexavalent forms of chromium are found. Molybdenum usually occurs as oxyanions in its highest oxidation state (Mo^{VI}), and aqueous selenium species are expected to be in either the selenite or selenate form (De Zuane, 1997).

Table 1.3: Oxidation states and ionic radii of B, Cr, Mo, and Se (Å), after Faure (1991).

Element	Valence	Coordination Numbers		
		III	IV	VI
B	+3	0.10	0.20	
Cr	+2			0.81
	+3			0.70
	+4		0.52	0.63
	+5		0.43	
	+6		0.38	0.52
Mo	+3			0.75
	+4			0.73
	+5			0.71
	+6		0.50	0.68
Se	-2			1.88
	+4			0.50*
	+6		0.37	0.42

* After Greenwood and Earnshaw (1984)

The small boron (III) atom forms no simple cation in solution. Hydrolysis of borate involves a change in coordination from planar boric acid, $B(OH)_3$, to tetrahedral borate ion, $B(OH)_4^-$. The equilibrium constant for boric acid is $10^{-9.24}$, and polyborates are formed rapidly and reversibly at boric acid concentrations greater than 0.1 m (Baes and Mesmer, 1976). According to Baes and Mesmer (1976), chromium (VI) is hydrolyzed with $Cr_2O_7^{2-}$ dominating in acidic solutions at Cr (VI) concentrations above 0.01m, and CrO_4^{2-} dominating in basic solutions. Hydrolysis of Mo (VI) produces the tetrahedral monomeric molybdate ion MoO_4^{2-} at pH above 7 or 8. At lower pH values and at concentrations in excess of 10^{-4} M,

molybdate is extensively polymerized. The dominant species of Se (IV) in water below pH of 2 is H_2SeO_3. Trigonal pyramidal anions $HSeO_3^-$ and SeO_3^{2-} form above pH values of approximately 3 and 8, respectively. Selenate strongly resembles sulfate in its hydrolysis, with SeO_4^{2-} being dominant above pH 2.

The oxyanion forms of boron, chromium, molybdenum, and selenium are mobile in natural waters. This characteristic has been used in geochemical prospecting to locate deposits of molybdenum (Chappell, 1973). The mobilities of these oxyanions are high in alkaline environments, whereas in acidic waters they are usually bound to ferric oxyhydroxides. In addition, the concentrations of these oxyanions are sometimes controlled by the solubilities of mineral phases. However, their salts of alkaline and alkaline earth metals usually have high solubility. Powellite ($CaMoO_4$) is an exception, showing a solubility of approximately 10^{-4} mole Mo/L in pure water (Felmy *et al.*, 1992). Some alkaline earth metal selenites also have low solubility. Sharmasarkar *et al.* (1996) determined the solubility of $CaSeO_3 \cdot H_2O$ to be $10^{-3.57}$ mole Se/L.

1.1.2 Environmental aspects

Boron is an essential element for plant growth and development. Its presence is necessary for root development and structural integrity of plant membranes. The level of tolerance for human exposure to B in drinking water is 1 mg/L (Table 1.4). Limits on B in irrigation water are less than 2 mg/L, whereas limits for livestock are 5 mg/L (Siler and Sigel, 1998). Trivalent chromium is nutritionally essential with a safe intake level of up to 0.2 mg/day (De Zuane, 1997). Chromium, especially in the hexavalent form, is toxic at high levels to animals. Hexavalent chromium has a harmful effect on the liver, kidney, and respiratory organs. Molybdenum is considered an essential trace element in plants and animals (Jarrell *et al*, 1980). When molybdenum reaches 5-15 ppm, however, the plants can become toxic to livestock (Mertz and Underwood, 1986). High levels of molybdenum produce a disorder called molybdenosis, molybdenum-induced copper deficiency. It has been recommended that concentrations of Mo not exceed 0.01 mg/L in the irrigation water for continuous application on all soils (Albasel and Pratt, 1989). Recent discoveries have revealed that selenium can have many beneficial effects in metabolism and development of ruminants and livestock (Frankenberger and Engberg, 1998). Concentrations of selenium in animal diets in excess of 4 to 5 ppm, however, have resulted in depressed growth rates, infertility of eggs, or other undesirable effects (Allaway, 1968).

High concentrations of these trace elements in the hydrosphere may be derived from the weathering of rocks. In an extensive survey of surface waters in Colorado, Voegeli and King (1969) concluded that surface waters containing greater than 5 µg/l Mo may be related to the weathering of molybdenum deposits. Boron, chromium, molybdenum, and selenium are also introduced into the environment as a result of industrial activities through atmospheric emission and effluent to hydrologic systems. Emissions of chromium can be traced to metallurgical processing, fuel combustion, and other sources such as cement plants (Nriagu and Nieboer, 1988). Ambient air selenium originates mainly from the combustion of fossil fuels and from other industries (Siler and Sigel, 1998). These trace elements are concentrated in solid wastes, such as fly ash (Page *et al.*, 1979; Eary *et al.*, 1990), oil shale (Stollenwerk and Runnells, 1981), and municipal solid waste incinerator (MSWI) bottom ash (Kersten *et al.*, 1997). They also occur in municipal sewage sludge (Sterritt and Lester, 1980). Surface and subsurface disposal of these waste materials can potentially cause the contamination of surface and ground water (Fruchter *et al.*, 1990; Stark and Redente, 1986; Lahann, 1976).

Table 1.4: Drinking water standards for B, Cr, Mo, and Se (mg/l), after De Zuane (1997).

Organization	Standard	B	Cr	Mo	Se
WHO	guidelines		0.05	0.07	0.01
USEPA	MCLG, MCL	0.6-1*	0.1	0.04*	0.05
Ontario	DWO	5.0	0.05		0.01

MCLG = maximum contaminant level goals, * expected.

MCL = maximum contaminant level

DWO = drinking water objectives (MOE, 1983)

Various techniques have been developed to remove these trace elements from drinking water and from wastewaters. In the treatment of drinking water, removal of up to 90% chromium has been achieved with the addition of alum, lime, or ferrous or ferric sulfate (De Zuane, 1997). Chemical treatment for selenium, however, was rated as poor (0-30% removal) with alum, lime, and activated carbon; fair (30%-60% removal) with excess lime; and fair to good (more than 50% removal) with ferric sulfate (De Zuane, 1997). Nriagu and Nieboer (1988) summarized the technologies available for the removal of chromium from wastewaters. New remedial technologies for selenium have been recently developed,

involving bioreduction of oxidized soluble inorganic selenium species (SeO_3^{2-} and SeO_4^{2-}) into an insoluble selenium precipitate (Se^0) (Frankenberger and Engberger, 1998).

1.2 Ettringite and hydrocalumite

1.2.1 Natural occurrence

Hydrocalumite and ettringite are the two mineral phases examined in this study. Ettringite, a hydrated calcium aluminate sulfate, was originally found near Ettringen, Germany, and received its name from this locality (Palache *et al.*, 1951). Freeborn and Roy (1984) summarized the two main occurrences of ettringite. Ettringite, from localities in Jordan and Israel, appear to be the result of the retrograde alteration of a high temperature mineral assemblage. The high temperature minerals were produced by spontaneous combustion of organic matter in the bituminous limestone (Khoury and Nassir, 1982). Ettringite crystals were also formed at Scawt Hill (Ireland), the Eifel district (Germany), and at Puy-de-Dome, France, where a limestone has been metamorphosed or metasomatized by a basalt intrusion.

Hydrocalumite was first characterized by Tilley (1934), and was named for its composition of hydrated calcium aluminate. Hydrocalumite is often closely associated with ettringite. The association of these minerals, together with afwillite and portlandite was found in Puy-de-Dome, France. The phase assemblage hydrocalumite - ettringite - afwillite was also observed at Eifel and Scawt Hill (Freeborn and Roy, 1984). These occurrences of ettringite and hydrocalumite suggest that the parent rock should be enriched in calcium and poor in silica. Metamorphism at high temperature and low pressure causes decarbonation and dehydration, producing a mineral assemblage similar to that of Portland cement clinkers (Khoury and Nassir, 1982). Ettringite and hydrocalumite are subsequently formed during the hydration of the high temperature assemblage.

1.2.2 Chemical composition

Because the literature nomenclature for ettringite and hydrocalumite is confusing, it is necessary to clarify the terminology used for both phases. Hydrocalumite was originally named for the mineral with the composition of $Ca_2Al(OH)_{6.75}(CO_3)_{0.125}(H_2O)_{2.5}$ (Tilley, 1934). However, a variety of anions can substitute for hydroxyl and carbonate in hydrocalumite and therefore, a range of compositions (solid solutions) can be found in nature. Some of the end-

members of these solid solutions have been named as new minerals, e.g. *Friedel's Salt* is the mineral name for the Cl endmember. The term *hydrocalumite* has been used as a general mineral name for the entire solid solutions series. Taylor (1973) proposed this scheme by presenting the chemical formula for hydrocalumite as $Ca_2Al(OH)_6X{\cdot}nH_2O$, where X represents a monovalent anion. It is preferable, however, to double the formula to $Ca_4Al_2(OH)_{12}X_2{\cdot}nH_2O$, which allows divalent anionic endmember compositions to be expressed without using fractional stoichiometric coefficients.

Hydrocalumites are common solid phases that form during the hydration of Portland cement. In cement chemistry terminology, the hydroxyl-hydrocalumite is referred to as C_4AH_{13}, where C, A and H are used as abbreviations for CaO, Al_2O_3 and H_2O, respectively. Thus C_4AH_{13} corresponds to the OH-hydrocalumite $Ca_4Al_2(OH)_{12}(OH)_2{\cdot}6H_2O$. There is also a sulfate-rich phase that forms in cement-water systems and it is variously referred to as alumino-ferro-monosulfate (AFm), monoaluminosulfate or simply monosulfate. The compositional formula for AFm in cement terminology is given as $C_4A\bar{S}H_{12}$ although some Fe^{3+} substitutes for Al^{3+}. The $\bar{S}$ in the formula represents SO_3. The quantity is barred to distinguish it from S that is used to represent SiO_2. In this study, we adopt Taylor's approach and use the term *hydrocalumite* to refer to any calcium aluminate with the formula $Ca_4Al_2(OH)_{12}X_2{\cdot}nH_2O$. Endmembers, or solid solutions particularly enriched in one anion, are distinguished by prefixing the term with the name of the anion, such as SO_4-hydrocalumite for the AFm phase or Cl-hydrocalumite for Friedel's salt.

Ettringite is the accepted mineral name for the phase whose chemical composition is $Ca_6Al_2(OH)_{12}(SO_4)_3{\cdot}26H_2O$. However, there are compositional variations in natural ettringite due to substitution of other anions for SO_4^{2-}. For example, borate is reported to partially substitute for sulfate in two ettringite analogues: *charlesite* and *sturmanite* (Dunn *et al.*, 1983; Peacor *et al.*, 1983). Many other compositional varieties of ettringite have been synthesized such as those enriched in OH^-, CO_3^{2-}, and NO_3^- (Carlson and Berman, 1960; Pöllmann *et al.*, 1989). Partial solid solutions of borate, and complete solid solutions of chromate and selenate ettringites with the sulfate endmember have been synthesized and characterized by various authors (Pöllmann *et al.*, 1993; Kumarathasan *et al.*, 1990; Hassett *et al.*, 1990). Pöllmann *et al.* (1989) proposed to use the term *ettringite* as a general term for all solid solutions of acicular calcium aluminate hydrates with the general formula of $Ca_6Al_2(OH)_{12}(X)_3{\cdot}nH_2O$, where X represents a divalent anion. Ettringite is also an important early-formed phase during the hydration of Portland cement. In cement terminology, ettringite is represented as $C_6A\bar{S}_3H_{32}$ and referred to as the AFt or alumino-ferro-trisulfate phase (Taylor, 1990). Similarly, *ettringite* will be used in this study to refer to calcium aluminate phases with the formula $Ca_6Al_2(OH)_{12}X_3{\cdot}nH_2O$, where X is a divalent anion.

1.2.3 Crystal structure

The crystal structure of hydrocalumite is shown in Figure 1.1. It is composed of brucite-like octahedral layers in which Ca would normally be in 6-fold coordination with hydroxyl groups (Figure 1.1a). However, one third of the Ca^{2+} sites are occupied by Al^{3+}. The considerably higher ionic potential of Al^{3+} distorts the calcium octahedra and permits a water molecule from the interlayer position to enter into calcium's coordination sphere (Figure 1.1b). This results in a rare, seven-fold coordination of oxygen around calcium ions in the structure (Ahmed and Taylor, 1967). Ca and Al always occur in the stoichiometric 2:1 ratio in the principal layers. The substitution of Al^{3+} for Ca^{2+} generates net positive charge in the octahedral layers, and anions are incorporated into the interlayers to balance this charge. Hydrocalumite is, therefore, an anionic clay mineral. Along with anions, water molecules also occupy the interlayer positions (Taylor, 1973). The type of the interlayer anions in the structure has a remarkable effect on the water content. For example, the substitution of $2Cl^-$ by $2OH^-$ or CO_3^{2-} is accompanied with an increase in water content, so that a sufficient number of hydrogen-bonds between upper and lower principle layer are maintained (Sacerdoti and Passaglia, 1988). Polymorphism is a common phenomenon associated with hydrocalumite due to variations in the manner of stacking of successive layers (Roberts, 1957).

The structure of ettringite is shown in Figure 1.2. It is composed of columns of positively-charged chemical units with a composition of $\{Ca_6[Al(OH)_6]_2 \cdot 24H_2O\}^{6+}$. The $Al(OH)_6$ octahedra are linked with CaO_8 polyhedra in the columns. The columns are aligned parallel to the c-axis. Anions and water molecules reside between the columns with the composition of $\{(SO_4)_3 \cdot nH_2O\}^{6-}$ in each unit cell (Moore and Taylor, 1970). Figure 1.2 shows two projections of the ettringite structure, one parallel to the c-axis and the other perpendicular.

X-ray diffraction (XRD) analysis is an essential technique used in this study for the identification of solid phases. The d-spacing of the hydrocalumite phases varies with the anion present and with the amount of water contained in the interlayer (Taylor, 1973). The amount of water in the interlayer is dependent on the drying conditions. Relative to hydrocalumite, the cell constants of ettringite phases are less susceptible to change with anionic substitution and change in relative humidity. Table 1.5 summaries the potential hydrocalumite phases related to this study, along with their characteristic XRD parameters measured at 25 °C (Lea, 1970; Taylor, 1990). The d-spacing of each phase is underlined. The relative humidities at which these phases are equilibrated are also given.

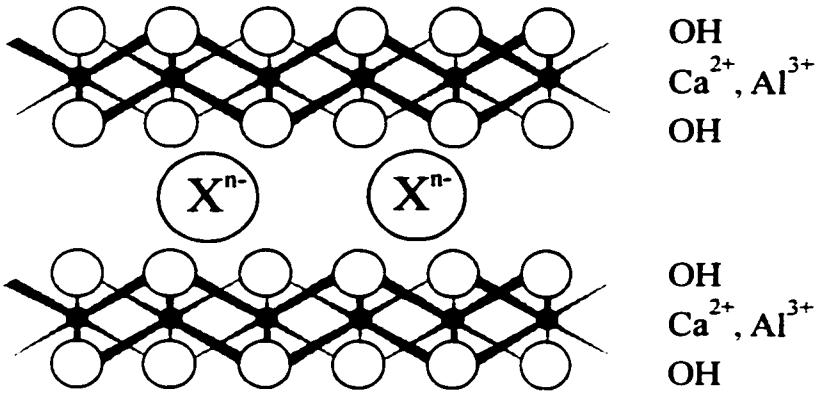

(a)

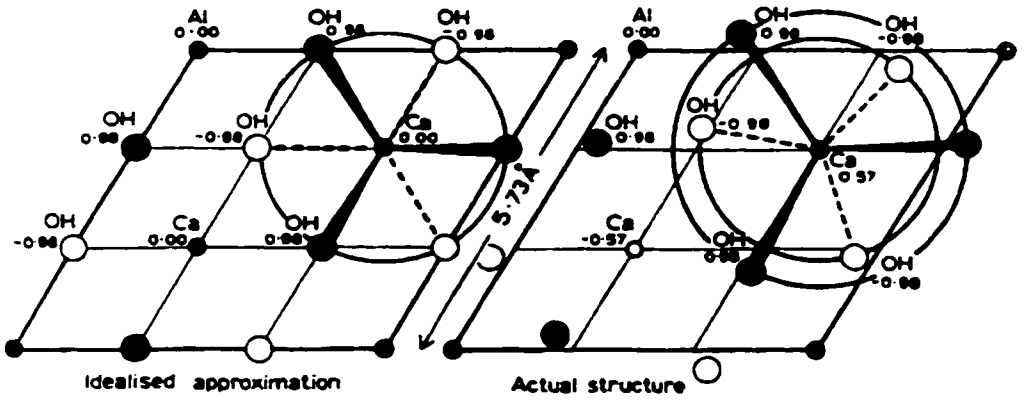

(b)

Figure 1.1: (a) A schematic representation of the structure of hydrocalumite, consisting of brucite-like layers intercalated by hydrated anions, modified from Constantino *et al.* (1995). (b) A comparison of the idealized model with the actual structure of hydrocalumite, from Taylor (1973).

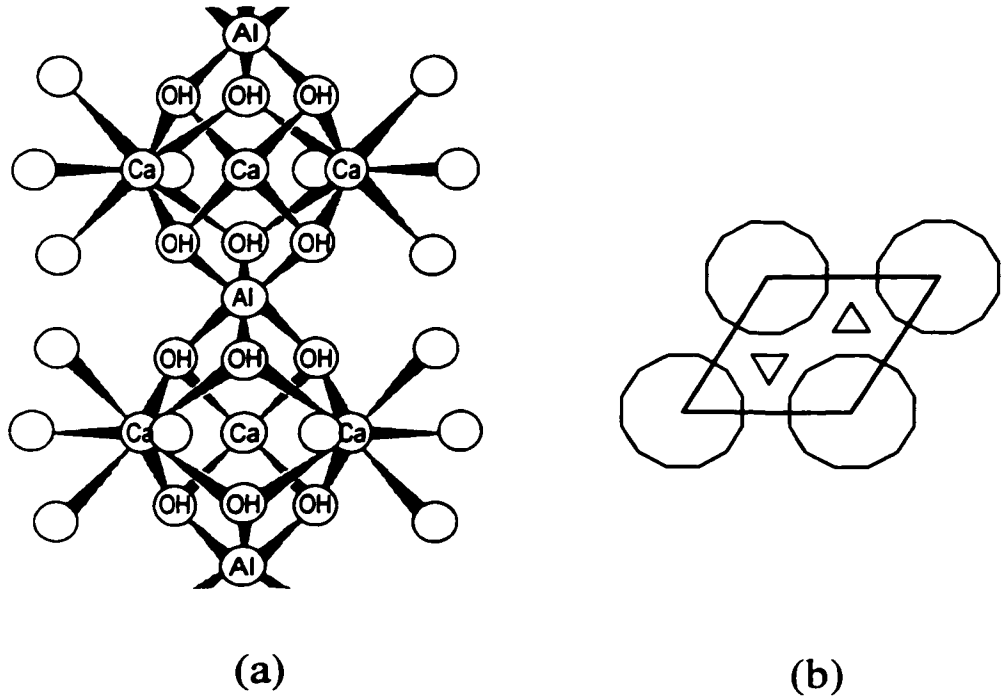

Figure 1.2: (a) A single column of ettringite projected on $(11\bar{2}0)$. Unmarked circles represent H_2O molecules. (b) A projection of the columns on (0001). The polygons represent the columns, whereas the triangles represent the anions and groups of H_2O molecules, modified from Taylor (1973).

Table 1.5: Hydrocalumite phases with $[Ca_2Al(OH)_6]^+$ principal layers

Solid Phase	One Formula Unit	Drying Conditions (% R.H.)	Characteristic X-ray powder spacings (Å)
C_4AH_{19}	$[Ca_2Al(OH)_6]_2[2OH^-\cdot 12H_2O]$	>88%	10.7, 5.35, 4.10
C_4AH_{13}	$[Ca_2Al(OH)_6]_2[2OH^-\cdot 6H_2O]$	12-88%	7.9, 3.95, 2.88
C_4AH_{11}	$[Ca_2Al(OH)_6]_2[2OH^-\cdot 4H_2O]$	<12%	7.4, 3.90, 3.70
C_2AH_8	$[Ca_2Al(OH)_6][(Al(OH)_4^-\cdot H_2O]$	12-100%	10.7, 5.36, 4.10
C_2AH_5	$[Ca_2Al(OH)_6][(Al(OH)_4^-]$	<12%	8.7, 4.34, 3.18
$C_4A\bar{S}H_{14}$	$[Ca_2Al(OH)_6]_2[SO_4^{2-}\cdot 8H_2O]$	100%	10.3, 5.15, 4.03
$C_4A\bar{S}H_{12}$	$[Ca_2Al(OH)_6]_2[SO_4^{2-}\cdot 6H_2O]$	20-95%	9.0, 4.48, 4.40
$C_4A\bar{C}H_{11}$	$[Ca_2Al(OH)_6]_2[CO_3^{2-}\cdot 5H_2O]$	37%	7.6, 3.8, 2.86
$C_4A\bar{C}_{0.5}H_{12}$	$[Ca_2Al(OH)_6]_2[(OH^-, \frac{1}{2}CO_3^{2-})\cdot 5.5H_2O]$	>37%	8.2, 4.10, 3.88
C_2ASH_8	$[Ca_2Al(OH)_6][AlSiO_3(OH)_2^-\cdot 4H_2O]$	37%	12.6, 6.3, 4.18

1.2.4 Other important anionic clays

Of all the anionic clays, *hydrotalcite* and its derivatives are the most extensively studied. Another important anionic clay is *green rust*, which has received much attention recently in the areas of remediation and corrosion science. Anionic clays possess positive charge in their principal layers. As a result, anions are needed by their structures to maintain charge balance. Anionic clays are rare in nature but simple and relatively inexpensive to prepare in the laboratory (Reichle, 1986).

Hydrotalcite consists of brucite layers in which Al^{3+} replaces some of the Mg^{2+} ions. The Mg/Al ratio, however, can vary from 2 to 3. Carbonate is often the interlayer anion and the formula is expressed as $Mg_6Al_2(OH)_{16}(CO_3)\cdot 4H_2O$. *Hydrotalcite-like* materials or *layered double hydroxides* (LDH) refer to compounds that have a general formula of $[M^{2+}_{3-x-2y}M^{3+}_{x-2y}(OH)_6]^{(x-2y)+}[xX^-\cdot yY^{2-}\cdot zH_2O]^{(x-2y)-}$, where M^{2+} and M^{3+} denote di- and trivalent cations, and X^- and Y^{2-} denote mono- and divalent anions (Brown and Gastuche, 1967). Many practical applications of the hydrotalcite-like compounds have been explored. They are widely used as sorbents, catalysts, and ion exchangers (Reichle, 1986). A large volume of data are available for the hydrotalcite-like phases in terms of preparation, characterization, properties, and applications (e.g. Miyata, 1980; Constantino and Pinnavaia, 1995). Considering the similarities in the structures between hydrocalumite and hydrotalcite, the studies on hydrotalcite-like phases are useful resources for the present study. Excellent

reviews of the current literature on hydrotalcite-like phases can be found in Cavani *et al.* (1991) and Rives and Ulibarri (1996).

Green rust is an intermediate ferrous-ferric compound that forms during the oxidation of the initial ferrous compound to the end rust product. This compound also has a brucite-like principal layer of $[Fe^{II}Fe^{III}(OH)_4]^+$, between which lie various anions. Based on the anions occupying the interlayer, green rust compounds are classified as *green rust 1* (planar anions such as CO_3^{2-}, Cl^-, and Br^-) or *green rust 2* (non-planar anions such as SO_4^{2-}) (Olowe and Génin, 1991). In addition to the occurrence during the corrosion of iron, green rust was also identified in soils (Trolard *et al.*, 1997). The presence of green rust in natural environments may influence the concentration of anions such as carbonate and sulfate in natural waters.

1.3 Objectives

Boron, chromium, molybdenum, and selenium are of environmental concern, because they are toxic at high concentrations, and usually occur as oxyanions, which are typically mobile in natural waters. Incorporation of these elements into mineral phases is an important mechanism for their removal from waters. The structural characteristics of ettringite and hydrocalumite indicate that both mineral phases are capable of incorporating anions into their structures. Previous studies have also demonstrated that boron, chromium, molybdenum, and selenium can be taken up by these phases (e.g. Kumarathasan *et al.*, 1990; Hassett *et al.*, 1990; Pöllmann *et al.*, 1993; Kindness, *et al.*, 1994).

Boron, chromium, molybdenum, and selenium are often enriched in fly ash, and the addition of lime to fly ash induces the formation of ettringite and hydrocalumite (Reardon and Della-Valle, 1997; Shi, 1996). Therefore, a study was initiated to examine the interaction between fly ash and lime water. Through a direct examination of the solid phases, Chapter 2 investigates the formation and transformation of secondary ettringite and hydrocalumite with reaction time in both the Class F and Class C fly ashes. An emphasis is placed on the stability of ettringite and hydrocalumite, and the compositional characteristics of these phases. Chapter 3 delineates the correlation between the solution composition and the development of the secondary phases. The affinities of the trace elements for these phases are also addressed. Chapter 4 examines the uptake behavior of borate, chromate, molybdate, and selenate in the pure ettringite-water and hydrocalumite-water systems in order to clarify the relationship between the decrease in anion concentrations and the precipitation of these phases in the lime-leached fly ashes. The preference of these oxyanions for ettringite and hydrocalumite is also determined. In Chapter 5, hydrocalumite solid solutions with OH as one endmember and

borate, chromate, molybdate, and selenate as the other endmembers are synthesized and characterized. This study focuses on the effect of the anions on mineral phase stability in the system $CaO\text{-}Al_2O_3\text{-}XO_3/Y_2O_3\text{-}H_2O$ ($X = Cr^{6+}$, Mo^{6+}, Se^{6+}, and S^{6+}; $Y = B^{3+}$). Some fundamental thermodynamic parameters are derived and the uptake capacity of hydrocalumite for these oxyanions is also determined. Because both ettringite and hydrocalumite are hydration phases of ordinary Portland cement, Chapter 6 explores the potential for removing these oxyanions from wastewaters using this commercially-available and cost-effective material.

Chapter 2

Fly ash-Lime-Water Interaction: I
Development of Secondary Phases with Time

2.1 Introduction

The large quantities of fly ash produced by thermal power plants are usually disposed of in landfills and surface impoundments, or utilized for different purposes. The major uses of fly ash are as a cement additive or as construction fill. Fly ash is also used in agriculture and land reclamation. However, there are restrictions on the disposal and utilization of fly ash due to the potential for leaching of toxic trace elements, which could cause degradation of surface and ground waters.

In both the disposal and utilization of fly ash, high pH environments are often generated. The leaching of trace elements is pH dependent, and therefore the presence of free lime will greatly affect the leaching properties of the fly ash and its potential for contamination. There are two different types of fly ash from the utilization scheme developed by the American Society for Testing and Materials: Class C and Class F (ASTM, 1988). Class C fly ash usually has a high CaO content, which may constitute up to 32% of its bulk composition (Thomas, 1997). When the fly ash is brought into contact with water, high pH leachates are created due to the presence of free lime. Significant amounts of free lime are also contained in the residues from "clean coal technology", where lime is injected to scavenge sulfur (Cobb *et al.*, 1997). When fly ash is used as a cement additive, high pH conditions are generated from the hydration of Portland cement (Reardon, 1992). Therefore, some understanding of the leaching of fly ash in high pH environments is necessary.

Fly ash is mainly composed of amorphous glassy particles. The relative percentage of the glassy matrix was reported to be 50, 60, and 70 to 90% by Wesche (1991), Henry and Knapp (1980) and Adriano *et al.* (1980), respectively. The amorphous component of fly ash was found to increase with decreasing particle size (Hansen *et al.*, 1981; Vempati *et al.*, 1994). Compositionally, the glassy phase is made up primarily of iron-aluminum-silicates or calcium-iron-aluminum-silicates (Henry and Knapp, 1980). Thomas (1997) documents that the Class F fly ashes are dominated by aluminosilicate glass with varying amounts of iron, whereas the amorphous phase in the Class C ash is mainly calcium aluminosilicate glass. Quartz, mullite, magnetite, and some soluble calcium phases such as anhydrite and lime are frequently identified in fly ashes (Natusch *et al.*, 1975; McCarthy *et al.*, 1984). Crystalline phases either occur as individual minerals or are enclosed in the glass matrix (Hulett and Weinberger, 1980; Warren and Dudas, 1984).

In this study, lime is added to fly ash to maintain the high pH conditions under which the glassy matrix of fly ash is severely leached (Reardon and Della-Valle, 1997). The leaching of the glassy phase liberates the associated elements, and as a result, secondary phases precipitate. These secondary phases reduce the solution concentrations of trace elements that occur as oxyanions. For example, ettringite is frequently identified as a leaching product of fly ash in alkaline solutions (Zhou and Dayal, 1989; Mattigod *et al.*, 1990; van der Hoek *et al.*, 1994). Sulfate and trace elements, such as As, B, Cr, Mo, Se, and V, have been shown to be incorporated into the ettringite structure (e.g. Carles-Gibergues and Aitcin, 1986; Kumarathasan *et al.*, 1990; Myneni *et al.*, 1997). In lime-treated fly ash, hydrocalumite has been identified as the major secondary phase, and the removal of anions such as borate, selenate, and sulfate has been correlated to the formation of hydrocalumite (Reardon and Della-Valle, 1997; Duchesne and Reardon, 1999).

Although some secondary precipitates have been identified in leached fly ash under alkaline conditions, and trace element removal has been observed, several questions remain unanswered. It is not yet clear when these phases form, why one phase forms preferentially over another, and which phases contribute to the fixation of trace elements. In the present study, the leaching of both Class F and Class C fly ashes is examined in the presence of excess lime. The objective of this study is to investigate the formation and transformation of secondary precipitates with time through a direct examination of the solid phases. An emphasis is placed on the stability of ettringite and hydrocalumite and the compositional characteristics of these phases.

2.2 Experimental

2.2.1 Materials

Three fly ash samples from Ontario Hydro's thermal generating stations were examined. The samples were collected from dry landfills at the Lakeview, Lambton, and Atikokan electric power plants. Both the Lakeview and Lambton fly ashes were generated by burning bituminous coal from eastern U.S. and are therefore categorized as Class F fly ash. Lignite from Saskatchewan was burned at Atikokan, which produces a Class C fly ash. The Atikokan fly ash contains 14% CaO, whereas the amount of CaO is less than 4% in the Lakeview and Lambton fly ashes (Section 3.2.1).

The crystalline phases in the fly ashes were identified using X-ray diffraction (XRD) analysis. The XRD patterns of the Lakeview and Lambton fly ashes are shown in Figure 2.1A. Quartz (SiO_2), mullite ($Al_6Si_2O_{13}$), magnetite (Fe_3O_4), and calcite ($CaCO_3$) were identified in the Lakeview fly ash. Based on the relative intensities of these minerals, quartz is the dominant crystalline phase. In the Lambton fly ash, quartz and mullite are the only phases identifiable using XRD. The relative amount of mullite to quartz, however, is higher in the Lambton fly ash than that in the Lakeview ash. Only the main peaks of quartz were observed in the Atikokan fly ash (Figure 2.1B). In the XRD patterns of the Lakeview and Lambton ashes, the diffuse glass band is centered at 25° 2θ (Figure 2.1A), close to the 2θ value of 26.8° given by Carles-Gibergues and Aitcin (1986) for the low calcium glassy phase. The glass band in the Atikokan fly ash occurred at 29° 2θ, indicating a high calcium aluminosilicate glassy phase (Diamond, 1983).

Quartz fragments were observed in all three ashes under an optical microscope. Mullite, which was identified in both the Lakeview and Lambton ashes, however, was not seen using either an optical microscope or a scanning electron microscope (SEM). The morphology of the glass particles varies widely between two different classes of fly ash. In the Lakeview and Lambton fly ashes, ash particles occur as spheres or as amorphous networks, in which small spheres were embedded (Figure 2.2A). This morphology is typical for fly ashes generated by burning eastern U.S. coal (Fisher *et al.*, 1976). The Atikokan fly ash consists mainly of individual spherical particles with various sizes (Figure 2.2B).

Reagent-grade $Ca(OH)_2$ was used as a form of hydrated lime in the experiments. Nanopure double-deionized water was used with a conductance of 0.1 μS/cm.

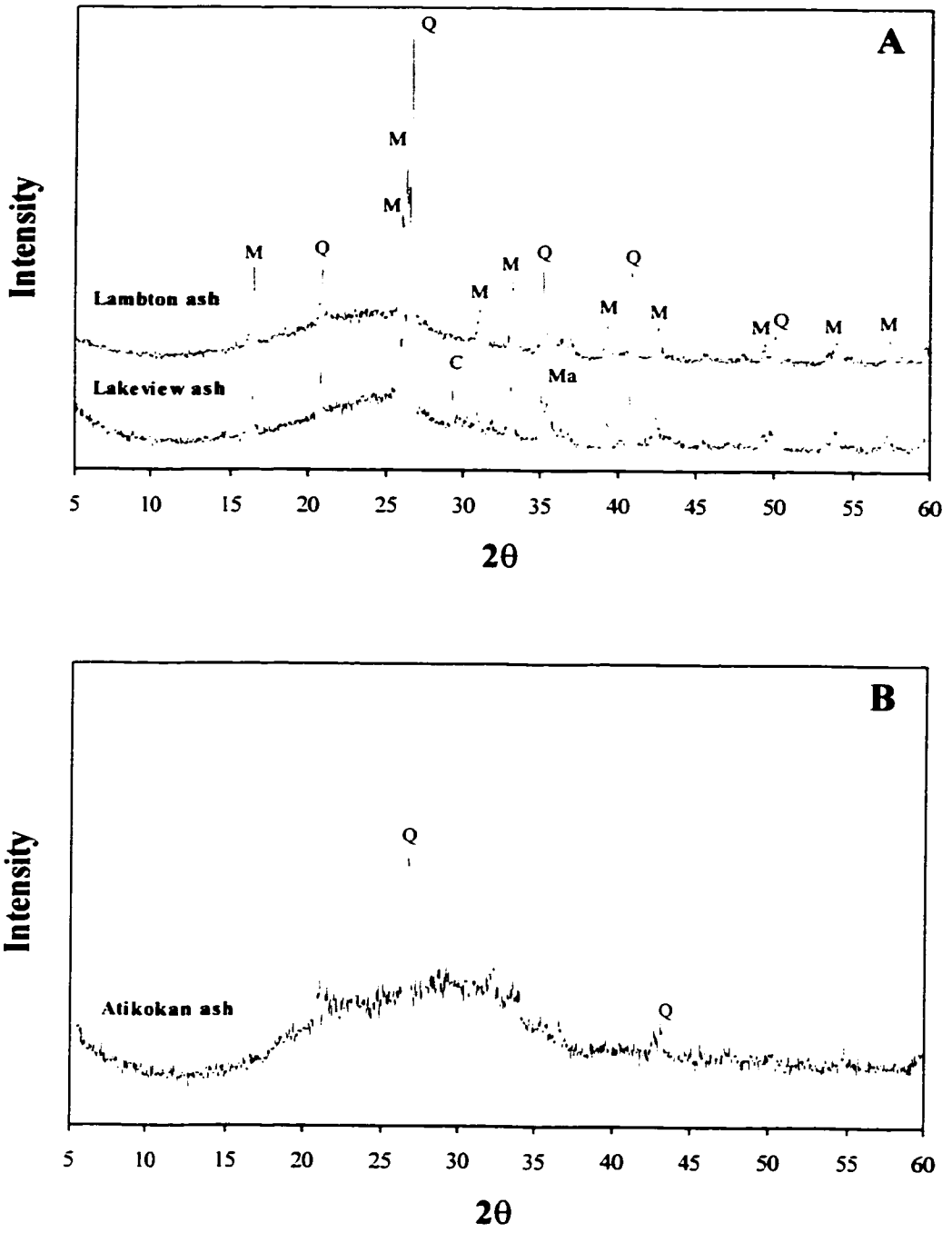

Figure 2.1: XRD patterns of the fly ashes. (A) Lakeview and Lambton fly ashes; (B) Atikokan fly ash. Q - quartz; M - mullite; C - calcite; Ma-magnetite.

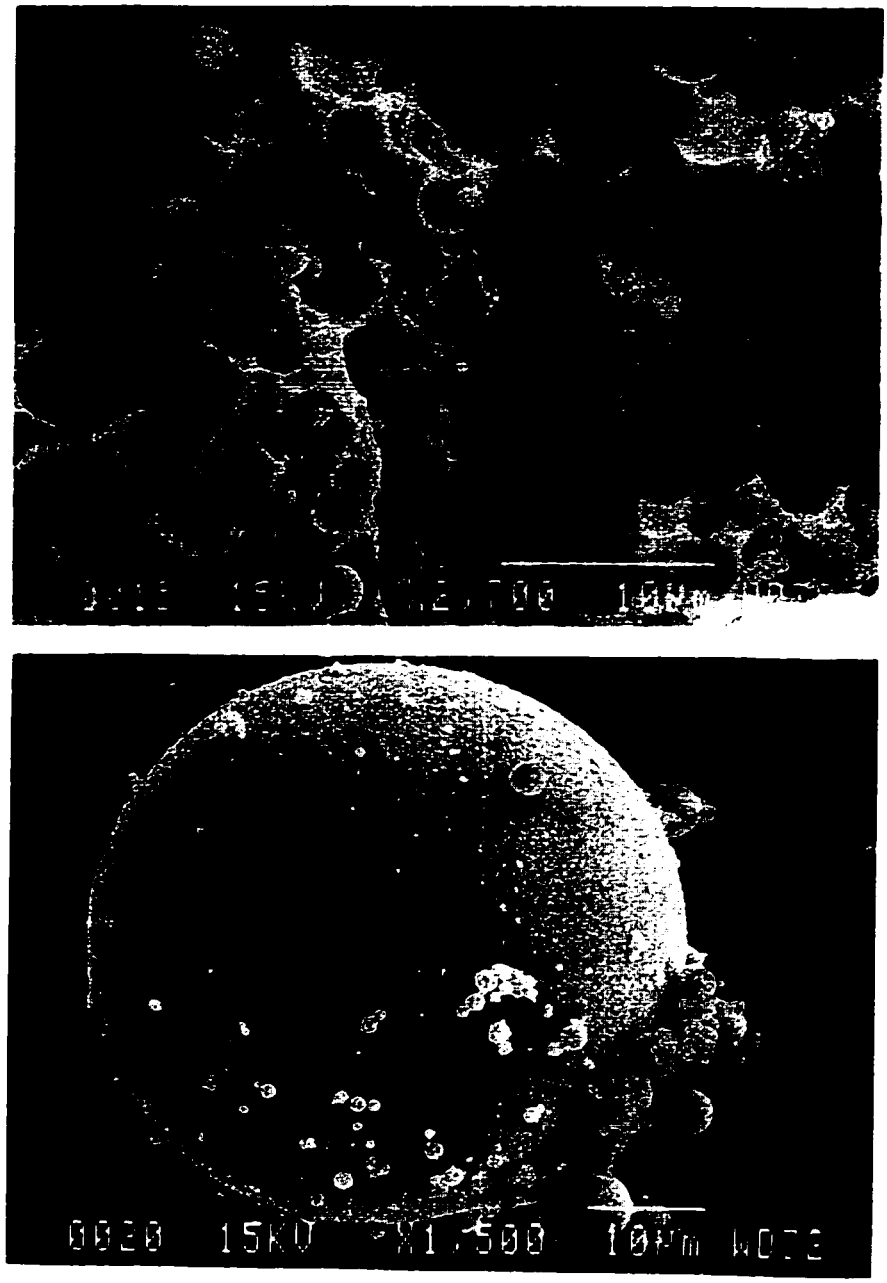

Figure 2.2: Micrographs of the fly ash particles. (A) spherical particles of Lambton fly ash occur individually or are imbedded in an amorphous glass network; (B) various sizes of spherical particles of Atikokan fly ash.

2.2.2 Procedure and analysis

The fly ashes were leached with lime at a water/ash ratio of 20:1. High density polyethylene (HDPE) bottles were used as the reaction vessels. For each sample, 40 g of water, 2 g of fly ash and 2 g of portlandite were massed and added to the bottle. The sample bottles were loaded on a carousel and immersed in a constant-temperature bath at a temperature of 25 ± 0.5 °C. The carousel was rotated continuously by the effluent from a circulation pump to ensure complete mixing. A duration of 30 days was allowed for the entire lime-leaching process. For each fly ash series, a slurry of the residue was collected after 1, 3, 7, 14, and 30 days of reaction. To ensure sample integrity and to avoid contamination, each reaction vessel was only sampled once. The solids were dried in a sealed desiccator over silica gel.

The reacted solids were examined under an optical microscope and also analyzed using X-ray diffraction (XRD) analysis, scanning electron microscopy (SEM) and energy dispersive X-ray (EDX) analysis. XRD analysis was conducted on random powder mounts using a Siemans D500 Diffractometer with Cu Kα radiation. Scanning parameters are typically 0.05° step size for 1-s count times over a range of 5 - 55° 2θ. SEM observations were made using a JEOL JSM-840 scanning electron microscope equipped with an energy dispersive X-ray spectrometer. The samples were coated with gold (thickness ≈ 400 Å) to reduce charging. The EDX spectra were obtained for 100 s of live time with no window between the sample and the X-ray detector.

2.3 Results

2.3.1 Microscopic examination

The lime-leached fly ashes were first examined using an optical microscope. Optical microscopy is a useful tool to determine the major mineral constituents and to identify minerals occurring at low percentages, which might not be identified by XRD or SEM. Large crystals of the precipitated phases can be readily observed under microscope even though their percentages are low. The disadvantages of optical microscopy are that identification of a mineral phase is sometimes limited by the resolution, and that the relative amount of secondary mineral phases may be underestimated using this technique.

Needle-like ettringite crystals were observed in the reacted Lakeview fly ash after 1 day of reaction. The amount of ettringite increased slightly and reached the maximum in the

3-d sample. At the end of the reaction period (after 30 days), ettringite crystals were seen only occasionally. Hexagonal hydrocalumite crystals were observed after 3 days of reaction. The amount of hydrocalumite increased with time and reached approximately 30% of the total solids in the 30-d sample. The crystallinity of hydrocalumite also improved with time.

In the reacted solids of the Lambton fly ash, needle-like ettringite crystals were also observed after 1 day of reaction. The amount of ettringite increased with reaction time, reaching a maximum after 3 days. Ettringite crystals were not seen in the 30-d sample. In this series, hydrocalumite was not seen until the reaction had proceeded for 7 days. Hydrocalumite accounted for approximately 10% of the total solids after 30 days of reaction. Isotropic hydrogarnet crystals were also seen in the 30-d sample.

In contrast to the above two series, ettringite occurred not only in greater abundance, but also as larger crystals in the Atikokan samples. Ettringite was present as needle-like crystals in the 1-d sample with a length ranging from 10 to 15 μm, and constituted over 5% of the solids. The maximum amount of ettringite was observed in the 7-d sample, and accounted for approximately 20 to 30% of the solids recovered. In the 14-d sample, the crystal size of ettringite increased but the quantity was reduced. Ettringite only accounted for 5% of the total solids after 30 days of reaction. Isotropic hydrogarnet crystals were found in the 30-d sample. Hexagonal hydrocalumite plates were not seen in this series.

2.3.2 X-ray diffraction analysis

Portlandite was the principal mineral phase identified in the reacted solids of all three fly ashes throughout the entire reaction period of 30 days (Figures 2.3, 2.4, and 2.5). Overall, the peak intensities of portlandite decreased with reaction time, indicating that this phase was being consumed as leaching progressed. However, there were still substantial amounts present at the termination of the reaction.

In the reacted Lakeview fly ash, quartz and mullite persisted throughout the entire reaction period and their relative intensities remained unchanged (Figure 2.3). Calcite, which also occurred in the fly ash as a primary mineral, was present only in the 1-d sample. The principal ettringite peak at a d-spacing of 9.6 Å was observed in the 1-d sample, and its intensity increased slightly in the 3-d sample. This phase was present throughout the whole course of reaction. Hydrocalumite was identified in the 7-d sample as indicated by the principal peaks at d-spacings around 7.4 and 7.9 Å. The peak at 7.9 Å corresponds to the OH-rich hydrocalumite, whereas the peak at the d-spacing of 7.4 Å is a dehydration phase of the

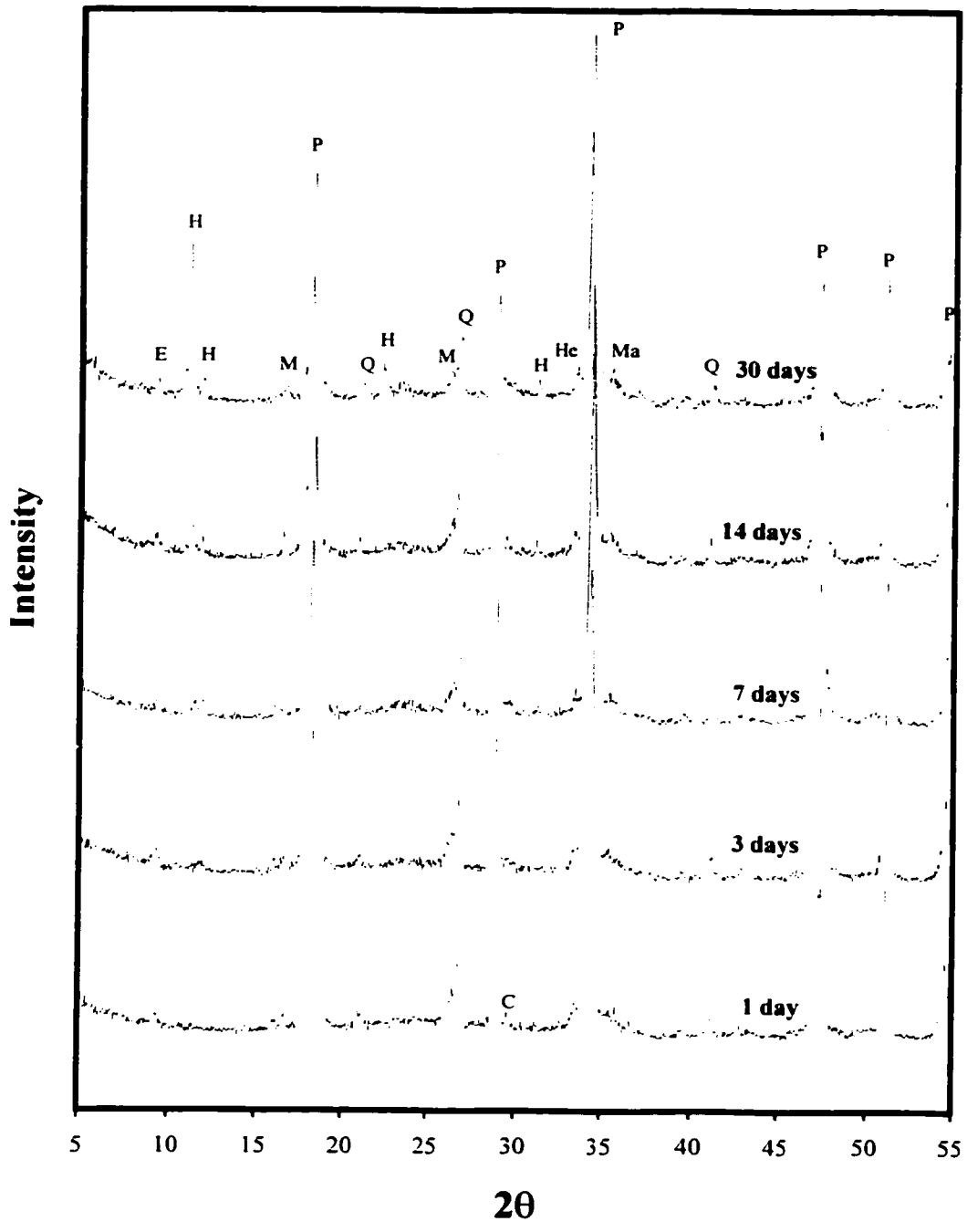

Figure 2.3: XRD patterns of the solid recovered from the lime-leached Lakeview fly ash. P-portlandite; H-hydrocalumite; E-ettringite; Q-quartz; M-mullite; Ma-magnetite; He-hematite; C-calcite.

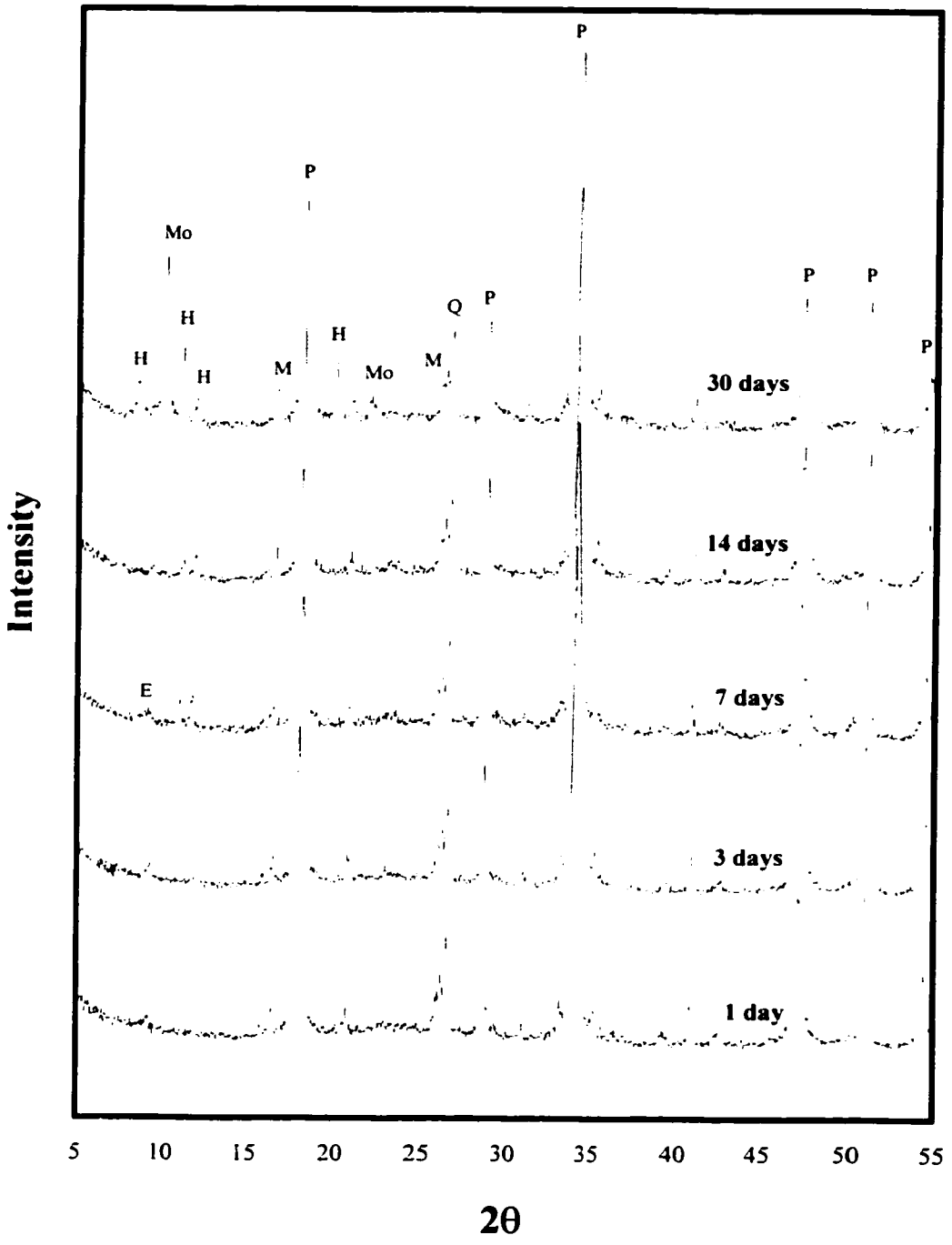

Figure 2.4: XRD patterns of the solid recovered from the lime-leached Lamton fly ash. P-portlandite; H-hydrocalumite; Mo-monosulfate; E-ettringite; Q-quartz; M-mullite.

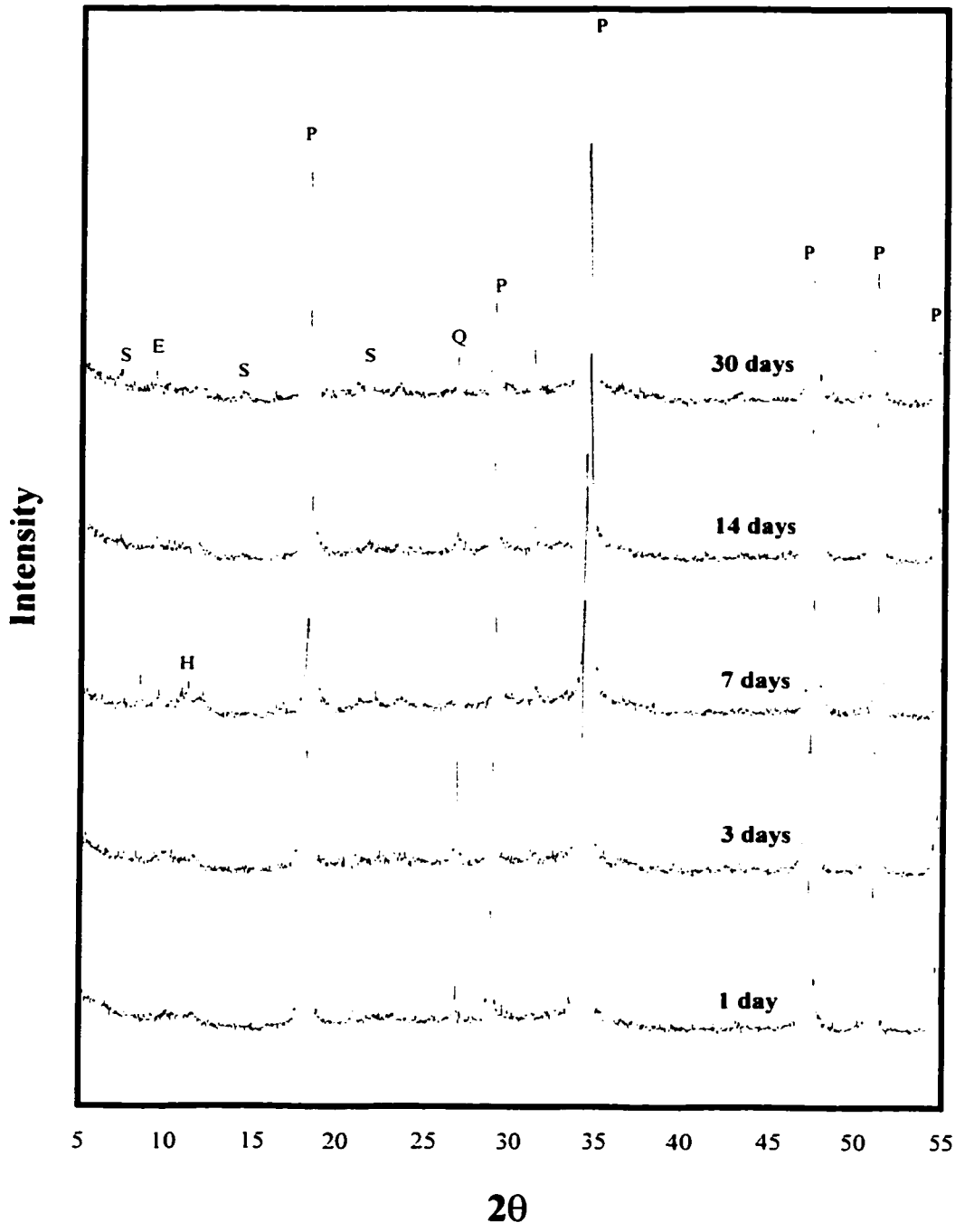

Figure 2.5: XRD patterns of the solids recovered from the lime-leached Atikokan fly ash. P-portlandite; H-hydrocalumite; S-strätlingite; E-ettringite; Q-quartz.

7.9 Å phase (Lea, 1970). The dehydration phase occurred due to the low-humidity drying conditions used in these experiments (samples were dried over silica gel). Both 7.4 and 7.9 Å phases should be regarded as an OH-rich hydrocalumite. CO_3^{2-}, dissolved from calcite, is also likely accommodated in the hydrocalumite. A marked increase in the peak intensities of hydrocalumite was seen between 14 days and 30 days, indicating that a large quantity of hydrocalumite formed during this time period.

Similar to the Lakeview series, the quantity of the primary crystalline phases quartz and mullite remained relatively constant in the Lambton samples (Figure 2.4). Ettringite was seen in the 1-d sample and the relative intensity reached a maximum in the 3-d sample. After 30 days of reaction, ettringite was no longer present in the XRD pattern. Hydrocalumite was not identified until the reaction had proceeded for 7 days. The d-spacing of the precipitated hydrocalumite was approximately 7.9 Å, and a dehydrated hydrocalumite phase with a d-spacing of 7.5 Å was also observed in the Lambton samples. The relative intensity of the OH-rich hydrocalumite peaks increased markedly between 14 days and 30 days of reaction. In the 30-d sample, the OH-rich hydrocalumite appeared to rehydrate during the XRD measurement, generating an additional peak at 10.5 Å. In this sample, another hydrocalumite phase was also seen at a d-spacing of 8.7 Å, suggesting that larger anions, such as SO_4^{2-}, reside in the interlayer of this hydrocalumite. These two immiscible hydrocalumite phases at 7.9 and 8.7 Å probably correspond to OH-rich and SO_4-rich solid solutions.

The primary mineral quartz was seen in all Atikokan samples, however, its relative intensity varied (Figure 2.5). Ettringite peaks were not seen in the XRD pattern of the 1-d sample although needle-like ettringite crystals were observed under the microscope in an amount over 5%. This phase was identified in the reacted solids after 7 days of reaction. Considering the amount of ettringite seen under the microscope, however, the peak intensity of this phase was low. In the Atikokan samples, identification of hydrocalumite was uncertain because the principal peak was broad and occurred at low intensity. In the 30-d sample, low-intensity peaks of strätlingite ($2CaO{\cdot}Al_2O_3{\cdot}SiO_2{\cdot}8H_2O$, or C_2ASH_8 in cement notation) were evident.

2.3.3 Scanning electron microscopy and energy dispersive X-ray analysis

2.3.3.1 Leached ash particles and secondary minerals

SEM examination of the reacted Lakeview and Lambton fly ashes revealed that leaching of the glass and the formation of secondary phases were similar between these two

Class F fly ashes. The results from both the Lakeview and Lambton samples will, therefore, be presented together. Leaching of the fly ash began at early reaction times. Figure 2.6A shows the leached glass surface of the Lakeview fly ash after 3 days of reaction. In addition to ash spheres, particles with smooth surfaces and an amorphous appearance were commonly seen. Occasionally, these particles were partly hexagonal in shape. Ettringite was formed in the early stages of the reaction and the amount decreased with time. It precipitated on the surface of ash particles (Figure 2.6A) or grew out from leached ash particles (Figure 2.6B). Hydrocalumite was seen after 3 and 7 days in the Lakeview and Lambton samples, respectively. After 14 days, hydrocalumite was dominant over ettringite (Figure 2.6 C). The transformation from ettringite to hydrocalumite is well illustrated in Figure 2.6 D, in which needle-like ettringite crystals and leached ash particles are encased by a growing hydrocalumite crystal. The transition point between ettringite and hydrocalumite is also shown in Figure 2.6E. In this picture, the formation of a well-formed hexagonal hydrocalumite crystal was almost complete and the residual ettringite needles can still be seen in the center of the hydrocalumite crystal. After 30 days of reaction, hydrocalumite occurred as perfect hexagonal platey crystals with a size over 10 μm and a thickness over 0.5 μm (Figure 2.7). The crystallinity of hydrocalumite also increased with time. Ettringite was observed occasionally in the Lakeview samples but not in the Lambton samples. At the termination of the reaction, the glass surface of ash particles had been leached away and the acicular mullite crystals can be seen (Figure 2.8A). A characteristic micrograph of the leached Lambton fly ash is shown in Figure 2.8B. The crust of the spherical ash particles (glassy phase) was deeply etched, and small spherical ash particles and moderately-corroded acicular mullite crystals were exposed.

The formation of secondary phases was quite different in the Atikokan fly ash. Ettringite was present as well-formed needle-like crystals throughout the reaction period (Figure 2.9), and the amount of ettringite was much higher in this series. The maximum quantity was observed in the 7-d sample. Hydrocalumite platey crystals were seen occasionally in the 3-d sample. After 14 days of reaction, Strätlingite occurred as rosette aggregates of thin platey crystals. Under the optical microscope, they are identical to the spherical ash particles, which made the identification of this phase impossible. The morphology of strätlingite is different from that of hydrocalumite formed in the Lakeview and Lambton fly ashes where it occurred as individual thick hexagonal plates. The strätlingite became the most common alteration phase in the 30-d sample. Figure 2.10A shows the coexistence of ash particles with strätlingite aggregates. A close-up of a strätlingite rosette is shown in Figure 2.10B.

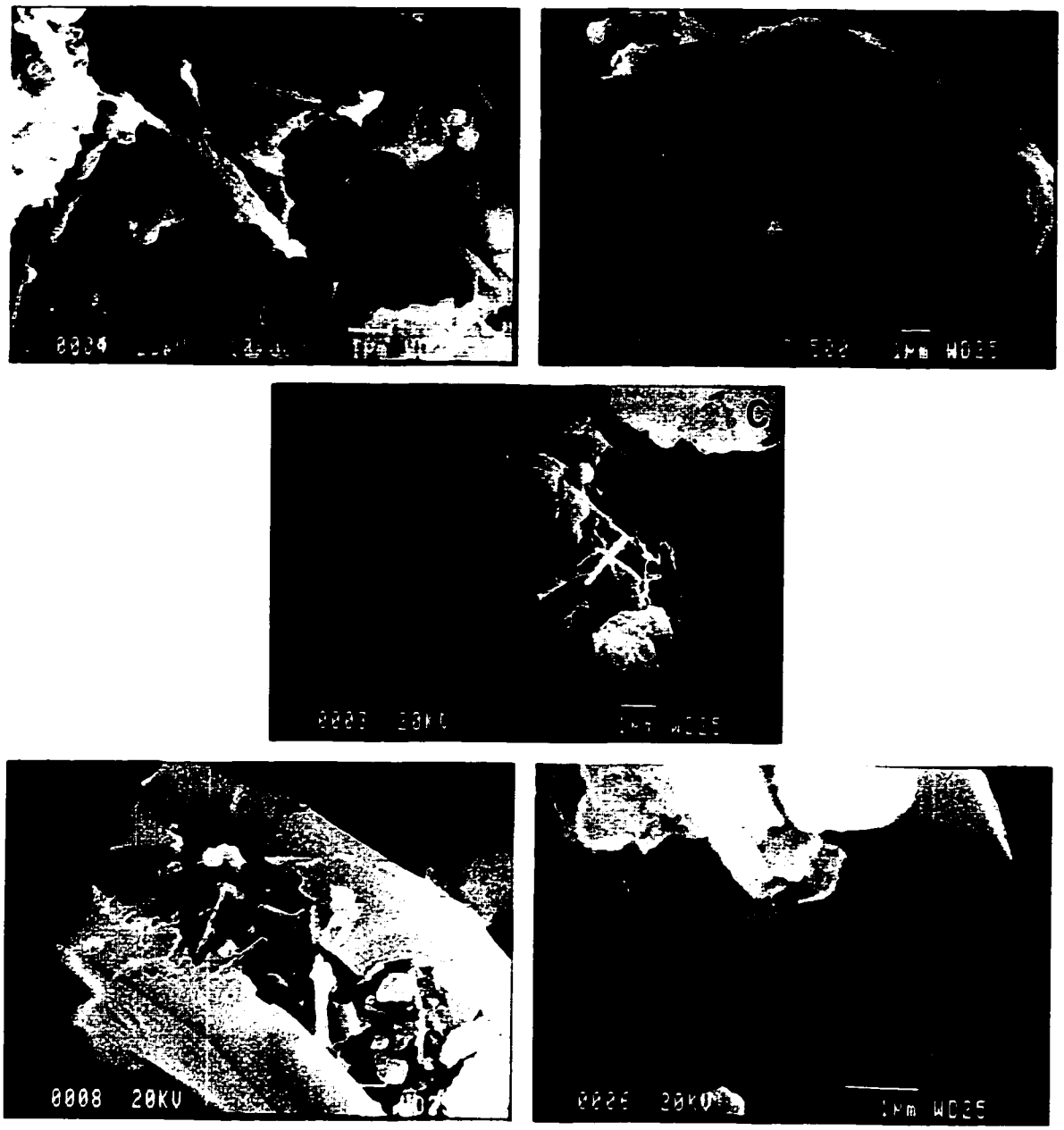

Figure 2.6: Micrographs of the solids recovered from the lime-leached Lakeview fly ash. (A) and (B) ettringite formed after 3 days of reaction; (C), (D), and (E) ettringite was transforming to hydrocalumite in the 14-d sample..

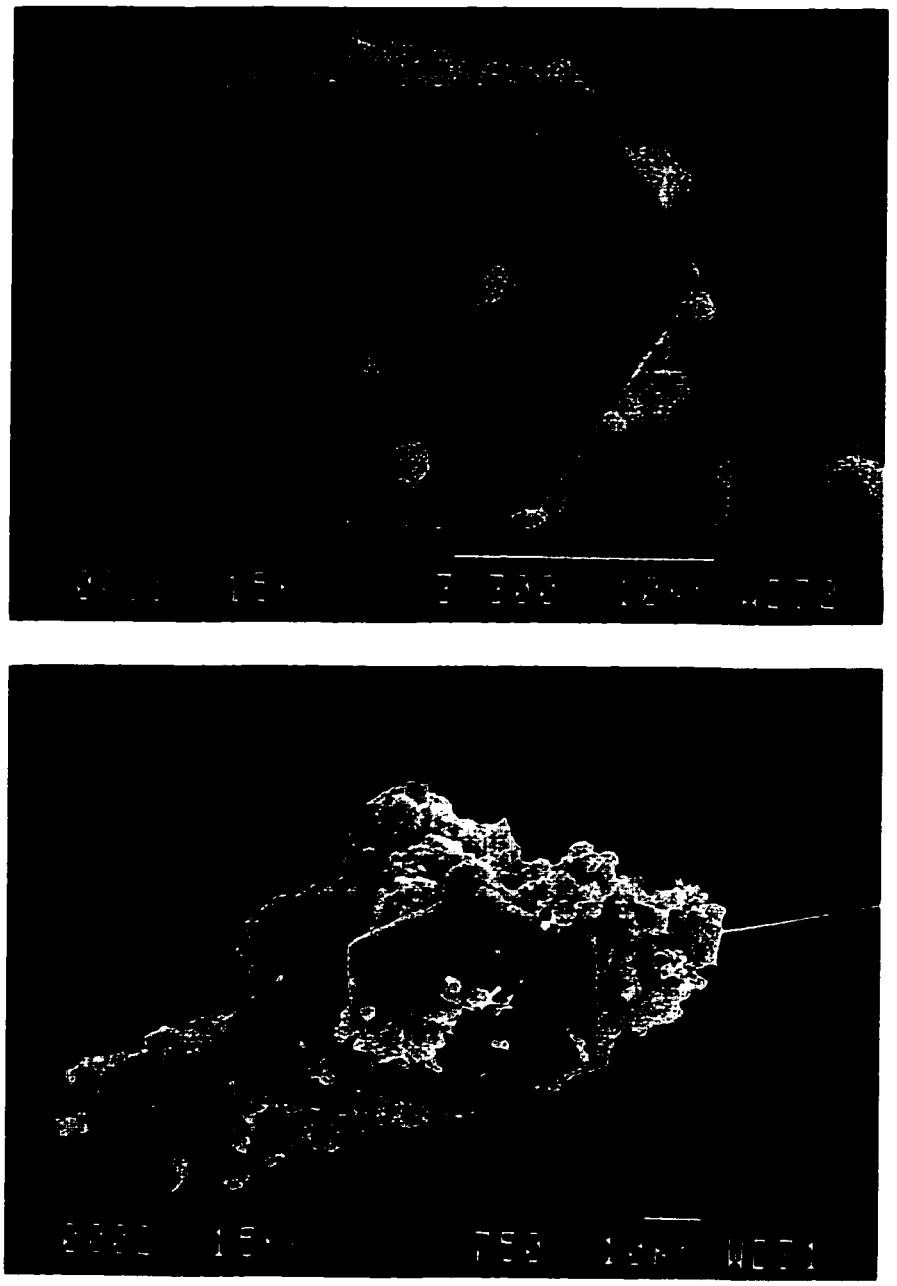

Figure 2.7: Micrographs of the thick, well-formed hexagonal hydrocalumite plates after 30 days of reaction. (A) from the lime-leached Lakeview fly ash; (B) from the lime-leached Lambton fly ash.

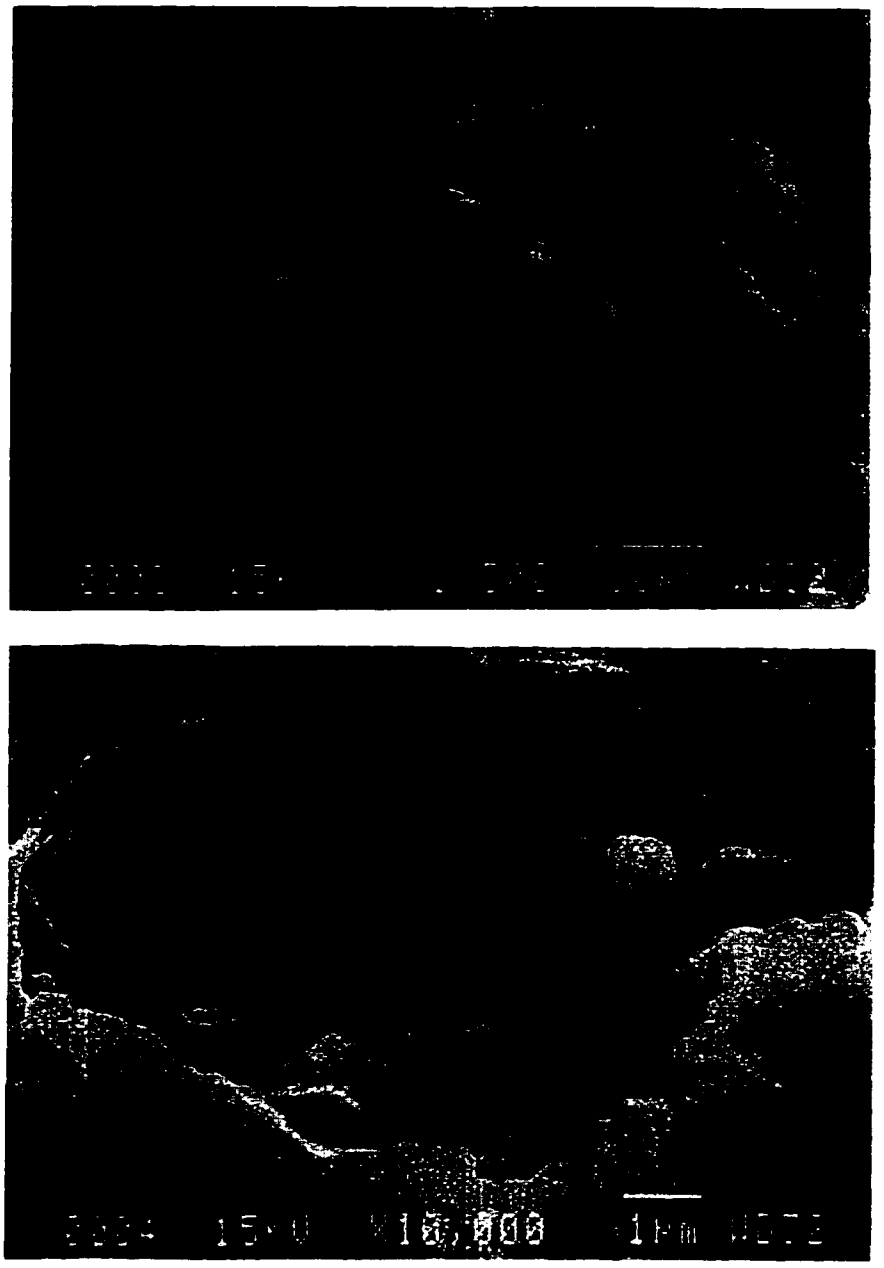

Figure 2.8: Micrographs of the leached fly ash particles after 30 days of reaction, showing that the glass crust of ash particles was removed and mullite crystals were exposed. (A) from the lime-leached Lakeview fly ash; (B) from the lime-leached Lambton fly ash.

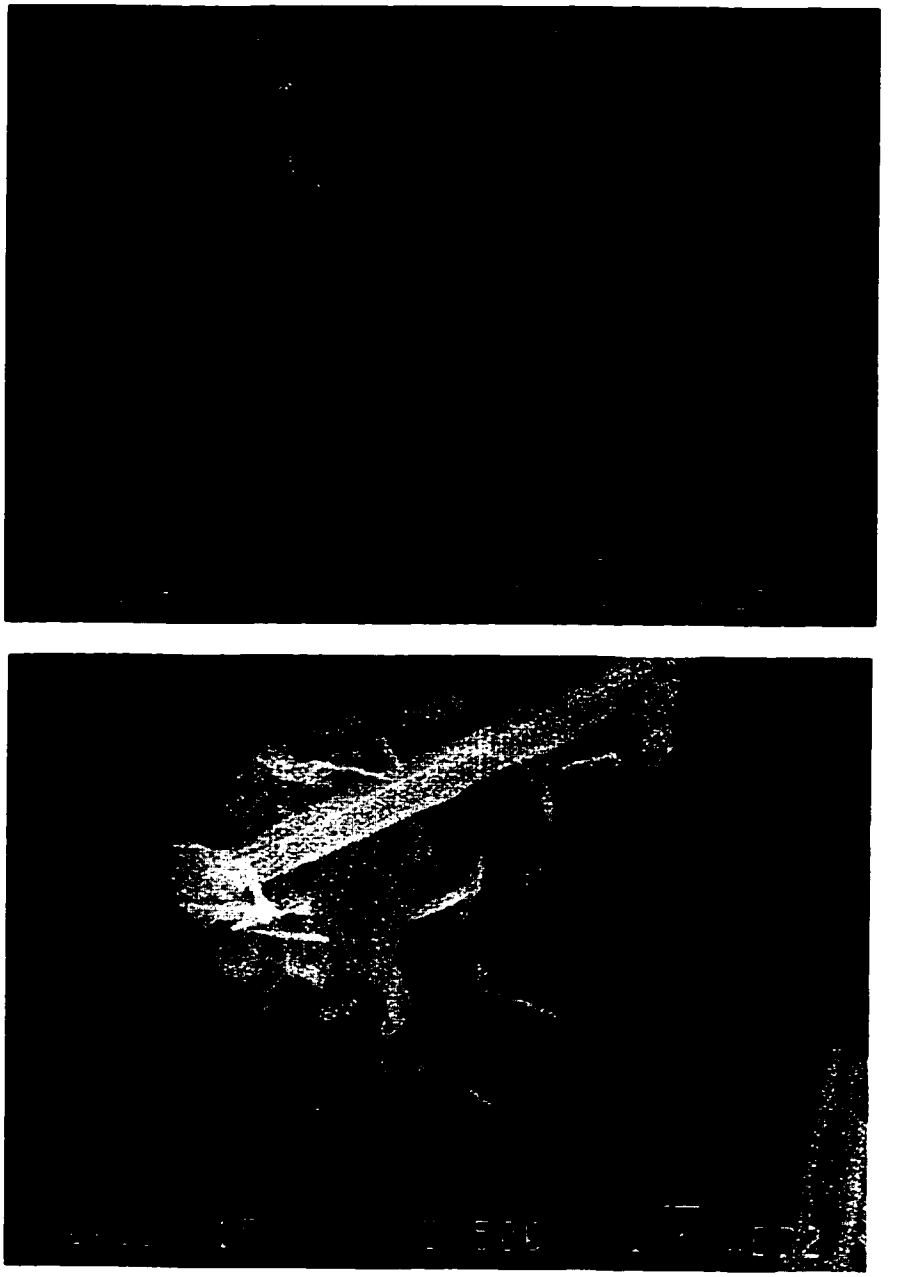

Figure 2.9: Micrographs of needle-like ettringite crystals from the lime-leached Atikokan fly ash. (A) after 7 days of reaction; (B) after 30 days of reaction.

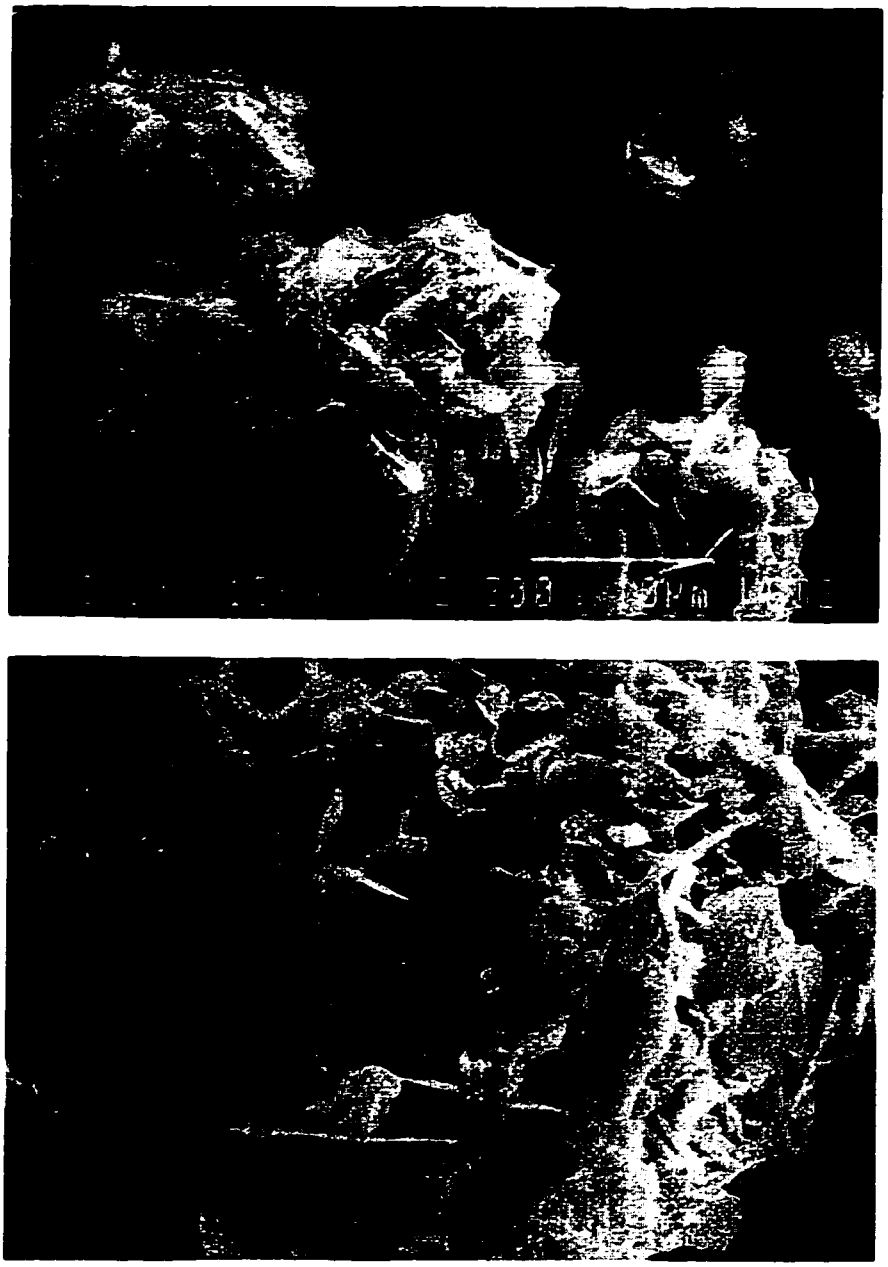

Figure 2.10: Micrographs of strätlingite rosettes from the lime-leached Atikokan fly ash after 30 days of reaction. (A) fly ash spheres and strätlingite rosettes; (B) a close-up of an aggregate, consisting of thin, platey strätlingite crystals..

2.3.3.2 The composition of secondary minerals

The major constituents of the leached fly ash spheres are Si, Al, and Fe in the Lakeview and Lambton samples. Ca and Ti were also detectable in the ash particles. The particles with an amorphous appearance are predominantly composed of Ca (> 85%), followed by Si (<10%). It is likely that these particles are a mixture of portlandite and CSH. In addition to Ca and Si, Al and Fe were also detectable. In both the Lakeview and Lambton samples, ettringite is predominantly composed of Ca, Al and Si (Figure 2.11A). Iron occurred as a minor constituent in the ettringite crystals. Similar to ettringite, the hydrocalumite crystals are also composed of Ca, Al and Si, with a detectable amount of Fe (Figure 2.11B). The content of Si in hydrocalumite decreased with time (Figure 2.11C). This corresponds to an increase in the crystallinity of the hydrocalumite crystals. In the Lambton samples, sulfur was also detected in some of the hydrocalumite crystals.

In the Atikokan samples, the leached ash particles consist mainly of Si, Al and Ca, followed by Na, Mg and Fe. The compositions of the ettringite crystals were similar to those found in the Lakeview and Lambton samples, and consisted of Ca, Al and Si (Figure 2.11D). The chemical composition of ettringite remained unchanged with reaction time (Figure 2.11E). The hexagonal platey crystals formed in the Atikokan fly ash showed a much higher Si content than those formed in Lakeview and Lambton ashes (Figure 2.11F). This is consistent with the XRD results, which identified these crystals as strätlingite.

2.3.4 Summary of ettringite and hydrocalumite formation

Ettringite was identified using XRD analysis in both the Lakeview and Lambton fly ashes, but was not shown or was only present at low relative intensities in the XRD patterns of the Atikokan samples. A large quantity of needle-like crystals, however, was observed in the Atikokan samples under the optical microscope and using SEM. EDX analysis of these needle-like crystals showed that their major constituents are Ca, Al and Si, similar to the ettringite formed in the Lakeview and Lambton ashes. On this basis, it is concluded that these needle-like crystals are ettringite. Ramachandran and Zhang (1986) also reported the absence of distinct ettringite peaks in samples where ettringite needles are evident. Further work is required to understand why ettringite was not detectable by XRD in the Atikokan samples. Between the Class F and Class C fly ashes, there were differences in the quantity of ettringite formed and in its persistence with continued reaction. Ettringite formed mainly at the early reaction stage in the Lakeview and Lambton (Class F) fly ashes and the maximum amount of ettringite did not exceed 10%. After 30 days of reaction, there was no ettringite left in the

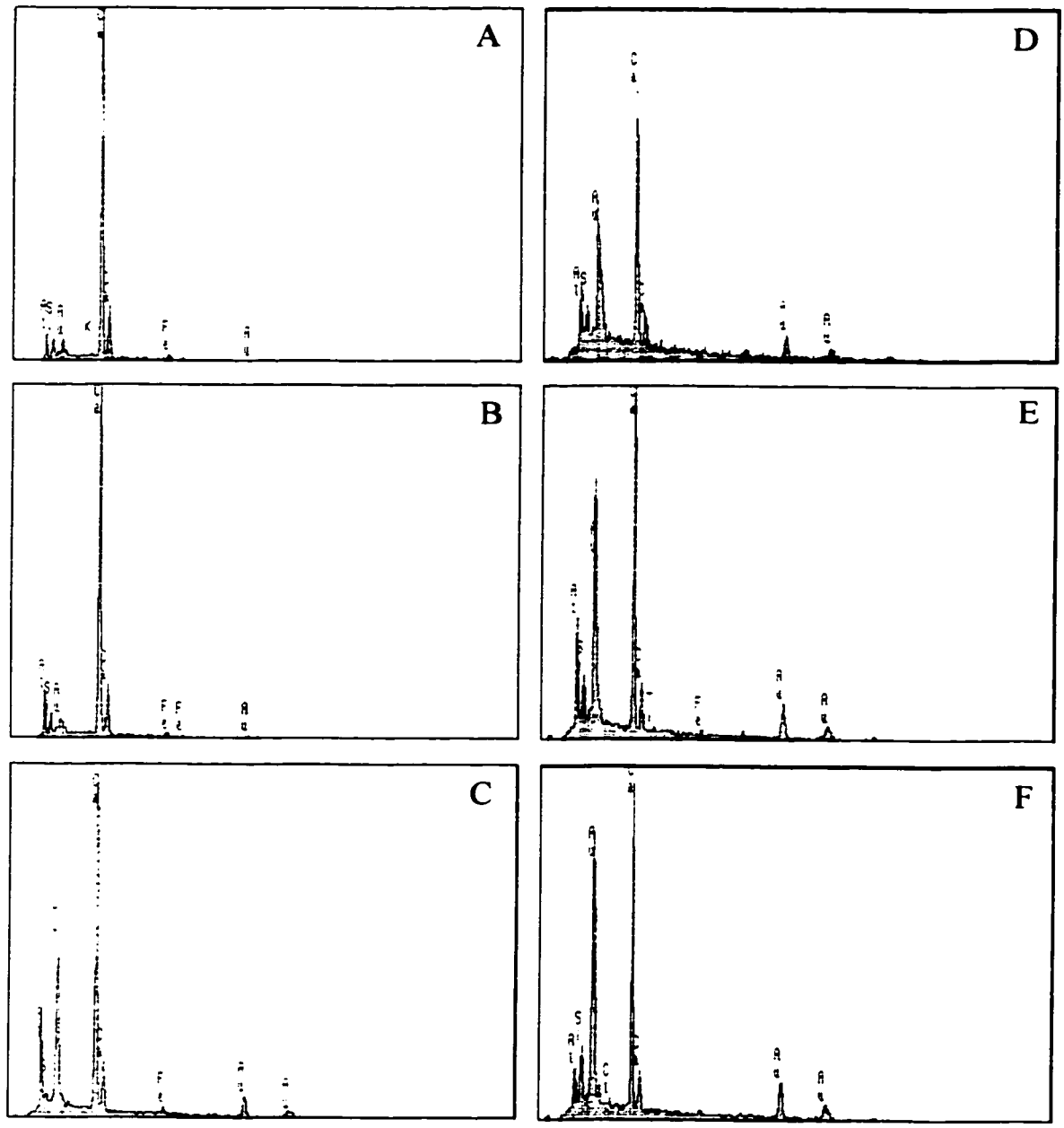

Figure 2.11 Energy dispersive analysis of ettringite and hydrocalumite formed in the lime-leached Lakeview (left column) and Atikokan (right column) fly ashes. (A) ettringite in the 3-d sample; (B) hydrocalumite in the 3-d sample; (C) hydrocalumite in the 30-d sample; (D) ettringite in the 7-d sample; (E) ettringite in the 30-d sample; (F) hydrocalumite in the 30-d sample.

Lambton fly ash and only a very small quantity was observed in the Lakeview fly ash. In contrast, the quantity of ettringite formed in the Atikokan (Class C) fly ash was much higher for the entire reaction period and the maximum amount reached approximately 30% of the total solids.

Hydrocalumite formed from Class F (Lakeview and Lambton) and Class C (Atikokan) fly ash showed differences in both morphology and composition. After 30 days of reaction, hydrocalumite was present as thick, well-crystallized hexagonal plates in both the Lakeview and Lambton fly ashes. Strätlingite (a hydrocalumite-like phase) formed in the Atikokan fly ash, however, occurred as aggregates of thin platey crystals. By the end of the reaction period, the hydrocalumite formed in the Lakeview fly ash appeared to be an OH-rich solid solution phase, whereas in the Lambton fly ash it likely occurred as two immiscible solid solutions: an OH-rich phase and a SO_4-rich phase. These solid solutions, however, were not distinct in the XRD pattern of the 30-d Atikokan samples. Instead, strätlingite peaks were present in the XRD pattern, and these crystals were seen as platey crystals using SEM. The low relative peak intensities of this phase in the XRD analysis, however, failed to reflect the large quantity of platey crystals actually present in the 30-d sample.

Table 2.1 summarizes the assemblages of calcium aluminate hydrates observed as a function of time. In this table, the relative amount of each phase is represented schematically.

2.4 Discussion

2.4.1 Leaching of fly ash

The amorphous glassy phase of the ash particles underwent substantial leaching during the course of the 30-day lime treatment. In both the Lakeview and Lambton (Class F) fly ashes, the amorphous crust of the spherical ash particles was removed and the inner mullite crystals were exposed (see Figure 2.8). In the Atikokan (Class C) fly ash, some of the original ash particles were completely decomposed and replaced by secondary mineral phases (see Figure 2.10). Crystalline phases such as quartz and mullite, however, were largely unattacked during 30 days of lime treatment. An analogue to fly ash leaching in high pH environments can be found in the reaction between fly ash and Portland cement. Hydration of Portland cement would also generate an alkaline solution with a pH over 13. In fly ash and cement pastes, Halse *et al.* (1984) observed that the glassy phase was heavily etched after 7 days of reaction and that the crystalline phases of the fly ash were inert in these reactions.

McCarthy *et al.* (1984) also pointed out that crystalline phases of fly ash did not participate in hydration reactions of cement.

Table 2.1: Secondary calcium aluminate hydrates in the lime-leached fly ashes. The numbers refer to the relative amount of each phase present.

Fly Ash	Reaction Period	Secondary Calcium Aluminate Hydrate				
		Ettringite	OH-rich hydrocalumite	SO_4-rich hydrocalumite	Strätlingite	Hydrogarnet
Lakeview	1 day	2	-	-	-	-
	3 days	3	1	-	-	-
	7 days	2	2	-	-	-
	14 days	2	3	-	-	-
	30 days	1	5	-	-	-
Lambton	1 day	2	-	-	-	-
	3 days	3	-	-	-	-
	7 days	2	2	-	-	-
	14 days	1	2	-	-	-
	30 days	-	3	3	-	1
Atikokan	1 day	2	-	-	-	-
	3 days	3	1	-	-	-
	7 days	5	1	-	-	-
	14 days	3	-	-	2	-
	30 days	2	-	-	5	1

The relative proportion of amorphous glass to crystalline phases appears to be the key factor that controls the extent of leaching of the fly ashes. Uchikawa (1986) also documented that the glass content tends to be the most important fly ash characteristic that influences reactivity. The size of the glass particles may also influence the extent of leaching. Small particles have a larger surface area, and small particles also contain lower quantities of crystalline phases (Hansen *et al.*, 1981; Vempati *et al.*, 1994). Hence, the chemical reactivity of fly ash will increase with decreasing particle size. It was observed that particles up to 1-2 μm in size were consumed by the hydration reaction of fly ash and cement within 28 days of reaction (Halse *et al.*, 1984). The chemical composition of the glassy material could also contribute to the degree of fly ash leaching. The reactivity of a glassy phase usually increases with its CaO content. In a lime solution, however, the CaO content of the glassy phase may have less influence on the reactivity.

The Atikokan fly ash showed more extensive alteration, with some of ash particles being completely replaced by the secondary phases. The XRD results (Figure 2.1) indicate that the Atikokan fly ash contains a lower quantity of the crystalline phases and more glassy phase than the other two ashes. In addition, the association of amorphous glass with crystalline minerals is different between these two types of fly ashes. The lack of crystalline phases inside the glass particles of the Atikokan fly ash may have allowed complete alteration and formation of aggregates of secondary phases, whereas the interlaced mullite in both Lakeview and Lambton limited the extent of reaction.

2.4.2 Coordination of Si in ettringite and hydrocalumite

Si was detected as a major constituent in the ettringite and hydrocalumite crystals produced in both the Class F and Class C fly ashes. The presence of Si in the structures of ettringite and hydrocalumite is, therefore, of significance in terms of ionic substitution. There are two possible positions for Si incorporation in the structures of ettringite and hydrocalumite. The radius ratio of Si^{4+} to O^{2-} (0.30) indicates that both four-fold (0.23) and six-fold (0.41) coordinations are possible. Being octahedrally coordinated, Si could substitute for Al in the main structural framework, i.e. (Ca, Al)-OH columns for ettringite and (Ca, Al)-OH sheets for hydrocalumite. The other possibility is that Si occurs as a tetrahedrally-coordinated anion residing in the interlayer positions of hydrocalumite or substituting for SO_4^{2-} in intercolumn positions in ettringite.

Si-bearing ettringite has been identified as a leaching product of fly ash and combusted oil shale (McCarthy and Solem-Tishmack, 1994; Essington, 1990). Regourd *et al*, (1976) reported the occurrence of this phase in the reaction of tricalcium silicate and tricalcium aluminate. Si-bearing ettringite was also synthesized by Flint and Wells (1944). The chemical formula of the Si-ettringite was expressed as $Ca_6Al_2(OH)_{12}(SiO_3)_3 \cdot 25H_2O$ by some authors (e.g. Flint and Wells, 1944; Regourd *et al*, 1976), in which Si was suggested to occur as SiO_3^{2-} and reside in the intercolumn of the ettringite structure. The coordination of Si, however, was determined in the structure of thaumasite (an ettringite-like phase). Edge and Taylor (1971) concluded that Si was six-fold coordinated and substituted for Al in the main structural columns of thaumasite. Taylor (1990) suggests that limited substitution of Si for Al probably occurs between ettringite ($Ca_6Al_2(OH)_{12}(SO_4)_3 \cdot 26H_2O$) and thaumasite ($Ca_6Si_2(OH)_{12}(SO_4)_2(CO_3)_2 \cdot 24H_2O$). The EDX results of this study indicate that Si-bearing ettringite formed in all three fly ashes. Based on the relative percentages of Si and Al, these phases are likely the solid solutions between ettringite and thaumasite with Si^{4+} partially

substituting for Al^{3+}. The XRD patterns obtained in this study, however, can not be used to resolve the difference between ettringite and thaumasite due to their identical principal peak positions (McCarthy and Solem-Tishmack, 1994) and due to the low intensities observed for the minor peaks. The partial substitution of Si^{4+} for Al^{3+} leads to the incorporation of more anions in the intercolumn positions to maintain charge balance in the mineral structure.

Previous studies suggested that Si occurred as the silicate anion and was present in the interlayer of the hydrocalumite structure (e.g. Flint and Wells, 1944; Van Aardt and Visser, 1981). By comparison to calcium monosulfate ($Ca_4Al_2(OH)_{12}(SO_4)\cdot 6H_2O$), Regourd *et al.* (1976) presented a formula of $Ca_4Al_2(OH)_{12}(SiO_3)\cdot 6H_2O$ for the Si-bearing hydrocalumite. SiO_3^{2-} was assumed to be the anion incorporated into the interlayer positions. No spectroscopic data, however, are available to support this assumption. Considering that $H_3SiO_4^-$ is the dominant species in the lime-leached fly ash at a pH value around 12.5, it is possible that $H_3SiO_4^-$ is directly incorporated into hydrocalumite. Similar to hydrocalumite, strätlingite also consists of positively-charged structural layers of $[Ca_2Al(OH)_6]^+$. Kuzel (1976) determined that Si was combined with Al to form the anion $AlSiO_3(OH)_2^-$ in the interlayer of strätlingite. Regardless of which silicate species is incorporated, the presence of Si in the interlayer positions of hydrocalumite and strätlingite will directly influence the incorporation of other anions that are competing with silicate or $AlSiO_3(OH)_2^-$.

2.4.3 Transformation of ettringite to hydrocalumite

Secondary ettringite and hydrocalumite formed extensively in the lime-leached fly ashes during the one-month reaction period. The formation of these phases can be divided into three stages: (1) formation of ettringite; (2) transformation of ettringite to hydrocalumite; and (3) coexistence of hydrocalumite and hydrogarnet. Ettringite was formed at the early stages of reaction. As leaching progressed, ettringite became unstable, and as the quantity of ettringite decreased, the amount of hydrocalumite increased. Transformation from ettringite to hydrocalumite is a common phenomenon in the hydration reaction of Portland cement (Taylor, 1990). In cement hydration, conversion of ettringite into monosulfate is usually related to the consumption of gypsum (e.g. Odler and Abdul-Maula, 1984; Singh *et al.*, 1990). The SO_4 concentration is described as a major factor controlling the stability of ettringite. The experimental observations demonstrated that ettringite was stable at high SO_4 concentrations and that the formation of the SO_4-bearing hydrocalumite (AFm phase in cement notation) was favored by low SO_4 concentrations (Gabrisová *et al.*, 1991). Based on modeling results, Höglund (1992) also predicts that ettringite may be transformed to hydrocalumite when the sulfate concentration in solution is reduced.

Two different mechanisms have been proposed to account for the transformation from ettringite to hydrocalumite. The first is a topochemical mechanism by which the decomposition of ettringite and formation of hydrocalumite occur in the solid state. Based on studies of Portland cement hydration, Taylor (1990) proposed a model to describe this transformation process. Initially, ettringite forms on the surface of C_3A ($3CaO \cdot Al_2O_3$) grains. It is suggested that hydrocalumite forms inside this ettringite rind by the reaction of C_3A with ettringite. Alternatively, the precipitation of hydrocalumite could occur by a through-solution mechanism, as a result of the dissolution of ettringite (Lea, 1970).

The temporal relationship between ettringite and hydrocalumite provides some information on the transformation mechanism. Shi (1996) observed that the diminishment of ettringite and the appearance of hydrocalumite occurred at the same time in a paste of fly ash and portlandite. Okushima *et al.* (1968) also showed that monosulfate appeared just when the amount of ettringite started to decrease. A transformation mechanism, however, can not be derived directly from this evidence. The spatial relationship between these two phases may be a more direct way to study the mechanism. However, direct observations of the transformation have not been made previously. Figures 2.3 E and F illustrate the transition point occurring in the conversion of ettringite to hydrocalumite. A solid-state conversion usually involves a replacement of original mineral by a new mineral, during which no morphological changes occur, such as in the case of magnetite to hematite conversion. However, a morphological change was observed from needle-like crystals of ettringite to hexagonal plates of hydrocalumite (Figure 2.3 F). Hydrocalumite appears to form from the outside of the ettringite aggregates. This association likely indicates a precipitation mechanism. The close relationship between these two phases, however, suggests that the formation of hydrocalumite was based on the consumption of ettringite. The presence of relict ettringite needles in the hydrocalumite crystals (Figure F and E) implies that solid-state mechanism may occur locally within the hydrocalumite crystals.

2.5 Conclusions

Substantial leaching of the glassy phase occurred when fly ash was reacted with lime and water. The primary crystalline minerals, such as quartz and mullite, were barely leached. Primary calcite, however, was dissolved in the lime solution. The extent of leaching depends largely on the relative quantity of amorphous glass to crystalline minerals. Other factors such as the particle size and the association between the glass and crystalline phases also influence the extent of alteration. Less leaching occurred with the Class F (Lakeview and Lambton) fly

ash, where there was a high percentage of crystalline quartz and mullite and where these phases were closely associated with the glassy phase. The Class C (Atikokan) fly ash, on the other hand, showed more extensive alteration. A higher percentage of the glassy phase was present in the ash, which was replaced by the secondary precipitates at the termination of 30-day reaction.

Secondary phases formed extensively during the 30-day lime-leaching process. Ettringite formed at the early reaction stage and reached a maximum value after 3 or 7 days. After 30 days of reaction, a small quantity of ettringite persisted in the Lakeview fly ash, whereas no ettringite was identified in the Lambton fly ash. Compared to these Class F fly ashes, the quantity of ettringite formed in the Class C fly ash was much higher. Hydrocalumite in the Class F fly ashes and strätlingite in Class C fly ash appeared at the time when the maximum amount of ettringite had formed. As the quantity of ettringite decreased, the amount of hydrocalumite or strätlingite increased. At the termination of reaction, there was more hydrocalumite or strätlingite than ettringite present. Hydrocalumite formed in the Class F fly ashes showed a euhedral hexagonal platey morphology. In the Class C fly ash, strätlingite occurred as rosettes, i.e. as aggregates of thin platey crystals.

High percentages of Si were measured in both ettringite and hydrocalumite. The needle-like crystals were determined to be solid solutions between ettringite and thaumasite. Sulfate and hydroxyl, and also carbonate in the case of Lakeview fly ash, are the main anions incorporated in these solid solution phases. Si occurs in six-fold coordination and substitutes for Al in the columns of the ettringite structure. Therefore, Si does not compete with other anions for the intercolumn positions. Moreover, the substitution of Si^{4+} for Al^{3+} in the main columns of ettringite results in the incorporation of more anions to balance the charge. In the hydrocalumite formed in the Lakeview and Lambton fly ashes, Si likely occurs in four-fold coordination as silicate anion and substitutes for hydroxyl in the interlayer of the structure. Substitution decreased with reaction time and with increased crystallinity of hydrocalumite. After 30 days of reaction, OH^- was the dominant anion in the hydrocalumite formed in the Lakeview fly ash. In the Lambton fly ash, hydrocalumite occurred as two immiscible solid solutions: an OH-rich phase and a SO_4-rich phase. The hexagonal platey crystals precipitated in the Atikokan fly ash had a high Si content. This phase is identified as strätlingite. $AlSiO_3(OH)_2^-$ is the anion present in the interlayer of the strätlingite structure. The presence of silicate anion in Si-hydrocalumite or $AlSiO_3(OH)_2^-$ in strätlingite would directly affect the incorporation of other anions into these phases.

It is the first time that direct visual evidence of the transformation from ettringite to hydrocalumite has been collected. The observation suggests that under the experimental

conditions, the transformation can be better described by a through solution mechanism. The close spatial relationship between these two phases, however, suggests that the formation of hydrocalumite is based on the consumption of ettringite. It appears that solid-state conversion from ettringite to hydrocalumite may also occur locally within a hydrocalumite crystal.

Chapter 3

Fly ash-Lime-Water Interaction: II. Temporal Change in Solution Composition

3.1 Introduction

A number of trace elements become enriched in fly ash during the coal combustion process. Some are concentrated principally on the surface of fly ash particles and are readily leachable. Trace elements, especially those that occur as anions, are often potential contaminants because they are relatively soluble in neutral to alkaline environments. Arsenic, boron, chromium, molybdenum, and selenium are the principal trace elements present at high concentrations in fly ash, and that also occur as oxyanions in leachates. For example, high concentrations of these trace elements were found in ash pond effluent (Dreesen *et al.*, 1977). High B concentrations were considered to be the limiting factor in the use of fly ash as a liming material for acidic soils (Warren, 1992), and the concentrations of Mo and Se in fly ash also greatly exceed their concentrations in soil (Page *et al.*, 1979).

Previous studies have demonstrated that arsenic is often enriched on the surfaces of ash particles. Surface forms of arsenic account for 65-100% and 50-80% of the total arsenic reported by Eary *et al.* (1990) and van der Sloot *et al.* (1985), respectively. Boron, as borate, is one of the most soluble trace elements in fly ash (Roy *et al.*, 1984). Ainsworth and Rai (1987) measured boron concentrations between 0.5 ppm and 82 ppm in hot water leachates at a w/s ratio of 20:1. In contrast, chromium was found to be mainly present in the trivalent cationic form and associated with ferric-rich compounds in fly ash which have low leachabilities (Hulett *et al.*, 1980; Furuya *et al.*, 1987; Polyák *et al.*, 1994). Molybdenum also shows a surface enrichment in fly ash, and is readily extractable in acid (Page *et al.*, 1979). Similar to arsenic, over 90% of selenium occurs on the surface of fly ash particles and is highly leachable by both water and acid (Eary *et al.*, 1990). In addition to these oxyanions,

high sulfate contents have been observed in fly ash, produced from the oxidation of iron sulfides in coal (Mattigod *et al.*, 1990). Sulfate is commonly the dominant anion in fly ash leachates.

Various mechanisms may be involved in the removal of sulfate and other oxyanionic trace elements from solution. Precipitation as individual mineral phases and incorporation into secondary mineral phases are the major mechanisms considered. For example, gypsum precipitates were identified in water-leached fly ash (Reardon *et al*, 1995). Amorphous iron and aluminum hydroxides are the main phases that adsorb the oxyanion forms of As, Cr, and Se from acid leachates of fly ash (Theis and Wirth, 1977; van der Hoek *et al.*, 1994). Ettringite and hydrocalumite, formed in alkaline leachates, are important host minerals for oxyanions released from fly ash (e.g. Hasset *et al*, 1989; Solem-Tishmack *et al.*, 1995; Reardon and Della-Valle, 1997; Duchesne and Reardon, 1999). Previous studies have shown that secondary ettringite and hydrocalumite have a substantial capacity to accommodate anions. This property is a function of their unique structures. Ettringite consists of positively-charged Ca-Al hydroxide columns, with sulfate and water molecules residing between these columns (Moore and Taylor, 1970). Sulfate in the ettringite structure can be replaced by other anions. Hydrocalumite is an anionic clay mineral that is composed of positively-charged portlandite-like layers. The positive charge is created by the substitution of one Al^{3+} for every two Ca^{2+}. Various anions can be incorporated into the interlayer to balance this charge (Taylor, 1973).

In this study, the formation of both ettringite and hydrocalumite was induced by adding lime to fly ash. Leaching studies of fly ash in lime solution have been conducted previously (e.g. Reardon and Della-Valle, 1997; Duchesne and Reardon, 1999). However, these authors did not document the change in solution chemistry with progressive leaching or characterize the development of secondary phases with reaction time. In Chapter 2, a systematic identification of the secondary phases with reaction time has been made. In this chapter, the solution composition is correlated to the development of the secondary phases, and the affinities of the trace elements for these phases are established.

3.2 Experimental

3.2.1 Materials

Three fly ash samples were obtained from Ontario Hydro's thermal generating stations and used in this study. Their bulk compositions were analyzed by XRAL

Laboratories and are summarized in Table 3.1. The Lakeview and Lambton fly ashes are Class F fly ashes (derived from bituminous coal), in which the sum of SiO_2 + Al_2O_3 + Fe_2O_3 is greater than 70%. The Atikokan fly ash is a Class C fly ash (derived from lignite), in which the sum of SiO_2 + Al_2O_3 + Fe_2O_3 is between 50% and 70%. The Atikokan fly ash contains 14% CaO, which is typical for Class C fly ashes (McCarthy *et al.*, 1990). Class F fly ashes, such as the Lakeview and Lambton ashes, have much lower percentages of CaO. In addition to high CaO, the Atikokan fly ash also contains high Na_2O and MgO. The K_2O content, however, is lower in this ash. Lee *et al.* (1986) also observed that Na contents of Class C ashes were higher than those of Class F, but that the opposite was true for K contents. All three fly ashes have similar sulfur contents. The Lakeview and Lambton fly ashes are dark gray in color, which is likely due to a higher percentage of unburned carbon. The presence of free carbon also contributes to the high *loss on ignition* (LOI) value. Atikokan fly ash is pale yellow, and has a low carbon content.

The concentrations of trace elements in the fly ashes are recorded in Table 3.2. Only the trace elements that typically form anionic species in water are listed. The Atikokan fly ash has an exceptionally high B concentration of 1470 ppm. The enrichment of B in the fly ashes derived from lignite was documented by Adriano *et al.* (1980). The Lakeview and Lambton fly ashes, however, are higher in As, Cr, Se, and V. Johnston and Eagleson (1989) reported 50 ppm Cl in both the Lakeview and Atikokan fly ashes.

3.2.2 Experimental design

The leaching of fly ash in lime solution was the major experiment carried out in this study, and a relatively long reaction time (30 days) was used. A fly ash - pure water leaching experiment was also conducted and the reactions were monitored over a short period of time (8 hours). A simple water-leaching experiment can provide information on whether an element occurs as a soluble phase or is associated with the glassy phase of the fly ashes. The solution composition data from the water-leaching system also serves as a baseline for interpreting the lime-leaching system results.

Although the major secondary phases formed in lime-leached fly ash have been described in Chapter 2, those that occur as amorphous phases or in low quantities may not have been identified. Additional information on the existence of a mineral phase, however, can be attained from the solution chemistry data. Reardon *et al.* (1995) recommended a simple procedure when conducting leaching tests to determine if the concentration of an element in the leachate is controlled by mineral solubility. Using the results of fly ash

leaching tests at two different water/ash ratios, these authors argue that if an element's concentration does not double when the water/ash ratio is halved, there must be a solid phase control on that element's concentration in solution. Therefore, two different water/ash ratios were used in this study. In accordance with the toxicity characteristic leaching procedure (TCLP), a water/ash ratio of 20:1 was used and an additional set of samples was prepared with a water/ash ratio of 40:1.

Table 3.1: Major element compositions of the fly ashes (mass%)

Fly Ash	SiO_2	Al_2O_3	CaO	MgO	Na_2O	K_2O	Fe_2O_3	MnO	TiO_2	P_2O_5	SO_3	LOI	Sum
Lakeview	41.5	22.3	3.09	0.70	0.49	1.61	11.5	0.02	1.07	0.36	1.07	17.5	101.0
Lambton	49.5	27.1	1.08	0.67	0.35	1.87	4.81	0.01	1.44	0.12	0.82	12.9	100.7
Atikokan	43.9	20.9	14.0	2.99	7.82	0.59	4.25	<0.01	0.99	0.56	1.15	0.15	98.3

Table 3.2: Trace element concentrations in the fly ashes (ppm)

Fly Ash	As	B	Cl	Cr	Mo	Se	V
Lakeview	75	383	50*	140	14	5	253
Lambton	36	70		130	7	21	281
Atikokan	26	1470	50*	62	9	3	118

* After Johnston and Eagleson (1989)

In the lime-leaching samples, 2 g of fly ash was added to 40 g of water for the samples with a water/ash ratio of 20:1. To the above mixture, 2 g of portlandite ($Ca(OH)_2$) was added as the source of lime. The same amount of water and half the mass of fly ash and portlandite were used in the samples prepared at a water/ash ratio of 40:1. In the water-leaching samples, the same quantities of fly ash and water were used with no addition of portlandite. Solution samples were taken after 1, 3, 7, 14, and 30 days of reaction in the lime-leaching experiment, whereas in the water-leaching experiment, solution samples were taken only after 1 and 8 hours of reaction. The details of the experimental procedure are described in Section 2.2.2.

3.2.3 Sampling and analyses

Solution samples were filtered through 0.45 μm cellulose acetate filter paper and split into three portions. The first aliquot of the solution was used for a pH measurement, which was made at the time of sampling. The second was diluted with water at a dilution factor of 1:4 for anion analysis, while the third was acidified with 1:1 HCl for cation analysis. The solution samples were stored in a refrigerator before use.

pH was measured using an Accumet pH meter coupled with a Ross® pH electrode. The electrode was calibrated against the buffer solutions of 4 and 7, or 7 and 9.18. Sulfate was analyzed using a Dionex AS3 Ion Chromatograph (IC). Arsenic and selenium were analyzed using a hydride-generating technique equipped with a Varian Atomic Absorption Spectrophotometer (AAS). The Mo concentrations were determined using the colorimetric method described by Savvin *et al.* (1980). The other elements were analyzed using a Jarrell-Ash Inductively Coupled Plasma Spectrophotometer (ICP). Analytical uncertainty for all techniques was better than ±5%.

3.3 Results

3.3.1 Solution composition

The solution compositions for the major elements are recorded in Tables 3.3 and 3.4 for the water/ash ratios of 20:1 and 40:1, respectively. The results from both the water-leaching and lime-leaching experiments are included in the same tables, but they will be summarized under the subsections entitled 'water-leaching system' and 'lime-leaching system', respectively. Potential solubility-controlling phases were predicted using the geo-chemical equilibria model SIMUL (Reardon 1990, 1992).

3.3.1.1 The water - leaching system

For each fly ash, the results of the water-leaching experiments are recorded in the first two rows (Tables 3.3 and 3.4). After 8 hours of reaction in water, Lakeview fly ash leachates were slightly alkaline and those of the Lambton fly ash were near neutral. The Atikokan leachates had a much higher pH value, approximately 11.8 after 8 hours. The glass matrix of the Atikokan fly ash may have been leached in the alkaline solution, whereas it is

probably inert at the near neutral pH values generated in the Lakeview and Lambton leachates.

Two common phenomena were observed for the Na and K solution concentrations in all three fly ashes: (1) the concentrations of Na and K are nearly constant with time during 8 hours of reaction; and (2) doubling the mass of fly ash relative to the mass of water doubled

Table 3.3: Concentrations of major ions in the fly ash leachates at a water/solid of 20:1 (ppm)

Fly Ash	Reaction	Time	Si	Al	Ca	Mg	Na	K	SO_4	pH
Lakeview	ash+water	1 hr	0.52	<0.2	193	1.63	5.29	2.73	372	7.66
"	ash+water	8 hr	1.03	0.38	191	2.04	5.85	3.36	338	8.40
"	ash+lime+water	1 d	0.43	<0.2	907	<0.01	17.2	16.3	16.1	12.63
"	ash+lime+water	3 d	0.33	<0.2	853	<0.01	20.6	27.5	2.33	12.64
"	ash+lime+water	7 d	0.53	0.41	815	<0.01	26.4	46.6	1.40	12.53
"	ash+lime+water	14 d	0.56	0.81	764	<0.01	48.7	124	1.03	12.60
"	ash+lime+water	30 d	0.33	1.58	661	<0.01	68.4	198	0.94	12.56
Lambton	ash+water	1 hr	1.65	0.27	105	5.56	10.0	16.2	264	6.24
"	ash+water	8 hr	1.72	<0.2	109	8.79	10.4	16.8	291	7.44
"	ash+lime+water	1 d	0.52	<0.2	922	<0.01	17.6	24.2	23.9	12.69
"	ash+lime+water	3 d	0.36	<0.2	848	<0.01	18.7	35.9	2.21	12.67
"	ash+lime+water	7 d	0.45	0.42	813	<0.01	20.7	57.7	1.14	12.64
"	ash+lime+water	14 d	0.53	0.83	751	<0.01	31.6	134	1.23	12.63
"	ash+lime+water	30 d	0.29	2.84	641	<0.01	40.5	195	0.82	12.59
Atikokan	ash+water	1 hr	1.26	39.6	226	<0.01	155	1.26	423	11.48
"	ash+water	8 hr	0.80	59.5	274	<0.01	172	1.46	473	11.80
"	ash+lime+water	1 d	0.44	<0.2	765	<0.01	257	6.02	23.5	12.62
"	ash+lime+water	3 d	0.64	<0.2	637	<0.01	343	12.2	5.44	12.69
"	ash+lime+water	7 d	0.91	1.54	514	<0.01	442	20.6	0.52	12.77
"	ash+lime+water	14 d	0.51	0.26	392	<0.01	570	30.0	0.69	12.75
"	ash+lime+water	30 d	0.46	0.99	262	<0.01	865	53.1	0.85	12.77

Table 3.4: Concentrations of major ions in the fly ash leachates at a water/solid of 40:1 (ppm)

Fly Ash	Reaction	Time	Si	Al	Ca	Mg	Na	K	SO_4	pH
Lakeview	ash+water	1 hr	0.43	<0.2	94.7	0.63	2.56	1.23	192	7.46
"	ash+water	8 hr	0.95	0.51	89.8	0.84	2.74	1.55	193	8.40
"	ash+lime+water	1 d	0.30	<0.2	957	<0.01	8.56	7.87	32.4	12.57
"	ash+lime+water	3 d	0.29	<0.2	874	<0.01	10.7	14.7	6.18	12.74
"	ash+lime+water	7 d	0.36	0.45	827	<0.01	14.8	25.9	1.07	12.67
"	ash+lime+water	14 d	0.73	<0.2	790	<0.01	24.2	59.7	1.33	12.66
"	ash+lime+water	30 d	0.23	1.08	730	<0.01	34.4	97.5	1.12	12.59
Lambton	ash+water	1 hr	1.02	<0.2	52.6	2.81	5.18	8.28	144	4.90
"	ash+water	8 hr	1.16	<0.2	53.8	4.23	5.06	8.16	149	5.51
"	ash+lime+water	1 d	0.20	<0.2	942	<0.01	8.29	11.9	28.7	12.53
"	ash+lime+water	3 d	0.48	<0.2	878	<0.01	9.18	18.3	1.38	12.74
"	ash+lime+water	7 d	0.38	0.44	833	<0.01	10.9	29.8	1.22	12.68
"	ash+lime+water	14 d	0.47	0.78	770	<0.01	16.8	68.3	1.25	12.66
"	ash+lime+water	30 d	0.15	2.62	705	<0.01	21.6	101	0.96	12.58
Atikokan	ash+water	1 hr	1.50	31.3	161	<0.01	78.9	0.52	251	11.34
"	ash+water	8 hr	0.98	42.8	202	<0.01	80.1	0.50	251	11.75
"	ash+lime+water	1 d	0.52	<0.2	849	<0.01	127	2.69	27.3	12.53
"	ash+lime+water	3 d	0.50	<0.2	358	<0.01	190	6.28	1.33	12.72
"	ash+lime+water	7 d	0.69	0.70	601	<0.01	255	11.9	1.01	12.64
"	ash+lime+water	14 d	0.48	5.05	554	<0.01	298	15.0	0.71	12.68
"	ash+lime+water	30 d	0.27	0.80	437	<0.01	472	27.3	0.80	12.65

the concentrations of Na and K in solution. These two observations indicate that a proportion of Na and K are enriched on the surface as readily soluble salts, which account for approximately 3, 8, and 6% of the total Na and 0.5, 2, and 0.6% of K in the Lakeview, Lambton and Atikokan fly ashes, respectively. The main portion of these elements, however, is associated with the less leachable glassy phase.

In both the Lakeview and Lambton leachates, calcium displayed the same doubling of concentration upon doubling the mass of fly ash as did Na and K. These results indicate

that a portion of Ca was in the form of readily soluble compounds and that no secondary mineral precipitate formed. Soluble calcium compounds account for 17% and 28% of the total Ca in the Lakeview and Lambton fly ashes, respectively. In contrast to the Lakeview and Lambton leachates, the Ca concentration in the high pH Atikokan leachates increased slightly during the water-leaching process. In addition to the dissolution of soluble compounds, some portion of the Ca may result from the leaching of glass at the high pH values generated in the Atikokan samples.

Generally, the SO_4 concentrations doubled when the water/ash ratio was halved within 8 hours of reaction. Based on the concentration of SO_4 at 40:1 water/ash ratio, approximately 60% of the total sulfur was readily dissolved from the Lakeview and Lambton ashes, whereas approximately 70% of the sulfur occurred as soluble phases in the Atikokan fly ash. Stinespring *et al.* (1985) determined that essentially all sulfur in fly ash was present as soluble sulfates. Sulfate was the dominant anion in all the leachates, which signifies that the soluble compounds of alkali and alkali earth metals occur mainly as sulfates. In the alkaline fly ash, Ca may also occur as CaO. Warren and Dudas (1984) suggested that the presence of submicron CaO particles contributed to the high pH values in alkaline fly ashes. Elseewi *et al.* (1980) also attributed the alkalinity of fly ash solutions to the dissolution of CaO.

The Si concentration in the Lakeview leachates increased with time during the 8-hour leaching process, whereas it remained essentially unchanged in the Lambton leachates. No doubling of Si concentration was shown upon doubling the mass of fly ash, implying that silicate mineral phases controlled its concentration. Atikokan leachates showed a decrease in the Si concentration with time, indicating a removal of Si from the solution. This is due to the precipitation of secondary silicates such as calcium silicate hydrates (CSH).

The Al concentrations were near or below detection in both Lakeview and Lambton leachates, in which amorphous $Al(OH)_3$ may control the Al concentrations. In contrast, the Al concentrations increased in the Atikokan leachates, with approximately 60 and 40 ppm Al measured after 8 hours for the water/ash ratios of 20:1 and 40:1, respectively. Although it is possible that ettringite precipitated in the alkaline Atikokan leachates, this process seems unlikely based on the fact that the SO_4 concentration increased with time.

In the Lakeview and Lambton leachates, the Mg concentration was twice as high in the samples with a water/ash ratio of 20:1 than in those with a 40:1 ratio, suggesting a lack of mineral solubility control. The concentration of Mg increased with time during the 8-hour water leaching process. A slowly dissolving phase apparently contributes to the Mg

concentration. Mattigod *et al.* (1990) suggested that periclase (MgO) might be the Mg-bearing compound in fly ash. In the Atikokan leachates, the concentrations of Mg were below detection (<0.01). Brucite ($Mg(OH)_2$) is insoluble at high pH and probably precipitated in these samples, removing Mg from solution.

3.3.1.2 The lime - leaching system

The results of the lime leaching experiments begin in the third row entry of Tables 3.3 and 3.4. For each fly ash, the pH of the leachates increased immediately to around 12.5 after addition of $Ca(OH)_2$. The pH values were slightly higher in the Atikokan leachates due to the higher alkali content of this fly ash.

In Figure 3.1, the saturation indices for portlandite, ettringite, monosulfate, hydrogarnet, and CSH are plotted vs. reaction time for the 20:1 samples. The leachates were slightly supersaturated with respect to portlandite initially, but the saturation index decreased with reaction time. After 30 days, the solutions were undersaturated with respect to this phase. Ettringite was highly supersaturated in the 1-d samples for all three fly ashes. Saturation with respect to ettringite was maintained in the Lakeview and Lambton samples throughout the reaction period. In the Atikokan fly ash, the leachates became undersaturated with respect to ettringite after 7 days. Supersaturation with respect to monosulfate was indicated in the 1-d samples, and an undersaturated condition was reached between 3 and 7 days. At later reaction times, saturation with respect to monosulfate was reached again in both the Lakeview and Lambton samples, but not in the Atikokan samples. The leachates were supersaturated with respect to hydrogarnet for all the fly ashes, and the saturation index showed an overall increase with time. Supersaturation with respect to CSH was also maintained throughout the entire reaction.

The results for all three fly ashes showed an abrupt increase in the concentrations of Na and K with the addition of lime. Combined with the results from the water-leaching experiments, this indicates that both Na and K are principally associated with the glassy phase. The association of these elements with the glassy matrix has also been documented previously (e.g. Hulett and Weinberger, 1980; Dudas, 1981). The abrupt increase in the concentrations of Na and K observed in this study reflects the aggressiveness of high pH solutions to the dissolution of aluminosilicate glass. After one day of reaction, the leached Na was 9.5 and 13.6% of the total Na in the Lakeview and Lambton fly ashes, respectively. In the Atikokan fly ash, 8.9% of the Na had been released into the leachates. During the same period, 3% of the total K was leached from these fly ashes, and both elements continued to

increase gradually with reaction time. After 30 days of reaction, the leached Na accounted for 37, 31, and 30% of the total Na in the Lakeview, Lambton and Atikokan leachates, respectively. Approximately 30, 25, and 22% of the total K had been released into the leachates of these three fly ashes.

In the lime-leaching system, an excess amount of portlandite was added and the leachates reached saturation with respect to this phase. The presence of portlandite was verified during the 30 days of lime-leaching process using XRD analysis (Chapter 2). The solution concentration of Ca decreased gradually with time for all three ashes. As the concentration of alkalis (Na and K) increased with time, the hydroxide concentration also increased. Therefore, if the Ca concentrations were controlled by portlandite solubility, they would decrease. At the termination of the reaction, the Ca concentration had dropped approximately 27, 30, and 66% in the 20:1 Lakeview, Lambton, and Atikokan samples, respectively. The decrease in the Ca concentration was less in the samples with a water/ash ratio of 40:1, where the concentrations of alkalis were lower. The saturation index of portlandite, however, also showed a gradual decrease with time for all three ashes (Figure 3.1). The observed undersaturation with respect to portlandite at the end of the reaction period must result from the formation of secondary phases, at a rate faster than portlandite is being dissolved.

Compared to the water-leaching samples, a substantial decrease in the SO_4 concentration occurred when lime was added. After one day of reaction, reductions of over 90% were measured, with only approximately 1% of the leached SO_4 remaining in solution after 3 days. The formation of secondary phases at early reaction times, such as ettringite, was likely responsible for the substantial removal of SO_4 from the leachates. Sulfate decreased slightly in both the Lakeview and Lambton samples with a further increase in reaction time. In the Atikokan leachates, a minimum SO_4 concentration was measured in the 7-d and 14-d samples for water/ash ratios of 20:1 and 40:1, respectively.

Both Si and Al showed similar concentration variations between the two water/ash ratios. Si concentrations remained relatively constant throughout the entire reaction, indicating that its concentration was controlled by a secondary mineral phase. CSH was likely the phase controlling the Si concentration. The concentration of Al was below detection for all three fly ashes at the early reaction times. A gradual increase in the Al concentration was observed as leaching continued. In the Atikokan leachates, the Al concentration reached a maximum after 7 and 14 days in the sample series of 20:1 and 40:1, respectively.

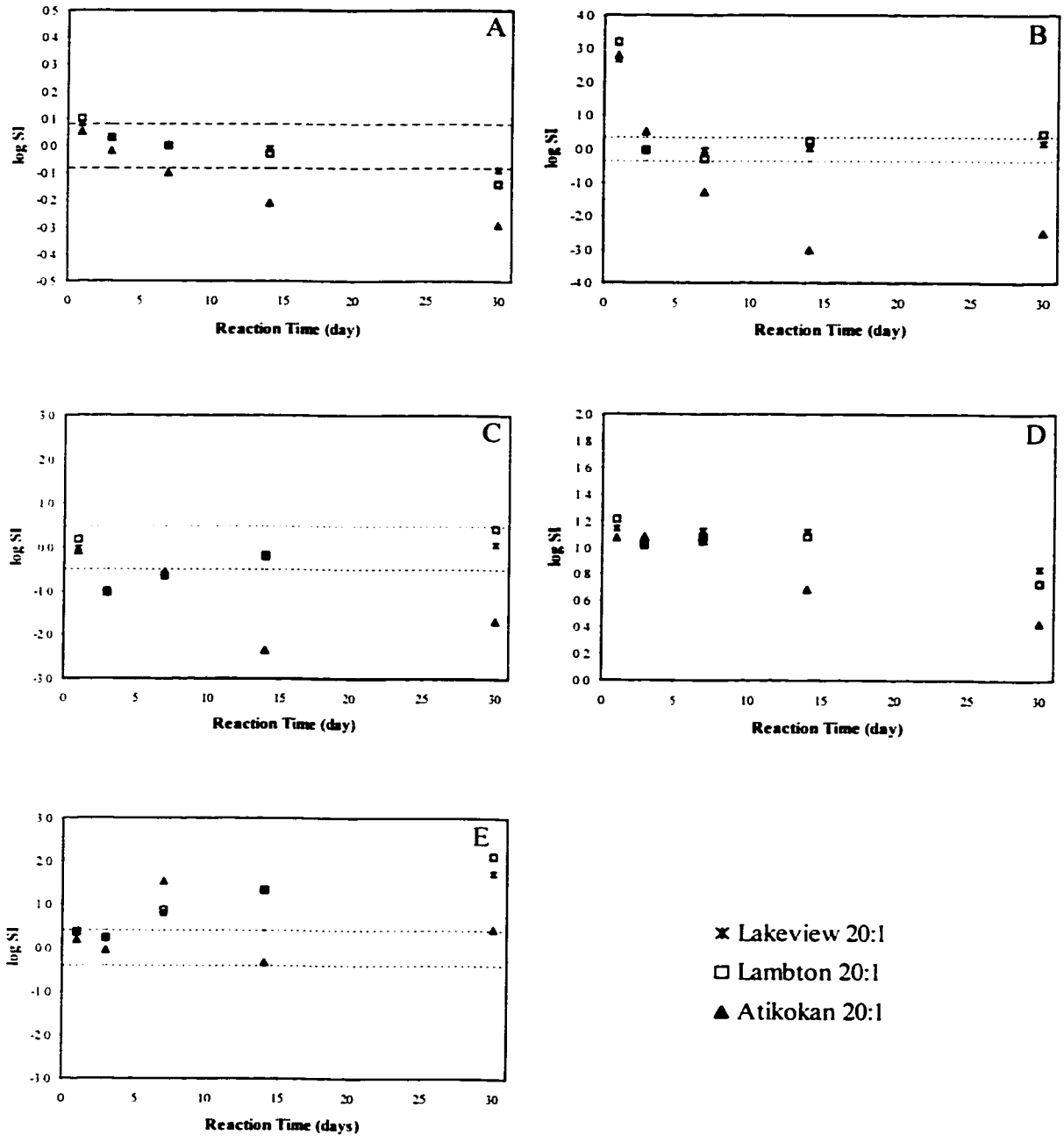

Figure 3.1:Saturation index vs. leaching time. (A) portlandite; (B) ettringite; (C) monosulfate; (D) CSH; (E) hydrogarnet. The dashed lines indicate the upper and lower uncertainty limits.

3.3.2 Trace elements

The concentrations of As, B, Cl, Cr, Mo, Se, and V were determined in the leachates for both the water-leaching and lime-leaching systems, and the results are recorded in Tables 3.5 and 3.6 for the water/ash ratio of 20:1 and 40:1, respectively. The concentrations of both Cr and V were below detection (<0.05 and <0.2 ppm, respectively) in all samples.

Table 3.5: Trace element concentration in the fly ash leachates at a water/solid of 20:1

Fly Ash	Reaction	Time	As (ppb)	B (ppm)	Cl (ppm)	Mo (ppm)	Se (ppb)
Lakeview	ash+water	1 hr	53	2.97	3.74	0.25	38
"	ash+water	8 hr	-	3.96	2.75	0.27	-
"	ash+lime+water	1 d	<20	<0.02	8.53	0.15	<20
"	ash+lime+water	3 d	<20	<0.02	8.98	0.10	<20
"	ash+lime+water	7 d	<20	<0.02	7.05	0.11	<20
"	ash+lime+water	14 d	<20	<0.02	3.26	0.09	<20
"	ash+lime+water	30 d	<20	<0.02	<2.0	<0.08	<20
Lambton	ash+water	1 hr	<20	1.70	2.71	<0.08	30
"	ash+water	8 hr	<20	1.77	3.08	0.21	51
"	ash+lime+water	1 d	<20	<0.02	8.04	0.29	<20
"	ash+lime+water	3 d	<20	<0.02	5.07	0.17	<20
"	ash+lime+water	7 d	<20	<0.02	4.42	0.15	<20
"	ash+lime+water	14 d	<20	<0.02	3.95	0.13	<20
"	ash+lime+water	30 d	<20	<0.02	2.57	<0.08	<20
Atikokan	ash+water	1 hr	<20	9.52	3.34	0.25	304
"	ash+water	8 hr	<20	12.7	3.93	0.26	392
"	ash+lime+water	1 d	<20	13.8	10.2	0.15	<20
"	ash+lime+water	3 d	<20	8.44	3.66	<0.08	<20
"	ash+lime+water	7 d	<20	0.26	2.26	<0.08	<20
"	ash+lime+water	14 d	<20	3.59	3.73	<0.08	<20
"	ash+lime+water	30 d	<20	6.01	4.16	<0.08	<20

Table 3.6: Trace element concentration in the fly ash leachates at a water/solid of 40:1

Fly ash	Reaction	Time	As (ppb)	B (ppm)	Cl (ppm)	Mo (ppm)	Se (ppb)
Lakeview	ash+water	1 hr	49	1.53	<2.0	0.13	28
"	ash+water	8 hr	73	1.94	2.22	0.14	37
"	ash+lime+water	1 d	<20	<0.02	4.16	0.12	<20
"	ash+lime+water	3 d	<20	<0.02	6.50	0.10	<20
"	ash+lime+water	7 d	<20	<0.02	3.37	0.09	<20
"	ash+lime+water	14 d	<20	<0.02	2.49	0.09	<20
"	ash+lime+water	30 d	<20	<0.02	<2.0	<0.08	<20
Lambton	ash+water	1 hr	<20	0.91	<2.0	<0.08	20
"	ash+water	8 hr	<20	0.95	<2.0	0.12	-
"	ash+lime+water	1 d	<20	<0.02	5.50	0.15	<20
"	ash+lime+water	3 d	<20	<0.02	4.34	0.13	<20
"	ash+lime+water	7 d	<20	<0.02	2.52	0.11	<20
"	ash+lime+water	14 d	<20	<0.02	2.27	0.11	<20
"	ash+lime+water	30 d	<20	<0.02	2.05	<0.08	<20
Atikokan	ash+water	1 hr	<20	6.99	2.42	0.15	96
"	ash+water	8 hr	<20	8.22	3.74	0.15	161
"	ash+lime+water	1 d	<20	8.51	4.35	<0.08	<20
"	ash+lime+water	3 d	<20	2.84	3.69	<0.08	<20
"	ash+lime+water	7 d	<20	<0.02	2.19	<0.08	<20
"	ash+lime+water	14 d	<20	1.34	2.09	<0.08	<20
"	ash+lime+water	30 d	<20	1.26	2.12	<0.08	<20

In the water-leaching system, only the Lakeview leachates showed measurable arsenic concentrations. Less than 3% of the total As was leached during 8 hours of reaction. In the same period, less than 10 and 30% of the total Se was released from the Lakeview and Lambton ashes, respectively. The low leachability of As and Se by water indicates either that these elements are closely associated with the glassy phase, or that removal of these elements from solution occurred by precipitation or coprecipitation. Previous studies, however, have

found that over 50% of the arsenic and 90% of the selenium in fly ash are enriched on the surface and are readily leachable (van der Sloot *et al.*, 1985; Eary *et al.*, 1990).

During the 8-hour water leaching, approximately 20% and 50% of the total B were leached from the Lakeview and Lambton fly ashes, respectively. The B concentrations doubled as the water/solid ratio was halved, implying that a portion of the B was present as a soluble phase and that no secondary precipitate formed. The highest B concentrations were measured in the leachates of the Atikokan fly ash, which has the highest B content. In the Atikokan leachates, the B concentration increased with time and was not doubled when the mass of solid was doubled relative to the mass of water. Only 17% of the total B in the fly ash was leached after 8 hours of reaction, indicating that the majority of the B is associated with the glassy phase. Elseewi *et al.* (1980) also suggested that B could be held in boro-silicate type phases.

Similar to B, the Cl concentrations were relatively constant in both the Lakeview and Lambton leachates during the water leaching process. However, the concentration of Cl increased with time in the Atikokan leachates. The leached Cl was found to be over 100% of the total Cl in the Lakeview and Atikokan fly ashes, when the Cl contents cited from Johnston and Eagleson (1989) are used. This is probably due to heterogeneities in the Cl concentrations of the fly ashes.

The Mo concentrations doubled in the leachates of all the fly ashes when the mass of ash was doubled, indicating no solubility control during water leaching. Soluble Mo accounted for approximately 40, 80 and 60% of the total Mo in the Lakeview, Lambton and Atikokan fly ashes, respectively.

After the addition of lime, further releases of the trace elements must have occurred, especially for elements such as B, which are predominantly associated with the glassy phase. The concentrations of these trace elements, however, showed an overall reduction with the addition of lime. Arsenic and selenium were reduced to below detection in all samples. The B concentrations also dropped below detection in the Lakeview and Lambton leachates. In the lime-leached Atikokan samples, an initial increase in the B concentration was observed. This increase is likely caused by the release of more B from the glassy phase of the fly ash upon lime addition. With increasing reaction times, the B concentrations decreased systematically for both water/ash ratios. The B concentration reached a minimum after 7 days of reaction. Compared to the water-leaching system, an increase of over 200% in the Cl concentrations were measured in the 1-d samples for all three fly ashes. These increases in the Cl concentrations are likely due to the dissolution of trace chloride impurities from the added

portlandite. After addition of lime, Cl concentrations gradually decreased as the reaction proceeded, with the Atikokan series showing a more rapid decrease. Similar to boron, a minimum Cl concentration was observed in the 20:1 sample after 7 days of reaction. During lime leaching, Mo concentration gradually decreased with time in the Lakeview and Lambton samples, whereas in the Atikokan leachates, its concentration was brought below detection after 1 day of reaction.

3.4 Discussion

3.4.1 Evolution of solution composition in the lime-leaching system

The fly ashes reacted in lime solution were characterized in Chapter 2. During the 30 days of reaction, the glassy phase of the ash particles underwent substantial leaching. Primary crystalline minerals such as quartz and mullite, however, are relatively stable in lime solution. This was evident from SEM and by their constant XRD peak intensities with reaction time. Extensive secondary mineral phases were formed during the leaching process. Ettringite was identified in the 1-d sample and reached a maximum amount after 3 or 7 days. With further leaching, ettringite transformed to hydrocalumite. After 30 days of reaction, hydrocalumite was the dominant calcium aluminate hydrate in the Lakeview and Lambton (Class F) fly ashes. In the Atikokan (Class C) fly ash, strätlingite (a Si-bearing hydrocalumite-like phase) was dominant. Hydrogarnet was also identified in both the Lambton and Atikokan fly ashes at the end of the reaction period. CSH likely formed throughout the entire leaching period.

The percentage of Na and K leached was used as a measure of the extent of glass leaching (Reardon and Della-Valle, 1997), because Na and K are closely associated with the glassy phase and behave conservatively. In this study, the leached Na accounts for 34, 23, and 24% of the total Na associated with the glassy phase of the Lakeview, Lambton and Atikokan fly ashes, respectively. The agreement between the leached Na and K were generally good. Approximately 29, 23, and 21% of the total K associated with glassy phase were leached from the Lakeview, Lambton and Atikokan fly ashes, respectively. The characterization of the solid phase, however, indicates that the most extensive leaching occurred in the Atikokan fly ash (Chapter 2). The difference between the observed leaching extent and the calculated results using Na and K concentrations may be due to heterogeneous distribution of these alkalis in fly ash particles.

The overall solution composition reflects a dynamic state between the flux of ions into solution from leaching of the glassy phase, and the flux of ions out of solution as they are

precipitated in secondary phases. Si is the major constituent of the glassy phase, and therefore leaching of glass would liberate a large quantity of Si. According to Carles-Gibergues and Aitcin (1986), CSH is the major sink for Si leached from the glassy phase. Geochemical equilibria modeling also indicates that CSH is a potential solubility controlling phase for Si. In addition to CSH, Si was detected in both the ettringite and hydrocalumite phases in the Lakeview and Lambton fly ashes (Chapter 2). In the Atikokan fly ash, ettringite and strätlingite appears to be a major host mineral for Si.

As one of the major constituents of the glassy phase, a large quantity of Al was released during the lime leaching process. High Al concentrations, however, were not measured in any of the solution samples. Compared to the water-leaching system, a sharp decrease in the Al concentration was observed with the addition of lime. These observations indicate that Al-bearing phases precipitated during lime leaching. The major Al-bearing phases identified were ettringite, hydrocalumite, and hydrogarnet. These phases are all calcium aluminate hydrates, and likely control the Al concentration at different reaction times. Ettringite formation was responsible for the initial drop in the concentrations of Al. As the reaction continued, ettringite was transformed to hydrocalumite. The Al concentrations were then controlled by hydrocalumite. In the case of the Atikokan fly ash, strätlingite was the main phase controlling the Al concentrations.

3.4.2 Relationship between anions and secondary phases

The extent of incorporation of trace elements in a solid phase depends on the aqueous speciation of the particular valence states that are present. Although the predominant form of arsenic in fly ash is As_2O_3, As (III) is hydrolyzed and oxidized to As (V) on contact with water (van der Sloot *et al.*, 1985). van der Hoek and Comans (1994) also determined that arsenate was the most important species in fly ash leachates. Under alkaline conditions, boron, chromium and molybdenum are mainly present as $B(OH)_4^-$, CrO_4^{2-} and MoO_4^{2-}, respectively (Eary *et al.*, 1990; van der Sloot *et al.*, 1985). In addition, the hydrolysis species of Cr (III) were also determined as the major soluble forms in ash pond leachate (Theis and Richter, 1979). Selenite (SeO_3^{2-}) was found to be dominant over selenate (SeO_4^{2-}) in fly ash leachate (Niss *et al.*, 1993; van der Hoek and Comans, 1994).

Precipitation of insoluble calcium salts is a potential mechanism for the removal of the trace elements in the lime-leaching system. Geochemical modeling, however, predicts that the leachates were undersaturated with respect to calcium salts of all the trace elements except for tetracalcium arsenate ($Ca_3(AsO_4)_2 \cdot Ca(OH)_2 \cdot 4H_2O$) (Kelleher, 1994). This phase

likely controlled the arsenic concentration. During lime leaching, the primary minerals in fly ash (e.g. mullite) may absorb some anionic trace elements, but the extent of incorporation is small (van der Hoek *et al.*, 1994). van der Hoek *et al.* (1994) also show that arsenic and selenium leached from fly ash are likely adsorbed onto hydrous iron oxides. However, this mechanism is only effective in acidic solutions. Of the secondary phases identified in the lime-leaching system, hydrogarnet is not likely a host mineral for anions based on structural considerations. Although incorporation of SO_4^{2-} into CSH has been documented (Gougar *et al.*, 1996), sulfate is more favored by the structure of ettringite. Therefore, from a structural point of view, ettringite and hydrocalumite (also strätlingite) are likely the most important host minerals for anions.

At early reaction times with lime, ettringite was the major secondary phase formed in all three fly ashes. Energy dispersive X-ray analyses showed that the ettringite crystals contain a substantial amount of Si (Chapter 2). The substitution of Si^{4+} for Al^{3+} in the ettringite structure requires more anions to balance the charge. A marked decrease in the SO_4 concentrations was measured after one day of reaction (Table 3.3), concurrent with the formation of ettringite. In reacted fly ashes, a correlation between decreasing sulfate concentrations and ettringite formation was also reported by Carles-Gibergues and Aitcin (1986) and Lecuyer *et al.* (1996).

Other oxyanionic trace elements can also be incorporated in ettringite, in addition to sulfate. A close relationship has been demonstrated between the formation of ettringite and reductions in B, Cr, and Se concentrations (Kumarathasan *et al.*, 1990; Solem-Tishmack *et al.*, 1995; Lecuyer *et al.*, 1996). In this study, the B concentrations dropped to below detection in lime-leached Lakeview and Lambton fly ashes after one day of reaction (Table 3.4). This corresponds to the appearance of ettringite, suggesting that borate is incorporated into the ettringite structure. The Se concentrations also decreased to below detection as ettringite formed. Considering the chemical similarities between selenate and sulfate, selenate likely substituted for sulfate in the ettringite structure. A small decrease in the Mo concentration was also measured with time in the Lakeview and Lambton leachates. This small change in the Mo concentrations is probably an indication that molybdate is not preferred by ettringite compared to borate and selenate. The concentration of Mo was reduced more quickly in the Atikokan leachates, probably due to the formation of larger quantities of ettringite with this fly ash.

When ettringite transforms to hydrocalumite, the incorporated anions are liberated to solution, and then likely accommodated in the structure of hydrocalumite as it precipitates. Hydrocalumite can incorporate anions that were previously held in ettringite, as well as those

released from the glassy phase with progressive leaching. The formation of hydrocalumite further reduced the concentrations of these anions in both the Lakeview and Lambton fly ashes. This further reduction implies that incorporation into hydrocalumite can lead to lower residual solution concentrations. The hydrocalumite formed in the Lakeview fly ash was a solid solution between the OH endmember and the SO_4 endmember, in which silicate and carbonate were also present (Chapter 2). Two immiscible OH-rich and SO_4-rich solid solutions formed in the Lambton fly ash. Silicate was also present in these hydrocalumite phases. Borate, molybdate and selenate competed with these major anions for interlayer positions in the hydrocalumite structure, and their low concentrations indicate the high affinity of these oxyanions for hydrocalumite.

The behavior of the Atikokan fly ash with lime leaching demonstrated a unique behavior in the change of the anion concentrations. Minimum concentrations of borate, sulfate, and chloride were observed in the 7-d sample at the water/ash ratio of 20:1. From XRD evidence, this is coincident with the maximum amount of ettringite formed. The increase in their solution concentration at later times could be a result of the transformation from ettringite to strätlingite. Strätlingite consists of positively-charged $[Ca_2Al(OH)_6]^+$ main structural sheets as does hydrocalumite. The major anion residing in the interlayer, however, is $[AlSiO_3(OH)]^-$ (Kuzel, 1976). Sulfate and other oxyanions must compete with $[AlSiO_3(OH)]^-$ for interlayer positions. Incorporation of borate and chloride into strätlingite appears to result in higher residual solution concentrations, which probably indicates that these anions are not favored by strätlingite. For borate, there may be an alternative explanation: that the amount of B released from the glassy phase is too large to be completely incorporated into strätlingite. Considering the large quantity of this phase formed in the late stage of the reaction, the second explanation seems less likely. Instead, if the minimum B concentration is related to the transformation from ettringite to strätlingite, ettringite appears to be able to incorporate more B into its structure.

3.5 Conclusions

Substantial leaching occurred when fly ash was reacted with lime and water. On the basis of the change in the concentrations of Na and K, leaching of the glassy phase was estimated to be 20 to 30% during the 30 days of reaction. However, from visual observations, the extent of leaching seems to be underestimated, especially for the Atikokan fly ash. Silica, the major constituent of fly ash, was leached from the glassy phase and removed by the precipitation of calcium silicate hydrates (CSH). Other secondary mineral phases, such as ettringite and hydrocalumite, were also found to accommodate Si. In the Atikokan fly ash,

strätlingite is an important host for Si. Aluminum, another major constituent of the glassy phase, was incorporated into the secondary calcium aluminate hydrates including ettringite, hydrocalumite, and hydrogarnet. The formation of ettringite was responsible for the initial reduction in the Al concentration, whereas hydrocalumite or strätlingite was likely the phase controlling Al concentrations at later reaction times. Calcium, contributed to the solution from either the dissolution of portlandite or the leaching of fly ash, was consumed by formation of secondary phases. Undersaturation with respect to portlandite at later reaction times indicates that the formation of the secondary phases was faster than the dissolution of portlandite.

Trace elements occurring as anions were removed from solution by incorporation into the secondary precipitates. At early reaction times, sulfate is the major anion accommodated in the structure of ettringite, but other anions are also taken up by ettringite. Borate seems to be preferred by ettringite, whereas molybdate is not preferred. The transformation from ettringite to hydrocalumite occurred after a few days of lime leaching. At the late reaction times, incorporation in hydrocalumite controlled the concentrations of the anionic trace elements in the leachates. Further reduction in the concentrations of the anions implies that incorporation in hydrocalumite could lead to lower residual solution concentrations than in ettringite. In the case of the Atikokan fly ash, a minimum in the concentration of B occurred after 7 days of reaction, which was coincident with the maximum formation of ettringite. The further release of B to solution is likely related to the transformation of ettringite to strätlingite, indicating that ettringite is a better candidate for incorporating B than strätlingite.

The results from this study further demonstrate that the addition of lime to fly ash is an effective technique to reduce the concentration of undesirable trace elements in solution. High pH environments promote the precipitation of ettringite and hydrocalumite phases, which incorporate anionic trace elements in their structures. However, it is also noted that some trace elements were released to solution during the transformation from ettringite to strätlingite. The possibility of trace element release after stabilization within a waste form is of major concern and an understanding of the physicochemical conditions that promote the transformation of ettringite to strätlingite is needed.

Chapter 4

Uptake of B, Cr, Mo, and Se by Hydrocalumite and Ettringite

4.1 Introduction

B, Cr, Mo, and Se are often enriched in solid wastes such as fly ash and spent oil shale and occur in high concentrations in their leachates. These elements are usually present as oxyanions in natural waters and are mobile at near neutral to alkaline pH values in hydrogeological environments. The solubilities of the common alkali and alkali earth salts of these anions are usually high. Their attenuation by other geochemical processes, e.g. sorption, is typically low due to the repulsion by negatively charged soil and sediment particle surfaces. Because of their high solubilities and mobilities in the environment, mechanisms for removing these oxyanions from wastewaters are of great importance.

Research on removal mechanisms for oxyanions has been focused on adsorption or coprecipitation with ferric oxides and hydroxides (e.g. Fendorf *et al.*, 1997; Bibak and Borggaard, 1994; Balistrieri and Chao, 1990). Incorporation of oxyanions into these solid phases is not only an important natural attenuation process, but also a potential technique for scavenging them from wastewaters (e.g. LeGendre and Runnells, 1975). The efficiency of incorporation, however, is greatly reduced in alkaline environments. In this study, we investigate two mineral phases: ettringite ($Ca_6Al_2(OH)_{12}(SO_4)_3 \cdot 26H_2O$) and hydrocalumite ($Ca_4Al_2(OH)_{12}(OH)_2 \cdot 6H_2O$), which are capable of removing anions from solution at high pH and can be induced to precipitate *in situ* from solid waste materials.

Although ettringite and hydrocalumite are not common naturally-occurring minerals, they are often precipitated during the hydration of solid wastes generated from the burning of fossil fuels. These phases were shown to develop as a result of fly ash-lime water interaction (Chapter 2). Ettringite is also commonly identified during the leaching of alkaline fly ash and gasification ash (Zhou and Dayal, 1990; Hassett *et al.*, 1989) and in leached spent oil shale (Essington, 1990). Kumarathasan and McCarthy (1987) observed that ettringite was replaced by hydrocalumite in an alkaline fly ash under leaching conditions.

In Chapter 2, the decrease in the anion concentrations of the fly ash leachates was correlated to the formation of both ettringite and hydrocalumite. This correlation has been observed by several authors. Hassett *et al.* (1989) suggested that the formation of ettringite was responsible for the concentration decrease of the oxyanion forms of As, B, Cr, Mo, Se, and V in fly ash leachates. Reardon and Della-Valle (1997) showed that the concentrations of B, Cl, Mo, and SO_4 decreased markedly in a long-term leaching experiment of lime-treated fly ash. Hydrocalumite, the most common secondary phase identified in the leached fly ash, was thought to be the host mineral for these anions. Both phases are also major hydration products of ordinary Portland cement (Taylor, 1990), therefore, there is considerable potential to stabilize undesirable anions in cement matrices.

This study examines the uptake behavior of borate, chromate, molybdate, and selenate in the pure ettringite-water and hydrocalumite-water systems in order to clarify the relationship between the decrease in anion concentrations and the precipitation of these phases observed in Chapter 2. The preferences of both ettringite and hydrocalumite for these oxyanions are also determined.

4.2 Experimental

4.2.1 Materials

All commercial chemicals used in this study were reagent grade. Solutions were prepared using Nanopure, double-deionized water with a conductance of 0.1 μS/cm. Monocalcium aluminate ($CaAl_2O_4$) was prepared by combusting a solution of calcium nitrate, aluminum nitrate, and urea at 500 °C for 5 minutes (Kingsley *et al.*, 1990). Prepared batches were routinely analyzed by X-ray diffraction (XRD) analysis to ensure purity. The solutions of B, Cr, Mo and Se used in both the uptake and control experiments were prepared from B_2O_3, K_2CrO_4, Na_2MoO_4 and Na_2SeO_4 compounds.

4.2.2 Experimental design

The uptake of B, Cr, Mo, and Se by hydrocalumite was studied by directly precipitating hydrocalumite from a solution containing low concentrations of the oxyanions of these elements. A stock solution containing approximately 10 ppm of each trace element was used in virtually all the uptake samples. Early results indicated that borate was least preferred by hydrocalumite, and therefore an additional sample was prepared using a 10 ppm B solution to determine if competition with other ions was responsible for the low B uptake.

Samples of hydrocalumite were prepared using a technique modified from Buttler *et al.* (1959). Hydrocalumite was precipitated by adding 7.0 mmoles of portlandite ($Ca(OH)_2$) and 1.6 mmoles of $CaAl_2O_4$ to 40 ml of stock solution. The resulting reaction is described by:

$$3Ca(OH)_2 + CaAl_2O_4 + 10H_2O \rightarrow Ca_4Al_2O(OH)_{12}(OH)_2 \cdot 6H_2O$$

The amount of $Ca(OH)_2$ added was in excess to that required to form hydrocalumite to ensure that the solution was saturated with respect to portlandite during the reaction period. This was done to simulate the conditions that exist in lime-leaching fly ash or cement-water systems, where both hydrocalumite and portlandite phases are present.

The uptake of B, Cr, Mo, and Se was also studied by coprecipitation with ettringite. The method described by Warren and Reardon (1994) was adopted to prepare the ettringite samples. Ettringite was precipitated by adding 7.0 mmoles of $Ca(OH)_2$ to 40 ml of 0.02 M $Al_2(SO_4)_3$ solution, which contained the same concentrations of B, Cr, Mo, and Se as in the hydrocalumite experiment. The reaction can be described as:

$$6Ca(OH)_2 + Al_2(SO_4)_3 + 26H_2O \rightarrow Ca_6Al_2(OH)_{12}(SO_4)_3 \cdot 26H_2O$$

When the results of this experiment indicated that molybdate was least preferred by ettringite, an additional run was carried out using a 10 ppm Mo solution, to determine if its uptake could be increased by removing the other anions. As in the hydrocalumite experiment, the amount of $Ca(OH)_2$ added was in excess to that required to produce ettringite.

To rule out the possibility that $Ca(OH)_2$ addition alone could cause reductions in borate, chromate, molybdate, and selenate concentrations, a control experiment was carried out. In the control samples, 2.70 mmoles of $Ca(OH)_2$ were added to 40 ml of the trace

element stock solution. This amount is slightly higher than the calculated excess $Ca(OH)_2$ present in the hydrocalumite and ettringite uptake experiments.

In all experiments, high density polyethylene bottles (60 ml) were used as reaction vessels. Once the solutions were prepared, the bottles were loaded on a wheel, immersed in a 25 ± 0.1 °C water bath and rotated continuously during the reaction period. All reactions were monitored by sampling both the solution and solid phases at various times over a period of 30 days. Sufficient duplicate samples were prepared so that each reaction vial was opened and sampled only once to avoid contamination.

4.2.3 Sampling and analysis

Samples of both solution and solids were taken after 1, 3, 7 and 30 days of reaction. The additional runs conducted with pure B and Mo solutions were sampled after 7 days of reaction. To prevent potential contamination from atmospheric CO_2, filtration was conducted in a glove box. All solution samples were passed through 0.22 μm cellulose acetate filters and acidified with 1:1 HCl to preserve them for chemical analyses. Solid samples were dried in a desiccator at a relative humidity of 37%.

B, Cr, Mo, and Se were analyzed using a Jarrell-Ash ICP spectrophotometer. The analytical uncertainties are within ±5%. Phase identification of solid samples was performed by X-ray powder diffractometry (XRD) using Cu Kα radiation generated at 30 mA and 50 kV. Specimens were step scanned as random powder mounts from 5 to 55° 2θ at 0.05° 2θ steps; integrated at 1 second per step. Selected solid samples were examined for morphology and crystallinity using a JEOL JSM-840 scanning electron microscope (SEM).

4.3 Results

The XRD results of the solid samples collected from the hydrocalumite uptake experiment are shown in Figure 4.1. Hydrocalumite formed after 1 day of reaction and was the principal phase produced in all samples. The peak intensities of this phase increased with time, especially between 7 days and 30 days, reflecting a possible increase in the amount of hydrocalumite precipitated. Excess $Ca(OH)_2$ was added in the original recipe to ensure the presence of portlandite, and the XRD results confirm its presence in all samples. Hydrogarnet ($3CaO{\cdot}Al_2O_3{\cdot}6H_2O$) was also identified with a quantity of less than 10%. The XRD patterns of the ettringite uptake samples are shown in Figure 4.2. Ettringite was identified as the

principal phase in all samples. With reaction time, the peak intensities of ettringite increased only slightly, indicating that the formation of ettringite was nearly complete after 1 day of reaction. The presence of portlandite was also confirmed in these samples.

SEM examination of the 1-d sample from the hydrocalumite uptake experiment showed anhedral to subhedral hydrocalumite crystals of 1 to 10 μm in size. After 7 days, the crystals were similar in size but appeared as well-formed hexagonal plates (Figure 4.3A). In the 30 d sample, the hydrocalumite crystals were substantially larger, reaching sizes greater than 50 μm. There were also abundant small hexagonal crystals, ranging from 1 to 5 μm, which occurred on the surfaces of the larger crystals (Figure 4.3B). These small crystals likely formed at later reaction times, supporting the XRD results, which suggest that the quantity of hydrocalumite increased with time. SEM micrographs of the ettringite uptake samples are shown in Figure 4.4. Ettringite occurred typically as needle-like crystals in the 7-d sample. The crystal size of ettringite appeared to increase slightly with time.

The solution compositions as a function of time from the hydrocalumite uptake experiment are shown in Table 4.1. The concentrations of Cr, Mo, and Se dropped to below detection after one day, with a decrease of over two orders of magnitude. The B concentration decreased by a factor of 10 in the first day, and by a factor of 2 again over the next 30 days. Because three of the anion concentrations were brought below detection limits, it is not possible to establish a specific order of preference of these anions by hydrocalumite. However, it is evident that borate is the least preferred anion. The B uptake results for the borate solution were similar to the solution containing all four anions. This suggests that anion competition, at least at these low solution concentrations, is not an important factor influencing the extent of uptake of the individual anions.

In comparison to hydrocalumite, anion uptake by ettringite is much lower (Table 4.2). Only borate, which was the least preferred by hydrocalumite, showed substantial concentration reductions. After one day of reaction, the B concentration dropped at least two orders of magnitude to below detection and remained below detection for the duration of the experiment. In contrast, the concentration reductions for Se, Cr and Mo were much less. After one day, the concentrations were reduced by 85, 60 and 45%, respectively. Their concentrations remained relatively constant with reaction time. The order of preference for all four elements by ettringite is B >> Se > Cr > Mo. The Mo uptake results for the solution containing only molybdate were similar to the solution containing all four anions. This suggests, as with hydrocalumite, that under the conditions of the experiment anion competition does not influence the extent of uptake of the individual anions by ettringite.

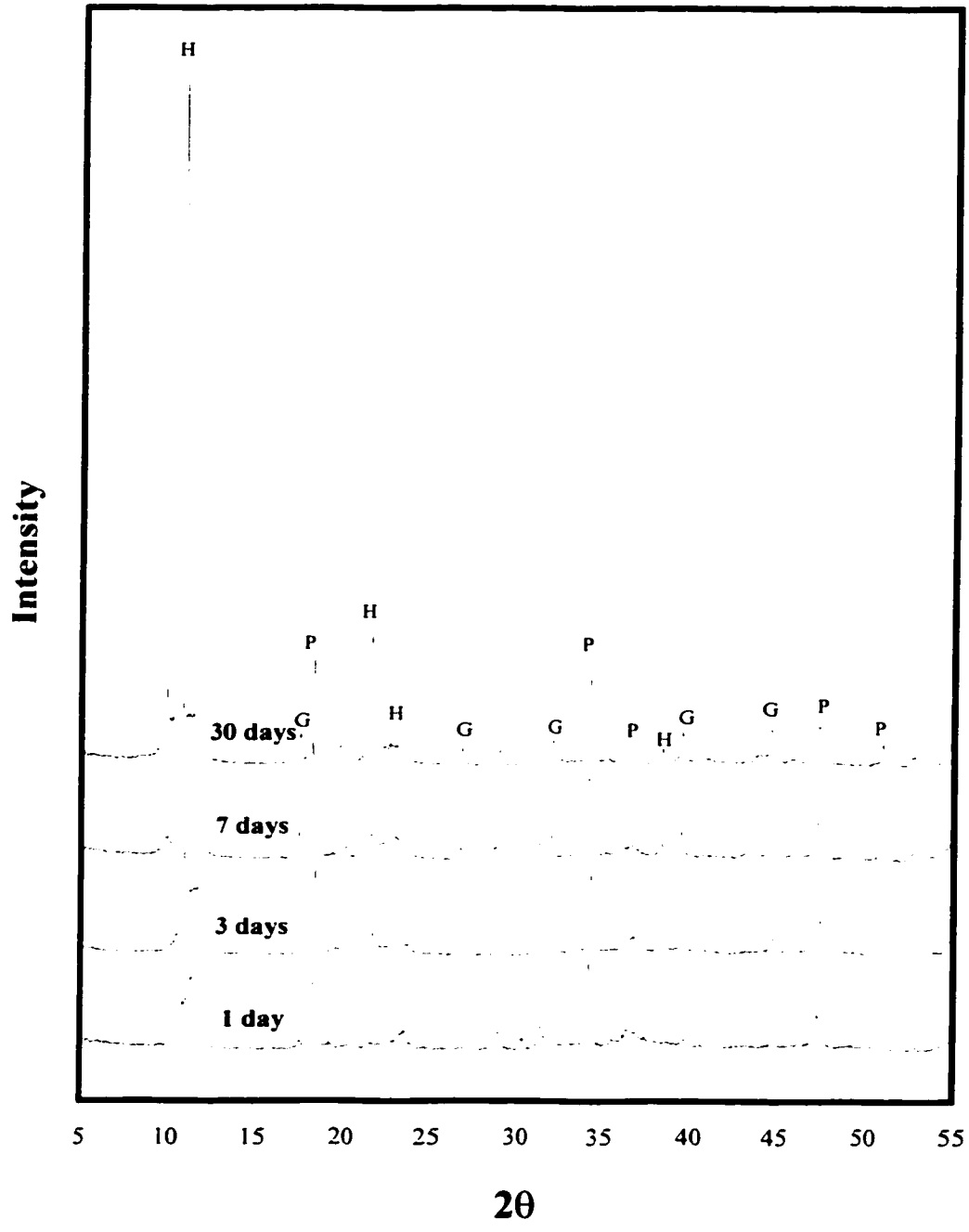

Figure 4.1: XRD patterns of the solids recovered from the hydrocalumite uptake experiment. H-hydrocalumite; P-portlandite; G-hydrogarnet.

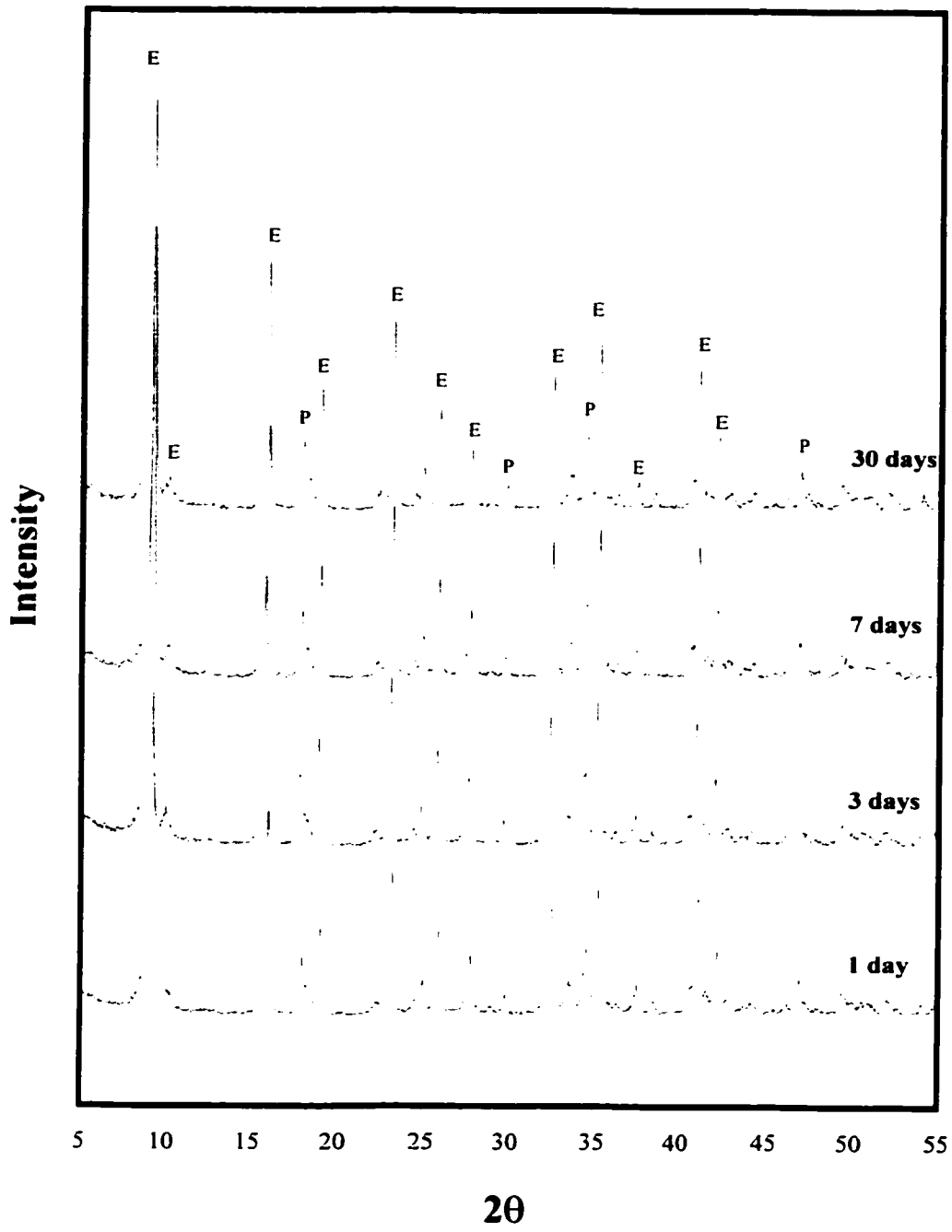

Figure 4.2: XRD patterns of the solids recovered from the ettringite uptake experiment. E- ettringite; P-portlandite.

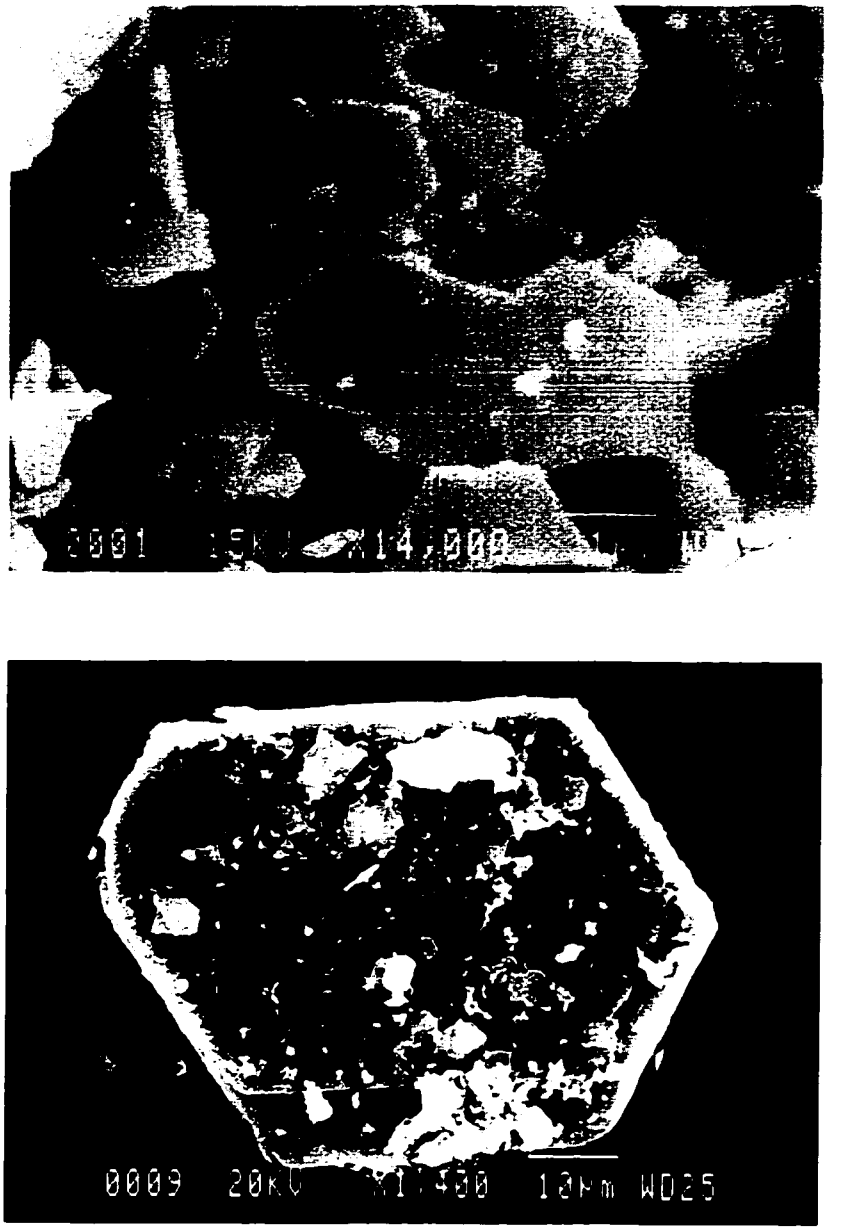

Figure 4.3: Micrographs of the solid recovered from the hydrocalumite uptake experiment, showing well-formed hexagonal plates of hydrocalumite. (A) after 7 days of reaction; (B) after 30 days of reaction.

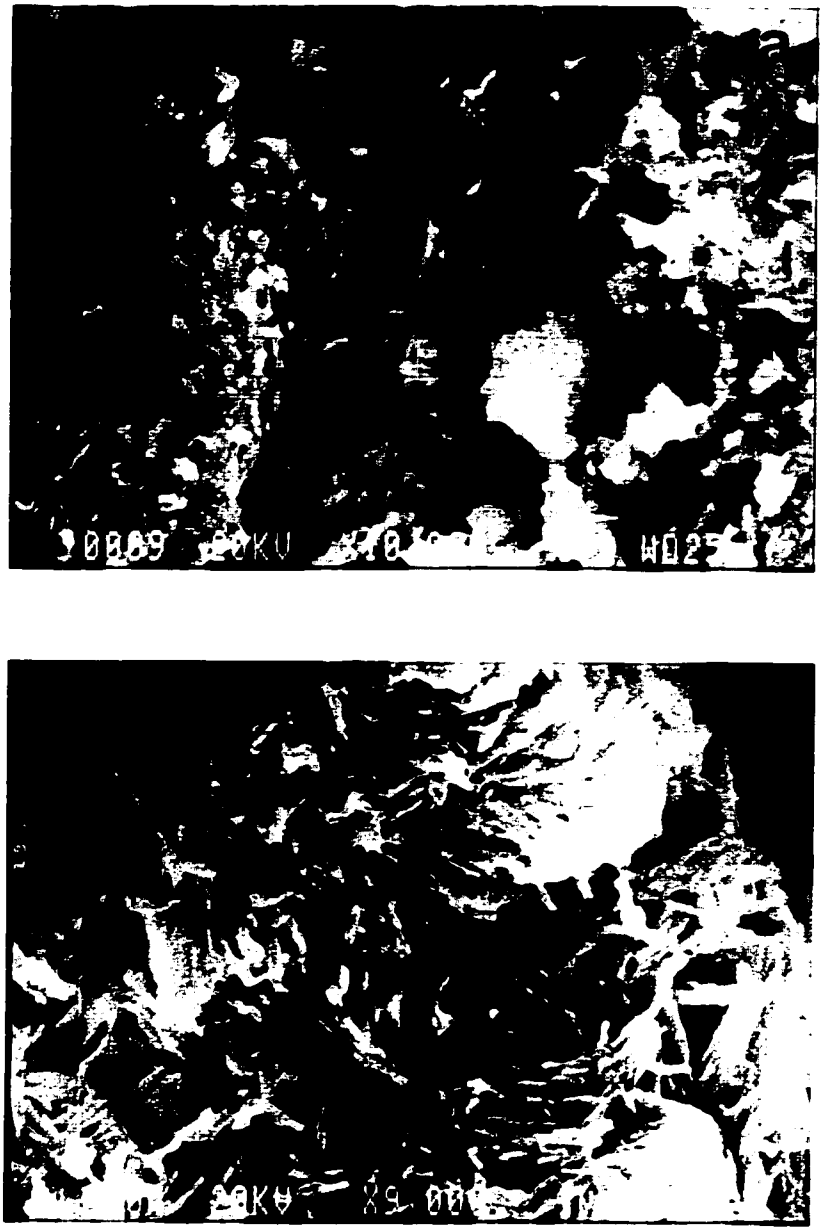

Figure 4.4: Micrographs of the solid recovered from the ettringite uptake experiment, showing needle-like crystals. (A) after 3 days of reaction; (B) after 30 days of reaction.

Table 4.1: Temporal changes in B, Cr, Mo, and Se solution concentrations in the hydrocalumite uptake experiment. The solution/hydrocalumite mass ratio was 40:0.9.

Trace Element	Reaction Period (days)	B (ppm)	Cr (ppm)	Mo (ppm)	Se (ppm)
B, Cr, Mo, Se	Original	9.44	10.11	9.81	11.57
"	1	0.94	<0.02	<0.08	<0.1
"	3	0.48	<0.02	<0.08	<0.1
"	7	0.40	<0.02	<0.08	<0.1
"	30	0.39	<0.02	<0.08	<0.1
B	Original	9.40			
"	7	0.31			

Table 4.2: Temporal changes in B, Cr, Mo, and Se solution concentrations in the ettringite uptake experiment. The solution/ettringite mass ratio was 40:1.

Trace Element	Reaction Period (days)	B (ppm)	Cr (ppm)	Mo (ppm)	Se (ppm)
B, Cr, Mo, Se	Original	9.44	10.11	9.81	11.57
"	1	<0.08	3.77	5.22	1.81
"	3	<0.08	3.80	5.39	1.99
"	7	<0.08	4.23	5.61	2.34
"	30	<0.08	3.99	4.55	2.04
Mo	Original			9.86	
"	7			4.09	

In Table 4.3, the change in the concentrations of B, Cr, Mo, and Se with time are reported for the control samples ($Ca(OH)_2$ present only). A comparison of the results for the original stock solution (top row entry) and the 1-d sample (second row entry) shows that only a slight concentration reduction occurred for each element upon addition of $Ca(OH)_2$. After this initial decrease, the concentrations remained stable for the next 30 days. The results of this control experiment provide important evidence: the reductions in anion concentrations observed in the hydrocalumite and ettringite uptake experiments must be a result of direct

incorporation into these phases rather than uptake by portlandite or precipitation as a calcium salt.

Table 4.3: Temporal changes in B, Cr, Mo, and Se solution concentrations in the control experiment.

Trace Element	Reaction Period (days)	B (ppm)	Cr (ppm)	Mo (ppm)	Se (ppm)
B, Cr, Mo, Se	Original	9.44	10.11	9.81	11.57
"	1	9.21	8.23	7.56	11.02
"	3	9.38	8.47	7.61	11.34
"	7	9.19	8.44	7.72	10.11
"	30	8.79	8.06	7.56	10.54

4.4 Discussion

4.4.1 Speciation of borate, chromate, molybdate, and selenate

The toxicity and mobility of a trace element in aqueous solution depends greatly upon the chemical properties of the species in which it is present. A number of valence states may be thermodynamically possible for a given element, and a number of hydrolysis products (*or hydrolysis species*) may exist for each of these valence states. The particular aqueous speciation of an element also determines the extent to which it is incorporated into precipitating mineral phases.

Polymerization is a common phenomenon for borate, chromate, and molybdate ions. However, extensive formation of polynuclear species only occurs with these ligands at low pH and high total dissolved metal concentrations. Under the experimental conditions (pH ≈ 12.5; total dissolved metal concentrations ≈ 10 ppm), only mononuclear hydrolysis species are important. The pertinent mononuclear hydrolysis reactions for borate, chromate, molybdate, and selenate and the corresponding equilibrium constants are presented in Table 4.4. In the aqueous phase, the deprotonated species is dominant when pH is greater than the pK. For example, $B(OH)_4^-$ is the prevailing species at pH values above 9.24. The most deprotonated or hydrolyzed species, i.e. $B(OH)_4^-$, CrO_4^{2-}, MoO_4^{2-}, and SeO_4^{2-}, are the dominant species for these elements at the pH conditions used in this study.

Table 4.4: The hydrolysis of borate, chromate, molybdate, and selenate at 25 °C and I = 0, after Smith and Martell (1976).

Hydrolysis Reaction	pK
$B(OH)_3° + H_2O \rightarrow H^+ + B(OH)_4^-$	9.24
$HCrO_4^- \rightarrow H^+ + CrO_4^{2-}$	6.51
$HMoO_4^- \rightarrow H^+ + MoO_4^{2-}$	4.24
$HSeO_4^- \rightarrow H^+ + SeO_4^{2-}$	1.70

4.4.2 Coordination of borate, chromate, molybdate, and selenate

The coordination and metal-oxygen bond length of the oxyanions examined are recorded in Table 4.5. Data for carbonate and sulfate anions are also listed for comparison. Borate can occur in both trigonal and tetrahedral coordinations in minerals (Hawthorne *et al.*, 1997). Tetrahedral CrO_4^{2-} is the only coordination found for hexavalent chromium in chromate minerals. Deviations of the CrO_4^{2-} tetrahedron have been measured with O-Cr-O angle ranging from 104 to 114° and mean Cr-O distances ranging from 1.60 to 1.67 Å (Wedepohl, 1969). Molybdate also shows a four-fold coordination, however, the molybdate tetrahedron is largely distorted in molybdate minerals. Geometrically, MoO_4^{2-} is intermediate in character between a regular tetrahedron and a square planar configuration (Evans, 1976). In contrast to molybdate, both sulfate and selenate are regular tetrahedra and show little distortion in hydrated sulfate and selenate minerals. The characteristics of SeO_4^{2-} are similar to SO_4^{2-} but the tetrahedrally coordinated bond length (Se-O) is 12% larger than that of sulfate.

Using IR spectroscopy, Wenda and Kuzel (1986) determined that boron was trigonally coordinated in their synthetic borate-hydrocalumite. Based on these results and on chemical analysis, they suggested that HBO_3^{2-} was present in the structure of hydrocalumite. Kindness *et al.* (1994) reported tetrahedral MoO_4^{2-} in the molybdate hydrocalumite endmember based on FTIR spectra. The coordination of chromate and selenate in hydrocalumite has not been determined. However, there have been some studies of chromate coordination in hydrotalcite, a close analogue to hydrocalumite. Hydrotalcite has a similar layered structure consisting of brucite-like principal layers instead of portlandite-like layers.

In chromate hydrotalcite, the presence of CrO_4^{2-} was determined from both IR and FTIR spectra (Miyata and Okata, 1977; Rhee *et al.*, 1997).

The coordinations of borate, chromate, and selenate have been directly determined in the ettringite structure. Pöllmann *et al.* (1989) determined that B was tetrahedral coordinated in borate-hydroxyl solid solution from Infrared (IR) adsorption spectra. The presence of $B(OH)_4^-$ in ettringite was also validated by Kumarathasan *et al.* (1990) using FTIR spectroscopy. Kumarathasan *et al.* (1990) and Pöllmann *et al.* (1993) established that tetrahedral CrO_4^{2-} existed in chromate-hydroxyl ettringite. Hassett *et al.* (1990) determined the presence of tetrahedral SeO_4^{2-} in ettringite solid solutions using FTIR spectroscopy. The coordination of molybdate in ettringite has not been examined.

Table 4.5: Coordination and bond length of the B, Cr, Mo, Se, C, and S species

Anion	Coordination	Bond Length (Å)	Reference
BO_3^{3-}	Trigonal planar	1.37	Grew and Anovitz (1996)
$B(OH)_4^-$	Tetrahedral	1.48	Grew and Anovitz (1996)
CrO_4^{2-}	Tetrahedral	1.66	Greenwood and Earnshaw (1984)
MoO_4^{2-}	Distorted tetrahedral	1.76	Pope (1991)
SeO_4^{2-}	Tetrahedral	1.64	Wedepohl (1969)
CO_3^{2-}	Trigonal planar	1.28	Wedepohl (1969)
SO_4^{2-}	Tetrahedral	1.47	Wedepohl (1969)

4.4.3 Substitution of the oxyanions in hydrocalumite

Hydrocalumite has unique structural characteristics which enable it to accommodate anions of various sizes. The thickness of the interlayer regions of hydrocalumite can vary as different anions are incorporated, e.g. 7.6 Å for CO_3^{2-} and 8.9 Å for SO_3^{2-} (Taylor, 1973). Therefore, the difference in ionic size between OH^- and a substituting anion is not likely a factor controlling the extent and preference for oxyanion incorporation. Studies on hydrotalcite, a similarly-structured compound, indicate that anion preference is determined by charge and bonding characteristics within the interlayer. It is known that trigonal planar carbonate is the most preferred anion in hydrotalcites, whereas tetrahedral sulfate is less favored. The carbonate triangle is oriented parallel to the principal layers, and therefore the bonding to the upper and lower surfaces of the interlayer region is equal (van der Pol *et al.*,

1994). Sulfate tetrahedra, however, are randomly distributed between the two possible orientations, with the apex of the tetrahedron pointing either up or down (Bish, 1980). Thus the bonding of an individual sulfate anion within the interlayer is anisodesmic, i.e. it is less strongly attached to one surface than it is to the other. This may explain why sulfate is more susceptible to replacement by trigonal planar anions like carbonate where the bonding to the layers is isodesmic.

The geometry of the anion and its orientation in the interlayer likely determine the total uptake capacity. In this study, the oxyanions occupy less than 2% of the anionic sites in the interlayer positions, the majority of the sites are occupied by OH^-. Incorporation of such a small percentage of these oxyanions would not disturb the overall structure. Therefore, it is unlikely that anion geometry is a major factor controlling incorporation. In fact, despite their tetrahedral coordination, CrO_4^{2-}, MoO_4^{2-}, and SeO_4^{2-} all showed a concentration decrease of over two orders of magnitude. Borate, on the other hand, occurring as trigonal HBO_3^{2-} in the structure of hydrocalumite, showed much lower uptake. Tetrahedral $B(OH)_4^-$ is the predominant borate species in the solution, therefore, the incorporation of borate into hydrocalumite involves a change in its coordination to trigonal HBO_3^{2-}. For this conversion to occur, an energy barrier must be overcome. This may explain the lower uptake of borate by this phase. Using a similar argument, Hemming *et al.* (1995) attributed the greater boron uptake by aragonite compared to calcite to the fact that borate is incorporated in aragonite in tetrahedral coordination, whereas a change in the coordination to trigonal is required for incorporation into calcite.

4.4.4 Substitution of the oxyanions in ettringite

In contrast to hydrocalumite, variations in the lattice dimensions of ettringite are more limited. However, some change is still allowable, e.g. the dimensions of the unit cell of ettringite increase gradually as more selenate replaces sulfate in the solid solution (Hasset*et al.*, 1990). In addition, anion substitution for SO_4^{2-} in ettringite does not appear to require an exact match in the anion geometry. For example, it has been observed that the uptake of pyramidal selenite is higher than that of tetrahedral selenate in ettringite (Solem-Tishmack*et al.*, 1995). This indicates that anion geometry is not the major factor controlling uptake. In ettringite, the size difference between sulfate and the substituting anion is probably more important.

The preference of ettringite for borate that was observed in this study is likely due to its similar size to sulfate. Kumarathasan *et al.* (1990) has suggested some possible charge

balance mechanisms which allow substitution of monovalent $B(OH)_4^-$ for SO_4^{2-}, such as coupled substitution of Na^+ or some other monovalent cation for Ca^{2+}. The order of preference of uptake for the anions that are divalent in solution is $SeO_4^{2-} > CrO_4^{2-} > MoO_4^{2-}$. This is likely related to an increase in the bond length observed in the same sequence (see Table 4.5). However, the size difference between SeO_4^{2-} and CrO_4^{2-} is too small to account for their difference in uptake. Since the incorporation of both SeO_4^{2-} and CrO_4^{2-} in ettringite is virtually a substitution for SO_4^{2-}, the difference in electronegativity between sulfur and selenium or chromium is also a possible factor influencing the substitution. Compared with sulfur, selenium has a very similar electronegativity to sulfur (2.4 vs. 2.5), whereas chromium has a much lower electronegativity (1.6). The similarity in electronegativity between selenium and sulfur would lead to a higher preference of selenate to substitute for sulfate in the structure of ettringite. Molybdate is least preferred by ettringite, likely because the size difference between molybdate and sulfate is the largest.

4.4.5 Environmental implications

In this study, ettringite and in particular hydrocalumite have shown a high capacity to incorporate oxyanions. Neglecting the small amount of hydrocalumite that dissolved in the solutions, the quantity of oxyanion taken up can be calculated. Under the experimental conditions used in this study, the uptake is approximately 400 mg/kg for boron and over 440 mg/kg for the other trace elements. The uptake of boron by ettringite is over 360 mg/kg if the same assumption is applied. The maximum uptake capacity for both mineral phases, however, could be much higher because substantial substitution of these oxyanions in both minerals has been reported. For example, a pure molybdate endmember of hydrocalumite has been synthesized (Kindness *et al.*, 1994), and borate substitution to 2/3 of the total anionic site capacity in ettringite has been achieved (Pöllmann *et al.*, 1993). Kumarathasan *et al.* (1990) have also shown the complete substitution of chromate and selenate for sulfate in ettringite. Based on the chemical formula derived for the borate, chromate, molybdate, and selenate hydrocalumite or ettringite endmembers, the maximum uptake capacities are calculated, and the results are summarized in Table 4.6.

The ability of hydrocalumite and ettringite to incorporate large quantities of anions into their structures is important for wastewater treatment applications. Not only do these phases have a large uptake capacity, but hydrocalumite in particular can reduce metal oxyanion concentration levels to below drinking water standards. Ettringite was able to reduce B to below detection in solution. It is worth noting that a large lattice uptake capacity for an oxyanion does not necessarily correspond to a low concentration level in solution.

Under the experimental conditions, about 40% of Cr remained in solution after ettringite recrystallized, although a complete substitution of chromate for sulfate can be achieved. Conversely, a small uptake capacity does not always correspond to a high residual concentration in solution. The removal of B from solution was nearly complete in the ettringite uptake experiments, but the borate endmember of ettringite has not been synthesized successfully. Further research is necessary to more fully understand the factors controlling uptake capacity and site preference of these oxyanions in hydrocalumite and ettringite, and to determine the solubilities of their solid solutions.

Table 4.6: Maximum uptake capacity (M.U.C.) of B, Cr, Mo, and Se by hydrocalumite and ettringite ($x10^3$ mg/kg).

Mineral Phase	Element	Chemical Formula	M.U.C.	Reference
Hydrocalumite	B	$Ca_4Al_2(OH)_{12}[HBO_3]\cdot 5.5H_2O$	18.7	Wenda and Kuzel (1986)
"	Cr	$Ca_4Al_2(OH)_{12}[CrO_4]\cdot 9H_2O$	74.7	Perkins and Palmer (unplished)
"	Mo	$Ca_4Al_2(OH)_{12}[MoO_4]\cdot 8H_2O$	133	Kindness *et al.* (1994)
"	Se	-	-	-
Ettringite	B	$Ca_6Al_2(OH)_{12}[B(OH)_4]_4[OH]_2\cdot 24H_2O$	33.8	Pöllmann *et al.* (1993)
"	Cr	$Ca_6Al_2(OH)_{12}[CrO_4]_3\cdot 26H_2O$	119	Kumarathasan *et al.* (1990)
"	Mo	-	-	-
"	Se	$Ca_6Al_2(OH)_{12}[SeO_4]_3\cdot 26H_2O$	170	Hassett *et al.* (1989)

4.5 Conclusions

Both hydrocalumite and ettringite have a high capacity to accommodate oxyanions, such as borate, chromate, molybdate, and selenate into their structures. For the examined oxyanions, hydrocalumite is more effective in incorporating anions and reducing their solution concentrations than ettringite. It has been established that the preference of the oxyanions by ettringite is in the order of $B(OH)_4^- > SeO_4^{2-} > CrO_4^{2-} > MoO_4^{2-}$. Preference of the anions can not be established for hydrocalumite because most oxyanion concentrations were brought below detection. It is evident, however, that borate was the least favored.

Borate occurs as trigonal HBO_3^{2-} in the structure of hydrocalumite. Although the trigonal coordination of borate is favored by the structure, a change in its coordination is required when $B(OH)_4^-$, the dominant species in solution, is incorporated into hydrocalumite. This change in coordination from tetrahedral to trigonal may be energetically or kinetically hindered, and therefore results in a lower borate uptake. At such low uptake levels (i.e. less than 2% of anionic sites), the geometry, size, and charge of the anions do not likely affect their uptake by hydrocalumite.

In the ettringite structure, differences in size and electronegativity between sulfate and the oxyanions are the major factors determining the extent of uptake. Anions with similar size, i.e. $B(OH)_4^-$, are highly preferred. Anions with dissimilar size and electronegativity, such as molybdate, are least preferred.

Chapter 5

Solid Solutions of B, Cr, Mo, and Se with OH-hydrocalumite

5.1 Introduction

It has been shown that solution concentrations of borate, chromate, molybdate, and selenate can be greatly reduced by incorporation into the hydrocalumite structure. Reductions in the concentrations of these oxyanions from 10 ppm to well below the drinking water standards have been achieved (Chapter 4). Incorporation of anions into hydrocalumite is a potential treatment process to remove these undesirable elements from contaminated drinking waters. If wastewater treatment is required, the uptake capacity of hydrocalumite is an important factor for consideration. The aim of this study is to determine the uptake capacity of hydrocalumite for these oxyanions, and to understand the effect of the anions on mineral phase solubility and stability in the system $CaO\text{-}Al_2O_3\text{-}XO_3/Y_2O_3\text{-}H_2O$ ($X = Cr^{6+}$, Mo^{6+}, Se^{6+}; $Y = B^{3+}$). Another primary objective was to derive or verify some fundamental thermodynamic parameters, such as the free energy, of the various hydrocalumite endmembers for inclusion into chemical equilibria models. To achieve these goals, hydrocalumite solid solutions with OH as one endmember and borate, chromate, molybdate, and selenate as the other endmembers have been synthesized and characterized in this study.

In addition to the four solid solution series described above, (OH, SO_4)-hydrocalumite solid solutions were also studied. There are two main reasons for adding sulfate to this investigation: (1) the system $CaO\text{-}Al_2O_3\text{-}SO_3\text{-}H_2O$ has been the subject of intensive research and therefore can serve as a reference for the other systems, and (2) ternary and quaternary compounds in the $CaO\text{-}Al_2O_3\text{-}SO_3\text{-}H_2O$ system are important constituents in most cements, comprising 10-20% of the hydration phases in ordinary Portland cement (Atkins *et al.*, 1991). Lamellar calcium aluminate hydrates and related basic salts, such as

OH-hydrocalumite ($Ca_4Al_2(OH)_{12}(OH)_2 \cdot 6H_2O$), or C_4AH_{13} in cement notation) and SO_4-hydrocalumite ($Ca_4Al_2(OH)_{12}(SO_4) \cdot 6H_2O$), or $C_4A\bar{S}H_{12}$ in cement notation), play important roles in the chemistry of cement hydration. Their impacts on the physicochemical properties of cement are marked. In addition, equilibria in this quaternary system are particularly important in connection with the chemical resistance of cement to attack by natural waters containing SO_4^{2-}. Finally, studies of this system may generate some useful information on the stability of the phase assemblages and on the prediction of solution compositions in cement - water systems.

Compounds containing the oxyanions are also used in the cement industry as additives to modify the properties of cement. Borate, in the form of either boric acid or sodium borate, has been added to rapid hardening cements to retard hydration reactions (Uchikawa and Uchida, 1977). The addition of calcium borate to high alumina cements was patented for preventing the conversion of CAH_{10} and C_2AH_8 into hydrogarnet at temperatures up to 60 °C (after Wenda and Kuzel, 1986). In the search for an alternative chloride-free accelerator, sodium molybdate, a corrosion inhibitor, was found to accelerate the hydration rate in both calcium aluminate and Portland cement (Thomas and Egan, 1989). Chromate, which passivates iron, is a good accelerator in Portland cement and is used in reinforced concrete (Thomas, 1987). Tashiro and Fukuyama (1975), however, reported a retardation of C_3A ($3CaO \cdot Al_2O_3$) hydration in $CaCrO_4$ solution. Although practical applications involve the use of these anions as additives, little effort has been devoted to understanding the mechanisms involved. In addition, stabilization and solidification (S/S) technology has been become the most common treatment for hazardous industrial wastes and for nuclear wastes. Of the toxic heavy metals, chromium and selenium are often stabilized using cement materials (Lin *et al.*, 1992; Cocke and Mollah, 1993). This study provides new knowledge on the binding mechanisms of oxyanions in cement and bridges the gap between observation of performance and the fundamental understanding of these mechanisms.

Although a large volume of data is available on both the solid characterization and solution composition for the system CaO-Al_2O_3-SO_3-H_2O, evidence for the stability of solid phases is contradictory (e.g. Jones, 1944; D'Ans and Eick, 1953; Roberts, 1969; Pöllmann, 1989; Glasser *et al.*, 1999). There is still disagreement over which solid solution phases exist between the endmembers of $Ca_4Al_2(OH)_{12}(OH)_2 \cdot 6H_2O$ and $Ca_4Al_2(OH)_{12}(SO_4) \cdot 6H_2O$ (e.g. Turriziani and Schippa, 1955; Pöllmann, 1989). Compared to the sulfate series, the number of studies on the solid solutions containing other oxyanions is much more limited. Hydrocalumite solid solutions between borate and hydroxyl have been studied by Wenda and Kuzel (1986), but their study focused on the solid phases. For chromate and molybdate, only the endmembers have been previously synthesized and characterized (Feitknecht and Buser,

1951; Kuzel, 1969; Kindness *et al.*, 1994). No literature has been published on hydrocalumite containing selenate. A few analytical and interpretational problems are apparent in a number of the previous studies. The contributions of early works were restricted by the techniques employed. For example, a complete solid solution between OH and SO_4 was proposed solely on the basis of the varying refractive indices of hydrocalumites (Jones, 1944a; D'Ans and Eick, 1953). Microscopic homogeneity, however, does not necessarily imply a single solid solution phase. The connection between the characterization of the solid and the solution composition has not been stressed in previous investigations. In addition, the results of many previous studies have been affected to some degree by the experimental difficulties inherent in studying the hydrocalumite phases. These phases are sensitive to the drying conditions employed, susceptible to contamination by atmospheric carbon dioxide, and slow to attain solid/aqueous phase equilibrium.

This study is the first attempt to systematically study hydrocalumite solid solutions of borate, chromate, molybdate, and selenate under well-controlled conditions. In addition to gathering experimental data for these solid solution series, two specific questions related to these systems have been addressed. Hydrocalumite is thought to be able to accommodate a variety of anions with different sizes and charges because its main structural sheets can either expand or shrink (Taylor, 1973). The capability of the hydrocalumite structure to accommodate different anions, however, has not been examined through comprehensive investigations of solid solution series with various anions. The question raised is: what is the limiting factor for anionic accommodation by this phase? It is usually observed that transformation from hydrocalumite to ettringite occurs when the sulfate content of the pore solution increases beyond a certain concentration (Damidot *et al.*, 1992). Transformation between these two phases is an important process that determines not only the timing of cement setting, but also its resistance to sulfate attack. The previous studies on this problem have been mainly empirical. It is still not clear why, when, or how the transformation occurs. Furthermore, no effort has been made to determine the effect of different anions on the phase transformation. As natural waters contain many different ions, this consideration is of practical importance.

5.2 Experimental

5.2.1 Materials

Monocalcium aluminate ($CaAl_2O_4$, or CA in cement notation) was prepared using the technique described in section 3.2.1. The chemical was ground to a fine powder before use.

CaO was prepared by calcining $CaCO_3$ (Aldrich reagent-grade $CaCO_3$ with purity between 99.95 to 100.05 %) in a muffle oven at 950 °C for 3 hours. The product was cooled in the oven for half an hour, then transferred to a desiccator and placed under vacuum until it reached room temperature. Completion of the reaction was verified based on the mass difference before and after heating. Double deionized Nanopure water was used throughout the experiments.

Powellite ($CaMoO_4$) was synthesized by titrating a molybdic acid solution with a $Ca(OH)_2$ saturated solution at room temperature. The titration was terminated when the pH reached approximately 6.5. This is the optimal pH to minimize both polymerization of molybdate and precipitation of calcite due to contamination by atmospheric CO_2. Powellite was precipitated after the mixture was heated to 80 °C for half an hour. The precipitated crystals were allowed to age in the mother liquid for two days. They were then filtered and rinsed with water, followed by ethanol. XRD analysis shows that pure powellite was produced. $CaMoO_4$ was used in the molybdate solid solutions. Reagent-grade B_2O_3, K_2CrO_4, Na_2SeO_4, and $CaSO_4 \cdot 2H_2O$ were used as the sources of borate, chromate, selenate, and sulfate, respectively. All chemicals were dried at 110 °C for at least three hours before use.

5.2.2 Experimental design

Monocalcium aluminate (2.0×10^{-3} mole) and freshly calcined CaO were used to prepare all the solid solution samples. For each endmember of the hydrocalumite series, stoichiometric amounts of CaO, compounds containing the oxyanions, and $CaAl_2O_4$ were combined to promote the following reactions:

$$CaAl_2O_4 + 3CaO + 13H_2O \rightarrow Ca_4Al_2(OH)_{12}(OH)_2 \cdot 6H_2O$$

$$CaAl_2O_4 + 3CaO + B_2O_3 + (n+4)H_2O \rightarrow Ca_4Al_2(OH)_{12}[B(OH)_4]_2 \cdot nH_2O$$

$$CaAl_2O_4 + 3CaO + K_2CrO_4 + nH_2O \rightarrow Ca_4Al_2(OH)_{12}(CrO_4) \cdot nH_2O + 2K^+$$

$$CaAl_2O_4 + 2CaO + CaMoO_4 + nH_2O \rightarrow Ca_4Al_2(OH)_{12}(MoO_4) \cdot nH_2O$$

$$CaAl_2O_4 + 3CaO + Na_2SeO_4 + nH_2O \rightarrow Ca_4Al_2(OH)_{12}(SeO_4) \cdot nH_2O + 2Na^+$$

$$CaAl_2O_4 + 2CaO + CaSO_4 \cdot 2H_2O + 10H_2O \rightarrow Ca_4Al_2(OH)_{12}(SO_4) \cdot 6H_2O$$

Hexavalent chromium, molybdenum, selenium, and sulfur usually occur as tetrahedral CrO_4^{2-}, MoO_4^{2-}, SeO_4^{2-}, and SO_4^{2-} in crystal structures. Trivalent boron, however, occurs in both tetrahedral ($B(OH)_4^-$) and trigonal ($B(OH)_3^\circ$) coordinations when it is incorporated into crystal structures (Sen *et al.*, 1994). In this study, it is assumed that boron is tetrahedrally coordinated with oxygens as $B(OH)_4^-$ in the structure of hydrocalumite. This assumption is based on the fact that $B(OH)_4^-$ is the dominant species in alkaline solution, and that reactions between $B(OH)_4^-$ and OH-hydrocalumite are ion exchange. During the ion-exchange process, it is thought that the coordination of an ion does not alter. In preparing a particular solid solution composition, it was assumed that the solubilities of the hydrocalumite phases were negligible.

For each solid solution series, 10 samples were prepared with the molar percentages of the anion in hydrocalumite of 10, 20, 30, 40, 50, 60, 70, 80, 90, and 100, respectively. Only six samples were prepared for the chromate solid solutions, containing 20, 40, 50, 60, 80, and 100 percent CrO_4, respectively. The ID number of a sample starts with the symbol of element (as anion) and followed by the molar percent. For example, the solid solution with an ideal formula of $Ca_4Al_2(OH)_{12}(SO_4)_{0.2}(2OH)_{0.8}\cdot nH_2O$ is referred to as S20. To prepare this solid solution, the amount of SO_4 added was based on the stoichiometric ratio of the solid solution phase, i.e. the molar ratio of $SO_3/Al_2O_3 = 0.2:1$ in the starting materials. The actual quantities of the chemicals added to each sample are given in the Appendix.

To monitor reaction process, two additional samples from each series containing either 50 or 100 molar percentage of anions were prepared for periodic conductance measurements. Conductance was measured after 3, 6, 14, 28, 56, 106, 147, and 208 days of reaction.

For each sample, the chemicals were weighed and transferred to a 60 ml high density polyethylene (HDPE) bottle. Approximate 50 ml of water was added to each bottle. During preparation and reaction, precautions were taken against contamination arising from carbonation by avoiding wherever possible contact with atmospheric CO_2. The addition of water would trigger the reaction and therefore this step was performed in a glove box under CO_2-free conditions. Glass mason jars were used to host the samples. This maintained a closed system during the long-term reaction. Soda lime, a CO_2 absorbent, was placed in the glass bottles to scavenge any possible leaking of CO_2 from the atmosphere. This setup was used for B, Cr, and Mo solid solution samples. For Se and S series, the sample bottles were wrapped with aluminum foil and jacketed with Ziplock bags. The reactions took place in constant-temperature water baths with the temperature controlled at 25 ± 0.1 °C. Samples were loaded on a wheel, and continuous vertical rotation was provided by a water pump.

5.2.3 Sampling and analysis

Samples of borate solid solutions were taken after a minimum reaction time of nine months. The other series of solid solutions were sampled between one year and one and half years of reaction. The reaction times for the samples are also listed in the Appendix. To prevent CO_2 contamination, all filtration of the products was conducted in the glove box. The samples were filtered through 0.22 μm filter paper. The filtered solids were retained and dried in a desiccator, over a $CaCl_2$ saturated solution (relative humidity of 37%). Solution samples were split into either two or three portions. To the cation samples (approximate 30 ml), 0.5 ml of 1:1 HCl was added. The samples for anion analysis (SO_4 solid solution series only) were diluted 1:2 with water. Both cation and anion samples were stored in a refrigerator before analysis. The remaining solution was used for pH and conductance measurements.

After equilibration at a R.H. of 37% for at least two weeks, a portion of the solid sample was used for X-ray diffraction analysis (XRD). The powder was randomly loaded on an aluminum sample holder. Specimens were step scanned from 5 to 55° 2θ at 0.05° steps; integrated at 1 second/step. Selected solid samples were examined for morphology and crystallinity using a JEOL JSM-840 scanning electron microscope (SEM). Chemical compositions of the solid phases were determined by energy dispersive X-ray analysis (EDX).

Solution samples were analyzed for Ca, Al, B, Mo, Cr, and Se using a Jarrell-Ash Inductively Coupled Plasma Spectrophotometer (ICP). The concentration of SO_4 was analyzed using a Dionex AS3 Ion Chromatograph (IC). pH was measured using an Orion Ross® pH electrode, which was calibrated against buffer solutions of 7.00 and 10.00. Conductance was measured using a Cole-Palmer® conductivity meter, and the probe was calibrated with a 0.01 m KCl solution. Conductance measurements for monitoring reaction progress were conducted in a glove box.

5.3 Results

5.3.1 Reaction kinetics

The reaction progress of each solid solution series was monitored for over 260 days using conductance measurements. The results are plotted in Figure 5.1. In this study, conductance measurements served as a criterion to judge if equilibrium conditions were

attained. It was assumed that equilibrium had been achieved once a stable conductance reading was attained. Sampling time was determined based on these measurements.

The relationship between the temporal changes in conductance and attainment of equilibrium, however, can be complex. If a stable mineral or a mineral assemblage forms initially, conductance should quickly level off. If a stable mineral forms but then recrystallizes, conductance should gradually decrease over time and level off when equilibrium is reached. If a metastable phase or assemblage forms first, there might be a period of constant conductance. The stable conductance during this period of time, however, does not represent an equilibrium condition. Conductance will remain constant until the metastable mineral phase or phases are consumed. Then there may be a period of marked conductance decrease until the last vestiges of the metastable phase are gone and the more stable phase or assemblage is all that remains. At this point, a true equilibrium condition is reached.

After 260 days of reaction, stable conductance readings were reached for all solid solution series except for sulfate. The conductance of the OH endmember remained constant after 3 days of reaction, indicating that an equilibrium or a metastable condition was established in a short period of time. Borate solid solution samples, however, showed a drop in conductance of approximate 70% and 60% within 60 days for B100 and B50, respectively. Afterwards, stable conductance values were exhibited by both samples. These results indicate that the reactions from the initial anhydrous, unstable phases to the stable phase(s) were complete for the borate series after two months. The conductance of the molybdate solid solution samples decreased gradually with time and stabilized after 200 days of reaction. The slow change in the conductance could be a result of either slow reaction with the added $CaMoO_4$ or a slow recrystallization process of early-formed material. Relatively stable conductance readings were achieved after approximate 60 and 100 days for Cr50 and Cr100, respectively. For sample Se50, the conductance remained constant for the first 100 days of reaction, after which a drop of 12% occurred between 100 to 200 days. A constant conductance was reached again after 200 days. The selenate endmember (Se100) showed a gradual decrease in the conductance over the entire monitoring period. The variation in conductance was different with the sulfate series. After a long period of stabilization (60 days for S100 and over 200 days for S50), the conductance decreased by 62% and 28% for S100 and S50, respectively. These large reductions likely resulted from a phase transformation rather than simple recrystallization. By the time of the last measurement, a stable reading had still not been reached.

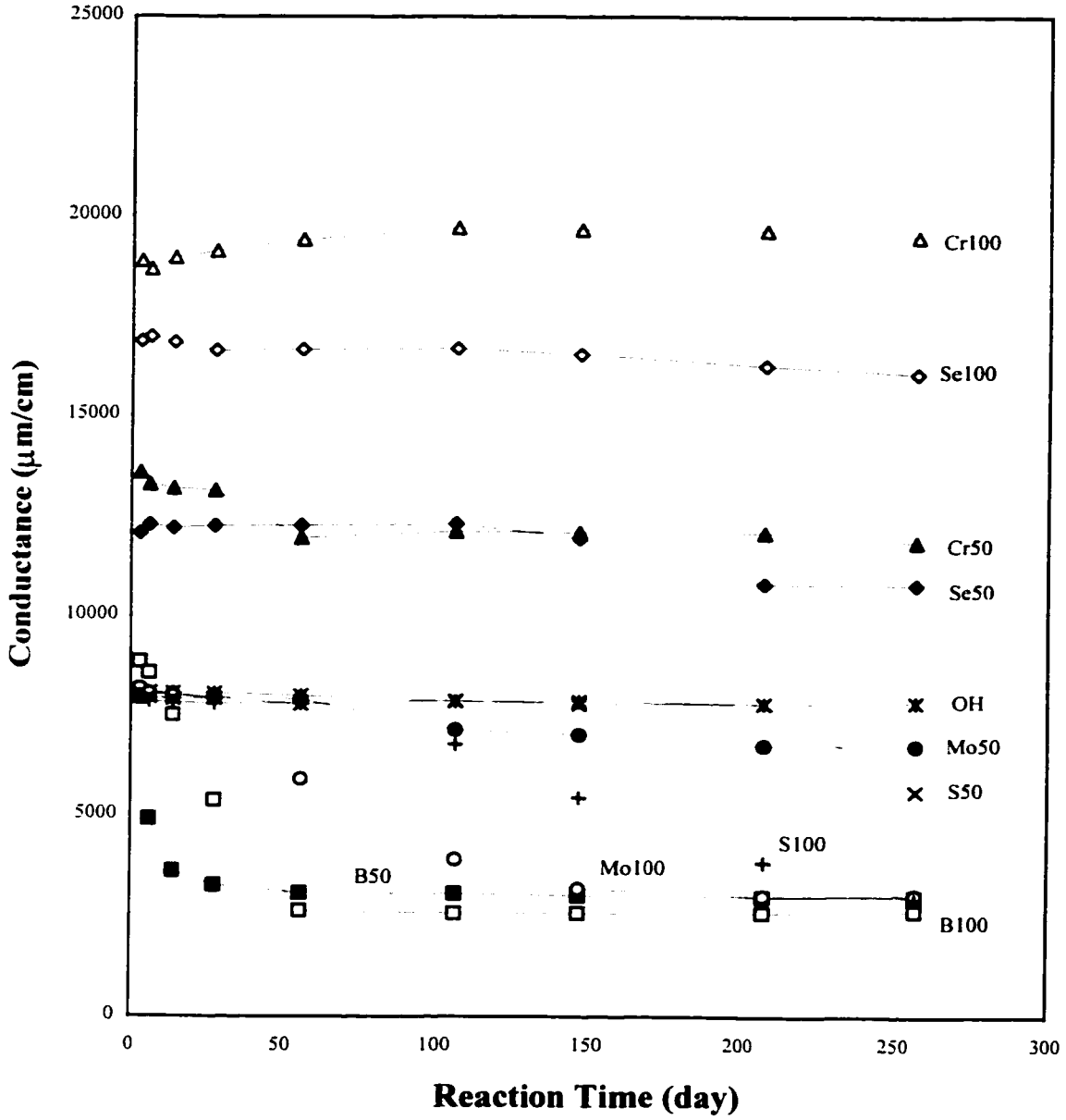

Figure 5.1: Conductance vs. reaction time for each solid solution series. Measurements were taken on the end members and the solid solutions containing 50% OH and 50% oxyanion. The curves are labelled with their sample ID.

Borate solid solution samples showed a much lower conductance than that of the OH endmember, whereas the molybdate series had an intermediate conductance. High conductances were generated in both the chromate and selenate series due to the presence of either K or Na, which was dissolved from the starting materials. From the trend of conductance change, the conductance of sulfate series is expected to be close to or even lower than that of borate. With the exception of the chromate and selenate series, the lowest conductance was always shown by the oxyanion endmembers. The samples with 50% oxyanion and 50% OH had a conductance higher than their corresponding endmembers and lower than the OH endmember. If a single hydrocalumite solid solution phase was formed in each sample as designed, a high conductance value corresponds to high solubility of this phase. This assumption allows us to determine the relative solubilities of the following endmembers as: $OH > MoO_4 > B(OH)_4 \approx SO_4$. The solubility of the chromate and selenate hydrocalumite can not be compared with the other endmembers in this manner due to the presence of other ions in the solutions (K^+ and Na^+).

5.3.2 X-ray diffraction analysis

The XRD results for the synthesized solid solutions are shown in Figures 5.2 to 5.7. For all 48 samples examined, no calcite peaks were found. Since the solution was at or near saturation with respect to portlandite for most of the samples, any contamination with atmospheric carbon dioxide would have caused precipitation of calcite. The absence of calcite indicates a CO_2-free system. Contamination of CO_2 could also result in the formation of $Ca_4Al_2(OH)_{12}(CO_3)\cdot 5H_2O$ which has a basal spacing of 7.6 Å. According to Turriziani and Schippa (1955), this compound is formed very readily from aqueous suspensions when small amounts of CO_2 are present. No peak at the d-spacing of 7.6 Å was shown in the XRD patterns. Instead, a phase with the d-spacing of 8.2 Å is present, which could be the compound $Ca_4Al_2(OH)_{12}(\frac{1}{2}CO_3, OH)_2\cdot 6H_2O$. This compound forms when OH-hydrocalumite ($Ca_4Al_2(OH)_{12}(OH)_2\cdot 6H_2O$, or C_4AH_{13}) is exposed to atmosphere and reacts with CO_2 (Roberts, 1969). Considering the precautions taken to exclude atmospheric CO_2 during the experimental procedures in this study, if CO_2 contamination occurred, it likely occurred when the samples were exposed to the atmosphere during the XRD measurements.

5.3.2.1 XRD results from the system CaO-Al_2O_3-H_2O

The XRD patterns for the OH endmember are shown in Figure 5.2. Samples OH1 and OH2 are replicates but had different reaction times. Similar XRD patterns were shown

between these two samples. Instead of OH-hydrocalumite (C_4AH_{13}) being the dominant phase as expected, the products consisted principally of hydrogarnet and portlandite. In addition, peaks at d-spacings of both 8.2 Å and 10.6 Å were present at lower relative intensities. C_4AH_{13} has a typical d-spacing of 7.9 Å. The phase with the d-spacing of 8.2 Å is likely derived from C_4AH_{13}, which carbonated to form $Ca_4Al_2(OH)_{12}(\frac{1}{2}CO_3, OH)_2 \cdot 6H_2O$ during the XRD measurements.

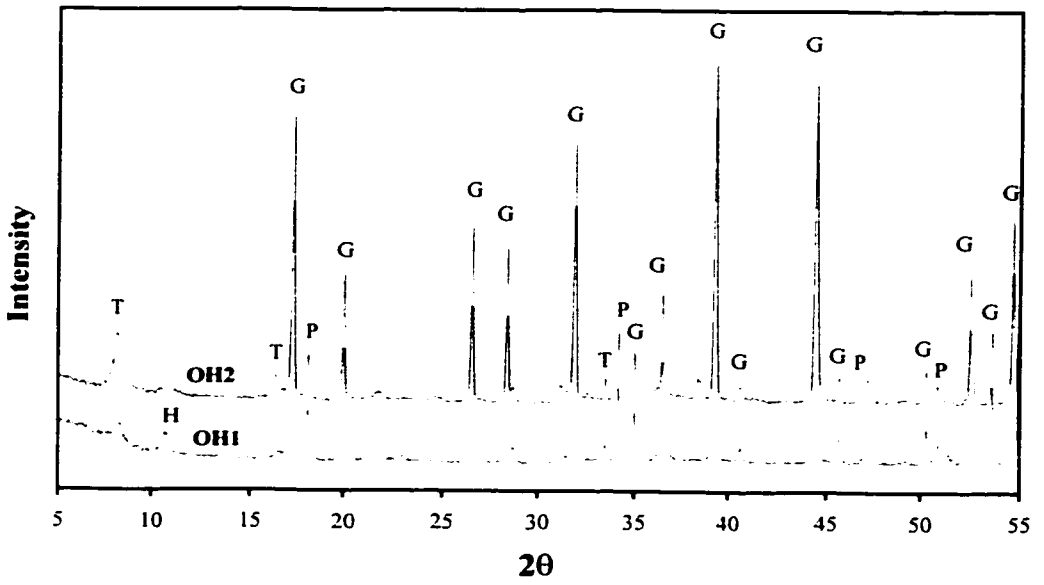

Figure 5.2: XRD patterns of the solids recovered from the OH hydrocalumite endmember. G-hydrogarnet; P-portlandite; H-hydrocalumite (C_4AH_{13}); T-C_4AH_{19}.

The peak at 10.6 Å could be attributed to either C_2AH_8 or C_4AH_{19} since these two phases have major peaks with practically identical positions. C_4AH_{19} is the stable tetracalcium aluminate hydrate in aqueous solution at room temperature (Roberts, 1969). According to Roberts (1969), dehydration of C_4AH_{19} takes place rapidly at relative humidities below 88%, and a conversion to C_4AH_{13} occurs. C_4AH_{19} has the same structure as C_4AH_{13} but contains an additional layer of water molecules in the interlayer region. Dicalcium aluminate hydrate (C_2AH_8) also has a similar structure to C_4AH_{13} except that $Al(OH)_4^-$ is the interlayer anion rather than OH^- (Richard *et al.*, 1995). C_2AH_8, however, is only formed when the ratio of CaO/Al_2O_3 in initial mixture is about 2 (Turriziani, 1964). At

high lime content, C_4AH_{19} should be produced instead of C_2AH_8. In this experiment, the initial CaO/Al_2O_3 ratio was 4.0 and the final solution is at equilibrium with portlandite. These conditions rule out the presence of C_2AH_8. Under the drying conditions (at 37% R.H.) employed for the solid samples, C_4AH_{19} should convert to C_4AH_{13}. The presence of C_4AH_{19} may be due to the fact that equilibrium had not been reached within two weeks or that rehydration occurred during the XRD measurements. Because C_4AH_{13} and C_4AH_{19} are essentially the same phase, they will be treated as one phase in the following text. This phase also appeared in the solid solution series at a similar basal spacing and will be referred to as a *highly hydrated hydrocalumite*.

5.3.2.2 XRD results from the system $CaO-Al_2O_3-XO_3/Y_2O_3-H_2O$

In the borate solid solution series, borate hydrocalumite was the dominant phase in all samples (Figure 5.3), and appeared as a single solid solution phase in all the XRD patterns. The d-spacing of hydrocalumite varied from 8.10 to 8.26 Å. However, no systemic trend with composition was observed. At the low end of the borate solid solutions, hydrogarnet was present, but its peak intensity decreased from B10 to B40. Portlandite peaks were also seen in sample B10. In both the B50 and B60 samples, borate hydrocalumite was the only phase identified. A new phase, borate ettringite, was present in samples B70 to B100. The peak intensity of ettringite increased with an increase in the molar percentage of borate except between samples B90 and B100. Highly hydrated borate hydrocalumite was also present in samples B90 and B100.

Throughout chromate solid solution series, hydrocalumite was always present as two or more immiscible solid solution phases as indicated by peak splitting (Figure 5.4). Splitting peaks correspond to phases of different layer thickness. The d-spacing for the chromate hydrocalumites varied widely from 7.9 to 9.6 Å. At the low end of the solid solutions (samples Cr20 to Cr50), the d-spacings of chromate hydrocalumite were consistent with one around 7.9 Å and the other around 8.6 Å. The principle peak of hydrocalumite shifted to a lower 2θ angle at the high end, splitting at 9.6 Å and 8.8 Å in Cr60, at 9.6 Å and 8.4 Å in Cr80, and at 8.9 Å and 8.3 Å in Cr100. Although the peak at 9.6 Å is close to that of ettringite, the overall pattern does not match with ettringite. This peak likely belongs to chromate hydrocalumite solid solution phase. Ettringite was not identified in this series. In addition to hydrocalumite, hydrogarnet and portlandite were also present at the low end of the solid solution. Sample Cr80 showed an unusually high amount of portlandite.

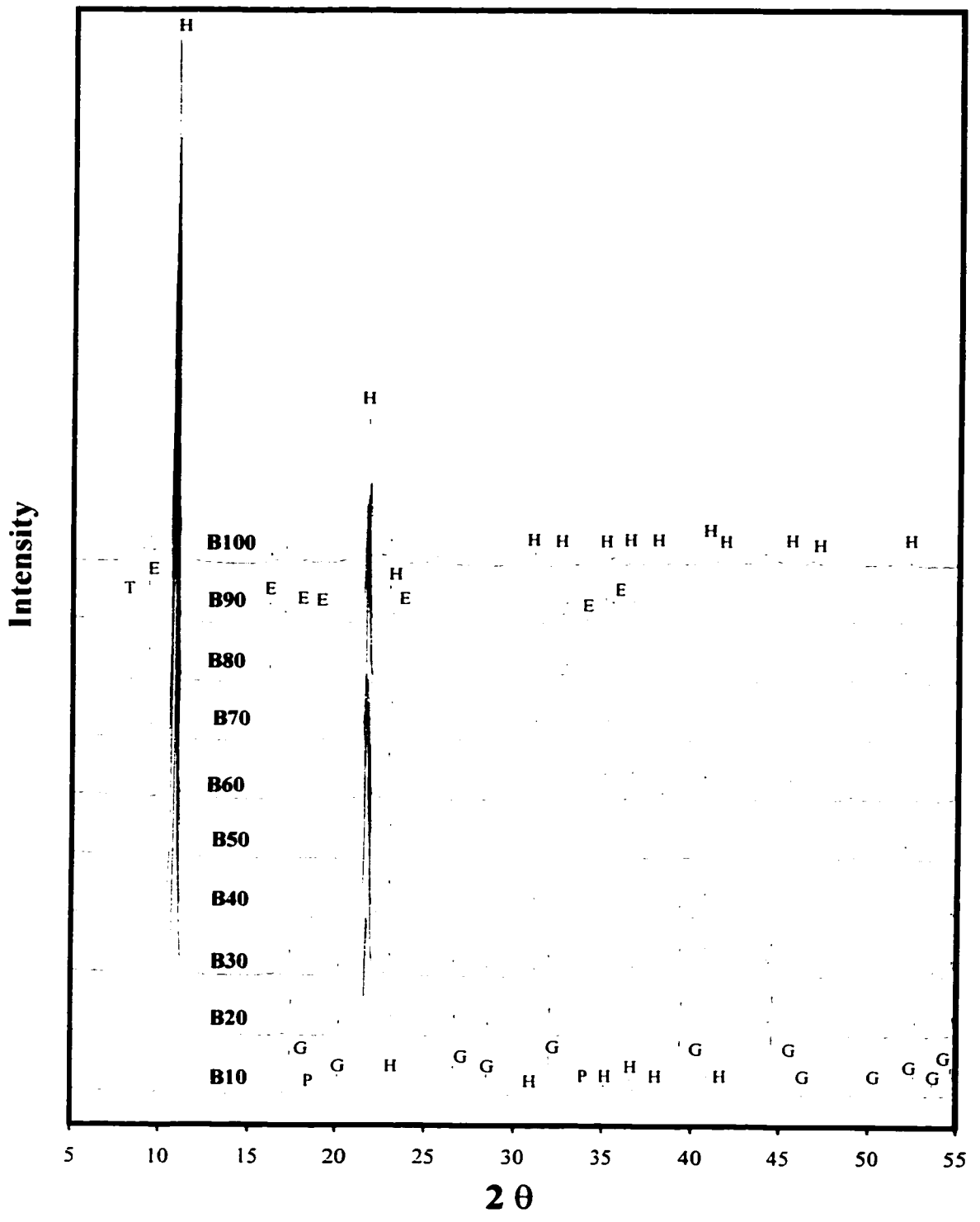

Figure 5.3: XRD patterns of the solids recovered from the borate solid solution series. H-hydrocalumite; G-hydrogarnet; E-ettringite; P-portlandite; T-highly hydrated hydrocalumite.

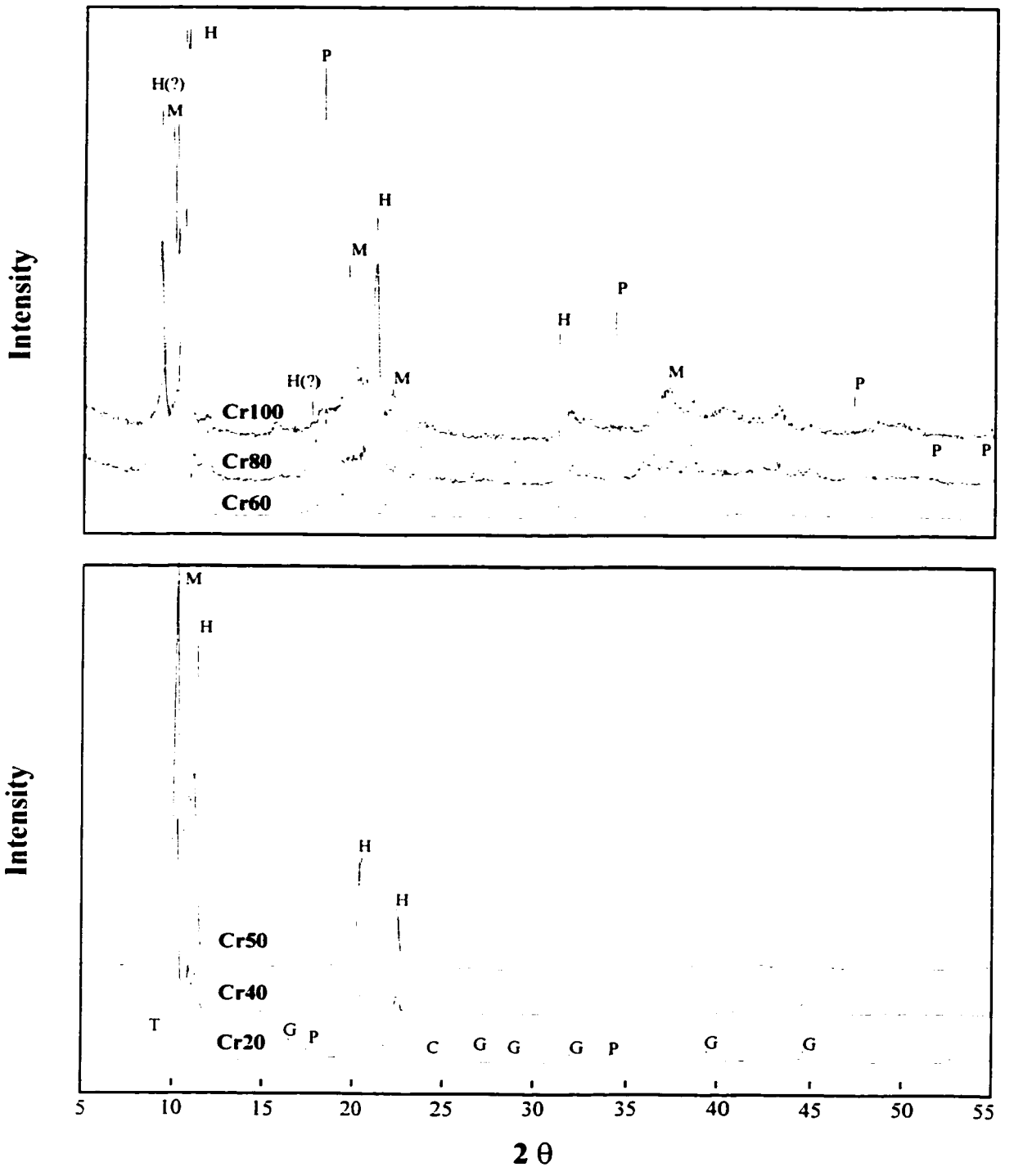

Figure 5.4: XRD patterns of the solids recovered from the chromate solid solution series. H-hydrocalumite; M-monosulfate; G-hydrogarnet; P-portlandite; T-highly hydrated hydrocalumite.

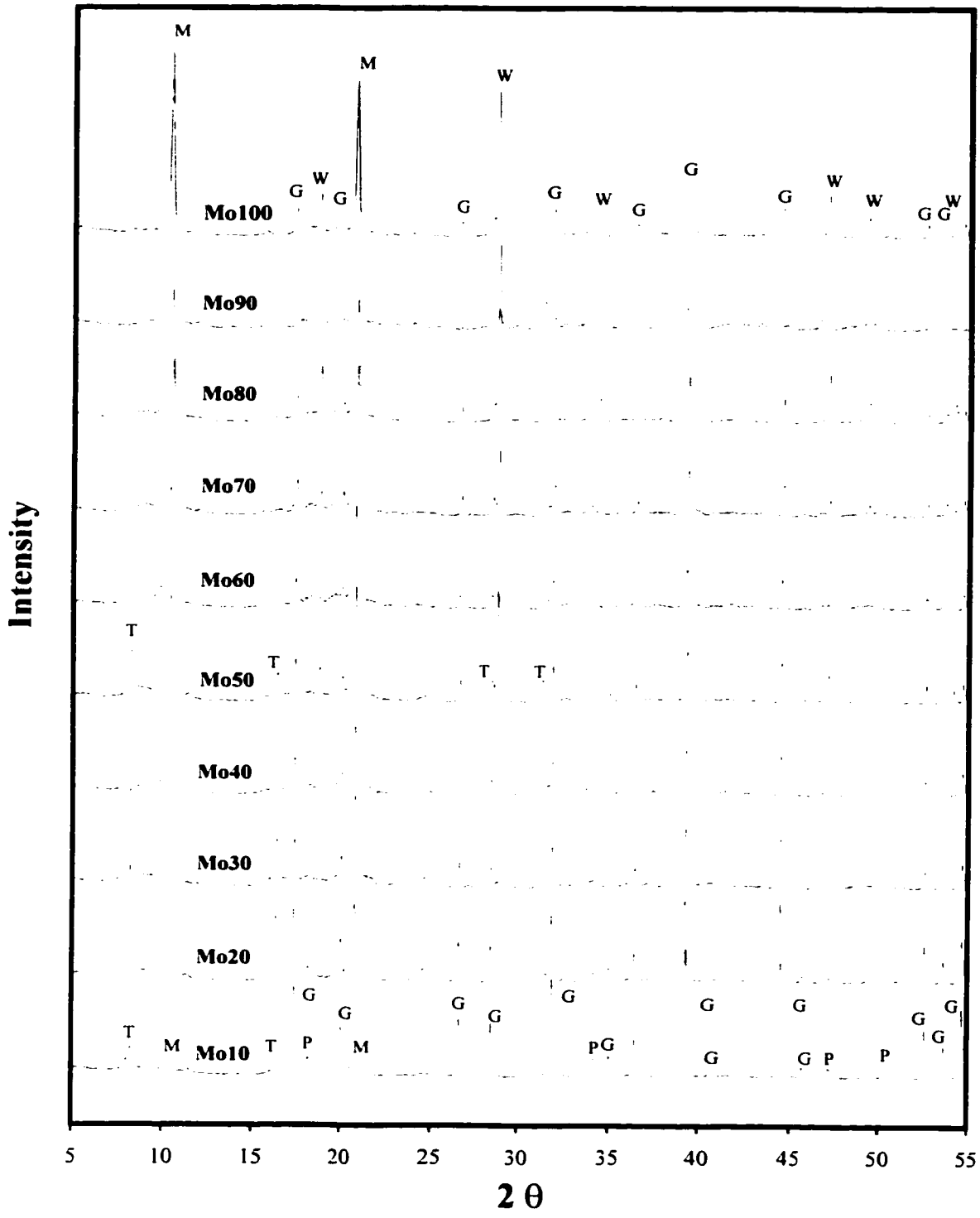

Figure 5.5: XRD patterns of the solids recovered from the molybdate solid solution series. M-monomolybdate; G-hydrogarnet; W-powellite; P-portlandite; T-highly hydrated hydrocalumite.

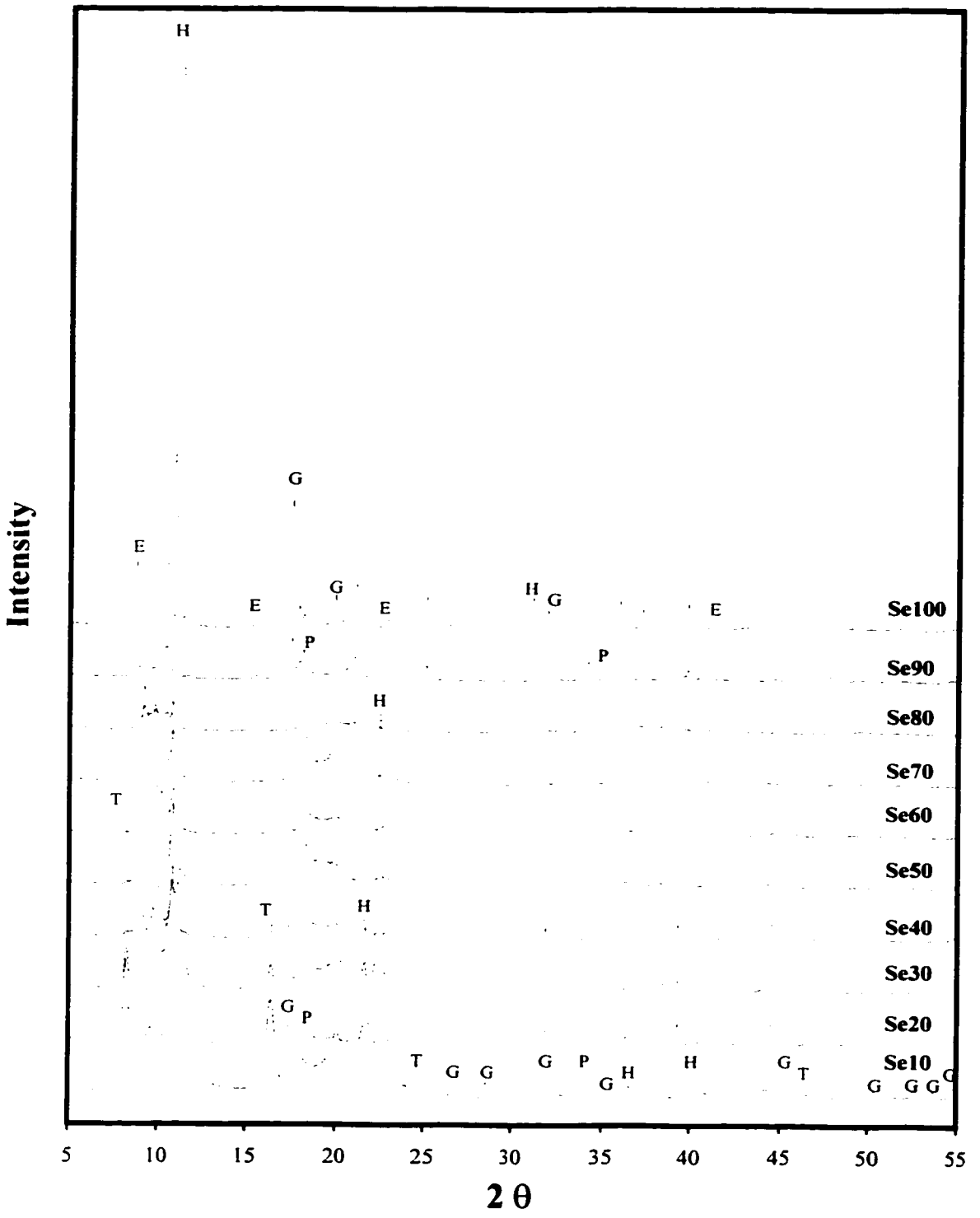

Figure 5.6: XRD patterns of the solids recovered from the selenate solid solution series. H-hydrocalumite (C_4AH_{13}); G-hydrogarnet; E-ettringite; P-portlandite; T-highly hydrated hydrocalumite.

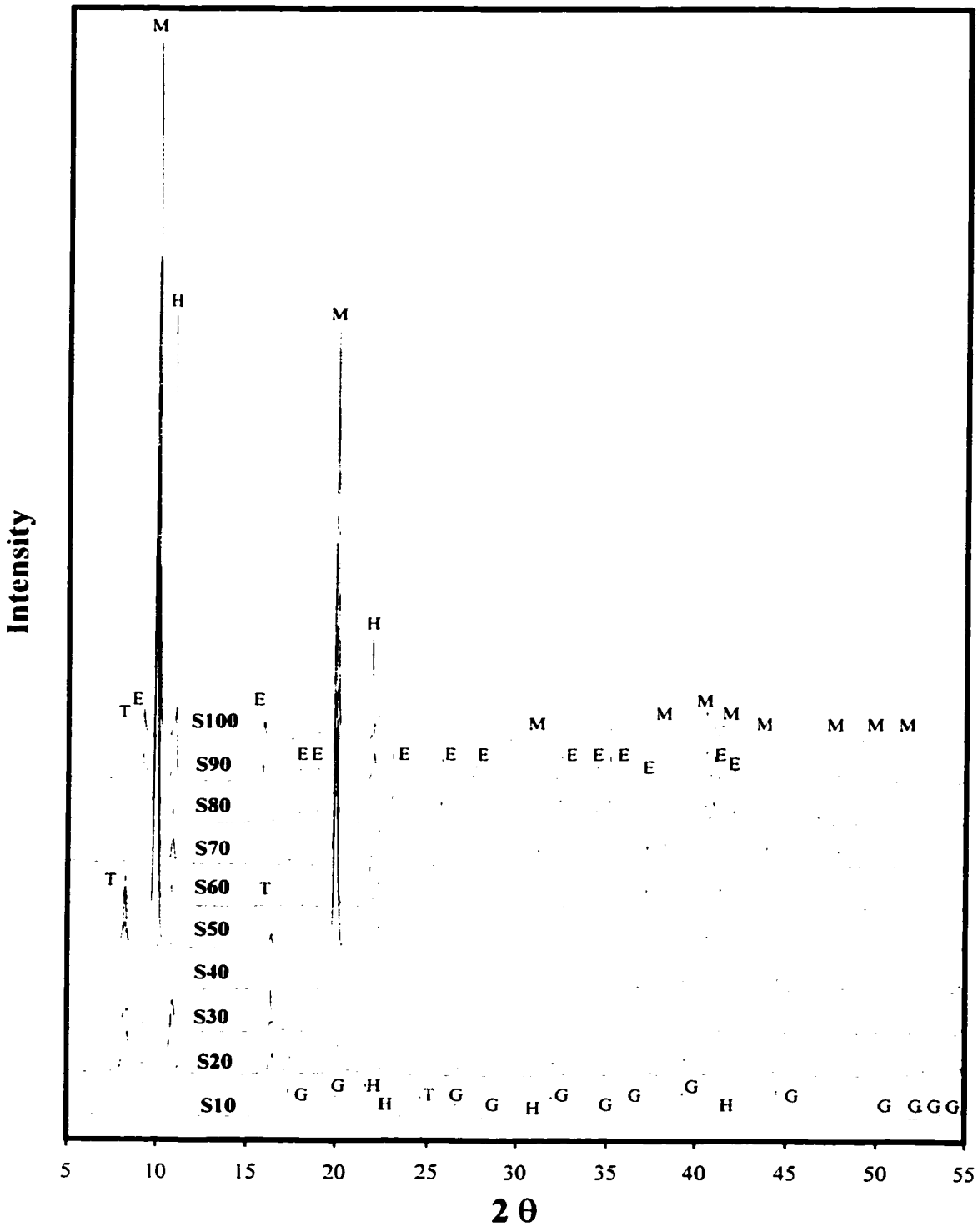

Figure 5.7: XRD patterns of the solids recovered from the sulfate solid solution series. H-hydrocalumite (C_4AH_{13}); M-monosufate; G-hydrogarnet; E-ettringite; P-portlandite; T-highly hydrated hydrocalumite.

The molybdate hydrocalumites had a very consistent d-spacing (around 8.5 Å) for the entire solid solution series (Figure 5.5). The XRD pattern of molybdate hydrocalumite is similar to that of monosulfate except for the lower d-spacing (8.5 vs. 8.9 Å). Highly hydrated hydrocalumite was present in most of the samples (Mo10 to Mo80). The d-spacing of 10.6 to 10.8 suggests that this phase is an OH-hydrocalumite. The peak intensities of this phase decreased with an increase in the molar percentage of molybdate, whereas the relative amount of molybdate hydrocalumite increased. Hydrogarnet was the dominant phase in sample Mo10. Hydrogarnet was present throughout the entire solid solution series, however, the relative amount decreased with an increase in the molar percentage of molybdate. The change in the amount of portlandite showed the same trend as hydrogarnet. Portlandite was not identified in samples Mo50 and higher. Powellite ($CaMoO_4$) was identified in all samples except for Mo10. A relatively high amount of powellite was observed in the samples above Mo50.

OH-hydrocalumite peaks were predominant in sample Se10, followed by hydrogarnet, and portlandite (Figure 5.6). Hydrogarnet showed a decrease in peak intensity with an increase in the molar percentage of selenate and was not seen in Se60. The precipitated hydrocalumite in this solid solution series exhibited miscibility gaps as indicated by peak splitting and broadening. These immiscible phases had a wide range of d-spacings varying from 7.9 to 9.5 Å. Hydrocalumite in this series had low peak intensities overall. Selenate ettringite was found at the high end (Se90 and Se100) and the amount increased greatly from Se90 to Se100. Selenate ettringite had a much larger d-spacing than sulfate ettringite (10.0 Å vs. 9.2 Å) as documented by Hassett *et al.* (1990). Hydrogarnet and portlandite were also observed in these two samples. Both phases only occurred in the low end of solid solutions for the other oxyanion series, except that portlandite was present in sample Cr80.

In the sulfate solid solution series, the major peak of hydrocalumite was always present as two splits with one close to OH-hydrocalumite (8.0 Å) and the other close to monosulfate (8.9 Å) (Figure 5.7). Overall, the relative amount of SO_4-rich phase increased and that of OH-hydrocalumite decreased with an increase in the molar percentage of sulfate. Sample S80, on the other hand, showed an opposite trend with the presence of high intensity OH-hydrocalumite peaks. Highly hydrated hydrocalumite phase was seen in most of the samples except for S70, S80, and S90. Hydrogarnet was present as low intensity peaks, and persisted up to S70. The relative intensity of hydrogarnet changed in a similar manner to the other series, decreasing with an increase in the molar percentage of sulfate. Ettringite formed at the high end of the solid solutions (from S80 to S100). The relative intensity was quite similar between S80 and S90, but lower in S100.

5.3.2.3 Summary of the XRD results

The solid solution series containing different oxyanions showed similar trends in their phase assemblages except for molybdate. In the OH endmember, the dominant phases are hydrogarnet and portlandite. OH-hydrocalumite (C_4AH_{13}) is present only as a minor phase. With the presence of an oxyanion, hydrocalumite became the dominant phase throughout the entire solid solutions. At the low end of the solid solutions (i.e. low anion content), hydrogarnet coexists with hydrocalumite. Portlandite is usually identified as well except in the sulfate series. The relative amount of hydrogarnet, however, decreases as the molar percentage of oxyanion increases. As hydrogarnet and portlandite are diminished around the middle of the solid solution series, the hydrocalumite solid solution phase(s) become the only identified solid(s). With higher anion content, ettringite forms along with hydrocalumite solid solution(s), and they become the new mineral assemblage. Some exceptions to these trends exist. For example, portlandite was seen at the high end of the chromate solid solutions. Both hydrogarnet and portlandite coexist with ettringite and hydrocalumite at the high end of selenate series. Molybdate solid solutions exhibited a different phase assemblage from the others. The starting material powellite was present in most of the samples, indicating the reaction had not reached completion. The presence of hydrogarnet persisted throughout the entire solid solutions series and the relative amount of hydrocalumite was low. No ettringite was found at the high end of the solid solution.

The precipitated hydrocalumite appeared either as a single solid solution phase (in the borate series) or as two or more immiscible solid solution phases (in the other series). In the XRD patterns of the chromate and selenate solid solution series, the principle peak of immiscible solid solutions exhibited either peak splitting or broadening with a wide range of d-spacings. In the molybdate and sulfate series, hydrocalumite occurred as two distinct solid solution phases with constant d-spacings: one close to the OH endmember and the other close to the oxyanion endmember. For all the immiscible solid solutions, it is generally observed that the OH-rich phase is dominant over the oxyanion-rich phase at the low end of the solid solutions. With an increase in the molar percentage of oxyanion, the order of dominance reverses.

5.3.3 Scanning electron microscopy and energy dispersive X-ray analysis

Selected solid samples were examined using SEM, and the micrographs are shown in Figures 5.8 to 5.12. Hydrogarnet occurs as isometric crystals. Hydrocalumite has a typical hexagonal or pseudohexagonal platey form, and ettringite is commonly present as needle-like

crystals. These phases can be recognized easily based on their morphology. The only difficulty encountered was that a series of hydrocalumite plates were sometimes piled together and showed only their edges, which gave them a needle-like appearance. So-called 'needle-like' hydrocalumite was documented by different authors (e.g. Steinour, 1951; Lea, 1970). Phase identification was assisted or further confirmed by the analysis of chemical compositions by EDX. Except for boron, all of the constituents in the solids can be detected using EDX analysis.

5.3.3.1 SEM/EDX examination

Sample OH1 consisted mainly of isometric hydrogarnet with crystal sizes varying from 1 to 10 μm (Figure 5.8A and C), some crystals showed a layered-growth feature (Figure 5.8B). Portlandite had an irregular appearance and occurred as precipitates on the surface of hydrogarnet crystals. A small percentage of hydrocalumite was also observed as single platey crystals (Figure 5.8A and C).

Hydrocalumite was the dominant mineral phase in sample B30. The crystals were mainly anhedral to subhedral plates (Figure 5.9A). Portlandite also appeared as plates similar to hydrocalumite and was identified with the assistance of EDX. Hydrogarnet was present as small octahedral and trapezohedral crystals (Figure 5.9B). Although no hydrogarnet was identified in sample B50 based on the XRD results, octahedral crystals of hydrogarnet were observed in this sample. The amount of this phase, however, only accounted for 1-2% of the total solids. In sample B60, hydrocalumite was the only phase observed. Most hydrocalumite crystals occurred as subhedral to euhedral plates (Figure 5.9C). Bladed aggregates of hydrocalumite were also observed (Figure 5.9D). In addition to hydrocalumite, needle-like ettringite crystals were prevalent in sample B90. Figure 5.9E shows a close spatial association of ettringite with hydrocalumite. Well-formed hexagonal hydrocalumite crystals can be seen in Figure 5.9F along with ettringite needles for sample B90.

Hydrocalumite in sample Cr20 occurred mainly as either hexagonal plates or plates with round edges. The crystal size was quite large, ranging from 20 to 50 μm. EDX analysis showed that the ratio of Ca:Cr in this phase varied from 4:0.1 to 4:0.6. Hydrogarnet appeared mainly as small octahedral crystals (around 1 μm). Figure 5.10A shows a hydrogarnet crystal that is a combination of an octahedron and a cube. Sample Cr80 consisted mostly of hydrocalumite crystals of different sizes. The crystals of hydrocalumite ranged from 1 to 20 μm and were subhedral to euhedral hexagonal plates (Figure 5.10B). The molar ratio of Ca:Cr in the hydrocalumite ranged from 4:0.8 to 4:1.0. Although large portlandite peaks were

shown in the XRD pattern, portlandite crystals were not often seen with SEM. This is probably due to its small crystal size and irregularly-shaped appearance. A variety of hydrocalumite morphologies were observed in sample Cr100. The hydrocalumite crystal in Figure 5.10C has a crystal form that is a combination of trigonal prisms and trigonal pyramids. Figure 5.10D shows a rhombohedral crystal (upper left) and a twin, and each half of the twin is a combination of a ditrigonal prism and a trigonal pyramid. Subhedral hydrocalumite crystals are shown in Figure 5.10E with a three dimensional appearance rather than plates. The typical thin hexagonal plates, however, were still seen occasionally in this sample (Figure 5.10F). The ratio of Ca to Cr in this sample was almost ideal at 4:1. No K was detected in the EDX spectra of the examined solids.

Two samples (Mo30 and Mo100) were examined from the molybdate solid solution series. Conspicuous octahedral crystals of hydrogarnet were present in sample Mo30 with a crystal size of approximately 1 μm (Figure 5.8D). Hydrogarnet was the dominant phase in this sample. Hydrocalumite appeared as round or hexagonal plates with the sizes ranging from 15 to 20 μm. The Ca to Mo ratio in the hydrocalumite crystals was about 4:0.8. In sample Mo100, hydrocalumite was the dominant phase. Hydrocalumite occurred as well-formed plates, with size ranging from 5 to 15 μm (Figure 5.8E and F). The molar ratio of Ca to Mo varied from 4:0.9 to 4:1, close to the endmember of molybdate hydrocalumite. Hydrogarnet crystals were also seen in this sample with octahedral, trapezohedral, and spherical forms.

In sample Se30, hydrocalumite typically occurs as large, subhedral to euhedral plates. The crystal size ranged from 20 to 80 μm (Figure 5.11A), and the molar ratio of Ca:Se varied from 4:0.3 to 4:0.5. Hydrogarnet crystals were plentiful in this sample with sizes varying from 0.2 to 5 μm, and most commonly occurred with an octahedral crystal form (Figure 5.11B). Hydrocalumite in sample Se70 was also present as plates in both hexagonal and round forms (Figure 5.11C). In this sample, rhombohedral crystals of hydrocalumite were also seen (Figure 5.11D). The Ca:Se ratio in the hydrocalumite was similar between different crystals, around 4:0.6. Although hydrogarnet was not identified from the XRD analysis of this sample, octahedral crystals were observed under SEM. The Ca/Al ratio in hydrogarnet was close to the ideal number of 3:2. Hydrocalumite crystals appeared as thick, well-formed hexagonal plates (Figure 5.11E). The Ca:Se ratio was around 4:1. The presence of ettringite was indicated from the XRD results. Typical needle-like crystals, however, were not seen in this sample. Ettringite also occurred as plates (Figure 5.11F), which has a Ca/Se ratio around 6:2. Na was not detected in any of the solid phases.

Figure 5.8: Micrographs of the solids recovered from the OH-hydrocalumite endmember and the molybdate solid solutions. (A) hydrogarnet crystals of various sizes in sample OH1; (B) layered-growth on the hydrogarnet crystal in sample OH1; (C) platey crystals and bladed aggregates of hydrocalumite in sample OH1; (D) octahedral hydrogarnet crystals in sample Mo30 (x8000); (E) Well-formed hexagonal hydrocalumite crystals in sample Mo100; (F) platey hydrocalumite and spherical form of hydrogarnet in sample Mo100.

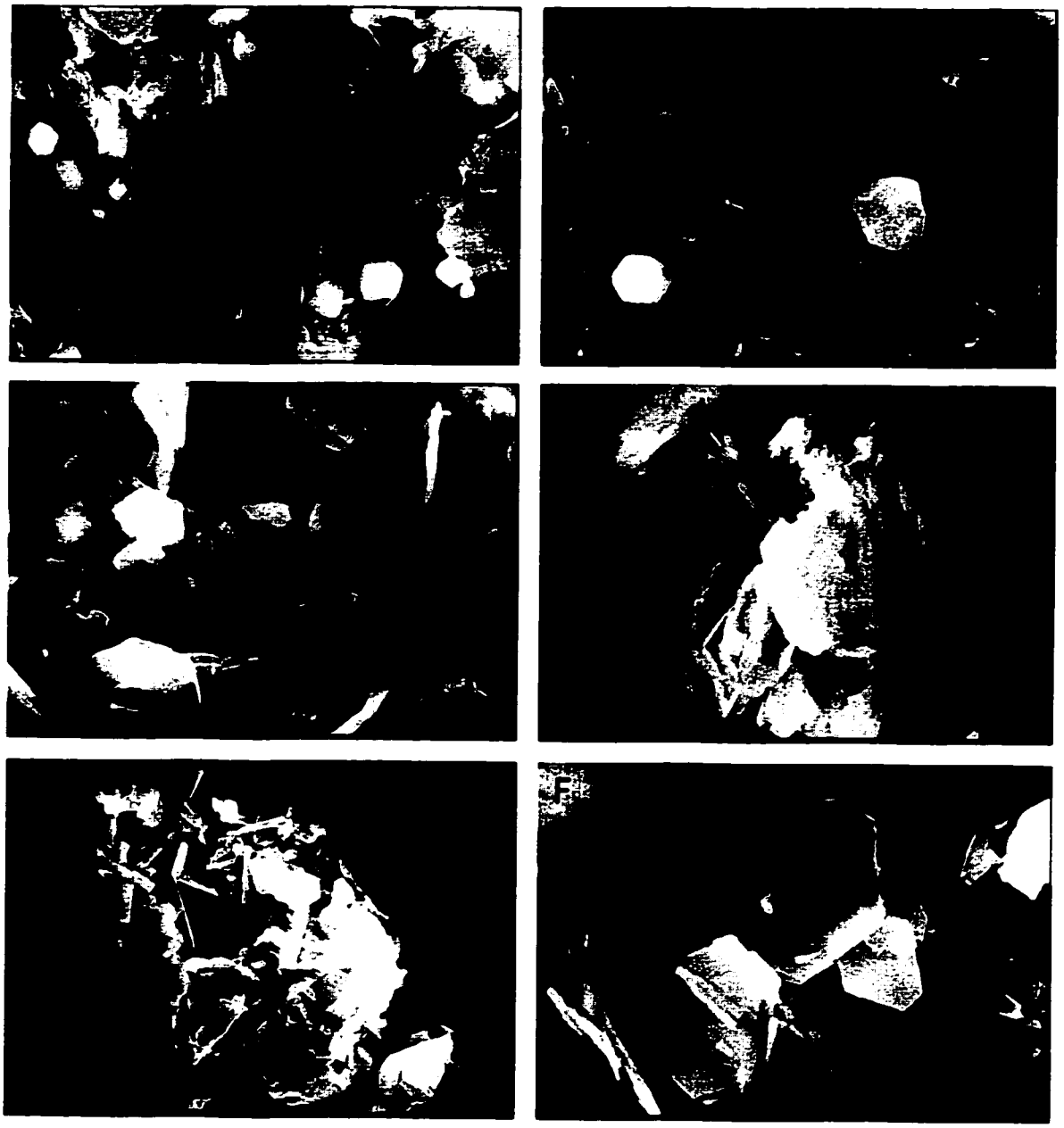

Figure 5.9: Micrographs of the solids recovered from the borate solid solutions. (A) anhedral to subhedral hydrocalumite plates in sample B30 (x7000); (B) octahedral and trapezohedral hydrogarnet crystals in sample B30 (x9000); (C) subhedral to hexagonal hydrocalumite in sample B60 (x5000); (D) bladed aggregates of hydrocalumite in sample B60 (x8000); (E) needle-like ettringite and hexagonal hydrocalumite in sample B90 (x3500); (F) well-formed hexagonal hydrocalumite plates and needle-like ettringite crystals in sample B90 (x4500).

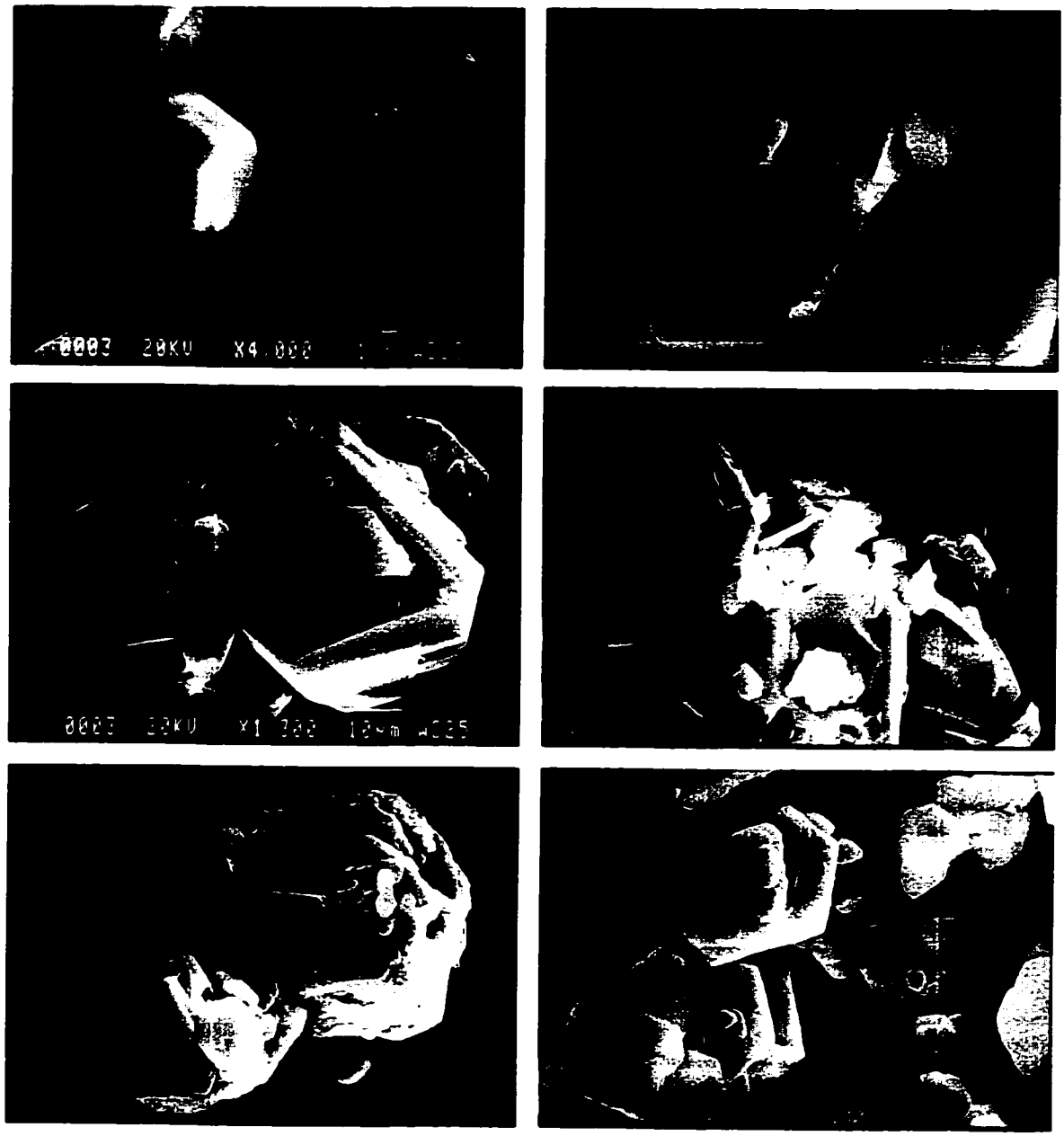

Figure 5.10: Micrographs of the solids recovered from the chromate solid solutions. (A) a hydrogarnet crystal (combination of a cube and a octahedron) in sample Cr20; (B) well-formed hydrocalumite plates of various sizes in sample Cr80 (x3500); (C) hydrocalumite crystals (combination of trigonal prisms and pyramids) in sample Cr100; (D) hydrocalumite -- a rhombohedral crystal (upper left) and a twin (middle) in sample Cr100 (x3000); (E) round hydrocalumite crystals in sample Cr100 (x1900); (F) hexagonal hydrocalumite plates in sample Cr100 (x1400).

Figure 5.11: Micrographs of the solids recovered from the selenate solid solutions. (A) hydrocalumite subhedral crystals in sample Se30; (B) octahedral hydrogarnet crystals in sample Se30; (C) round or hexagonal hydrocalumite plates in sample Se70; (D) rhombohedral hydrocalumite crystals in sample Se70; (E)Well-formed hydrocalumite plates of various sizes in sample Se100 (x600); (F) thick plates of selenate ettringite (upper left) in sample Se100 (x3000).

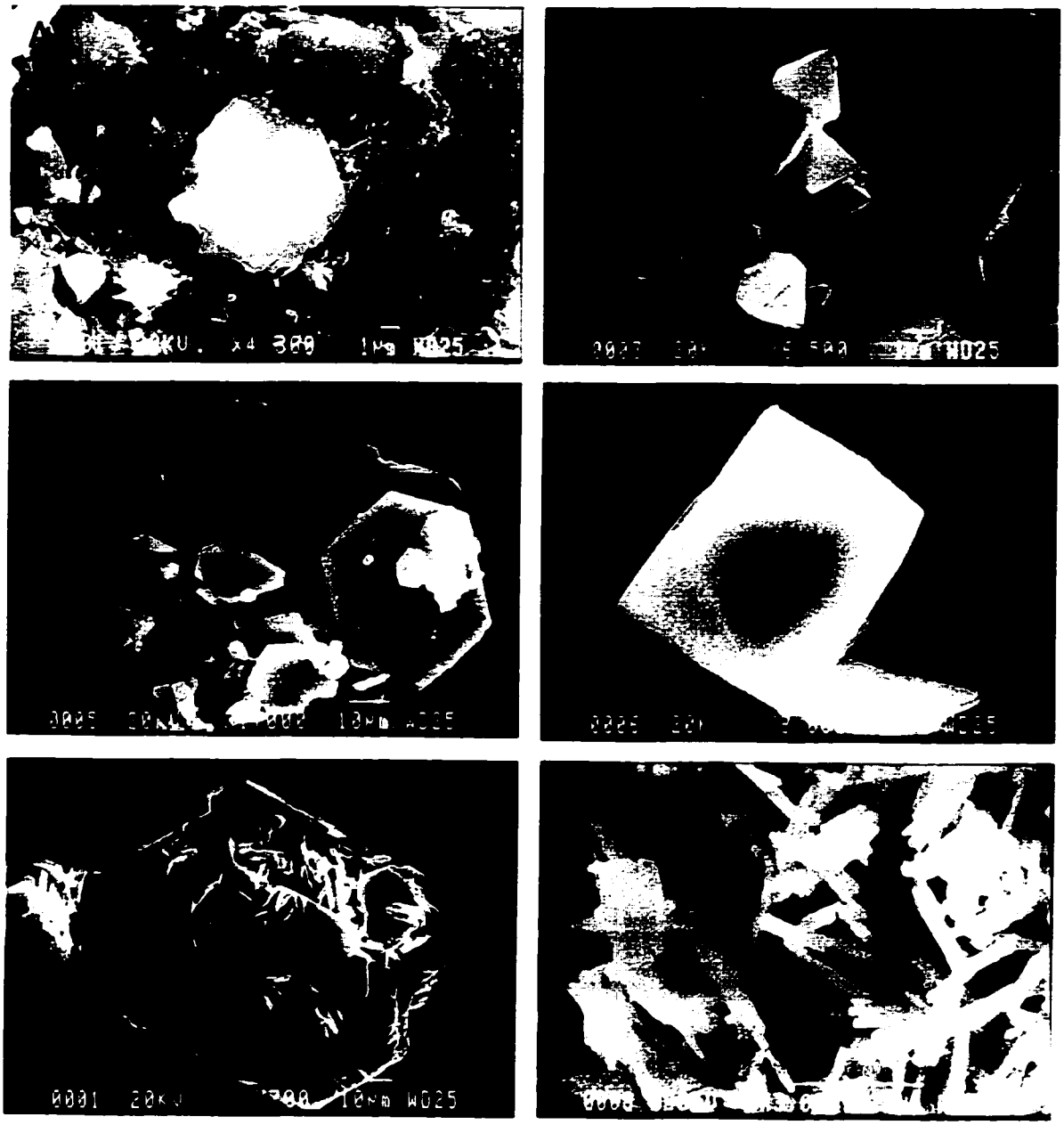

Figure 5.12: Micrographs of the solids recovered from the sulfate solid solutions. (A) anhedral to subhedral hydrocalumite plates in sample S30; (B) octahedral hydrogarnet crystals in sample Se30; (C) well-formed hydrocalumite crystals of various sizes in sample S70; (D) octahedral hydrogarnet crystal in sample S70; (E) thick, hexagonal hydrocalumite plates and needle-like ettringite crystals in sample S100; (F) needle-like ettringite crystals in sample S100.

In sample S30, hydrocalumite was mainly present as anhedral to subhedral plates of approximately 10 μm in size (Figure 5.12A). The Ca:S ratio varied from 4:0.3 to 4:0.5. Although hydrocalumite occurred as two immiscible solid solution phases as shown in the XRD results, there was no indication of the presence of two different hydrocalumites either morphologically or compositionally. Hydrogarnet was present as individual, well-formed octahedral crystals with sizes from 0.5 to 2 μm (Figure 5.12B). In sample S70, hydrocalumite was present in a well-crystallized hexagonal crystal form with a variety of crystal sizes, ranging from over 100 μm to less than 1μm (Figure 5.12C). In this sample, hydrogarnet crystals of about 8 μm in size were seen (Figure 5.12D). Hydrocalumite occurred as thick, well-formed hexagonal plates in S90. The crystal size of hydrocalumite was quite uniform, being approximately 100 μm (Figure 5.12E). The molar ratio of Ca:S in the hydrocalumites of both S70 and S90 was very close to 4:1. In sample S90, a large quantity of needle-like ettringite crystals with lengths of approximate 10 μm were present (Figure 5.12E and F). The ettringite showed an ideal stoichiometric ratio of 6:2:3 for Ca, Al and S.

5.3.3.2 Summary of the SEM/EDX results

There are several trends observed for the abundance and crystal habit of the hydrocalumite in all the solid solution series. The amount of oxyanion hydrocalumite increased from the low end of solid solutions to the high end just before the occurrence of ettringite. The crystal size of hydrocalumite also usually increased in the same direction. It was observed that many small hexagonal crystals (<1 to 5 μm) were precipitated on the surface of large hexagonal crystals (50 to 100 μm) at the high end of the solid solutions. The degree of crystallinity of hydrocalumite also increased with an increase in the molar percentage of anions. Hydrocalumite was generally precipitated as anhedral to subhedral plates at the low end of solid solutions and crystallized as well-formed hexagonal plates at the high end. The crystal form also changed from thin plates to thick plates, rhombohedra, and trigonal prisms (more equant or 3-dimensional in appearance). This is especially true for the chromate and selenate solid solution series. Compositionally, it was found that the anions were usually enriched in hydrocalumite, i.e. the molar ratio of anion to calcium was higher than what was expected.

Ettringite occurred as needle-like crystals with lengths varying from 2 to 10 μm. It formed only at the high end of the solid solutions and was conspicuously present in borate and sulfate solid solutions. Instead of a typical needle-like crystal form, ettringite in the selenate solid solution samples occurred as thick plates. Identification of this phase was based on EDX analysis. Hydrogarnet crystals were predominantly octahedral, however, other

crystal forms, such as trapezohedron, were also seen. At the high end of the Mo solid solution series, hydrogarnet was also present as spheres. The crystal size of hydrogarnet was commonly between 1 and 5 μm. The molar ratio of Ca/Al was close to the ideal ratio of 3:2. B, Cr, Mo, Se, and S were not detected in hydrogarnet. Portlandite was observed only occasionally due to its low abundance in the samples.

5.3.4 Solution composition and geochemical modeling

The compositions of all solution samples were analyzed and the results are presented in Tables 5.1 to 5.6. Systematic changes in the concentrations of calcium and aluminum were seen in these solid solution series. Overall, calcium concentrations decreased with an increase in the molar percentage of oxyanion, whereas the concentration of aluminum increased. The concentrations of oxyanions were generally low at the low end of the series. Compared to the other oxyanions, boron concentration was nearly two orders of magnitude higher at the low end. Boron concentration showed a gradual increase from the low end of the solid solutions to the high end. The concentrations of chromate and selenate, however, remained relatively constant at the low end and increased abruptly near the high end. Molybdenum concentration showed no systematic variation throughout the entire solid solutions. In the sulfate solid solutions, only the samples at the high end (S80 to S100) had the sulfate concentrations above detection. Generally, pH values decreased slightly with an increase in the molar percentage of oxyanion for all the solid solution series.

Table 5.1: Solution compositions of OH hydrocalumite (mmolal)

Sample ID	Ca	Al	pH
OH1	23.48	0.1207	12.16
OH2	22.48	0.1444	12.64

Ion activities used to calculate saturation indices (SI) of the potential precipitates were calculated using the geochemical model SIMUL (Reardon, 1990; 1992). Because thermodynamic data for the oxyanion-bearing hydrocalumites are not available, the prediction was based only on OH-hydrocalumite. In the database, solubility data for OH-hydrocalumite was cited from the experimental results of Wells *et al.* (1943). The saturation

indices (SI) calculated for hydrogarnet, OH-hydrocalumite, portlandite, and gibbsite for each solid solution series are plotted in Figure 5.13.

Table 5.2: Solution compositions of (B, OH) solid solutions (mmolal)

Sample ID	Ca	Al	B	pH
B10	25.39	0.1129	0.1961	12.53
B20	19.12	0.2667	0.4120	12.42
B30	14.18	0.4574	0.5140	11.79
B40	10.96	1.650	0.5771	12.25
B50	9.217	2.670	1.690	11.56
B60	10.46	2.654	5.984	11.61
B70	10.98	2.323	7.772	11.96
B80	10.59	2.378	9.630	11.82
B90	12.24	2.608	9.655	11.60
B100	11.45	2.323	8.998	11.58

Table 5.3: Solution compositions of (Cr, OH) solid solutions (mmolal)

Sample ID	Ca	Al	Cr	K	pH
Cr20	18.20	0.1526	0.0012	16.88	13.10
Cr40	12.31	0.2266	0.0014	33.00	13.16
Cr50	8.955	0.4290	0.0011	39.73	12.71
Cr60	6.419	0.7420	0.0010	45.81	13.19
Cr80	7.229	0.0189	0.1696	65.45	13.30
Cr100	1.719	0.1319	1.922	80.13	12.97

Table 5.4: Solution compositions of (Mo, OH) solid solutions (mmolal)

Sample ID	Ca	Al	Mo	pH
Mo10	22.52	0.1297	0.0070	12.64
Mo20	22.94	0.1247	0.0038	12.63
Mo30	23.02	0.1321	0.0073	12.57
Mo40	22.09	0.0849	0.0073	12.55
Mo50	16.68	0.2279	0.0056	12.47
Mo60	15.08	0.2962	0.0043	12.45
Mo70	11.35	0.8114	0.0052	12.33
Mo80	11.10	0.8325	0.0062	12.33
Mo90	8.176	2.405	0.0070	12.14
Mo100	8.625	2.182	0.0059	12.16

Table 5.5: Solution compositions of (Se, OH) solid solutions (mmolal)

Sample ID	Ca	Al	Se	Na	pH
Se10	21.07	0.1315	<0.0025	8.136	12.67
Se20	17.60	0.1726	<0.0025	15.93	12.71
Se30	13.83	0.2421	<0.0025	24.38	12.72
Se40	10.70	0.2684	0.0035	32.21	12.73
Se50	7.478	0.4817	0.0030	39.58	12.49
Se60	4.797	0.7214	0.0070	45.56	12.76
Se70	3.817	0.8043	0.0176	60.03	12.82
Se80	2.903	1.051	0.0342	65.92	12.56
Se90	7.134	0.0208	1.283	64.16	12.91
Se100	7.028	0.0208	1.268	71.57	12.84

Table 5.6 Solution compositions of (S, OH) solid solutions (mmolal)

Sample ID	Ca	Al	S	pH
S10	21.12	0.0955	<0.0020	12.62
S20	19.12	0.2910	<0.0020	12.43
S30	17.22	0.2557	<0.0020	12.44
S40	15.39	0.5302	<0.0020	12.50
S50	13.57	0.4995	<0.0020	12.46
S60	11.16	0.9759	<0.0020	12.35
S70	10.80	0.5170	<0.0020	12.38
S80	12.90	0.1469	0.0087	12.46
S90	11.44	0.2146	0.0093	12.41
S100	6.037	1.450	0.0071	11.87

Some similarities in the SI patterns are observed between the borate, molybdate, and sulfate solid solution series. The chromate and selenate series also showed close trends to each other, in which alkalis (either K or Na) were present. The presence of alkali is probably responsible for the similarities between these two solid solutions.

In the borate, molybdate and sulfate series, hydrogarnet had a positive SI value throughout the entire solid solutions. The SI of OH-hydrocalumite generally decreased with an increase in the molar percentage of oxyanion. At the high end of the solid solution series, the solutions became undersaturated with this phase. In these solid solutions, saturation or near saturation with respect to portlandite was only reached at the low end. The SI values of portlandite decreased with an increase in the molar percentage of oxyanion. Gibbsite showed an opposite trend to portlandite. The solutions were saturated with this phase at the high end of these solid solutions. It is noted that the SI of powellite was close to zero, within the range of uncertainty, for all of samples in the molybdate solid solution series, indicating that the solubility of powellite controls the Mo concentration. In addition, saturation indices above zero were calculated for both monosulfate and ettringite in the samples between S80 and S100.

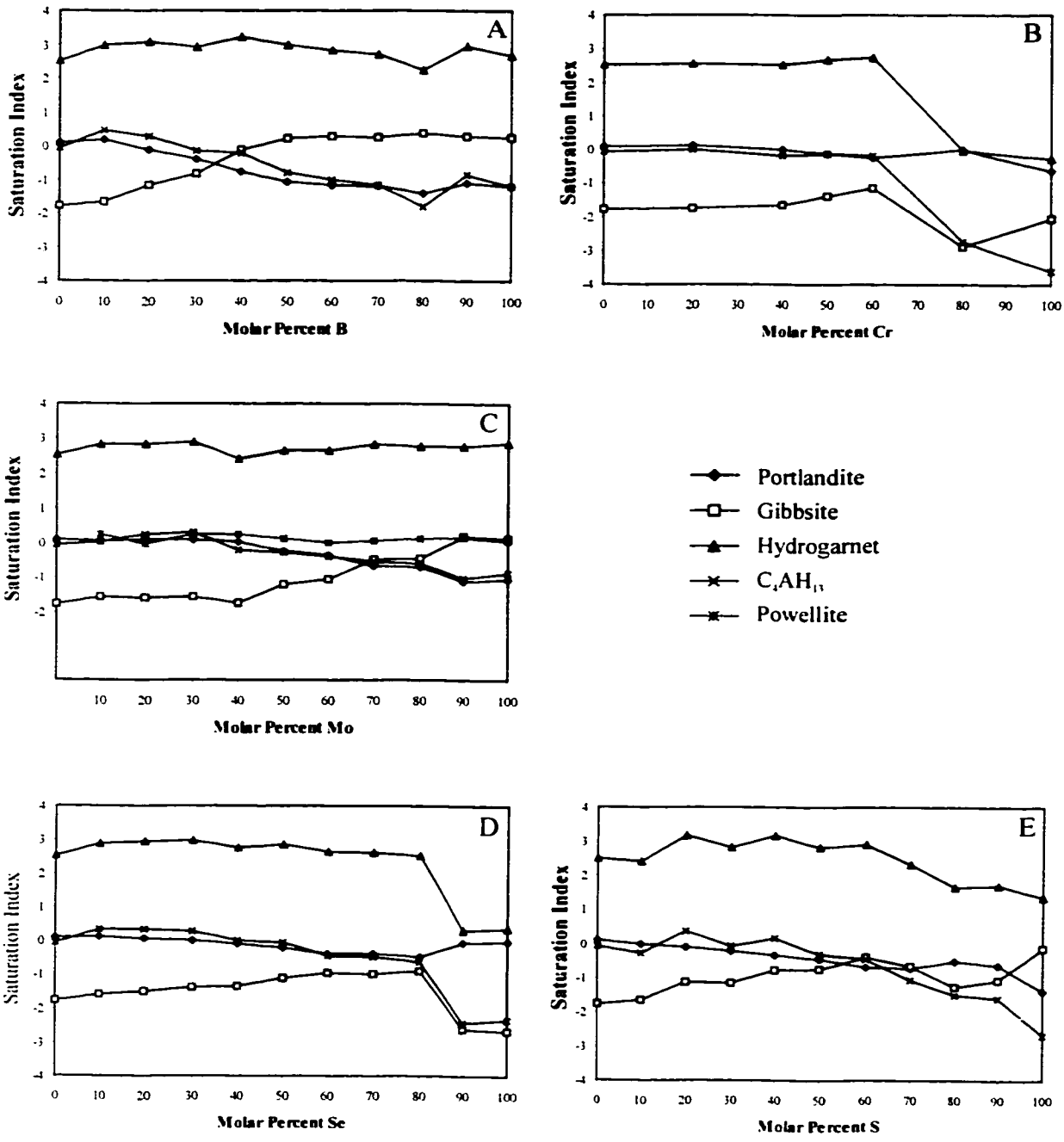

Figure 5.13:Saturation index vs. the predicted molar percent of oxyanion in the solid solution series. (A) the borate solid solutions; (B) the chromate solid solutions; (C) the molybdate solid solutions; (D) the selenate solid solutions; (E) the sulfate solid solutions.

The variation in SI value was very consistent between hydrogarnet and OH-hydrocalumite in the chromate and selenate series. The SI values for these two phases remained constant up to sample Cr60 and Se80 for the chromate and selenate series, respectively. In these samples, supersaturation and saturation was attained for hydrogarnet and OH-hydrocalumite, respectively. A sharp decrease in SI occurred at the high end of the solid solutions. The solution then became nearly saturated with respect to hydrogarnet and undersaturated with respect to OH-hydrocalumite. Portlandite was saturated from the low end to sample Cr80. In selenate solid solution series, portlandite was near saturation at both low and high ends. In both series, gibbsite always remained undersaturated. The saturation of portlandite and gibbsite is influenced by the presence of the alkali (Na or K), which increases the solution pH. This in turn, decreases the solubility of portlandite and increases the solubility of gibbsite.

5.3.5 Evolution of the solid phases

Phase evolution from the OH endmember to the oxyanion endmember has been determined based mainly on XRD results. XRD analysis, although a powerful tool for solid phase identification, is unable to detect phases which are amorphous in form, or phases which constitute less than 5% of the sample. SEM examination, supplemented by EDX analysis, can provide some additional information on the phase assemblage, e.g. to identify the presence of crystalline hydrogarnet when its mass is less than 5%. Predictions based on thermodynamic calculations of the SI values can also be used to support the identification of solid phases. The modeling results are mainly used to suggest the possible presence of gibbsite, which was not directly identified by XRD analysis and SEM examination. The existence of portlandite was also considered using the SI data as portlandite was present at low quantity and may not be detectable by XRD analysis.

Figure 5.14 illustrates the range of persistence of the various solid phases over each solid solution series based on all lines of evidence (XRD, SEM, EDX, and chemical modeling). It is a subjective schematic rather than a quantitative representation of the phase present.

5.4 Discussion

The pure CaO-Al_2O_3-H_2O system, i.e. OH-hydrocalumite endmember, will be addressed first in the following sections. With the presence of each oxyanion, a quaternary

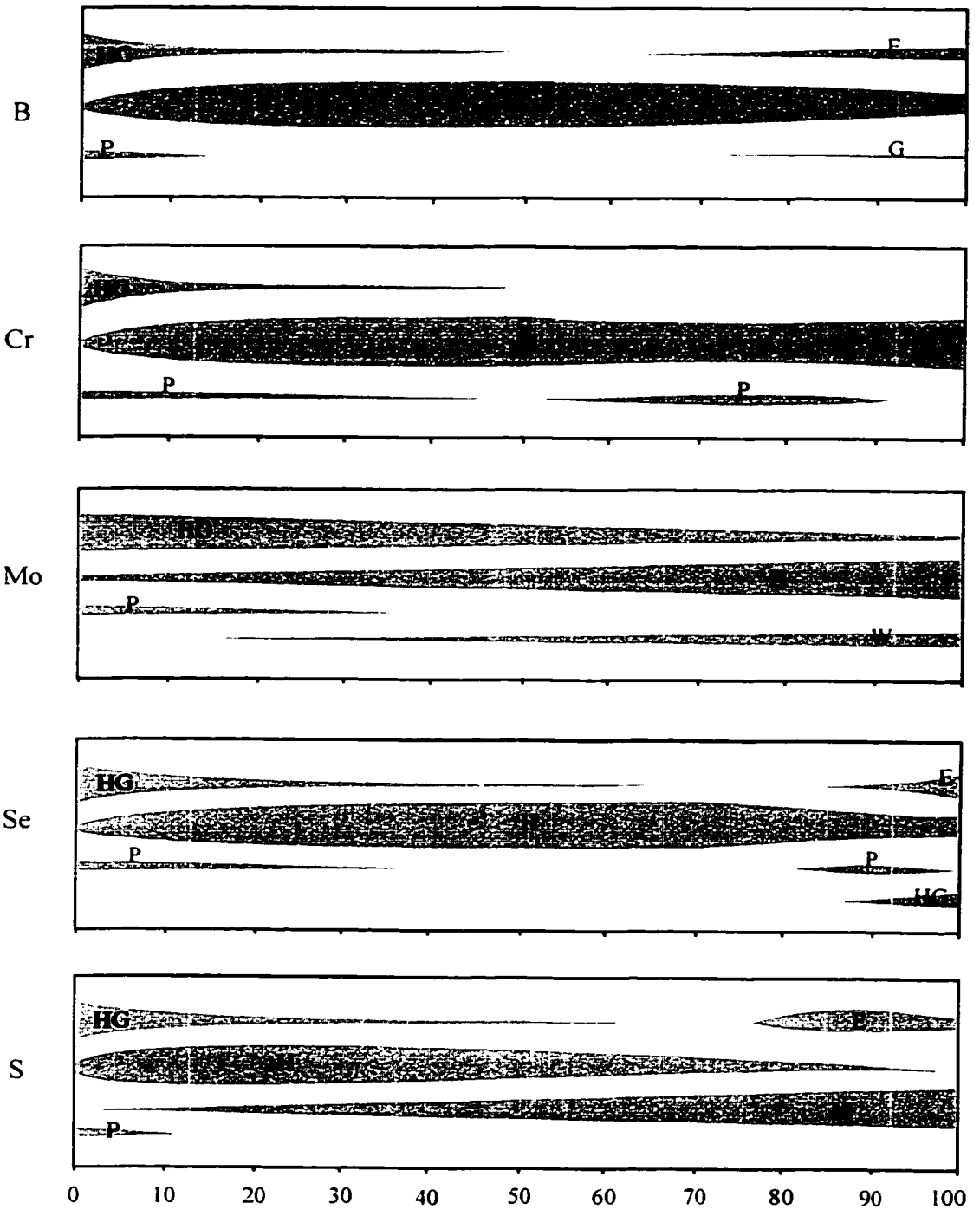

Figure 5.14: A schematic representation of phase assemblage in the borate, chromate, molybdate, selenate, and sulfate series. HG- hydrogarnet; H-hydrocalumite; M-monosulfate; P-portlandite; E-ettringite; G-gibbsite; W-powellite.

system $CaO\text{-}Al_2O_3\text{-}XO_3/Y_2O_3\text{-}H_2O$ is generated. The solid solution series of borate, chromate, molybdate, selenate, and sulfate will be discussed as quaternary systems. Common properties of the different systems are summarized in the section entitled 'Interrelationship between the systems', followed by a discussion of environmental applications and the implications of this study to cement chemistry.

5.4.1 $CaO\text{-}Al_2O_3\text{-}H_2O$ system

The XRD results demonstrate that hydrogarnet (C_3AH_6), portlandite, and OH-hydrocalumite (as both C_4AH_{13} and C_4AH_{19}) are present in this system after over one year of reaction. C_4AH_{13} and C_4AH_{19} should be regarded as one phase because C_4AH_{13} is derived from C_4AH_{19} by dehydration. The coexistence of hydrogarnet, portlandite, and OH-hydrocalumite indicates a long-term metastable condition, and that equilibrium had not been attained at the termination of the experiment.

The phase rule predicts that one of the three phases (hydrogarnet, portlandite, and hydrocalumite) must be converted at equilibrium. The predominance of hydrogarnet over the long term implies that this is a stable phase. It has been recognized that C_4AH_{13} is a metastable phase with respect to C_3AH_6 at room temperature (e.g. Wells*et al*, 1943; Roberts, 1957). Steinour (1951) reported conversion of C_4AH_{13} to hydrogarnet with time. Literature reviews on thermodynamic equilibria also reveal that hydrogarnet is the only stable calcium aluminate hydrate in the system $CaO\text{-}Al_2O_3\text{-}H_2O$ at room temperature (Jones, 1960; Taylor, 1961; Turriziani, 1964). In addition to hydrogarnet, the thermodynamically stable compounds in this system include portlandite ($Ca(OH)_2$) and gibbsite ($\gamma\text{-}Al_2O_3{\cdot}3H_2O$). Under the present experimental conditions (initial $CaO/Al_2O_3 = 4$), precipitation of gibbsite is not possible. It is likely that a supersaturated solution with respect to OH-hydrocalumite was generated from the dissolution of $CaAl_2O_4$ in lime solution. OH-hydrocalumite precipitated initially and transformed to hydrogarnet with time. This transformation can be described by the reaction:

$$Ca_4Al_2(OH)_{12}(OH)_2{\cdot}6H_2O \rightarrow Ca_3Al_2O_6{\cdot}6H_2O + Ca(OH)_2 + 6H_2O \qquad (5.1)$$

This reaction implies that portlandite may also precipitate as a decomposition product of hydrocalumite. In fact, portlandite was identified in the solids. At equilibrium, hydrocalumite should be completely converted to hydrogarnet and portlandite, which is ultimately the stable mineral assemblage.

Although OH-hydrocalumite is a metastable phase, successful synthesis of this phase has been achieved by many investigators. There are three main factors affecting the kinetics of the transformation reaction: temperature, lime content (or CaO/Al_2O_3 ratio), and water/solid ratio. Kinetically, low temperatures, e.g. 5 °C, favor the formation and preservation of metastable hydrocalumite (Glasser *et al.*, 1999). Buttler *et al.* (1959) prepared large crystals of C_4AH_{13} up to 50 μm by hydrating C_2A in strong lime water for 200 days at 5 °C. In contrast, at temperatures above 100 °C, tetracalcium aluminate hydrates only exists momentarily (Peppler and Wells, 1954). Preparation of C_4AH_{13} is usually conducted in lime water, i.e. portlandite-saturated solution (Lea, 1970). At low lime contents, other metastable phases, such as C_2AH_8, become dominant. When the CaO/Al_2O_3 ratio = 3, pure hydrogarnet is generated at room temperature within two weeks (Thorvaldson and Grace, 1929). Large w/s ratios and mixing also promote the conversion of C_4AH_{13} to hydrogarnet. In contrast, OH-hydrocalumite conversion is largely inhibited by the low w/s ratios used in cement paste.

The present study indicates that the reaction kinetics are very slow for the conversion of hydrocalumite to hydrogarnet. The transformation was not complete after over one year of reaction, although it probably started shortly after the formation of hydrocalumite. Atkins *et al.* (1991) observed that small amounts of hydrogarnet and portlandite existed in the reaction of C_3A with CaO (CaO/Al_2O_3 = 4, w/s = 1) after only two weeks. Many authors have reported the persistence of OH-hydrocalumite in aqueous solutions after long reaction times (Jones, 1960; Taylor, 1961; Turriziani, 1964). The formation of hydrogarnet by conversion from metastable hydrocalumite is likely by a 'through-solution mechanism', involving the dissolution of C_4AH_{13} and the crystallization of C_3AH_6 from solution. The solution composition is determined by the dissolution reaction. In the solution, the concentration of aluminum was low, approximately 5 ppm. Low Al concentration could be the limiting factor on the rate of transformation because precipitation of hydrogarnet requires the removal of Ca and Al at a stoichiometric ratio of CaO/Al_2O_3 = 3, whereas in the solution, the CaO/Al_2O_3 ratio was approximately 80 and 100 in samples OH1 and OH2, respectively.

After long reaction times, the solution becomes saturated with respect to OH-hydrocalumite by the removal of excess Ca and Al from the initially supersaturated solution. Because the formation of hydrogarnet is a very slow process, saturation with respect to hydrocalumite, and consequently supersaturation with respect to hydrogarnet are always maintained in the solution. Precipitation of hydrogarnet triggers the further dissolution of hydrocalumite to reestablish equilibrium. The analytical solution composition data, therefore, can be used to calculate the solubility product of hydrocalumite. By incorporating the solution composition into SIMUL, a solubility product (Log K_{sp}) of -25.35 ± 0.20 was calculated for OH-hydrocalumite ($Ca_4Al_2(OH)_{12}(OH)_2 \cdot 6H_2O$). The free energy value

calculated for this phase is -7336.14 ± 1.14 kJ·mol^{-1}. The uncertainties were estimated based on the maximum analytical uncertainty of 5%. Using the experimental data obtained for this phase at 21 °C by Wells *et al.* (1943), Log K_{sp} of -25.63 ± 0.15 was calculated, in agreement with the value calculated in the current study.

5.4.2 CaO-Al_2O_3-B_2O_3-H_2O system

5.4.2.1 Coordination of borate in hydrocalumite

The coordination of borate in the structure of hydrocalumite is important to determine the chemical formula of the borate hydrocalumite solid solution. In solutions with a pH value above 9.8, borate occurs as tetrahedral $B(OH)_4^-$. In the high pH solutions examined in this study, $B(OH)_4^-$ is the dominant species. When borate is incorporated into a mineral, the coordination of borate can persist or can be changed depending on the structural environment of the host mineral. For example, borate has been shown to occur in trigonal and tetrahedral coordinations in calcite and aragonite structures, respectively (Sen *et al*, 1994). Incorporation of anions into hydrocalumite, an anionic clay mineral, is usually described as an ion-exchange reaction. During the exchange process, it is assumed that no changes occur in the coordination of the anion. Based on these considerations, tetrahedral $B(OH)_4^-$ was assumed to be present in hydrocalumite, and the experiment was designed accordingly. An ongoing literature search, however, later revealed that the coordination of borate in the structure of hydrocalumite was determined experimentally by Wenda and Kuzel (1986). Based on the IR spectrum, borate was found to be trigonally-coordinated in hydrocalumite. Divalent HBO_3^{2-} was proposed as the anion existing in the interlayer of the hydrocalumite structure. Given that borate occurs as HBO_3^{2-}, only half of the designed molar percentage is needed in order to maintain charge balance in the hydrocalumite structure. The endmember in the borate solid solution of hydrocalumite would therefore occur in sample B50.

5.4.2.2 Formation of the solid phases

Four different phase assemblages developed as the concentration of borate was progressively increased. At the low end of the solid solution series (sample B10), the precipitates consisted of borate hydrocalumite solid solution, hydrogarnet, and portlandite. Over the compositional range B20 to B40, the mineral assemblage consisted of borate hydrocalumite and hydrogarnet. In B50 and B60, only borate hydrocalumite was observed. At higher borate contents (samples B70 and above), a new phase assemblage was identified with

borate hydrocalumite and borate ettringite as the dominant phases. Borate hydrocalumite was the dominant mineral phase thorough out the entire series.

In samples B10 to B40, the formation of hydrogarnet, however, means that the amount of hydrocalumite precipitated was less than expected. As a result, the molar percentage of borate was higher in the structure of the hydrocalumite solid solution than initially calculated. From reaction 5.1, the transformation to hydrogarnet is accompanied by the precipitation of portlandite. In the samples that showed the presence of hydrogarnet (B10 to B40), however, portlandite was only identified in sample B10 from the XRD patterns (Figure 5.3) and the modeling results (Figure 5.13). When only a small percentage of hydrocalumite converts to hydrogarnet, precipitation of portlandite may not occur due to the large w/s ratio used and relatively high solubility of portlandite. Under these conditions, the solution phase can accommodate the extra Ca^{2+} and OH^- ions without precipitating portlandite.

The two intermediate samples B50 and B60 are pure borate hydrocalumite by XRD measurements. SEM evidence, however, shows that approximately 1-2% hydrogarnet was present in sample B50. Ignoring the presence of hydrogarnet, the quantities of the starting materials used to prepare the solid solution allows a calculation of the composition of the borate hydrocalumite. After subtracting the solution composition for Ca, Al and B, the molar ratios of Ca/Al and Ca/B in borate hydrocalumite were calculated to be 4:2.05 and 4:1.02. These ratios are in agreement with the borate hydrocalumite endmember (Ca/Al = 4:2 and Ca/B = 4:1) suggested by Wenda and Kuzel (1986). These authors also presented a formula of $Ca_4Al_2(OH)_{12}(HBO_3)\cdot 5.5H_2O$ for this endmember using the measured water content. The overall formation reaction of borate hydrocalumite endmember is then:

$$CaAl_2O_4 + 3CaO + 0.5B_2O_3 + 12H_2O \rightarrow Ca_4Al_2(OH)_{12}(HBO_3)\cdot 5.5H_2O \qquad (5.2)$$

Using a similar approach for sample B60, the Ca/B ratio was calculated to be 4:1.12. This ratio indicates a higher borate content than that of the borate hydrocalumite endmember. Alternately, another solid phase containing borate such as borate ettringite may be present.

At higher borate concentrations (samples above B60), borate ettringite was identified in addition to borate hydrocalumite. Pöllmann *et al.* (1989, 1993) characterized the endmember of borate ettringite and proposed a formula of $Ca_6Al_2(OH)_{12}[B(OH)_4]_4[OH]_2\cdot 24H_2O$ for this phase. In borate ettringite, $B(OH)_4^-$ occupies 2/3 of the anionic sites and OH^- occupies 1/3 of the anionic sites. The ratio of Ca/Al is 3.0 in ettringite, and therefore, precipitation of this phase requires an Al-bearing phase as a product in order to balance the

reaction. Chemical modeling of the solution composition indicates that the solution was saturated with respect to gibbsite. This phase, however, was not observed in the XRD patterns. This is probably due to its low percentage, or its poor crystallinity (alumina gel instead of crystalline gibbsite). The constant B concentration between B80 and B100 may indicate that an invariant point has been reached, where borate hydrocalumite, borate ettringite and gibbsite coexist.

5.4.2.3 Free energy of borate hydrocalumite and borate ettringite

After two months of reaction, the conductance values remained stable for the duration of the experiment over 9 months. Constant conductance values suggest that saturation with respect to borate hydrocalumite and borate ettringite was attained. Using the solution composition for sample B50, where the borate hydrocalumite endmember is essentially the only phase present (over 98%), the free energy of the borate endmember of hydrocalumite ($Ca_4Al_2(OH)_{12}(HBO_3)\cdot 5.5H_2O$) can be derived. Assuming congruent dissolution, the reaction can be written as:

$$Ca_4Al_2(OH)_{12}(HBO_3)\cdot 5.5H_2O \rightleftarrows 4Ca^{2+} + 2Al(OH)_4^- + B(OH)_4^- + 5OH^- + 3.5H_2O \qquad (5.3)$$

The solubility product for the borate hydrocalumite endmember is defined as:

$$K_{sp} = [Ca^{2+}]^4\cdot[Al(OH)_4^-]^2\cdot[B(OH)_4^-]\cdot[OH^-]^5\cdot[H_2O]^{3.5}$$

Using SIMUL, the solubility product for borate hydrocalumite was calculated to be Log $K_{sp} = -27.31 \pm 0.21$. Analytical uncertainty was used to estimate the uncertainties in the K_{sp} values. Using the calculated K_{sp} and thermodynamic database assembled in SIMUL by Reardon (1990, 1992) for the constituent ions, the free energy of formation ($\Delta G°_{f,\,298}$) of the borate hydrocalumite endmember was calculated to be -7750.42 ± 1.20 kJ·mol^{-1}. The derived K_{sp} was then used to calculate the saturation indices of borate hydrocalumite in samples B10 to B40. They varied from –0.30 to 0.03 (very close to zero), indicating that the borate hydrocalumite solid solutions have similar solubility products.

The anionic sites are fully occupied by borate in sample B50. Further addition of borate should result in a sharp increase in the solution borate concentration until saturation with respect to another borate mineral occurs. This appears to occur around B60 (see Table 5.2), which is likely the first sample where borate ettringite existed. Borate ettringite was identified in B70 and the amount continued to increase through B100. The uniform B

concentrations in the solutions of samples B80 to B100 are likely due to the occurrence of an invariant point. At the invariant point, the solution composition is uniquely defined by three phases: borate hydrocalumite, borate ettringite, and gibbsite. The free energy and solubility product can be calculated for borate ettringite using the solution compositions measured in these three samples. Taking the ettringite precipitated in these samples as the endmember with the formula of $Ca_6Al_2(OH)_{12}[B(OH)_4]_4[OH]_2 \cdot 24H_2O$, the dissolution reaction can be written as:

$$Ca_6Al_2(OH)_{12}[B(OH)_4]_4[OH]_2 \cdot 24H_2O \rightleftarrows 6Ca^{2+} + 2Al(OH)_4^- + 4B(OH)_4^- + 6OH^- + 24H_2O \qquad (5.4)$$

The solubility product for the borate ettringite endmember is defined as:

$$K_{sp} = [Ca^{2+}]^6 \cdot [Al(OH)_4^-]^2 \cdot [B(OH)_4^-]^4 \cdot [OH^-]^6 \cdot [H_2O]^{24}$$

Using SIMUL, a value of -17408.22 ± 4.34 kJ·mol^{-1} was obtained for the free energy of borate ettringite, and the corresponding Log K_{sp} is -39.98 ± 0.76 (± 2 S.D.). Using the derived free energy data for borate hydrocalumite, borate ettringite and the free energy for gibbsite, the solution composition at the triple point can be calculated. The predicted data are tabulated in Table 5.7. For comparison, the average measured concentrations from B80 to B100 are also present as the 'measured' data. There are only small differences which may arise from the assumption of the presence of gibbsite. Amorphous alumina gel is probably the actual phase present, which would result in higher predicted Al and lower Ca concentrations in solution.

Table 5.7: A comparison of predicted and measured solution compositions (mmolal).

Source	Ca	Al	B	pH
Predicted	12.1	1.27	11.5	11.94
Measured	11.4	2.44	9.43	11.67

5.4.3 $CaO-Al_2O_3-CrO_3-K_2O-H_2O$ system

5.4.3.1 Mineral phase assemblage

Similar to the borate series, chromate hydrocalumite was the dominant phase in the solid solution series. In samples Cr20, 40 and 50, chromate hydrocalumite, hydrogarnet and portlandite coexisted. At higher molar percentages of chromate, only chromate hydrocalumite was observed, except in sample Cr80, which also contained portlandite. Chromate hydrocalumite occurred as more than one solid solution phase throughout the series, as shown by peak splitting in the XRD patterns. Generally, the peak intensity of the OH-rich phase was high at the low end of the series and decreased approaching the high end. EDX analysis revealed a large variation in the molar percentage of chromate in the hydrocalumites precipitated in these samples, e.g. ranging from 10 to over 60% in sample Cr20. This indicates that solid solutions of hydrocalumite with various compositions exist as separate crystals. At the high end, the molar percentage of chromate in hydrocalumite was relatively constant. Hydrocalumite was found to contain approximately 100% chromate in sample Cr100, although the XRD results showed the presence of more than one phase. The occurrence of chromate hydrocalumite as two or more solid solution phases does not allow the calculation of thermodynamic parameters from these data.

The d-spacing of the chromate hydrocalumite varied from 7.9 for the OH-rich to 9.6 Å for the CrO_4-rich solid solutions. Kuzel (1969) determined a d-spacing of 8.97 Å for the chromate hydrocalumite endmember based on a single crystal measurement. The chemical formula of this chromate endmember was given as $Ca_4Al_2(OH)_{12}(CrO_4)\cdot 6H_2O$. Perkin and Palmer (unpublished) determined a d-spacing of 10.3 Å for the highly hydrated chromate hydrocalumite. By analog to monosulfate, they proposed a formula of $Ca_4Al_2(OH)_{12}(CrO_4)\cdot 9H_2O$ for this phase. These two studies consistently suggest that chromate hydrocalumite has a similar d-spacing to monosulfate (8.97 Å) and to its highly hydrated form (10.3 Å). The reason for the discrepancy in the d-spacing measured in this study, and those determined by Kuzel (1969) and Perkin and Palmer (unpublished) is unclear. However, the discrepancy may be related to the fact that potassium chromate was used in this study, whereas calcium chromate was used in the other two studies.

Chromate ettringite was not identified in this solid solution series. This may indicate that the hydrocalumite structure has a high affinity to accommodate CrO_4^{2-}, or that chromate is not favored by ettringite. Chloride shows a similar structural affinity for hydrocalumite but not for ettringite (Höglund, 1992). For chromate, its large size and distorted tetrahedral geometry (see Section 4.4.2) probably lead to a poor fit in the ettringite structure.

Alternatively, the presence of high alkalis (in the form of K^+) may stabilize hydrocalumite. However, ettringite occurred in the selenate series, although Na was present. By comparison, it seems that it is the chromate, rather than the presence of alkali in solution, that is responsible for stabilizing hydrocalumite in the chromate series.

5.4.3.2 Uptake of chromium

The experiments in which chromate hydrocalumite solid solutions were synthesized, demonstrate that hydrocalumite has a large potential to remove chromate anions from contaminated waters. The chromate uptake by hydrocalumite is calculated for different chromate concentrations and is tabulated in Table 5.8. Calculation of the amount of hydrocalumite was made by assuming that chromate hydrocalumite solid solution was the only solid phase present and it contained the ideal amount of chromate. These assumptions overestimate the quantity of hydrocalumite because other phases (hydrogarnet and portlandite) were present. As a result, the uptake capacity of hydrocalumite may be slightly underestimated.

Table 5.8: Cr uptake by hydrocalumite vs. final Cr concentration ($H_2O/(CaAl_2O_4+CaO)$ ratio $\approx$ 75:1).

Sample ID	Original Cr Concentration (ppm)	Final Cr Concentration (ppm)	Uptake Capacity (mg/kg)
Cr20	416	0.06	18050
Cr40	832	0.08	35080
Cr50	1039	0.06	43230
Cr60	1248	0.05	51190
Cr80	1664	8.82	66100
Cr100	2080	99.9	77050

Uptake capacity of up to 50000 mg/kg has been achieved in the samples from Cr 20 to Cr60. In the coexisting solution samples, the concentration of chromium was reduced to less than 0.08 ppm, where the original Cr concentration ranged from over 400 to 1250 ppm. This demonstrates that hydrocalumite has not only a high uptake capacity, but is also capable

of reducing the Cr concentration level to below the drinking water standard (0.1 ppm). The maximum capacity of hydrocalumite to take up Cr is calculated to be over 77000 mg/kg from the experiments.

5.4.4 $CaO-Al_2O_3-MoO_3-H_2O$ system

5.4.4.1 Characterization of the system

There are three characteristics of the phase assemblages observed in this system that are unique: (1) Hydrogarnet exists throughout the entire series instead of being present only at the low end of the solid solution; (2) Powellite ($CaMoO_4$) was identified in the XRD patterns of most of the samples and was predicted to be present in all of the samples based on the geochemical modeling, whereas in the other series hydrocalumite and ettringite were the only oxyanion-bearing phases; and (3) The presence of molybdate in the structure of hydrocalumite stabilizes hydrocalumite as do the other anions, but the range of stable solid solution is much more limited.

Molybdate hydrocalumite occurred as a single solid solution phase with a relatively constant d-spacing of approximately 8.6 Å. Highly hydrated OH-hydrocalumite was also present (d-spacing of 10.6 to 10.8 Å) in all samples except Mo90 and Mo100. The molybdate hydrocalumite was a minor phase at the low end of the series, and became the dominant phase of samples Mo40 and above. The molar percentage of molybdate in molybdate hydrocalumite ranges between 80 and 100%. This is consistent with the constant d-spacing observed. Although other oxyanions were enriched in hydrocalumite at the low end of the solid solutions, an enrichment of 80% is unusually high. Molybdate hydrocalumite was also synthesized by Kindness *et al.* (1994). The molar percentage of molybdenum in their prepared hydrocalumite was reported to be 92%, close to the molybdate endmember. Under different drying conditions, two phases of molybdate hydrocalumite were identified with the d-spacing of 8.70 Å and 10.25 Å for $Ca_4Al_2(OH)_{12}(MoO_4)\cdot 4H_2O$ and $Ca_4Al_2(OH)_{12}(MoO_4)\cdot 8H_2O$, respectively. The d-spacing of the lower water content phase was close to the molybdate hydrocalumite obtained in this study.

5.4.4.2 Why does this system behave differently?

Some portion of molybdate occurred as powellite when the reaction was terminated. The existence of powellite indicates that the reaction was not complete after one and a half

years. Equilibrium was not reached as indicated by the coexistence of four phases (hydrogarnet, portlandite, molybdate hydrocalumite, and powellite) in the system. The low solubility of powellite could be a limiting factor responsible for the incomplete reaction. Other compounds of low solubility such as calcite, however, show much faster reaction kinetics. Carbonate hydrocalumite could be readily formed using calcite as the carbonate source. No calcite is identified by XRD analysis in the paste of C_3A ($3CaO \cdot Al_2O_3$) and 25% calcite after 3 days (Ramachandran and Zhang, 1986). The fast kinetics of carbonate hydrocalumite formation are probably related to the fact that carbonate is greatly preferred by the structure of hydrocalumite (see Section 4.4.3). Incorporation of carbonate ions into hydrocalumite, in turn, induces the dissolution of calcite. Compared with carbonate hydrocalumite, the formation of molybdate hydrocalumite appears to be difficult. If this is the case, the driving force for dissolving powellite will be small. The difficulties of forming (MoO_4, OH)-hydrocalumite solid solution are probably explained by the large difference in both geometry and anionic size between molybdate and hydroxyl (see Section 4.4.3).

The limited solid solution may be due to incompatibility between molybdate and hydroxyl. The results of this study show that only high percentages of MoO_4^{2-} can stabilize the structure of hydrocalumite. When 80% or more of the anionic sites are occupied by molybdate, a stable solid solution forms. As a result, large quantities of hydrogarnet were produced at the low end of the solid solution. The presence of powellite also accounts for the large quantity and persistence of hydrogarnet in this series. When the starting materials are mixed initially, the precipitates likely consist of OH-rich solid solution, due to the low solubility of powellite. If molybdate can not readily enter the structure to stabilize hydrocalumite, the initially precipitated OH-hydrocalumite will convert to hydrogarnet. Once hydrogarnet forms, the unreacted powellite is less likely to be used to produce molybdate hydrocalumite. A long-term metastable condition is then maintained.

5.4.5 CaO-Al_2O_3-SeO_3-Na_2O-H_2O system

5.4.5.1 Mineral phase assemblage

Selenate hydrocalumite was the dominant mineral phase in this solid solution series. At the low end of the series, hydrogarnet and portlandite were present, in addition to selenate hydrocalumite. In samples Se40 to Se70, hydrogarnet and selenate hydrocalumite were present, however, in sample Se80, only selenate hydrocalumite was observed. Four phases were observed at the high end of the solid solution series: selenate hydrocalumite, selenate ettringite, hydrogarnet and portlandite.

Similar to the chromate solid solution series, a variety of (SeO_4, OH) - hydrocalumite phases formed with d-spacing ranging from 7.9 for an OH-rich to 9.5 Å for a SeO_4-rich hydrocalumite, with the OH-rich solid solution dominant at the low end. At the high end, a selenate hydrocalumite endmember with a molar percentage of selenate close to 100% was generated. Literature on selenate hydrocalumite is not available. However, a comparison with SO_4-hydrocalumite endmember can be made due to the similarities in the anionic radius between selenate and sulfate. Selenate has larger ionic radius than sulfate (2.43 vs. 2.30 Å). As a result, the d-spacing of selenate hydrocalumite might be slightly larger than that of SO_4-hydrocalumite (8.9 Å). However, the highest d-spacing measured in this study (9.5 Å) seems too large for selenate hydrocalumite endmember. This deviation in d-spacing also occurred in the chromate solid solution series. Considering the sample preparation for these systems, it is likely the presence of alkali in solution that causes the occurrence of a wide range of d-spacings.

Selenate ettringite was identified in samples Se90 and Se100 from the XRD patterns. The d-spacing of selenate ettringite is larger than that of sulfate ettringite (10.0 vs. 9.2 Å). Hassett *et al* (1993) also observed the peak shift from high 2θ to low 2θ angle as more selenate was accommodated. The needle-like crystal form, which is typical of ettringite, was not seen using SEM. Instead, there was no obvious difference in morphology between selenate ettringite and selenate hydrocalumite. Jones (1938) also documented that no needle crystals were seen in the preparation of selenate ettringite.

5.4.5.2 Uptake of selenium

The Se uptake by hydrocalumite was calculated based on the same assumptions made for the chromate series (Table 5.9). Selenate hydrocalumite was assumed to occur as a single solid solution phase with an ideal molar percentage of selenate in its structure. In the entire series, water/solid ($H_2O/CaAl_2O_4$+CaO) ratio was maintained at approximately 75:1. The concentration of selenium was less than 0.2 ppm in the samples Se30 and below, where the highest original Se concentration was approximately 950 ppm. When the original concentration was in the range from 1250 to 2500 ppm, the residual Se solution concentration increased from 0.3 to approximately 3 ppm. Within this range, selenate hydrocalumite solid solutions were the solid phases accommodating Se. The residual Se concentration in solution was constant at 100 ppm in samples Se90 and Se100, where selenate ettringite coexisted with selenate hydrocalumite. It is likely that the solubility of selenate ettringite controlled the Se concentration in these samples. Due to the fact that selenate ettringite formed at the high end,

a larger uptake capacity for the solid products could be expected if the initial Se concentration was higher than that in sample Se100. In this case, more selenate ettringite would form to take up the additional selenate.

Table 5.9: Se uptake by hydrocalumite vs. final Se concentration ($H_2O/(CaAl_2O_4+CaO)$ ratio $\approx$ 75:1)

Sample ID	Original Se Concentration (ppm)	Final Se Concentration (ppm)	Uptake Capacity (mg/kg)
Se10	316	<0.2	13840
Se20	631	<0.2	27140
Se30	948	<0.2	39960
Se40	1264	0.28	52300
Se50	1579	0.23	64170
Se60	1891	0.55	75650
Se70	2210	1.39	86780
Se80	2526	2.70	97440
Se90	2839	101	104090
Se100	3159	100	114210

5.4.6 $CaO-Al_2O_3-SO_3-H_2O$ system

As one of the most important systems in cement chemistry, the formation and transformation of the solid phases in the system $CaO-Al_2O_3-SO_3-H_2O$ have been the subject of extensive research. In addition to a large body of original work, the literature on this subject has been reviewed by many authors (e.g. Steinour, 1951; Jones, 1960; Taylor, 1961; Turriziani, 1964; Lea, 1970; Taylor, 1990). Examination of the previous work, however, reveals contradictory presentations related to two fundamental questions: (1) Is there a partial solid solution between sulfate and hydroxyl hydrocalumite? (2) Could a SO_4-hydrocalumite endmember or a (SO_4, OH)-hydrocalumite solid solution (i.e. AFm phase in cement notation) be a stable phase under certain conditions? These questions will be addressed in the following section. Conclusions will be drawn based on both previous studies and the results from the present investigation.

5.4.6.1 Solid solution of (SO_4, OH)-hydrocalumite

At the low end of the solid solution series, hydrocalumite, hydrogarnet and portlandite were present (sample S10). Hydrocalumite and hydrogarnet were observed in samples between S20 to S70. At higher sulfate contents, hydrocalumite, and ettringite were the only phases directly observed. Hydrocalumite exists as two immiscible phases throughout the entire sulfate solid solution series. Peak splitting occurred with the longer basal spacing close to the sulfate endmember (8.9 Å) and the lower one close to the hydroxyl endmember (7.9 Å). With an increase in the molar percentage of SO_4^{2-}, the peak height of the sulfate-rich hydrocalumite increased and that of hydroxyl endmember decreased.

The results indicate that partial solid solutions between sulfate and hydroxyl are not present. These results agree well with the findings of Turriziani and Schippa (1954). Based on their XRD results, these authors also identified two immiscible phases of hydrocalumite ($Ca_4Al_2(OH)_{12}(OH)_2{\cdot}6H_2O$ and $Ca_4Al_2(OH)_{12}(SO_4){\cdot}6H_2O$) when the molar ratio of $CaSO_4/Al_2O_3$ in the preparation ranged from 0 to 1. Similarly, the peak intensity of OH-hydrocalumite decreased with increasing sulfate content, whereas that of the sulfate endmember increased along the same direction. Glasser *et al.* (1999) determined the sulfate content in a large number of synthesized hydrocalumites using EDX analysis. A frequency distribution plot revealed two peaks in the sulfate contents of the hydrocalumite solid solutions. One was at approximately 6% sulfate and the other at 80 to 85% sulfate. These compositions correspond to the solid solution phases close to the hydroxyl-rich and sulfate-rich hydrocalumites, respectively.

Partial solid solutions between sulfate and hydroxyl were determined over the same molar ratio of $CaSO_4/Al_2O_3$ from 0 to 1 by Roberts (1969) and Pöllmann (1989). Roberts (1969) prepared a partial solid solution at $CaSO_4/Al_2O_3$ ratios from 0.5 to 1.0. The longest basal spacing of this solid solution increased linearly from 8.77 to 8.96 Å. The composition of $Ca_4Al_2(OH)_{12}(\frac{1}{2}SO_4)(OH){\cdot}6H_2O$ was given to the phase with the basal spacing of 8.77 Å, and the phase at 8.96 Å was determined to be the sulfate endmember. At molar ratios of $CaSO_4/Al_2O_3$ between 0.1 and 0.5, it was determined that two phases, $Ca_4Al_2(OH)_{12}(OH)_2{\cdot}6H_2O$ and $Ca_4Al_2(OH)_{12}(\frac{1}{2}SO_4)(OH){\cdot}6H_2O$ coexisted. Ettringite was identified along with $Ca_4Al_2(OH)_{12}(SO_4){\cdot}6H_2O$ at $CaSO_4/Al_2O_3$ ratios over 1.0. These results have been verified by the experimental work of Pöllmann (1989). A gradual increase in d-spacing was measured in the solid solutions of $Ca_4Al_2(OH)_{12}[xSO_4, (1\text{-}x)(OH)_2]{\cdot}6H_2O$ when $0.5 \leq x \leq 1.0$ with the d-spacings ranging from 8.79 to 8.94 Å, very close to the values obtained by Roberts (1969). The d-spacing remains essentially constant at 8.79 Å when $0.5 \leq x \leq 1$, where $Ca_4Al_2(OH)_{12}(\frac{1}{2}SO_4)(OH){\cdot}6H_2O$ was found to coexist with $Ca_4Al_2(OH)_{12}(OH)_2{\cdot}6H_2O$.

Either partial solid solutions or two immiscible phases of hydrocalumite have been produced in the system CaO-Al_2O_3-SO_3-H_2O when the $CaSO_4/Al_2O_3$ ratio is less than 1. The formation of different products is likely a condition-dependent process. Synthesis of SO_4-hydrocalumite was conducted at or near 25 °C in the studies mentioned above. Temperature, therefore, can not explain the different results of these studies. Other possible factors that could cause differences include starting material, water/solid ratio, and reaction time. Roberts (1969) used similar starting materials to those used in the present experiment, and a partial solid solution was produced after one week of reaction. Pöllmann (1989) synthesized the solid solution by hydration of a paste, reacted for 8 months. In the latter case, although a long period of time was allowed for the reaction, hydration might have been inhibited due to the low w/s ratio used in the pastes. Considering that the formation of partial solid solutions between sulfate and hydroxyl takes approximately a week, it is probably a long-term reaction that results in two immiscible endmembers. The presence of hydrogarnet in the present study (over 16 months of reaction) indicates that the reaction is more mature.

Although two immiscible hydrocalumite phases were observed in the XRD patterns, these two phases could not be distinguished on the basis of morphology using SEM. EDX analysis also failed to give distinct compositions for the OH-hydrocalumite and SO_4-rich solid solution. For example, the sulfate content of the hydrocalumite crystals varied from 30% to 50% in sample S30. If these two immiscible phases were present as separate crystals, the molar percentage of sulfate should be either close to 0 or 100. The intermediate composition measured suggests that a single hydrocalumite crystal may be composed of the two phases. Turriziani and Schippa (1954) measured the refractive indices of sulfate hydrocalumite solid solutions. Their data suggested a complete solid solution between the hydroxyl and sulfate endmembers. In contrast, two immiscible phases were identified in the XRD patterns. These observations also suggest a mixture of two hydrocalumite phases in a single crystal.

Taylor (1990) points out that a continuous solid solution series based on the optical properties could be a true solid solution, an oriented intergrowth, or a random interstratification of layers of different types. The hydrocalumite precipitated in this study showed no difference in either morphology or chemical composition. A single hydrocalumite crystal likely consists of a mixture of two immiscible phases. If it was a partial solid solution that formed during the initial precipitation, two immiscible phases probably developed with time. Exsolution is a common phenomenon in geological processes, and refers to the separation of an initial solid solution into two endmembers (which still occur in a single

crystal) under new physicochemical conditions. This process might explain the coexistence of OH-hydrocalumite and a SO_4-rich hydrocalumite phase in a single crystal.

5.4.6.2 Stable vs. metastable

There are many discussions on the metastability of SO_4-hydrocalumite based on the results of Jones (1944) and D'Ans and Eick (1953). For example, Turriziani (1964) summarizes Jones' work and suggests that the stable solid phases in the system CaO-Al_2O_3-SO_3-H_2O are portlandite, gypsum, hydrogarnet, ettringite, and gibbsite, but notes that monosulfate can coexist metastably with ettringite. Lea (1970) states that the only quaternary compound appearing as a stable phase is ettringite. SO_4-hydrocalumite has also been determined to be metastable by researchers at the University of Aberdeen. Atkins *et. al.* (1992) state that ettringite is thermodynamically more stable than SO_4-hydrocalumite in water at 25 °C. Three observations were used to back up their statement: (1) dissolution of monosulfate gives sulfate concentration two orders of magnitude lower than if it dissolved congruently; (2) ettringite precipitates during the dissolution of monosulfate; and (3) solutions saturated with respect to monosulfate are supersaturated with respect to ettringite. Based on thermodynamic calculations, Damidot and Glasser (1993) also find that monosulfate never appears to be a stable phase and is always metastable with respect to hydrogarnet and ettringite. In contrast, Seligmann and Greening (1968) document that $Ca_4Al_2(OH)_{12}(OH)_2 \cdot xH_2O$ and $Ca_4Al_2(OH)_{12}(SO_4) \cdot 6H_2O$ solid solutions can occur as stable phases and that there is a stable invariant point at low sulfate concentrations, at which portlandite, hydrogarnet and a solid solution of hydrocalumite with the composition of $Ca_4Al_2(OH)_{12}(\frac{1}{2}SO_4)(OH) \cdot 6H_2O$ are in equilibrium. Their conclusion was drawn from observations on paste hydration of C_3A and gypsum. Pöllmann (1989) also considers that (SO_4, OH)-hydrocalumite solid solutions are stable because they are present after reaction times of up to 8 months. Kaprálik and Hanic (1989) proposed that both the sulfate hydrocalumite endmember and the intermediate phase $Ca_4Al_2(OH)_{12}(\frac{1}{2}SO_4)(OH) \cdot 6H_2O$ are stable.

A thermodynamically stable phase is one that is present at equilibrium under specific conditions (e.g. temperature and pressure). The determination of the stability of ettringite and hydrocalumite was mainly based on the observation of phase assemblages. If a phase existed after long term reaction, it was described as a stable phase (e.g. Pöllmann, 1989). Long reaction times, however, do not always result in an equilibrium condition, especially in the system CaO-Al_2O_3-SO_3-H_2O, in which reaction rates tend to be sluggish. Thermodynamic calculations were also used to predict phase stability. The stability of ettringite and

hydrocalumite, however, can not be determined from thermodynamic calculations because of uncertainties in $\Delta G°_f$ values for the calcium aluminate hydrates (Warren and Reardon, 1994). The phase rule is the only criterion that can be used to judge if equilibrium has been attained.

If temperature is fixed at 25 °C and pressure is fixed at atmospheric pressure, the stability of SO_4-hydrocalumite and ettringite is determined by the solution composition. Theoretically, from the dissolution reactions of these phases, a solution composition can be found to satisfy their stability:

$$Ca_6Al_2(OH)_{12}(SO_4)_3 \cdot 26H_2O \rightleftarrows Ca_4Al_2(OH)_{12}(SO_4) \cdot 6H_2O + 2Ca^{2+} + 2SO_4^{2-} + 20H_2O \qquad (5.5)$$

Based on the dissolution reaction of hydrocalumite and ettringite, and on their solubility products, a stability field for each phase can be found in the stability diagram constructed at a specified Ca concentration with log $[SO_4^{2-}]$ as the y-axis and (log $[Al(OH)_4^-]$ + 2pH) as the x-axis. Perkin and Palmer (unpublished) constructed a similar diagram to describe the stability of chromate-hydrocalumite and chromate ettringite. The dependence of ettringite and SO_4-hydrocalumite stability on solution composition is commonly observed in cement hydration. Hydration of the cement components C_3A and C_4AF in the presence of gypsum produces ettringite. Once gypsum is consumed and the concentration of sulfate in solution decreases, further hydration of C_3A and C_4AF result in the formation of monosulfate (SO_4-hydrocalumite). Under these conditions, ettringite formed at earlier stages is also converted to monosulfate.

The question is then 'could monosulfate be stable when it is assembled with other phases that occur in this system?'. Jones (1944) has documented that monosulfate is metastable within the following phase assemblages: monosulfate-ettringite-gibbsite; monosulfate-ettringite-portlandite; monosulfate-gibbsite; and monosulfate-portlandite. From the present study, a phase assemblage generated at the low end of the solid solution (i.e. low SO_3/Al_2O_3 ratios) was hydrocalumite (as hydroxyl endmember and a sulfate-rich solid solution), hydrogarnet, and portlandite. The existence of four phases indicates that equilibrium was not reached. As discussed in section (5.4.1), OH-hydrocalumite is not a stable phase and will convert to hydrogarnet. As a result, hydrogarnet, portlandite, and SO_4-hydrocalumite will be the stable phase assemblage. In addition, the low SO_4 concentration in solution measured in this study ($<2x10^{-3}$ mmolal) will not favor the conversion of monosulfate to ettringite. Similar assemblages were observed in both the $CaO-Al_2O_3-B_2O_3-H_2O$ and $CaO-Al_2O_3-MO_3-H_2O$ systems, emphasizing that hydrocalumite could be a stable phase in the presence of hydrogarnet and portlandite. The phase assemblage hydrogarnet,

portlandite, and SO_4-hdyrocalumite was not studied by Jones (1944), and warrants further investigation.

5.4.7 Interrelationship between the systems

A comparison of the solid phase assemblages and of the solution compositions between these different systems is beneficial to reveal the underlying relationships. The experimental data show that most of the OH-hydrocalumite converted to hydrogarnet after one year of reaction. Hydrocalumite phases containing borate, chromate, molybdate, selenate and sulfate, however, were dominant after a reaction period between 9 and 18 months. This demonstrates that the incorporation of these oxyanions into the structure of hydrocalumite stabilized the hydrocalumite phases. In the CaO-Al_2O_3-$CaCl_2$-H_2O system, Birnin-Yauri (1993) found that after 9 months of reaction, the initially-formed OH-hydrocalumite had converted to hydrogarnet, whereas the Cl-hydrocalumite phase remained stable.

Phase assemblages in the systems CaO-Al_2O_3-XO_3/Y_2O_3-H_2O show that the presence of the oxyanion greatly increases the stability of the oxyanion-bearing hydrocalumite phases. Based on the fact that OH-hydrocalumite is an unstable phase, it is reasonable to infer that the OH-rich solid solutions are also not stable. If this reasoning is correct, only solid solutions containing a certain percentage of oxyanion can exist under equilibrium or long-term metastable conditions. This conjecture is supported by the enrichment of oxyanions in hydrocalumite at the low end of the solid solution series examined. Oxyanion may be enriched by the formation of two immiscible phases with an oxyanion-rich solid solution and the OH endmember. Alternatively, a solid solution that forms initially may separate into the OH and SO_4-rich phases with progressive reaction. OH-hydrocalumite will convert to hydrogarnet with reaction time. Accompanying this conversion, portlandite also forms. This explains the coexistence of oxyanion-bearing hydrocalumite, hydrogarnet and portlandite at the low end of each solid solution series from this study. This particular phase assemblage can also be predicted to occur in any solid solution series between OH endmember and a hydrocalumite endmember.

Substitution in solid solutions is generally restricted by differences in ionic radius, geometry, and charge of the substituting ions. Glasser *et al.* (1999) state that extensive or complete solid solution of hydrocalumite occurs between anions of the same charge and geometry, whereas only limited solid solution occurs between anions of the same charge but differing in geometry. Ordering (i.e. immiscible phases) occurs between ions differing in both charge and geometry. When substitution occurs between hydroxyl and other anions,

geometric fitting of the substituting anion in the interlayer position is likely the key factor controlling the behavior of the solid solution. In the structure of hydrocalumite, borate has trigonal planar coordination and divalent charge as does carbonate. By analogy, borate is likely arranged parallel to the principle structural sheet, as is carbonate in carbonate hydrotalcite (van der Pol *et al.*, 1994). From structural considerations, trigonal planar borate fits well in between the principal layers and, therefore borate and hydroxyl are compatible in the structure. As a result, an extensive solid solution forms between hydroxyl and borate. Extensive solid solutions were also observed between the OH^- and trigonal planar SO_3^{2-} endmembers (Motzet and Pöllmann, 1999). In terms of the compatibility in the interlayer positions, similar results can also be expected for the anions such as fluoride and chloride. For sulfate anion, which occurs in regular tetrahedral coordination, a structural balance could not be easily achieved with hydroxyl. Consequently, the solid solution between sulfate and hydroxyl is limited to the region near the hydroxyl and sulfate endmembers. Molybdate occurs as distorted tetrahedron and is the largest in size. The large difference in ionic size and geometry between molybdate and hydroxyl limits the formation of extensive solid solutions. Instead, only the solid solutions near the molybdate endmember are formed.

The chromate and selenate hydrocalumites consist of immiscible solid solution phases with a broad range of d-spacings. The solids in both series were precipitated from alkaline solutions. The OH-rich solid solution phase is probably more stable under highly alkaline conditions, in which the hydroxyl ion is largely enriched. With the existence of the foreign ion (K^+ or Na^+), the actual systems in these two solid solution series are quinary. As a result, the precipitated hydrocalumites may not be comparable to those in the quaternary systems where no alkali ions are present.

Ettringite was observed in the borate, selenate and sulfate series. For the borate series, ettringite precipitation occurs when the amount of borate exceeds the amount required to form the borate endmember of hydrocalumite, i.e. at a B_2O_3/Al_2O_3 ratio > 0.5. The situation is different in the sulfate solid solution series. Ettringite formed at SO_3/Al_2O_3 ratios of 0.8 and above. Ettringite was also observed in the selenate solid solutions at a SeO_3/Al_2O_3 ratio between 0.9 and 1.0. The affinity of anion by the structures of hydrocalumite and ettringite is likely the factor that determines where ettringite would occur. For instance, incorporation of Cl into ettringite appears to cause its structure unstable. As a result, Cl-ettringite failed to be produced in aqueous solutions under ambient conditions (Höglund, 1992). It is expected that the stability of Cl-hydrocalumite can be extended to a much higher Cl/Al_2O_3 ratio than 1.0.

5.4.8 Environmental applications

Two parameters are important for the application of this technique in wastewater treatment. First, the uptake capacity of each undesirable element by the precipitates, and second, the residual concentration of these oxyanions in the solution phase. This study showed that hydrocalumite not only has large uptake capacity for these anions, but also results in low residual solution concentrations. Based on the characteristics of the hydrocalumite structure, other anions may also be removed effectively by this phase.

It is shown that two or more minerals, rather than a single hydrocalumite phase, coexist in most of the samples. In addition to hydrocalumite, the coexisting ettringite phase also incorporates anions into its structure. The uptake of anions would be greatly increased if they were also incorporated into ettringite phases. If a higher amount of anion were initially present, more ettringite would form to reduce the concentrations of the anions in solution. This potential has been demonstrated in the borate, selenate, and sulfate series. The coexistence of other solid phases causes some difficulties in estimating the amount of hydrocalumite precipitated. For engineering purposes, however, the solid products can be treated as a bulk material and the uptake capacity can be defined as the ratio of the removed trace element (mg) over the starting material $CaAl_2O_6$ (kg). Table 5.10 gives the calculated capacity for the oxyanions based on the results of the current study. High uptake capacities were shown in the range of five orders of magnitude (mg/kg) for all the elements examined.

These oxyanions usually have high solubilities as common alkali and alkali earth salts, and therefore conventional chemical precipitation is not an effective treatment to reduce their concentrations. Coprecipitation and adsorption methods are often used to remove these anions from solution, however, the materials employed in these processes have low uptake capacities. Various techniques have been developed, including electrochemical reduction and solvent extraction. Compared to these techniques, the capability of hydrocalumite to remove these oxyanions is extraordinary. For example, electrolytic ferrite treatment was claimed to be capable of very high chromium removals, in which hexavalent chromium was reduced from 200 ppm to less than 0.05 ppm (Nriagu and Nieboer, 1988). In the CaO-Al_2O_3-CrO_3-K_2O-H_2O system from this study, however, a reduction of chromate from 2500 ppm to less than 0.08 ppm was achieved.

The materials for precipitating hydrocalumite are not difficult to produce. Monocalcium aluminate ($CaAl_2O_4$, or CA in cement notation) is a major component in high aluminum cement. This compound can also be replaced by tricalcium aluminate ($Ca_3Al_2O_6$, or C_3A in cement notation), which is one of the major constituents in ordinary Portland

cement. In other words, high aluminum cement or Portland cement may potentially be used as a material in wastewater treatment. The most important condition that must be maintained with this technique is the pH. Since both hydrocalumite and ettringite are only stable in alkaline solutions, a pH value of 10.7 must be maintained to stabilize ettringite and a pH value 11.6 to stabilize hydrocalumite (Gabrisová *et al.*, 1991). To remove undesirable anions from wastewaters, a two-step process can be employed. In the first step, wastewater with high concentrations of anions is passed through calcium aluminate materials causing the precipitation of ettringite. In the second step, the pre-treated water is passed through fresh materials, reducing the concentration levels to below the drinking water standards. Hydrocalumite solid solutions will host the anions in the second step. The treatment can also be applied *in situ* by adding the compounds (either CA or C_3A with lime) to oxyanion-containing wastewater and allowing the reaction to occur. Better results could be achieved if mixing is provided. After the solids have settled, the treated water can be pumped out. Further treatment may be needed to return the pH to near neutral values before the water is discharged.

Table 5.10: Maximum uptake capacity of hydrocalumite measured for B, Cr, Mo, Se, and S.

Sample ID	Uptake Capacity		Mineral Assemblage
	mg/kg $CaAl_2O_6$	mmole/mole $CaAl_2O_6$	
B100	$1.21x10^5$	$1.77x10^3$	Hydrocalumite Ettringite
Cr100	$3.14x10^5$	$9.52x10^2$	Hydrocalumite
Mo100	$6.07x10^5$	$1.00x10^3$	Hydrocalumite Powellite
Se100	$4.84x10^5$	$9.68x10^2$	Hydrocalumite Ettringite
S100	$2.03x10^5$	$9.99x10^2$	Hydrocalumite Ettringite

The results from this study highlight the high binding potential of oxyanions by calcium aluminates. The binding mechanisms are important for the stabilization and solidification (S/S) technology because they directly control the leaching process. As implied by the results of the present study, borate and chromate are incorporated into hydrocalumite when the molar ratios of B_2O_3/Al_2O_3 and CrO_3/Al_2O_3 are less than 0.5 and 1.0, respectively.

Selenate may be accommodated in hydrocalumite or in both hydrocalumite and ettringite within the same composition range (SeO_3/Al_2O less than 1). Powellite would be an important host mineral for molybdate although molybdate would be also partially associated with hydrocalumite. The presence of multiple anions would enhance the stability of ettringite and result in the formation of ettringite at lower XO_3/Al_2O ratios.

5.4.9 Implications to cement chemistry

In the ternary system $CaO-Al_2O_3-H_2O$, the transformation from OH-hydrocalumite to hydrogarnet is inevitable at room temperature. The kinetics for the conversion, however, are very sluggish even at large w/s ratios and under well-mixed conditions. OH-hydrocalumite therefore persists for periods of up to one year and a half as shown in this study. As a result, hydrogarnet is rarely observed in cement pastes cured at room temperature. In addition, the presence of oxyanions greatly enhances the stability of hydrocalumite. The oxyanion hydrocalumite are stabilized at certain concentration ranges in pore solution. Stabilization of hydrocalumite by the oxyanions may be generalized to other anions, which is significant to studies on the effectiveness of various salts to change the rates of cement hydration and setting.

The hydration of high alumina cement produces CAH_{10} and CAH_8. The addition of borate prevents the conversion of these phases to hydrogarnet by the formation of stable borate hydrocalumite. Of the examined oxyanions, borate may be most effective at stabilizing hydrocalumite. Based on the geometric fitting of the anion in the layered structure of hydrocalumite, a prediction can be made as to which phase will preferentially incorporate a specific anion. For example, there is ever-increasing interest in the use of chemical admixtures to modify concrete characteristics in order to meet specific requirements. Calcium nitrite is commonly used as an additive to prevent corrosion of reinforcement in concrete. The results of this study suggest that nitrite might be preferred over sulfate in the structure of hydrocalumite. However, when the ratio of calcium nitrite to C_3A is high, nitrite may reside in ettringite.

This study determined that sulfate hydrocalumite could be a stable phase and that the stabilities of sulfate hydrocalumite and ettringite are dependent on solution composition. These are consistent with the observations on the transformation between ettringite and sulfate hydrocalumite in cement. Transformation between these two phases is a subject that has received much attention. It is closely related to the hydration of cement, during which

ettringite precipitates first and converts to monosulfate as the solution becomes depleted in sulfate. The transformation reaction can be described by the reaction:

$$Ca_6Al_2(OH)_{12}(SO_4)_3{\cdot}26H_2O + 2Ca_3Al_2O_6 \rightarrow 3Ca_4Al_2(OH)_{12}(SO_4){\cdot}6H_2O + 2H_2O \quad (5.6)$$

Although expressed as the sulfate hydrocalumite endmember, the actual phases present are the solid solutions between sulfate and hydroxyl. The results from this investigation predict that further reaction would result in a separation of the solid solutions into two immiscible phases. The relative amount of the sulfate-rich to the hydroxyl-rich phase would depend on the initial SO_3/Al_2O_3 ratio in cement.

It is well known that sulfate-rich waters, seawater and some groundwater, can cause volumetric expansion and cracking of cement due to the phase transformation from hydrocalumite to ettringite (Lea, 1970). The formation of secondary ettringite is considered to be a result of hydrocalumite reacting with a SO_4-containing solution:

$$3Ca_4Al_2(OH)_{12}(SO_4){\cdot}6H_2O + 2Ca^{2+} + 2SO_4^{2-} + 20H_2O \rightarrow Ca_6Al_2(OH)_{12}(SO_4)_3{\cdot}26H_2O \quad (5.7)$$

Sulfate concentration is a major factor that triggers the conversion. Based on the results from this study, it can also be predicted that the presence of other anions in water may also contribute to the transformation process.

5.5 Conclusions

In the ternary CaO-Al_2O_3-H_2O system, OH-hydrocalumite is a metastable phase, which converts to the stable phase, hydrogarnet. After over one year of reaction, most of the OH-hydrocalumite had converted to hydrogarnet. At oxyanion contents greater than ≈10%, the hydrocalumite phase(s) becomes dominant in all the quaternary systems CaO-Al_2O_3-XO_3/Y_2O_3-H_2O for reaction periods between 9 and 18 months. This suggests that a hydrocalumite phase can be stabilized when an anion other than OH is present in the structure. The results also show that only the hydrocalumites in which anions are enriched to certain percentage are stable. The enrichment of the oxyanion in the structure of hydrocalumite appears to be accomplished by the formation of two immiscible phases (the OH endmember and an anion-rich solid solution phase). In the sulfate solid solution series, the enrichment of SO_4 in hydrocalumite is likely achieved by disproportionating the initially-formed complete solid solution into the OH and SO_4-rich phases. In the quaternary systems examined, OH-hydrocalumite transforms to hydrogarnet and portlandite with reaction time.

Therefore, the stable phase assemblage generated in these systems consists of hydrocalumite, hydrogarnet, and portlandite.

The difference in geometry and anionic radius controls the type of solid solution formed. Extensive solid solutions are formed between the borate and hydroxyl hydrocalumite endmembers. This is because trigonal planar borate fits well in the principal layers and is compatible with hydroxyl in the structure. For the sulfate anion, which occurs in regular tetrahedral coordination, the arrangement between linear OH and tetrahedral sulfate ions in the interlayer results in an unstable structure. Consequently, the solid solution between sulfate and hydroxyl is only limited to the region near the hydroxyl and sulfate endmembers. For the molybdate solid solution, the large difference in ionic size and geometry between molybdate and hydroxyl limits the formation of extensive solid solutions. Therefore, only the solid solutions near the molybdate endmember are formed. The chromate and selenate hydrocalumites consist of immiscible solid solution phases with a broad range of d-spacings. The solids in both series were precipitated from alkaline solutions.

Ettringite was observed in the borate, selenate and sulfate series. For the borate series, ettringite precipitation occurs when the amount of borate exceeds the amount required to form the borate endmember of hydrocalumite, i.e. at a B_2O_3/Al_2O_3 ratio > 0.5. Ettringite formed at SO_3/Al_2O_3 ratios between 0.8 and 1.0 in the sulfate solid solutions. Ettringite was also observed in the selenate solid solutions at a SeO_3/Al_2O_3 ratio between 0.9 and 1.0. The affinity of anion by the structures of hydrocalumite and ettringite is likely the factor that determines where ettringite would occur.

Thermodynamic data were derived from the solution composition data measured in this study. A free energy of formation, $\Delta G°_{f,298}$, of -7336.14 ± 1.14 kJ·mol^{-1} was determined for OH-hydrocalumite ($Ca_4Al_2(OH)_{12}(OH)_2 \cdot 6H_2O$). Solution composition data in the CaO-Al_2O_3-B_2O_3-H_2O system allowed the first determination of the free energies of borate hydrocalumite and borate ettringite. The free energy of formation of the borate hydrocalumite endmember, $Ca_4Al_2(OH)_{12}(HBO_3) \cdot 5.5H_2O$, was determined to be -7750.42 ± 1.20 kJ·mol^{-1}. For borate ettringite, $Ca_6Al_2(OH)_{12}[B(OH)_4]_4[OH]_2 \cdot 24H_2O$, the free energy of formation was calculated to be -17408.22 ± 4.34 kJ·mol^{-1}. These values allow predictions of the equilibrium boron concentration in solution to be made in the CaO-Al_2O_3-B_2O_3-H_2O system. Determination of the free energies of the hydrocalumites containing other oxyanions, however, is not applicable due to the presence of immiscible solid solutions.

In this study, the determination of the maximum uptake capacity of the various anions by hydrocalumite was based on the mass of $CaAl_2O_4$ (starting material) rather than

that of hydrocalumite due to the presence of other phases. At a $H_2O/(CaAl_2O_4+CaO)$ ratio of approximately 75:1, the maximum capacity was calculated to be in the range of 100,000 mg/kg $CaAl_2O_4$ for B, Cr, Mo, Se, and S. Compared to conventional treatment techniques, these uptake capacities are extraordinary. Hydrocalumite is the major host mineral for the oxyanions under the experimental conditions used in this study. Ettringite also incorporates a moderate amount of oxyanion in the borate, selenate, and sulfate series. In the $CaO-Al_2O_3-MoO_3-H_2O$ system, powellite is also responsible for the removal of Mo. From the trends of the uptake results, higher capacities than the maximum values are indicated. Overall, the results of this study demonstrate that the system $CaO-Al_2O_3-XO_3/Y_2O_3-H_2O$ not only has a high uptake capacity for anions, but also has the capability to reduce their solution concentration to an acceptable level.

Chapter 6

Immobilization of B, Cr, Mo, and Se by Portland Cement

6.1 Introduction

Both ettringite and hydrocalumite are important hydration phases of ordinary Portland cement. They comprise 10 to 20% of the total mass of the hydration phases (Atkins *et al.*, 1991). In Chapter 4, it was shown that ettringite and hydrocalumite incorporate borate, chromate, molybdate, and selenate into their structures. In Chapter 5, extensive solid solutions between the hydroxyl endmember and borate endmember were characterized. Solid solutions are more limited in the molybdate and sulfate series. In the chromate and selenate series, solid solution phases with various percentages of chromate and selenate were found. At high contents of borate, selenate and sulfate, hydrocalumite and ettringite coexisted. Pöllmann *et al.* (1989, 1993) characterized the partial solid solutions of borate and chromate with SO_4-ettringite, and Hassett *et al.* (1990) determined the presence of a complete ettringite solid solution between selenate and sulfate. These studies have demonstrated that ettringite and hydrocalumite not only possess large uptake capacities for these oxyanions, but also lead to low residual solution concentrations. In addition to ettringite and hydrocalumite, CSH can also take up oxyanions such as sulfate and chromate (Odler, 1980; Omotoso *et al.*, 1998a). These studies suggest that incorporation of oxyanions into Portland cement could be a potential method for removal of anions from wastewaters. An understanding of the uptake of oxyanions by Portland cement is, therefore, of practical importance. It was this consideration that initiated the present investigation.

Portland cement is composed of four major components: C_3S (Ca_3SiO_5), C_2S (Ca_2SiO_4), C_3A ($Ca_3Al_2O_6$), and C_4AF ($Ca_4Al_2Fe_2O_{10}$) (Taylor, 1990). Other phases such as alkali sulfate, magnesium oxide and calcium oxide, are present in minor amounts. Gypsum

($CaSO_4 \cdot 2H_2O$) is usually added to Portland cement to retard the setting rate (Collepardi *et al.*, 1979). Cement reacts with water to yield a number of hydration phases, and produces high pH pore solution (Birchall *et al.*, 1978). The hydration of C_3S and C_2S produces calcium silicate hydrates (CSH). Reactions of C_3A and C_4AF with SO_4^{2-} dissolved from gypsum initially produce ettringite (an AFt phase), but as the pore solution becomes depleted in sulfate, ettringite transforms to hydrocalumite (an AFm phase). Further hydration results in a compositional change of the hydrocalumite from SO_4-rich to OH-rich (Taylor, 1990).

Cementitious, or cement-based waste forms are often used for the disposal of radioactive and hazardous wastes. Portland cement is the most common material used in cementitious solidification/stabilization (S/S) technologies. Heavy metals, such as Cr (III), Pb, Zn, Cd, Hg, and Ba, are often the elements of concern (Cocke and Mollah, 1993). Less attention has been drawn to oxyanions, despite the fact that arsenate, chromate, and selenate are priority pollutants. The radioisotopes of some elements generated by the nuclear industry also occur as anions, e.g. CO_3^{2-}, I^-, Cl^- and MoO_4^{2-}, (Gougar *et al*, 1996). Knowledge on the incorporation of borate, chromate, molybdate, and selenate in Portland cement will enhance the current understanding of the mechanisms involved in the immobilization of anions in cement matrices.

The objective of this study is to determine the capability of ordinary Portland cement to incorporate borate, chromate, molybdate, and selenate. The effect of the presence of these oxyanions on cement hydration is also addressed. The uptake behavior of these anions by Portland cement is compared with that by ettringite and hydrocalumite alone, to elucidate the partitioning of these anionic species by the hydration phases.

6.2 Experimental

6.2.1 Materials

Commercial Portland cement (CSA CAN 3-A5) was used in this study. The bulk composition of this cement is recorded in Table 6.1. Compared to the percentage of SO_3 typical of Portland cement (1.7 ~ 2.3) (Bogue, 1955), this material has a higher sulfur content. Table 6.2 shows the concentrations of the trace elements in the cement that occur as anions in solution. The concentrations of Cr, Mo, and Se are all below 5 ppm, whereas the concentration of B is much higher (41 ppm). Approximately 0.02% Cl is present in this material.

Table 6.1: Bulk composition of the Portland cement (in mass%).

Oxides	Al_2O_3	CaO	Fe_2O_3	K_2O	MgO	MnO	P_2O_5	Na_2O	SO_3	SiO_2	TiO_2	LOI	Sum
mass%	4.86	60.9	2.98	0.82	3.82	0.07	0.09	0.35	3.57	19.7	0.26	4.00	101.4

Table 6.2: Composition of minor and trace elements in the Portland cement (ppm).

Element	B	Cr	Mo	Se	Cl
Concentration	41	2	5	<3	215

According to a procedure developed by Bogue (1955), the quantitative phase composition for the principle cement components (Bogue index) was calculated and the results are presented in Table 6.3. C_3S is the predominant component, followed by C_2S, C_4AF, and C_3A. The quantity of gypsum was also calculated, assuming that all SO_3 occurs as gypsum. This assumption results in a high calculated percentage of gypsum, compared to the amount typically added to cement (between 3.4% to 5%) (Bogue, 1955). In this calculation, no correction was made for free lime.

Table 6.3: Potential phase composition of the Portland cement

Component	C_3S	C_2S	C_3A	C_4AF	Gypsum	Other Constituents
mass%	51.1	18.0	7.84	9.07	7.68	6.31

The crystalline phases in this material were identified using X-ray diffraction (XRD) analysis, and the XRD patterns are presented in Figure 6.1. Based on their relative intensities, C_3S, C_3A, and anhydrite are the dominant phases in this cement. Gypsum, arcanite (K_2SO_4), and free lime (CaO) are present as minor phases. Because of the overlapping of the major peaks of C_2S with those of C_3S, the relative amount of C_2S can not be determined from the XRD analysis.

A stock solution containing approximately 200 ppm B and 100 ppm of each of Cr, Mo, and Se was used in the uptake experiments. This solution was prepared using reagent-grade B_2O_3, K_2CrO_4, Na_2MoO_4, and Na_2SeO_4. Nanopure water with a conductance of 0.1 μS/cm was used in the control experiment.

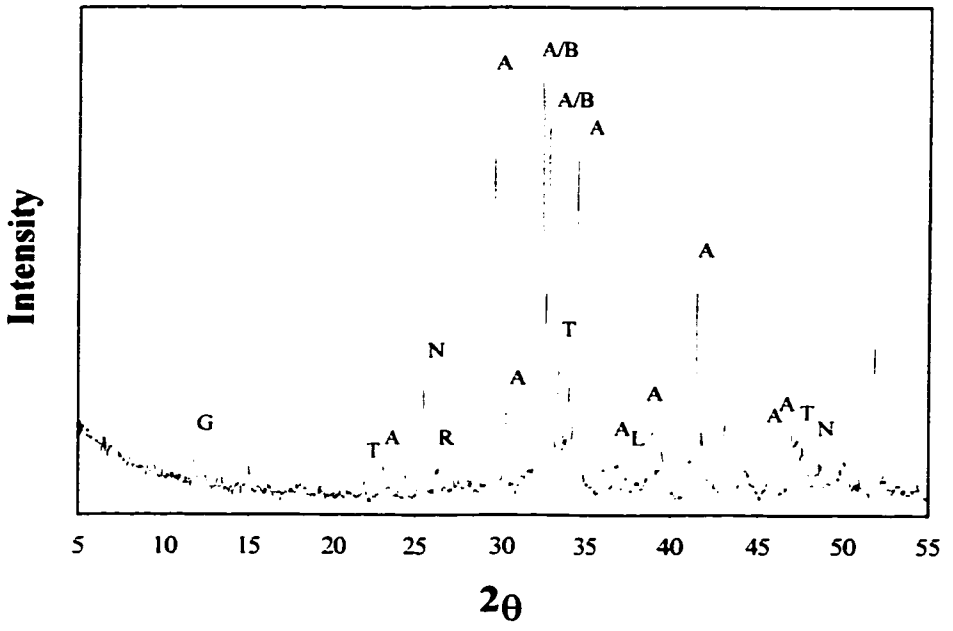

Figure 6.1: XRD pattern of the Portland cement. A - alite (C_3S); B - belite (C_2S); T - tricalcium aluminate (C_3A); N-anhydrite ($CaSO_4$); G - gypsum ($CaSO_4 2H_2O$); L - lime (CaO); R - arcanite (K_2SO_4).

6.2.2 Experimental procedure and analysis

The uptake of borate, chromate, molybdate, and selenate was studied at water to cement ratios much higher than those normally used in waste solidification technology. In order to study the change in the solution concentration of these oxyanions with progressive hydration, a larger volume of solution is required. Cement hydration was examined with and without the oxyanions present in solution. Both the solution composition and the solid phases were monitored as a function of time.

In the uptake experiment, Portland cement was mixed with the stock solution at two different w/s ratios of 20:1 and 40:1. Two w/s ratios were used to determine whether or not the concentration of an element is controlled by mineral solubility (Reardon *et al.*, 1995). In the control experiment, Portland cement was mixed with pure water at a w/s ratio of 20:1 only. Reactions were conducted in 60 ml high density polyethylene (HDPE) bottles. The bottles were loaded on a carousel and submerged in a constant temperature water bath maintained at 25 ± 0.5 °C. The carousel was rotated vertically at speeds from 10 to 20 rpm using the effluent from a water pump to ensure continuous mixing of the samples.

For each experimental series, samples were taken after 1h, 8h, 1d, 3d, 7d, 14d, and 30d of reaction. Solutions were filtered through a 0.22 μm filter paper. The solids were retained on the filter, and then air-dried. The solution samples were split into two portions for cation and anion analyses, respectively. The cation samples were preserved with 1:1 HCl, and the anion samples were diluted 1:2 with Nanopure water.

The solution compositions of the cation samples were determined using a Jarrell-Ash Inductively Coupled Plasma Spectrophotometer (ICP). The concentration of SO_4 was analyzed using a Dionex AS3 Ion Chromatograph (IC). The analytical uncertainties are within ±5% for both techniques. The solids were examined using X-ray diffraction (XRD) analysis. XRD analyses were made on random powder mounts using a Siemans D500 Diffractometer with Cu Kα radiation. For all samples, diffraction intensities were obtained between 5° and 55° 2θ at 40 kV and 110 mA. The samples were step scanned at 0.05° intervals integrated at 1s per interval.

6.3 Results

6.3.1 Concentration of major elements vs. time

The solution compositions of the samples from the control experiment are presented in Table 6.4. The results from the uptake experiment are recorded in Tables 6.5 and 6.6 for w/s ratios of 20:1 and 40:1, respectively. The geochemical equilibria model SIMUL (Reardon, 1990; 1992) was used to calculate the saturation indices for the mineral phases.

After one hour of reaction between cement and water, the solution was predicted to be nearly saturated with respect to both portlandite and gypsum. The solution then remained slightly supersaturated with respect to portlandite throughout the entire reaction period. The

saturation index of gypsum, however, decreased markedly after 1 day due to a substantial drop in the sulfate concentration. After 3 days of reaction, the sulfate concentration had been reduced by more than 500 times, and remained relatively constant in concentration with further reaction. Soluble K and Na were released into solution upon dissolution. Substantial percentages of K and Na, typically 30 and 45 %, respectively, are associated with anhydrous cement phases (Taylor, 1990). These are released as the hydration reactions progress. After 30 days of reaction, nearly 100% of both K and Na in the cement had been released into solution. The concentration of Si was low (approximately 2 ppm) in the 1-hr sample, but dropped after 1 day of reaction to 0.3 ppm and remained constant with increased reaction time. Aluminum, magnesium, and iron were all below detection during the course of reaction in the control samples.

In the uptake experiments, saturation with respect to portlandite was reached after 8 hours in the 20:1 series and after 1 day in the 40:1 series. Slight supersaturation was maintained in these two series for the duration of the experiment. The highest SO_4 concentrations were measured in the 1-hr samples for both series. Approximately 50% of the total sulfur remained in solution after the first hour of reaction. The SO_4 concentrations then decreased substantially with increased reaction time, especially in the 20:1 samples. In these samples, a decrease of almost two orders of magnitude occurred during the course of reaction, whereas the SO_4 concentration decreased only about 1/5 in the 40:1 samples.

Table 6.4: Concentration (ppm) of the major elements in solution after the reaction of cement with water. Water/solid ratio is 20:1.

Reaction Time	Al	Ca	Fe	K	Mg	Na	Si	SO_4	pH
1 hour	<0.1	982	<0.1	327	<0.05	95.5	2.24	995	12.44
1 day	<0.1	803	<0.1	314	<0.05	77.6	0.34	148	12.54
3 days	<0.1	900	<0.1	316	<0.05	106	0.32	1.04	12.61
7 days	<0.1	860	<0.1	324	<0.05	113	0.26	2.35	12.60
14 days	<0.1	855	<0.1	333	<0.05	120	0.20	1.76	12.60
30 days	<0.1	829	<0.1	341	<0.05	127	0.16	1.90	12.60

Table 6.5: Concentration (ppm) of the major elements in solution after the reaction of cement with a solution containing oxyanions. Water/solid ratio is 20:1.

Reaction Time	Al	Ca	Fe	K	Mg	Na	Si	SO_4	pH
original	3.01	0.56	<0.1	159	<0.05	113	1.01	<0.05	9.02
1 hour	1.90	747	<0.1	464	0.07	181	10.46	933	12.14
8 hours	1.63	1123	<0.1	480	<0.05	190	2.32	907	12.46
1 day	1.02	1605	<0.1	473	<0.05	188	1.04	756	12.67
3 days	0.57	1135	0.35	489	0.33	208	2.39	416	12.58
7 days	<0.1	855	<0.1	497	<0.05	217	0.50	75.5	12.63
14 days	<0.1	798	<0.1	504	<0.05	227	0.39	20.3	12.64
30 days	<0.1	760	<0.1	517	<0.05	236	0.32	12.3	12.64

Table 6.6: Concentration (ppm) of the major elements in solution after the reaction of cement with a solution containing oxyanions. Water/solid ratio is 40:1.

Reaction Time	Al	Ca	Fe	K	Mg	Na	Si	SO_4	pH
original	3.01	0.56	<0.1	159	<0.05	113	1.01	<0.05	9.02
1 hour	1.89	537	<0.1	305	0.19	147	34.2	546	11.88
8 hours	2.39	730	<0.1	324	0.06	154	6.25	530	12.22
1 days	1.72	1078	<0.1	315	<0.05	150	2.03	491	12.47
3 days	1.19	1529	<0.1	319	<0.05	155	1.14	422	12.66
7 days	0.88	1260	<0.1	322	<0.05	161	0.77	390	12.62
14 days	0.68	1103	<0.1	331	<0.05	166	0.76	228	12.62
30 days	0.47	1022	<0.1	333	<0.05	169	0.64	116	12.63

The concentration of Na, and to a lesser extent K, showed a slight but steady increase with time for both w/s ratios. Based on the solution composition measured, over 85% of the total K in the cement was released to solution within the first hour of reaction. 52% of the total Na was present in solution after the same reaction time. Therefore, the quantities of K and Na accommodated in the principal cement components are less than 15% for K and over 45% for Na. The amount of K associated with the cement component is low, compared to that typically occurring in cement (Taylor, 1990). At the end of reaction period, the quantities of both Na and K in solution were close to 100% of the total amounts in the original cement (within analytical error).

Approximately 3 ppm Al was introduced from the stock solution used in the uptake experiments. Overall, the Al concentrations showed a decreasing trend with time, with a larger decrease observed in the sample series of 20:1. A large release of Si into solution was seen in the 1-hr samples. However, the Si concentrations had dropped by over 90% after one day of reaction, and gradually decreased with reaction time. For the 1-hr samples, the Si concentration in the 40:1 sample was more than three times that measured in the 20:1 sample.

6.3.2 Concentration of trace elements vs. time

The changes in the concentrations of B, Cr, Mo, and Se with time are shown in Table 6.7 for the uptake experiment. In the control experiment, the concentrations of these elements were all below detection.

During the 30-day hydration process, the concentrations of B, Cr, Mo, and Se in the sample series at a w/s ratio of 20:1 decreased by factors of 115, 16, 8, and 6, respectively. Except for boron, substantial decreases in concentration of these elements did not occur until after 8 hours of reaction. After three days of reaction, the concentrations of these elements had decreased by between 40 and 80 percent.

A much smaller reduction in the concentrations of B, Cr, Mo, and Se were measured in the sample series at a w/s ratio of 40:1. Essentially no change in their concentrations was measured after one day of reaction. Between one day and three days, reductions of 18, 18, 9, and 6.5% occurred for B, Cr, Mo, and Se, respectively. After 30 days of reaction, B and Se had decreased by factors of 4.3 and 1.5, respectively. Similar to the 20:1 sample series, borate

was most preferred and selenate was least preferred by the hydration phases of Portland cement.

The solutions in the uptake samples were supersaturated with respect to powellite ($CaMoO_4$) during the 30 days of reaction. Precipitation of powellite, therefore, could be a factor controlling the concentration of Mo. No solubility controls were identified for the other oxyanions. However, Mo showed a similar decrease in its solution concentration compared to the other trace elements. In addition, higher Mo concentrations were measured in 40:1 samples, where the concentrations of Ca were also higher. If the Mo concentrations were controlled by the solubility of powellite, a lower Mo concentration would have been generated in these samples. Therefore, a powellite solubility control on Mo is unlikely.

Table 6.7: Concentration (ppm) of trace elements in solution after the reaction of cement with a solution containing oxyanions.

Reaction Time	Water/Solid = 20:1				Water/Solid = 40:1			
	B	Cr	Mo	Se	B	Cr	Mo	Se
Original	182	107	101	100	182	107	101	100
1 hour	170	101	99.7	102	173	101	100	100
8 hours	145	96.9	98.2	93.6	165	104	103	98.2
1day	108	85.7	88.6	86.3	136	92.8	95.4	94.7
3 days	31.1	39.6	47.0	62.6	111	75.6	86.9	88.5
7 days	9.81	18.4	26.5	38.1	79.3	64.8	73.4	82.7
14 days	3.77	8.24	15.2	20.7	55.3	56.7	63.4	74.0
28 days	1.58	6.53	12.2	15.9	42.1	48.6	54.3	66.9

6.3.3 X-ray diffraction analysis

Figure 6.2 is a plot of the XRD patterns for the control samples. In these samples, portlandite, ettringite, hydrocalumite, and calcite were identified. Unhydrated C_3S was also

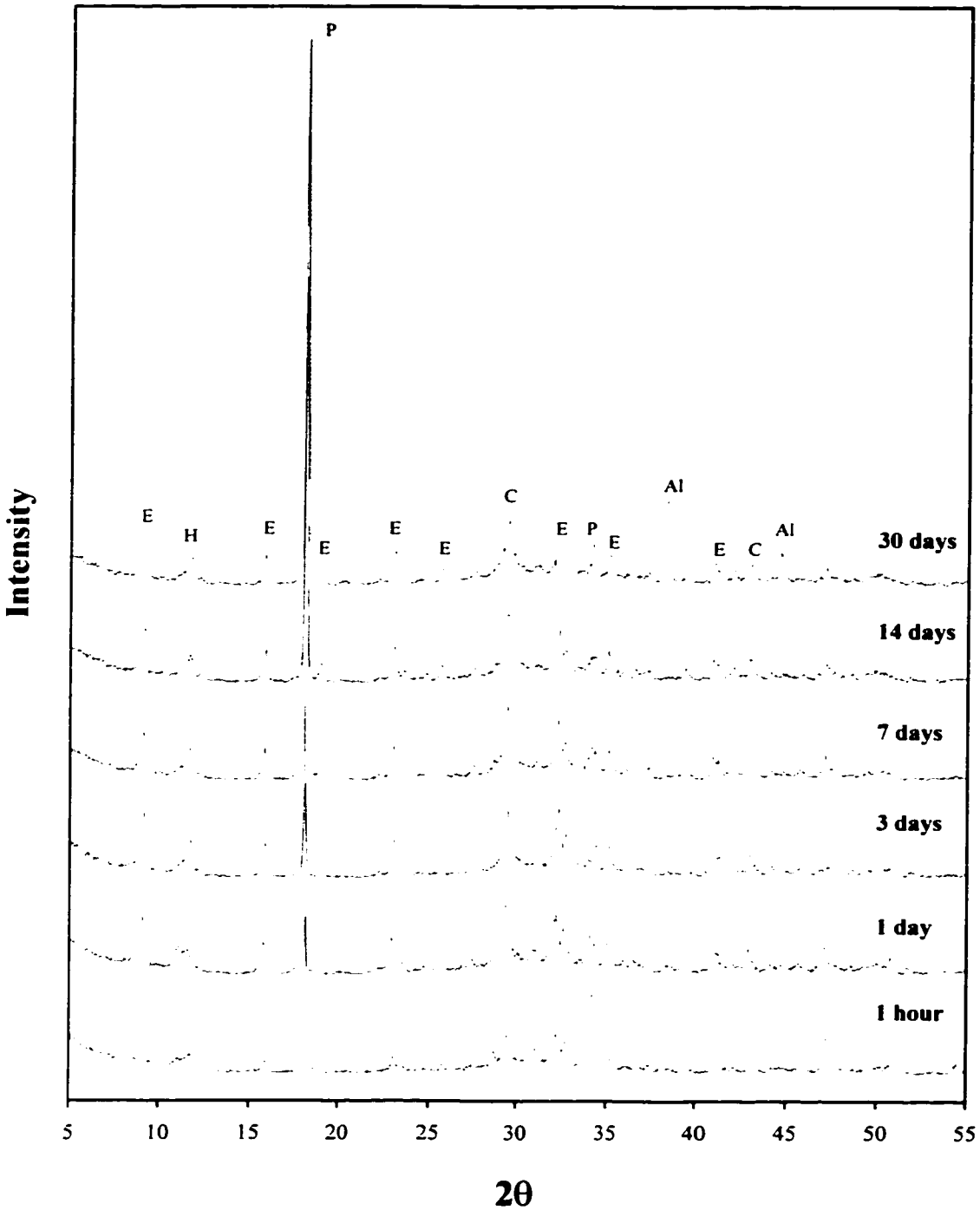

Figure 6.2: XRD patterns of the solids recovered from the control experiment with a w/s ratio of 20:1. H-hydrocalumite; E-ettringite; P-portlandite; C-calcite; Al-aluminum metal from the sample mount.

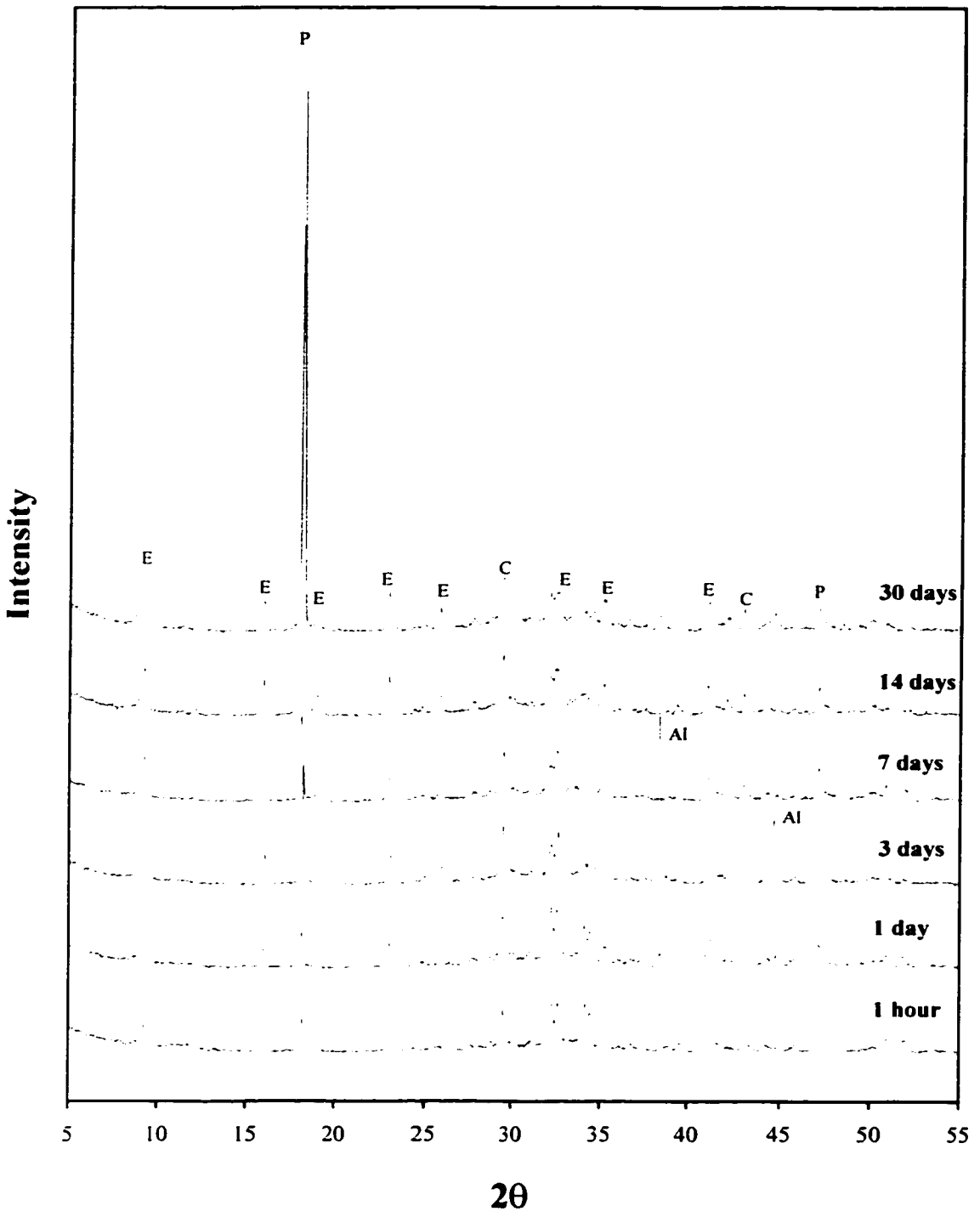

Figure 6.3: XRD patterns of the solids recovered from the uptake experiment with a w/s ratio of 20:1. E-ettringite; P-portlandite; C-calcite; Al-aluminum metal from the sample mount.

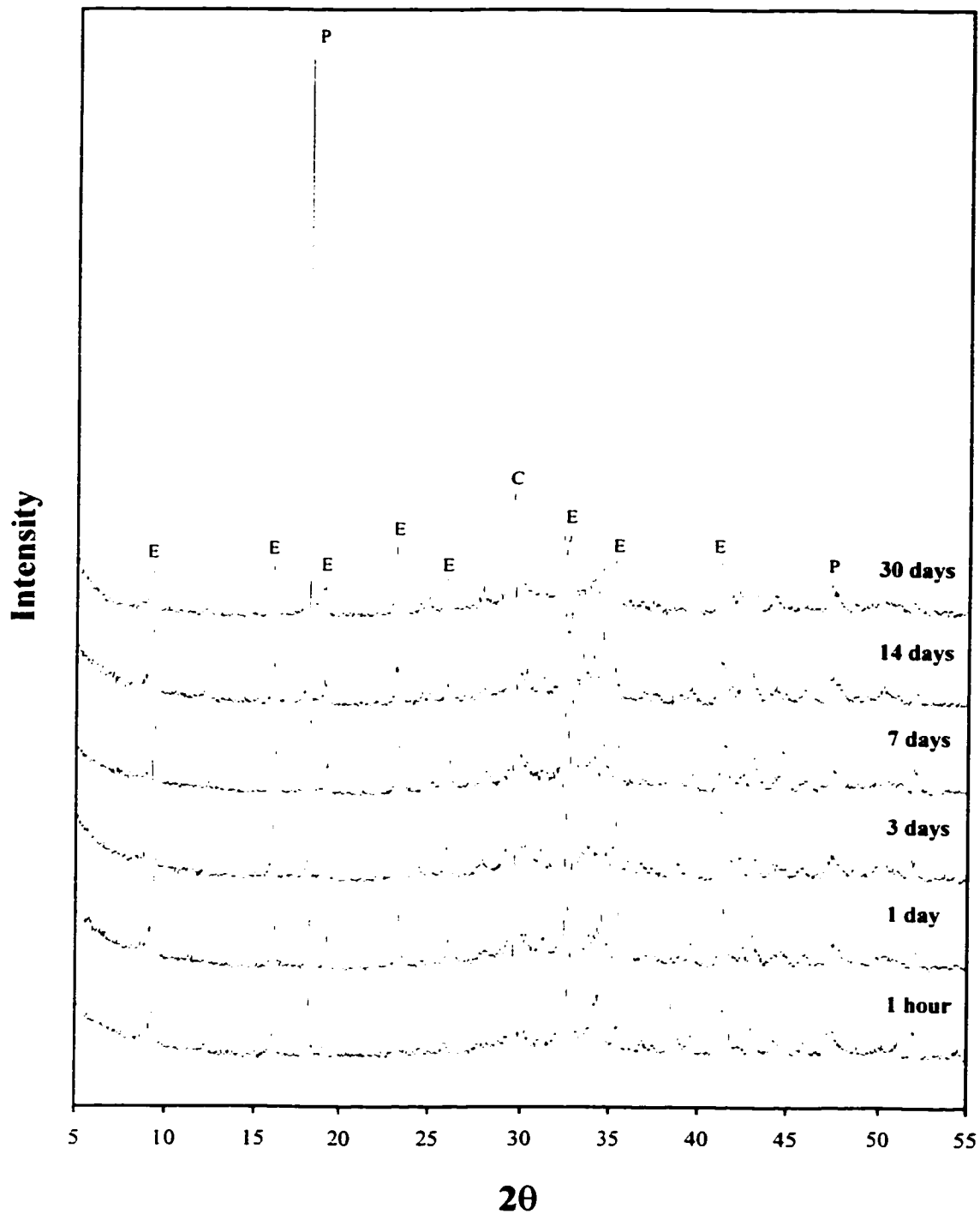

Figure 6.4: XRD patterns of the solids recovered from the uptake experiment with a w/s ratio of 40:1. E-ettringite; P-portlandite; C-calcite.

present at early reaction times. The peak intensities of portlandite increased with time, indicating a close correlation between the precipitation of portlandite and cement hydration. Ettringite formed after one hour of reaction and a large increase in its peak intensity occurred after one day, after which the quantity of ettringite remained relatively constant. Hydrocalumite was also observed after one hour of reaction. The principal peak of hydrocalumite was broad and had two splits of low relative intensity in both the 1-hr and 1-d samples. The position of hydrocalumite principal peak and its peak intensity remained unchanged between 3 and 30 days of reaction. Based on the position of the principal peak, the hydrocalumite formed at the early reaction times is likely a SO_4-rich phase, which converts to an OH-rich phase with time. Calcite likely precipitated during the drying process of the solid samples under atmospheric conditions.

The XRD patterns of the solid samples recovered from the uptake experiments with a w/s ratio of 20:1 are shown in Figure 6.3. The solid samples consist mainly of portlandite, ettringite, and calcite. Similarly, unhydrated C_3S was seen in the early time samples. Compared to the control samples, the identified phases are similar, except that hydrocalumite is not observed in the uptake samples. Overall, the relative amount of portlandite increased with time. The peak intensities, however, were much lower in the early hydration samples, compared to the corresponding control samples. As in the control samples, ettringite was seen after one hour of reaction, but its peak intensities were lower. The peak intensities of ettringite increased with time, and a large increase was shown in the 3-d sample. After this time, the relative amount of ettringite remained constant.

Solid samples at a w/s ratio of 40:1 have the same constituent phases as the 20:1 samples (Figure 6.4). However, the changes in the relative amount of the solid phases are different for these two series. Compared with the 20:1 series, the relative amount of portlandite was much lower in the 40:1 series between 3 days and 14 days of reaction, and a large increase in the amount of portlandite occurred in the 30-d sample. Ettringite had formed within one hour of reaction, and its peak intensity increased with increasing reaction time up to 3 days.

6.4 Discussion

6.4.1 Hydration of Portland cement

When Portland cement is brought into contact with water, the soluble alkali sulfates, e.g. arcanite (K_2SO_4), dissolve, releasing K and Na ions in solution. Calcium sulfates

(anhydrite and gypsum in this case) also dissolve quickly, leading to an initial increase in both the Ca and SO_4 concentrations. Ca ions are also released from the hydration of the principal cement components (C_3S, C_2S, C_3A and C_4AF) and free lime if present. This was observed in the control experiment, where the solution was nearly saturated with respect to both gypsum and portlandite after one hour of cement hydration.

The initial hydration of calcium silicates (mainly C_3S) can be inferred from the high Si concentration generated in solution. In cement pore solution, however, the concentration of Si measured is very low (< 2 ppm) even at very early hydration times (Birchall *et al.*, 1978). Greene (1960) suggested that liberation of Si from the hydration of cement clinker must have occurred and the Si concentration reached high values immediately upon mixing. In the uptake samples, 10 ppm and 34 ppm Si were measured in the samples with w/s ratio of 20:1 and 40:1, respectively. These results confirm that the low Si concentrations measured in cement pore solutions results from the removal of Si by the precipitation of CSH immediately after mixing cement with water. In solutions saturated with respect to CSH, there is a well-established inverse relationship between the concentration of Si and Ca (Reardon, 1992). The higher Si concentrations measured in the uptake samples compared to the control samples is likely due to their lower Ca concentrations.

Aluminum ions released from C_3A and C_4AF react rapidly with Ca^{2+}, OH^-, and SO_4^{2-} to yield ettringite. After one hour of reaction, the SO_4 concentration in solution only accounts for 50% of the total amount of sulfate. During this time, removal of SO_4 from solution must have occurred by incorporation into secondary phases. Ettringite ($Ca_6Al_2(OH)_{12}(SO_4)_3 \cdot 26H_2O$) was identified in the XRD analysis, and is likely responsible for removing a major percentage of the SO_4. In addition to ettringite, hydrocalumite ($Ca_4Al_2(OH)_{12}(SO_4) \cdot 6H_2O$) was also present, and is capable of accommodating a substantial quantity of sulfate.

The extent of cement hydration may be estimated based on the change in peak intensities of the anhydrous phases in the XRD patterns. However, a better approach is to use the rate of release of the alkali elements into solution as a measure of the hydration rate. For the Portland cement used in this study, approximately 15% of K and 45% Na were associated with the principal cement components (see Section 6.3.1). After 30 days of reaction, the quantities of both Na and K in solution were close to 100% of the total amounts in the original cement. This is true for both control and uptake samples. Therefore, it is reasonable to conclude that hydration of the Portland cement was essentially complete after 30 days of reaction.

6.4.2 Influence of the oxyanions on cement hydration

The presence of borate, chromate, molybdate, and selenate have no obvious effect on the rate of cement hydration. After subtracting the quantities of K and Na introduced from the stock solution, these elements showed a very similar change in their concentrations with time in both the uptake and control samples. The relative amount of portlandite precipitated, however, was much higher in the control samples, especially at early reaction times. Portlandite is produced mainly by the hydration of the principal cement components. The smaller percentage of portlandite formed in the uptake samples, however, is likely related to the presence of the oxyanions. The higher anion concentrations in solution balance much of the charge of the soluble alkalis, which would otherwise be balanced by OH^-. This then permits a higher Ca^{2+} concentration in solution at portlandite saturation. According to Kantro (1975), most soluble salts accelerate the hydration of C_3S. Although K^+ and Na^+ are not considered as effective accelerators (Jawed *et al.*, 1983), CrO_4^{2-} is quite effective (Thomas, 1987). It is likely that the concentration levels of these salts in this experiment were not high enough to modify the hydration rate.

A comparison of the XRD results between the uptake and control experiments reveals that hydrocalumite was produced by hydration of cement in water, but not in the solutions containing approximately 200 ppm B and 100 ppm Cr, Mo, and Se. In other words, hydrocalumite could be a stable phase in Portland cement-water system (at w/s ratio of 20:1), whereas the presence of high concentrations of borate, chromate, molybdate, and selenate shifts the stabilities of ettringite and hydrocalumite, and enhances the stability domain of ettringite. When considering the stability of these phases in cement hydration, sulfate concentration is usually used as a criterion. High concentrations of sulfate are thought to favor the formation of ettringite (e.g. Scrivener, 1989). The subsequent transformation of ettringite to hydrocalumite is attributed to sulfate depletion in solution as hydration proceeds (e.g. Skalny *et al.*, 1978). The results from the current study indicate that borate, chromate, molybdate, and selenate have a similar effect on the stability of ettringite.

6.4.3 Incorporation of the oxyanions into hydration phases

The concentrations of B, Cr, Mo, and Se were substantially reduced in the samples at a w/s ratio of 20:1. In the 40:1 sample series, however, the extent of reduction was over two times lower. Table 6.8 shows the calculated uptake of these oxyanions for Portland cement based on the change in their solution concentrations and the quantity of the cement initially added. The uptake of Cr, Mo, and Se is very similar for the two w/s ratios, especially after 30

days of reaction. Therefore, the high concentration of these oxyanions in solution is likely due to the fact that the amount of oxyanions added in the 40:1 samples is in excess of the maximum uptake capacity.

Table 6.8: Uptake of B, Cr, Mo, Se, and SO_4 by Portland cement (mg/kg).

Reaction Time	Water/Solid = 20:1					Water/Solid = 40:1				
	B	Cr	Mo	Se	SO_4	B	Cr	Mo	Se	SO_4
1 hour	240	120	30	0	24140	360	240	40	0	20960
8 hours	740	200	60	130	24660	680	120	0	70	21600
1day	1480	430	250	270	24680	1840	570	220	210	23160
3 days	3020	1350	1080	750	34480	2840	460	560	460	25920
7 days	3440	1770	1490	1240	41290	4110	1690	1100	690	27200
14 days	3570	1980	1720	1590	42390	5070	2010	1500	1040	33680
28 days	3610	2010	1780	1680	42550	5600	2340	1870	1320	38160

When sulfate was the only oxyanion present (in the control samples), the reduction in sulfate concentration was substantial, i.e. a decrease of more than 500 times was observed in the control samples, whereas the uptake samples only showed a decrease in sulfate of 75 times after 30 days of reaction. This lower reduction must have been caused by the competition between sulfate and the other oxyanions added. The presence of borate, chromate, molybdate, and selenate decreased the extent of sulfate uptake, however, sulfate showed the highest uptake by the hydration phases (Table 6.8).

Hydration of Portland cement in water produced CSH, portlandite, ettringite, and hydrocalumite. In the solutions containing B, Cr, Mo, and Se, the same hydration products were generated except that hydrocalumite was not present. The reason that hydrocalumite forms in OPC during the hydration process after early-formed ettringite is that once gypsum is consumed and solution sulfate concentration decreases, the system becomes 'starved' for sulfate. So further hydration of C_3A and C_4AF result in the formation of the lower sulfate content hydrocalumite (monosulfate) rather than ettringite. Even early-formed ettringite is

consumed to furnish sulfate for the formation of hydrocalumite. This process does not occur in the oxyanion uptake reactions because these oxyanions can substitute for sulfate in ettringite and so the system never becomes sulfate-starved.

In Chapter 4, it was shown that the decrease in the concentration of B, Cr, Mo, and Se in the presence of portlandite was less than 10%. Portlandite therefore, is likely not the phase responsible for the concentration reductions observed in the experiments. The removal of these oxyanions from solution likely resulted from incorporation into ettringite and CSH.

The preference of these oxyanions by the hydration phases of Portland cement decreases in the following order: $B(OH)^-$ >> CrO_4^{2-} > MoO_4^{2-} > SeO_4^{2-}. If ettringite is the major phase responsible for the uptake, the order of preference should be $B(OH)^-$ >> SeO_4^{2-} > CrO_4^{2-} > MoO_4^{2-} as determined in Chapter 4. The only difference between these orders of preference is the position of selenate. This difference implies that a hydration phase other than ettringite is incorporating these anions, and that chromate and molybdate are more preferred than selenate by this phase. In addition to ettringite, CSH is the likely phase responsible for incorporating these anions, based on its abundance and layered structure.

CSH comprises approximately 70% (on a mass basis) of the hydration products in cement (Birchall *et al.*, 1978). Kalousek (1965) provided some evidence for the immobilization of sulfate ion by showing that the concentrations of crystalline sulfate compounds were too low to account for the total sulfate concentration. Both Copeland *et al.* (1967) and Odler (1980) found that a few percent of sulfate could be bound in hydrated C_3S. Ramachandran (1971) and Beaudoin *et al.* (1990) studied the interaction of Cl^- with CSH and determined the presence of Cl^- in CSH. The incorporation of small amount of chromate in CSH was determined by Omotoso *et al.* (1998a). By analogy, it seems reasonable that borate, chromate, molybdate, and selenate could also be incorporated into this phase.

Different mechanisms are proposed for incorporation of anions into CSH. Odler (1980) concludes that sulfate is physically adsorbed to the large surface of the CSH gel and can be readily desorbed. Beaudoin *et al* (1990) suggests that Cl^- can reside both in interlayer positions and on the surface of the C-S-H sheets where it is water extractable. A small percent chloride is also thought to substitute in the crystal lattice. Omotoso *et al.* (1998b) suggests that some CrO_4^{2-} units may be located in tetrahedral SiO_4^{4-} sites in the C-S-H. Richardson and Groves (1992) attributed the presence of sulfate in C-S-H to the structural intermixture with varying amounts of AFm and hydrotalcite-type layers. The incorporation mechanism, however, can not be determined based on the bulk solution composition obtained in this

study. Further work is required to understand the preference of these oxyanions by CSH, the extent of uptake, and the incorporation mechanisms.

6.5 Conclusions

Ordinary Portland cement has a large capacity to accommodate a variety of oxyanions. Over a period of 30 days of hydration (w/s = 20:1), the concentrations of B, Cr, Mo, and Se were reduced by over 115, 16, 8, and 6 times, respectively. For the series at w/s of 40:1, however, a much lower decrease was measured. The concentrations of the above elements decreased by 1.5 to 4 times over the same reaction period. This is because the amount of oxyanions added in the 40:1 samples is in excess of the maximum uptake capacity.

Sulfate, initially dissolved from anhydrite and gypsum in the cement, showed the quickest and largest decrease in its concentration among the anions. Borate, chromate, molybdate, and selenate compete with sulfate for incorporation. With the presence of other anions, the residual SO_4 solution concentrations were higher. The preference of these oxyanions by Portland cement decreases in the order of $B(OH)^-$ >> CrO_4^{2-} > MoO_4^{2-} > SeO_4^{2-} for both w/s ratios examined.

Portlandite, ettringite, and CSH are the main products generated by the hydration of cement in the solutions containing approximately 200 ppm B and 100 ppm Cr, Mo, and Se. Of these hydration phases, ettringite is the major sink for these oxyanions. CSH is also likely involved in the removal of the oxyanions from solution. A comparison on the order of preference by ettringite and by Portland cement suggests that selenate is least preferred by CSH.

This study demonstrates that the presence of oxyanions other than sulfate prevents the transformation of ettringite to hydrocalumite. Ettringite is usually considered as the product under the conditions of high sulfate concentration, i.e. the presence of sulfate stabilizes ettringite. The coexistence of other oxyanions, however, enhances the stability of ettringite by being able to substitute for sulfate. This finding is important to cement technology, specifically to the deterioration of concrete caused by the formation of secondary ettringite during sulfate attack. A variety of anions will be present when concrete is exposed to natural hydrological environments. The results of this study have shown that these anions will also contribute to the formation of secondary ettringite.

Chapter 7

Summary

7.1 Incorporation of B, Cr, Mo, and Se into hydrocalumite and ettringite

In this study, the incorporation of borate, chromate, molybdate, and selenate into hydrocalumite and ettringite was examined in several different experiments. The results demonstrate that both phases have a high uptake capacity for these trace elements, and that hydrocalumite is capable of reducing oxyanion concentrations to below drinking water standards. It is the structural characteristics of the mineral phases that determine the uptake of these anions and the type of solid solution formed between the OH and anion endmembers. The factors controlling the incorporation of these anions into hydrocalumite depends upon the dominant phase present: (1) OH-rich hydrocalumite; (2) solid solutions between the OH endmember and the oxyanion endmember; (3) oxyanion hydrocalumite endmember.

When low concentrations of B, Cr, Se, and Mo (e.g. 10 ppm) are added to OH-hydrocalumite, their concentrations are reduced to close to or below detection. This observation suggests that there are no structural constraints on the incorporation of the anions by hydrocalumite. In this case, the number of sites occupied by the oxyanion in the structure of OH-hydrocalumite is low ($\approx$ 2%). At these low percentages, incorporation does not appear to disturb the structure of hydrocalumite, and as a result, a variety of anions can be accommodated. The size, geometry, and charge of an anion, therefore, do not affect the extent of uptake under these conditions.

As the concentrations of these oxyanions increase, incorporation into hydrocalumite produces solid solutions, which then control their solution concentrations. The type of solid

solution formed is largely dependent on the compatibility between the anion and hydroxyl in the interlayer. Trigonal planar borate is orientated parallel to the principal layers and therefore is compatible with hydroxyl in the structure. Extensive solid solutions are formed between the borate and hydroxyl hydrocalumite endmembers. A structural balance is not easily established for the accommodation of linear OH^- ions and tetrahedral ions (e.g. SO_4^{2-}). Consequently, the solid solution between sulfate and hydroxyl is limited to the region near the hydroxyl and sulfate endmembers. This suggests that an extensive solid solution will form between OH^- and a halogen or a trigonal planar anion (e. g. SO_3^{2-} and NO_3^-), and that more limited solid solutions will occur between OH^- and tetrahedral anions.

In the endmembers, the arrangement of anions is different in the structure of hydrocalumite depending on the geometry of the anion. Anions with trigonal planar geometry are equally bonded to the upper and lower surfaces of the interlayer, whereas tetrahedral anions are randomly distributed between the two possible orientations. These tetrahedral anions are less strongly attached to one surface of the interlayer than to the other. Despite the differences in their structures, the chromate, molybdate and selenate hydrocalumite endmembers still form. The maximum uptake capacity of B, Cr, Mo, and Se is determined to be over 100,000 mg/kg $CaAl_2O_4$ in their hydrocalumite endmember samples, where hydrocalumite is the major phase. Ettringite also takes up a moderate amount of oxyanion in the borate, selenate, and sulfate series.

Unlike hydrocalumite, the structure of ettringite is more restricted in terms of anion substitution. Therefore, the factors that commonly control lattice incorporation such as ionic size, geometry, and charge influence the extent of uptake. This study establishes that the preference of the oxyanions by ettringite is in the order $B(OH)_4^- > SeO_4^{2-} > CrO_4^{2-} > MoO_4^{2-}$. The substitution of other anions for sulfate appears to be limited mainly by differences in size. Similarity in electronegativity also favors substitution.

7.2 Stability of hydrocalumite and ettringite

Based on the observed phase assemblages in the system $CaO\text{-}Al_2O_3\text{-}XO_3/Y_2O_3\text{-}H_2O$ ($X = Cr^{6+}$, Mo^{6+}, Se^{6+}, and S^{6+}; $Y = B^{3+}$), the stability of hydrocalumite and ettringite is controlled by the relative quantity of anion to Al_2O_3. This is also demonstrated by observations on the phases formed during the hydration of Portland cement, and during reactions between fly ash and lime. Anions other than sulfate also appear to enhance the stability of ettringite.

The phase assemblages in the solid solution series with OH as one endmember and the anionic B, Cr, Mo, Se, and S as the other endmember were characterized. After over one year of reaction, most of the OH-hydrocalumite had converted to hydrogarnet. Oxyanion-hydrocalumite solid solution phases, however, were dominant after reaction periods between 9 and 18 months, even for the samples with lowest percentage of anion (e.g. XO_3/Al_2O_3 ratio = 10%). The results also show that only the hydrocalumites in which anions are enriched to certain percentage are stable. This can be accomplished by the formation of two immiscible hydrocalumite phases: an OH endmember and an oxyanion-rich solid solution. Alternatively, an initial solid solution phase may separate into OH-hydrocalumite and an anion-rich hydrocalumite with time, as in the sulfate solid solution series. With time, OH-hydrocalumite transforms to hydrogarnet and portlandite. Therefore, a stable phase assemblage at the low content of anion (i.e. low XO_3/Al_2O_3 or Y_2O_3/Al_2O_3 ratio) in these systems consists of hydrocalumite, hydrogarnet, and portlandite.

With the presence of high percentage of anion, ettringite formed along with hydrocalumite in the borate, selenate and sulfate series. Ettringite, however, occurred at different XO_3/Al_2O_3 or Y_2O_3/Al_2O_3 ratios, depending on the anion. For the borate series, ettringite forms when the amount of borate exceeds the amount required to form the borate endmember of hydrocalumite, i.e. at a B_2O_3/Al_2O_3 ratio > 0.5. Ettringite forms at SO_3/Al_2O_3 ratios between 0.8 and 1.0 in the sulfate system, and between SeO_3/Al_2O_3 ratios of 0.9 and 1.0 in the selenate system. It is likely that the affinity of an anion for the structures of hydrocalumite and ettringite is the factor that determines the ratio at which ettringite occurs. For instance, incorporation of Cl into ettringite appears to cause an unstable structure. As a result, Cl-ettringite has not been produced in aqueous solutions under ambient conditions, even at high chloride concentrations.

Hydrocalumite is the calcium aluminate phase commonly observed in mature cement paste. The molar ratio of SO_3/Al_2O_3 in Portland cement ranges from 0.4 to 0.6 (Bogue, 1955). It is the low ratio of SO_3/Al_2O_3 that stabilizes hydrocalumite in cement-water systems. The formation of ettringite during initial hydration is due to the quick dissolution of sulfates, which results in a high concentration of sulfate ions relative to C_3A. As sulfate is consumed, ettringite transforms to hydrocalumite. Direct observations suggest that this transformation is best described as a through solution mechanism, however it appears that solid-state conversion may also occur locally within a hydrocalumite crystal. The formation of ettringite initially, and its conversion to hydrocalumite with time, were observed in reactions of fly ash with lime and water in the present study. In the Lambton fly ash, where the reaction was matured, the phase assemblage consisted of hydrocalumite, hydrogarnet, and portlandite. Hydrocalumite occurred as two immiscible solid solutions: an OH-rich and a SO_4-rich phase.

This phase assemblage is the same as observed in the pure sulfate-OH hydrocalumite solid solutions.

The occurrence of ettringite in the borate and selenate hydrocalumite solid solution series examined in this study demonstrates that ettringite can form when the concentrations of anions other than sulfate are high. An enhancement in the stability of ettringite by these anions is also shown in the reaction between Portland cement and a solution containing 200 ppm B and 100 ppm Cr, Mo, and Se. Ettringite was the only calcium aluminate phase formed in cement hydrated in this solution, whereas both ettringite and hydrocalumite formed during the hydration of Portland cement with water.

7.3 Practical implications

The potential leaching of undesirable anionic trace elements from fly ash can be reduced by adding lime to fly ash. High pH environments promote the precipitation of ettringite and hydrocalumite, which incorporate anions into their structures. The results from the interaction of fly ash with lime and water demonstrate that ettringite was responsible for removal of the anions at the early reaction times. Further reaction causes the transformation of ettringite to hydrocalumite in the Class F fly ash and to strätlingite in the Class C fly ash. Hydrocalumite and strätlingite incorporate anions that originally were coprecipitated with ettringite and that were released with the progressive leaching of the ash particles. Transformation to hydrocalumite further reduced the concentration level of anions, whereas a release of anion was observed with the transformation to strätlingite, which could cause a potential problem to the environment. In concrete, ettringite persists much longer than was observed in this study, where large w/s ratios were used and complete mixing was provided. By analogy, ettringite may persist in a fly ash disposal site. Both hydrocalumite and ettringite are also hydration phases of ordinary Portland cement. In the utilization of fly ash as cement additive, release of the trace elements is unlikely to occur due to their incorporation into ettringite and hydrocalumite.

Ordinary Portland cement has a large capacity to accommodate a variety of oxyanions. This capability allows Portland cement to be used as a material for removal of anions from wastewaters and for the solidification/stabilization of liquid wastes. Depending on the concentrations, either ettringite or ettringite and hydrocalumite form, serving as the major sink for anions. CSH may also be involved in the removal of anions from solution. Of the oxyanions examined, borate showed the highest extent of uptake and selenate showed the lowest by ordinary Portland cement. When high solution concentrations are encountered,

precipitation of insoluble salts (e.g. powellite) may also take up a certain proportion of an anion. Ettringite has larger uptake capacity than hydrocalumite, whereas hydrocalumite can reduce anion at lower solution concentration levels. By manipulating the formation of either ettringite or hydrocalumite, the optimal conditions for removal of anions can be achieved.

Bibliography

Adriano D. C., Page A. L., Elseewi A. A., Chang A. C., and Straughan I. (1980) Utilization and disposal of fly ash and other coal residues in terrestrial ecosystems: A review. *J. Environ. Qual.* **9**, 333-344.

Ahmed S. J. and Taylor H. F. W. (1967) Crystal structures of the calcium aluminate hydrates. *Nature* **215**, 622-623.

Ainsworth C. C. and Rai D. (1987) Chemical characterization of fossil fuel combustion wastes. Electric power research institute. Report No. EA-5321.

Albasel N. and Pratt P. F. (1989) Guidelines for molybdenum in irrigation waters. *J. Environ. Qual.* **18**, 259-264.

Allaway W. H. (1968) Agronomic controls over the environmental cycling of trace elements. *Adv. Agron.* **20**, 235-274.

ASTM (1988) Standards specification for fly ash and raw or calcined natural pozzolan for use as a mineral admixture in Portland cement concrete. C618-88, The American Society for Testing and Materials, Philadelphia (PA) ASTM, 1988.

Atkins M., Macphee D., Kindness A., and Glasser F. P. (1991) Solubility properties of ternary and quaternary compounds in the CaO-Al_2O_3-SO_3-H_2O system. *Cem. Concr. Res.* **21**, 991-998.

Baes C. F. Jr. and Mesmer R. E. (1976) *The Hydrolysis of Cations*. John Wiley & Sons, New York.

Balistrieri L. S. and Chao T. T. (1990) Adsorption of selenium by amorphous iron oxyhydroxide and manganese dioxide. *Geochim. Cosmochim. Acta* **54**, 739-751.

Beaudoin J. J., Ramachandran V. S., and Feldman R. F. (1990) Interaction of chloride and C-S-H. *Cem. Concr. Res.* **20**, 875-883.

Bibak A. and Borggaard O. K. (1994) Molybdenum adsorption by aluminum and iron oxides and humic acid. *Soil Sci.* **158**, 323-328.

Birchall J. D., Howard A. J., and Bailey J. E. (1978) On the hydration of Portland cement. *Proc. R. Soc. Lond.* **A. 360**, 445-453.

Birnin-Yauri, U. A. (1993) Chloride in cement: study of the system CaO-Al_2O_3-$CaCl_2$-H_2O. Ph.D. thesis, University of Aberdeen.

Bish D. L. (1980) Anion-exchange in takovite: applications to other hydroxide minerals. *Bull. Mineral.* **103**, 170-175.

Bogue R. H. (1955) *The Chemistry of Portland Cement* (2nd ed.). Reinhold Publishing Corporation, New York.

Bowen H. J. M. (1979) *Environmental Chemistry of the Elements*. Academic Press, London.

Brown G. and Gastuche M. C. (1967) Mixed magnesium-aluminium hydroxides. II. Structure and structural chemistry of synthetic hydroxycarbonates and related minerals and compounds. *Clay Minerals* 7, 193-201.

Brownlow A. H. (1996) *Geochemistry* (3rd ed.). Prentice Hall, New Jersey.

Buttler F. G., Dent Glasser L. S., and Taylor H. F. W. (1959) Studies on $4CaO{\cdot}Al_2O_3{\cdot}13H_2O$ and the related natural mineral hydrocalumite. *J. Amer. Ceram. Soc.* **42**, 121-126.

Carles-Gibergues A. and Aitcin P-C. (1986) Analysis of the cementitious and pozzolanic properties of a silico-aluminous (Class F) fly ash. In 2nd Symposium on fly ash and coal conversion by-products: characterization, utilization and disposal. Boston, MA. 1985, *Mater. Res. Soc. Symp. Pro.* **65**, 125-130.

Carlson E. T. and Berman H. A. (1960) Some observations on the calcium aluminate carbonate hydrates. *J. Res. Nat. Bur. Std.* **64A**, 333-341.

Cavani F., Trifiro F., and Vaccari A. (1991) Hydrotalcite-type anionic clays: preparation, properties and applications. *Catalysis Today* **11**, 173-301.

Chappell W. R. (1973) Transport and biological effects of molybdenum in the environment. In *Heavy Metals in the Aquatic Environment: Proceedings of the International Conference held in Nashville, Tennessee, December 1973,* (edited by P. A. Krenkel) Pergamon Press, New York, pp.167-188.

Cobb J. T. Jr., Clifford B. V., Neufeld R. D., Pritts J. W., Beeghly J. H., and Bender C. (1997) Laboratory evaluation and commercial demonstration of hazardous waste treatment using clean coal technology by products. *International ash utilization symposium*, pp. 286-296.

Cocke D. L. and Mollah M. Y. A. (1993) The chemistry and leaching mechanisms of hazardous substances in cementitious solidification/stabilization systems. In *Chemistry and microstructure of solidified waste forms* (edited by R. D. Spence). Lewis Publishers, pp. 187-242.

Collepardi M., Baldini G., and Pauri M. (1979) Retardation of tricalcium aluminate hydration by calcium sulfate. *J Amer. Ceram. Soc.* **62**, 33-35.

Constantino V. R. L. and Pinnavaia T. J. (1995) Basic properties of $Mg^{2+}_{1-x}Al^{3+}_x$ layered double hydroxides intercalated by carbonate, hydroxide, chloride, and sulfate anions. *Inorg. Chem.* **34**, 883-892.

Copeland L. E., Bodor E., Chang T. N., Weise C. H. (1967) Reactions of tobermorite gel with aluminates, ferrites, and sulfates. *J. PCA Res. Dev. Lab.* **9**, 61-74.

Cotton F. A., Wilkinson G., Marillo C. A., and Bochman M. (1999) *Advanced Inorganic Chemistry (6th ed.)*. John Wiley & Sons, New York.

Damidot D., Atkins M., Kindness A., and Glasser F. P. (1992) Sulphate attack on concrete: limits of the AFt stability domain. *Cem. Concr. Res.* **22**, 229-234.

Damidot D. and Glasser F. P. (1993) Thermodynamic investigation of the $CaO-Al_2O_3-CaSO_4-H_2O$ system at 25 °C and the influence of Na_2O. *Cem. Concr. Res.* **23**, 221-228.

D'Ans J. and Eick H. (1953) The system $CaO-Al_2O_3-CaSO_4-H_2O$ at 20 °C. *Zement-Kalk-Gips* **6**, 302-311.

De Zuane J. (1997) *Handbook of Drinking Water Quality*. Van Nostrand Reinhold, New York.

Diamond S. (1983) On the glass present in low-calcium and in high-calcium fly ashes. *Cem. Concr. Res.* **13**, 459-464.

Dreesen D. R., Gladney E. S., Owens J. W., Perkins B. L., Wienke C. L, and Wangen L.E. (1977) Comparison of levels of trace elements extracted from fly ash and levels found in effluent waters from a coal-fired power plant. *Environ. Sci. Technol.* **11**, 1017-1019.

Drever J. I. (1998) *The Geochemistry of Natural Waters (2nd ed.)*. Prentice Hall, New Jersey.

Duchesne J. and Reardon E. J. (1999) Lime treatment of fly ash: characterization of leachate composition and solid/water reactions. *Waste Management* **19**, 221-231.

Dudas M. J. (1981) Long-term leachability of selected elements from fly ash. *Environ. Sci. Technol.* **15**, 840-843.

Dunn P. J., Peacor D. R., Leavens P. B., and Baum J. L. (1983) Charlesite, a new mineral of the ettringite group, from Franklin, New Jersey. *Amer. Miner.* **68**, 1033-1037.

Eary L. E., Rai D., Mattigod S. V., and Ainsworth C. C. (1990) Geochemical factors controlling the mobilization of inorganic constituents from fossil fuel combustion residues: II. Review of the minor elements. *J. Environ. Sci.* **19**, 202-214.

Edge R. A. and Taylor H. F. W. (1971) Crystal structure of thaumasite, $[Ca_3Si(OH)_6 \cdot 12H_2O](SO_4)(CO_3)$. *Acta Cryst.* **B27**, 594-601.

Elseewi A. A., Page A. L., and Grimm S. R. (1980) Chemical characterization of fly ash aqueous systems. *J. Environ. Qual.* **9**, 424-428.

Essington M. E. (1990) The composition and solubility of ettringite precipitated from combusted oil shale. *Oil Shale Symp. Pro.* 23rd. Colorado School of Mines Press, pp. 16-25.

Evans R. C. (1976) *An Introduction to Crystal Chemistry (2nd ed.)*. Cambridge University Press, Cambridge.

Faure G. (1991) *Principles and Applications of Inorganic Geochemistry*. Macmillan Publishing Company, New York.

Feitknecht W. and Buser H. W. (1951) Calcium-aluminum basic compounds. IV. The structure of the platelike calcium aluminum basic salts. *Helv. Chim. Acta* **34**, 128-142.

Felmy A. R., Rai D., and Mason M. J. (1992) The solubility of $CaMoO_{4(c)}$ and an aqueous thermodynamic model for Ca^{2+}-MoO_4^{2-} ion-interactions. *J. Soln. Chem.* **21**, 525-532.

Fendorf S., Eick M. J., Grossl P., and Sparks D. L. (1997) Arsenate and chromate retention mechanisms on goethite. 1. Surface structure. *Environ. Sci. Technol.* **31**, 315-326.

Fisher G. L., Chang D. P. Y., and Brummer M. (1976) Fly ash collected from electrostatic precipitators. Microcrystalline structures and mystery of the spheres. *Science* **192**, 553-555.

Flint E. P. and Wells L. S. (1944) Analogy of hydrated calcium silicoaluminates and hexa-calcium aluminate to hydrated calcium sulfoaluminates. *J. Res. Nat. Bure. Std.* **33**, 471-477.

Frankenberger W. T. Jr. and Engberger R. A. (1998) *Environmental Chemistry of Selenium.* Marcel Dekker, New York.

Freeborn W. P. and Roy D. M. (1984) The stability of ettringite. Technical Report prepared by The Pennsylvania State University for Office of Nuclear Waste Isolation, Battelle Memorial Institute, Columbus, OH.

Fruchter J. S., Rai D., and Zachara J. M. (1990) Identification of solubility-controlling solid phases in a large fly ash field lysimeter. *Environ. Sci. Technol.* **24**, 1173-1179.

Furuya K., Miyajima Y., Chiba T., and Kikuchi T. (1987) Elemental characterization of particle size-density separated coal fly ash by spectrophotometry, inductively coupled plasma emission spectrometry, and scanning electron microscopy-energy dispersive X-ray analysis. *Environ. Sci. Technol.* **21**, 898-903.

Fyfe W. S. (1974) *Geochemistry*. Oxford University Press, Oxford.

Gabrisová A., Havlica J., and Sahu S. (1991) Stability of calcium sulphoalumina hydrates in water solutions with various pH values. *Cem. Concr. Res.* **21**, 1023-1027.

Glasser F. P., Kindness A., and Stronach S. A. (1999) Stability and solubility relationships in AFm phases. Part I. Chloride, sulfate, and hydroxide. *Cem. Concr. Res.* **29**, 861-866.

Gougar M. L. D., Scheetz B. E., and Roy D. M. (1996) Ettringite and C-S-H Portland cement phases for waste ion immobilization: a review. *Waste Management* **16**, 295-303.

Greene K. T. (1960) Early hydration reactions of Portland cement. In *Proc. 4th Intl. Congress on the Chemistry of Cements*, Washington **I**, 359-374.

Greenwood N. N. and Earnshaw A. (1984) *Chemistry of the Elements*. Pergamon Press, Oxford.

Grew E. S. and Anovitz L. M. (1996) Boron: Mineralogy, Petrology and Geochemistry. In *Reviews in Mineralogy*, **33**. Mineralogy Society of America.

Halse Y., Pratt P. L., Dalziel J. A., and Gutteridge W. A. (1984) Development of microstructure and other properties in flyash OPC system. *Cem. Concr. Res.* **14**, 491-498.

Hansen L. D., Silberman D., and Fisher G. L. (1981) Crystalline components of stack-collected, size-fractionated coal fly ash. *Environ. Sci. Technol.* **15**, 1057-1062.

Hassett D. J., McCarthy G. J., Kumarathasan P., and Pflughoeft-Hassett D. (1990) Synthesis and characterization of selenate and sulfate-selenate ettringite structure phases. *Mat. Res. Bull.* **25**, 1347-1354.

Hassett D. J., Pflughoeft-Hassett D. F., Kumarathasan P., and McCarthy G. J. (1989) Ettringite as an agent for the fixation of hazardous oxyanions. In *Proc. 12th Annual Madison Waste Conference on Municipal and Industrial Waste*, 471-482.

Hemming N. G., Reeder R. J., and Hanson G. N. (1995) Mineral-fluid partitioning and isotopic fraction of boron in synthetic calcium carbonate. *Geochim. Cosmochim. Acta* **59**, 371-379.

Henry W. M. and Knapp K. T. (1980) Compound forms of fossil fuel fly ash emissions. *Environ. Sci. Technol.* **14**, 450-456.

Höglund L. O. (1992) Some notes on ettringite formation in cementitious materials: Influence of hydration and thermodynamic constraints for durability. *Cem. Concr. Res.* **22**, 217-228.

Hulett L. D. Jr., Weinberger A. J. (1980) Some etching studies of the microstructure and composition of large aluminosilicate particles in fly ash from coal-burning power plants. *Environ. Sci. Technol.* **14**, 965-970.

Jarrell W. M., Page A. L., and Elseewi A. A. (1980) Molybdenum in the environment. *Residue Reviews* **74**, 1-43.

Jawed I., Skanly J., and Young J. F. (1983) In *Structure and performance of cement* (edited by P. Barnes) Applied Science. Barking, Essex. p. 237.

Jones F. E. (1938) The calcium aluminate complex salts. *Proc. Intl. Congress on the Chemistry of Cements*, Stockholm, 231-245.

Jones F. E. (1944) The quaternary system $CaO-Al_2O_3-CaSO_4-H_2O$ at 25 °C. *J. Phys. Chem.* **48**, 311-356.

Jones F. E. (1960) Hydration of calcium aluminates and ferrites. *Proc. 4th Intl. Congress. Chemistry of the Cements*, Washington **I**, 205-246.

Johnston H. M. and Eagleson K. E. (1989) Chemical characteristics of Ontario Hydro coal fly ash: A Review. Ontario Hydro Report No. 89-155-K, pp.64.

Kalousek, G. L. (1965) Analyzing SO_3-bearing phases in hydrating cements. *Mater. Res. Stand.* **5**, 292-304.

Kantro D. L. (1975) Tricalcium silicate hydration in the presence of various salts. *J. Test. Eval.* **3**, 312-321.

Kaprálik I. and Hanic F. (1989) Phase relations in the subsystem $C_4A\bar{S}-C\bar{S}H_2-CH-H_2O$ of the system $CaO-Al_2O_3-C\bar{S}-H_2O$ referred to hydration of sulfoaluminate cement. *Cem. Concr. Res.* **19**, 89-102.

Kelleher E. (1994) The stability and solubility of the calcium arsenates in water as a function of pH at 25 °C. MSc. Thesis, University of Waterloo.

Kersten M., Moor H. C., and Johnson C. A. (1997) Speciation of trace metals in leachate from a MSWI botton ash landfill. *Applied Geochem.* **12**, 675-683.

Khoury H. N. and Nassir S. (1982) High temperature mineralization in the bituminous limestone in Maqarin area — north Jordan. *N. Jb. Miner. Abh.* **144**, 197-213.

Kindness A., Lachowski E. E., Minocha A. K., and Glasser F. P. (1994) Immobilization and fixation of molybdenum (VI) by Portland cement. *Waste Management.* **14**, 97-104.

Kingsley J. J., Suresh K., and Patil K. C. (1990) Combustion synthesis of fine-particle metal aluminates. *J. Mater. Sci.* **25**, 1305-1312.

Klein C. and Hurlbut C. S. Jr. (1999) *Manual of Mineralogy* (revised 21st ed.). John Wiley & Sons, New York.

Kumarathasan P. and McCarthy G. J. (1987) Laboratory modeling and XRD characterization of the hydration reactions of lignite gasification and combustion ash codisposal waste forms. *Mat. Res. Symp. Proc.* **86**, 159-170.

Kumarathasan P., McCarthy G. J., Hassett D. J., and Pflughoeft-Hassett D. F. (1990) Oxyanion substituted ettringites: synthesis and characterization and their potential role in immobilization of As, B, Cr, Se and V. In *Fly Ash and Coal Conversion By-Products: Characterization, Utilization and Disposal V*, pp. 83-104.

Kuzel H. J. (1969) X-ray investigation of some complex calcium aluminate hydrates and related compounds. *Proc. 5th. Intl. Congress on the Chemistry of Cements*, Tokyo **II**, 92-97.

Kuzel, H. J. (1976) Crystallographic data and thermal decomposition of synthetic gehlenite hydrate $2CaO{\cdot}Al_2O_3{\cdot}SiO_2{\cdot}8H_2O$. *N. Jb. Miner.* 319-325.

Lahann R. W. (1976) Molybdenum hazard in land disposal of sewage sludge. *Water, Air, and Soil Pollution* **6**, 3-8.

Lea F. M. (1970) *The Chemistry of Cement and Concrete.* (3rd ed.). Edward Arnold (Publishers).

Lecuyer I., Bicocchi S., Ausser P., and Lefevre R. (1996) Physico-chemical characterization and leaching of desulphurization coal fly ash. *Waste Manag. Res.* **14**, 15-28.

Lee C., Schlorholtz S., and Demirel T. (1986) Available alkalis in fly ash. In 2nd Symposium on fly ash and coal conversion by-products: characterization, utilization and disposal. Boston, MA. 1985. *Mater. Res. Soc. Symp. Pro.* **65**, 125-130.

LeGendre G. R. and Runnells D. D. (1975) Removal of dissolved molybdenum from wastewaters by precipitates of ferric iron. *Environ. Sci. Technol.* **9**, 744-749.

Lerch W., Ashton F. W., and Bouge R. H. (1929) The sulfoaluminates of calcium. *J. Res. Nat. Bur. Stand.* **2**, 715-731.

Lin C. F., Rou W., and Lo K. S. (1992) Treatment strategy for Cr(VI)-bearing wastes. *Wat. Sci. Technol.* **26**, 2301-2304.

Mattigod S. V., Rai D., Eary L. E., and Ainsworth C. C. (1990) Geochemical factors controlling the mobilization of inorganic constituents from fossil fuel combustion residues: I. Review of the major elements. *J. Environ. Qual.* **19**, 188-201.

McCarthy G. J., Swanson K. D., Keller L. P., and Blatter W. C. (1984) Mineralogy of western fly ash. *Cem. Concr. Res.* **14**, 471-478.

McCarthy G. J. and Solem-Tishmack J. K. (1994) Hydration mineralogy of cementitious coal combustion by-products. In *Advances in Cement and Concrete* (edited by M. W. Grutzeck and S. L. Sarkar). American Society of Civil Engineers. pp. 103-121.

Mertz W. and Underwood E. J. (eds.) (1986) *Trace Elements in Human and Animal Nutrition* (5th ed.). Academic Press, Orlando.

Miyata S. (1975) The syntheses of hydrotalcite-like compounds and their structures and physico-chemical properties —I: The systems Mg^{2+}-Al^{3+}-NO_3^-, Mg^{2+}-Al^{3+}-Cl^-, Mg^{2+}-Al^{3+}-ClO_4^-, Ni^{2+}-Al^{3+}-Cl^- and Zn^{2+}-Al^{3+}-Cl^-. *Clays and Clay Minerals* **23**, 369-375.

Miyata S. and Okada A. (1977) Synthesis of hydrotalcite-like compounds and their physico-chemical properties — the systems Mg^{2+}-Al^{3+}-SO_4^{2-} and Mg^{2+}-Al^{3+}-CrO_4^{2-}. *Clays and Clay Minerals* **25**, 14-18.

MOE. Ontario Drinking Water Objectives. Ontario Ministry of Environment, Toronto, ON, 1983.

Moore A. E. and Taylor H. F. W. (1970) Crystal structure of ettringite. *Acta Cryst.* **B26**, 386-393.

Motzet H. and Pöllmann H. (1999) Synthesis and characterization of sulfite-containing AFm phases in the system CaO-Al_2O_3-SO_2-H_2O. *Cem. Concr. Res.* **29**, 1005-1011.

Myneni S. C. B., Traina S. J., Logan T. J., and Waychunas G. A. (1997) Oxyanion behavior in alkaline environments: sorption and desorption of arsenate in ettringite. *Environ. Sci. Technol.*, **31**, 1761-1768.

Natusch D. F. S., Bauer C. F., Matusiewicz H., Evans C. A., Baker J., Loh A., Linton R. W., and Hopke P. K. (1975) Characterization of trace elements in fly ash. *Proc. Intl. Conf. on Heavy metals in the Environment.* Toronto, Canada. **II**, Part 2, 553-575.

Niss N. D., Schabron J. F., and Brown T. H. (1993) Determination of selenium species in coal fly ash extracts. *Environ. Sci. Technol.* **27**, 827-829.

Nriagu J. O. and Nieboer E. (editor) (1988) *Chromium in the Natural and Human Environments*. Advances in Environmental Science and Technology **20**. John Wiley & Sons.

Odler I. (1980) Interaction between gypsum and the C-S-H phase formed in C_3S hydration. *Proc. 7th Intl. Congress on the Chemistry of Cements*, Paris **IV**, 493-495.

Odler I. and Abdul-Maula S. (1984) Possibilities of quantitative determination of the AFt-(ettringite) and AFm-(monosulfate) phases in hydration cement pastes. *Cem. Concr. Res.* **14**, 133-141.

Okushima M., Kondo R., Muguruma H., and Ono Y. (1968) Development of expansive cement with calcium sulphoaluminous cement clinker. *Proc. 5th Intl. Congress on the Chemistry of Cements*, Tokyo **IV**, 419-438.

Olowe A. A. and Génin J. M. R. (1991) The mechanism of oxidation of ferrous hydroxide in sulphated aqueous media: importance of the initial ratio of the reactants. *Corrosion Science* **32**, 965-984.

Omotoso O. E., Ivey D. G., and Mikula R. (1998a) Hexavalent chromium in tricalcium silicate. Part I Quantitative X-ray diffraction analysis of crystalline hydration products. *J. Mater. Sci.* **33**, 507-513.

Omotoso O. E., Ivey D. G., and Mikula R. (1998b) Hexavalent chromium in tricalcium silicate. Part II Effects of Cr^{VI} on the hydration of tricalcium silicate. *J. Mater. Sci.* **33**, 515-522.

Page A. L., Elseewi A. A., and Straughan I. R. (1979) Physical and chemical properties of fly ash from coal-fired power plants with reference to environmental impacts. *Residue Rev.* **71**, 83-120.

Palache C., Berman H., and Frondel C. (1951) *The System of Mineralogy* (7^{th} ed.), *Vol. II.* John Wiley & Sons, New York.

Peacor D. R., Dunn P. J., and Duggan M. (1983) Sturmanite, a ferric iron, boron analogue of ettringite. *Can. Mineral.* **21**, 705-709.

Peppler R. B. and Wells L. S. (1954) The system of lime, alumina, and water from 50 to 250 °C. *J. Res. Nat. Bur. Stand.* **52**, No. 2, 75-92.

Perkins R. B. and Palmer C. D. (unpublished) Solubility of $3CaO{\cdot}Al_2O_3{\cdot}CaCrO_4{\cdot}nH_2O$, the chromate analog of monosulfate; 5-75 °C. Submitted to *Cem. Concr. Res.*

Pöllmann H. (1989) Solid solution in the system $3CaO{\cdot}Al_2O_3{\cdot}CaSO_4{\cdot}aq$-$3CaO{\cdot}Al_2O_3{\cdot}Ca(OH)_2{\cdot}aq$ - H_2O at 25 °C, 45 °C, 60 °C, 80 °C. *N. Jb. Miner. Abh.* **161**, 27-40.

Pöllmann H., Kuzel H. J., and Wenda R. (1989) Compounds with ettringite structure. *N. Jb. Min. Abh.* **160**, 133-158.

Pöllmann H., Auer St., Kuzel H. J., and Wenda R. (1993) Solid solution of ettringite. Part II: Incorporation of $B(OH)_4^-$ and CrO_4^{2-} in $3CaO{\cdot}Al_2O_3{\cdot}3CaSO_4{\cdot}32H_2O$. *Cem. Concr. Res.* **23**, 422-430.

Polyák K., Bódog I., and Hlavay J. (1994) Determination of chemical speices of selected trace elements in fly ash. *Talanta* **41**, 1151-1159.

Pope M. T. (1991) Molybdenum oxygen chemistry: oxides, oxocomplexes, and polyoxoanions. In *Progress in Inorganic Chemistry* **39**, pp.181-257.

Ramachandran V. S. (1971) Possible states of chloride in the hydration of tricalcium silicate in the presence of calcium chloride. *Matériaux et Constructions* **4**, No. 19. 3-12.

Ramachandran V. S. and Zhang C. M. (1986) Hydration kinetics and microstructural development in the $3CaO{\cdot}Al_2O_3$-$CaSO_4{\cdot}2H_2O$-$CaCO_3$-H_2O system. *Matériaux et Constructions* **19**, No. 114, 437-444.

Reardon E. J. (1990) An ion interaction model for the determination of chemical equilibria in cement/water systems. *Cem. Concr. Res.* **20**, 175-192.

Reardon E. J. (1992) Problems and approaches to the prediction of the chemical composition in cement/water system. *Waste Management* **12**, 221-239.

Reardon, E. J., Czank, C. A., Warren, C. J., Dayal, R., and Johnston, H. M. (1995) Determining controls on element concentrations in fly ash leachate. *Waste Manag. Res.* **13**, 435-450.

Reardon E. J. and Della-Valle S. (1997) Lime treatment of fly ash slurries: anion sequestering by the formation of anionic clays. *Environ. Sci. Technol.* **31**, 1212-1223.

Regourd M., Hornain H., and Mortureux B. (1976) Evidence of calcium silicoaluminates in hydrated mixtures of tricalcium silicate and tricalium aluminate. *Cem. Concr. Res.* **6**, 733-740.

Reichle W. T. (1986) Anionic clay minerals. *CHEMTECH* **16**, 58-63.

Rhee S. W., Kang M. J., Kim H., and Moon C. H. (1997) Removal of aquatic chromate ion involving rehydration reaction of calcined layered double hydroxide (Mg-Al-CO_3). *Environ. Technol.* **18**, 231-236.

Richard N., Lequeux N., and Boch P. (1995) Local environment of Al and Ca in CAH_{10} and CAH_8 by X-ray absorption spectroscopy. *Eur. J. Solid State Inorg. Chem.* **t. 32**, 649-662.

Richardson I. G. and Groves G. W. (1992) The incorporation of minor and trace elements into calcium silicate hydrate (C-S-H) gel in hardened cement pastes. *Cem. Concr. Res.* **23**, 131-138.

Rives V. and Ulibarri M. A. (1999) Layered double hydroxide (LDH) intercalated with metal coordination compounds and oxometalates. *Coordination Chemistry Reviews* **181**, 61-120.

Roberts M. H. (1957) New calcium aluminate hydrates. *J. Appl. Chem.* **7**, 543-546.

Roberts M. H. (1969) Calcium aluminate hydrates and related basic salt solid solutions. *Proc. 5th. Intl. Congress on the Chemistry of Cements,* Tokyo **II**, 104-117.

Rollinson, C. L. (1973) 36. Chromium, molybdenium and tungsten. In *Comprehensive Inorganic Chemistry, Vol. 3* (edited by. J. C. Bailar, H. J. Emeleus, R. Nyholm, and A. F.Trotman-Dickenson). Pergamon Press. pp. 623-769.

Roy W. R., Griffin R. A., Dickerson D. R., and Schuller R. M. (1984) Illinois basin coal fly ashs 1. Chemical characterization and solubility. *Environ. Sci. Technol.* **18**, 734-739.

Sacerdoti M. and Passaglia E. (1988) Hydrocalumite from Latium, Italy: its crystal structure and relationship with related synthetic phases. *N. Jb. Miner. Mh.* **10**, 462-475.

Savvin S. B., Chernova R. K., and Beloliptseva G. M. (1980) Reaction of molybdenum (VI) with bromopyrogallol red in the presence of cetylpyridinium chloride. *J. Anal. Chem.* **33**, 757-764.

Scrivener K. L. (1989) The microstructure of concrete. In *Material Science of Concrete*. **1**, pp. 127-161.

Seligmann P. and Greening N. R. (1968) Studies of the early hydration reactions of Portland cement by X-ray diffraction. *Proc. 5th Intl. Congress on the Chemistry of Cements*, Tokyo **IV**, 80-104.

Sen S., Stebbins J. F., Hemming N. G., and Ghosh B. (1994) Coordination environments of B impurities in calcite and aragonite polymorphs: a ^{11}B MAS NMR study. *Amer. Miner.* **79**, 819-825.

Sharmasarkar S., Reddy K. J., and Vance G. F. (1996) Preliminary quantification of metal selenite solubility in aqueous solutions. *Chem. Geology.* **132**, 165-170.

Shi C. (1996) Early microstructure development of activated lime-fly ash pastes. *Cem. Concr. Res.* **26**, 1351-1359.

Siler H. G. and Sigel H. (1998) *Handbook on Toxicity of Inorganic Compounds*. Marcel Dekker Inc., New York.

Singh N. B., Singh A. K., and Singh S. P. (1990) Hydration study of the system $Ca_3Al_2O_6$-$CaSO_4{\cdot}2H_2O$-$Ca(OH)_2$-H_2O with and without citric acid. *J. Am. Ceram. Soc.* **10**, 3063-3068.

Skalny J., Jawed I., and Taylor H. F. W. (1978) Studies on hydration of cement – recent developments. *World Cem. Technol.* **9**, 183-195.

Smith R. M. and Martell A. E. (1976) *Critical Stability Constants. Vol. 4: Inorganic Complexes.* Plenum Press.

Solem-Tishmack J. K., McCarthy G. J., Docktor B., Eylands K. E., Thompson J. S., and Hassett D. J. (1995) High-calcium coal combustion by-products: engineering properties, ettringite formation, and potential application in solidification and stabilization of selenium and boron. *Cem. Concr. Res.* **25**, 658-670.

Stark J. M. and Redente E. F. (1986) Composition of leachates from surface retorted oil shale disposal sites. *J. Environ. Qual.* **15**, 282-288.

Steinour H. H. (1951) Aqueous cementitious systems containing lime and alumina. *PCA Bull.* **34**, 1-100.

Sterritt R. M. and Lester J. N. (1980) Concentrations of heavy metals in forty sewage sludges in England. *Water, Air, and Soil Pollution.* **14**, 125-131.

Stinespring C. D., Harris W. R., Cook J. M., and Casleton K. H. (1985) Surface studies of coal, oil, and coal-oil-mixture ash using Auger electron spectroscopy and solvent leaching techniques. *Applied Spectroscopy* **39**, 853-856.

Stollenwerk K. G. and Runnells D. (1981) Composition of leachates from surface-retorted and unretorted Colorado oil shale. *Environ. Sci. Technol.* **15**, 1340-1346.

Tashiro, G. and Fukuyama, M. (1975) Hydration of C_3A in $CaCrO_4$ solution. *Rev. 29th Gen. Mtg. Cement Assoc. Japan*, 42.

Taylor H. F. W. (1961) The chemistry of cement hydration. *Progress in Ceramic Science* **1**, 89-145.

Taylor, H. F. W. (1973) Crystal structures of some double hydroxide minerals. *Miner. Mag.* **39**, 377-389.

Taylor H. F. W. (1990) *Cement Chemistry*. Academic Press, London.

Theis T. L. and Richter R. O. (1979) Chemical speciation of heavy metals in power plant ash pond leachate. *Environ. Sci. Technol.* **13**, 219-224.

Theis T. L. and Wirth J. L. (1977) Sorption behavior of trace metals on fly ash in aqueous system. *Environ. Sci. Technol.* **12**, 1096-1100.

Thomas M. D. A. (1997) The use of fly ash in concrete: a question of classification. *International Ash Utilization Symposium*, 333-341.

Thomas N. L. (1987) Corrosion problems in reinforced concrete: why accelerators of cement hydration usually promote corrosion of steel. *J. Mater. Sci.* **22**, 3328-3334.

Thomas N. L. and Egan P. J. (1989) Assessment of sodium molybdate as an accelerator of cement hydration and setting. *Adv. Cem. Res.* **2**, 89-98.

Thorvaldson, T. and Grace, N. S. (1929) The hydration of the aluminates of calcium. *Can. J. Res.* **1**, 36-47.

Tilley C. E. (1934) Hydrocalumite ($4CaO{\cdot}Al_2O_3{\cdot}12H_2O$), a new mineral from Scawt Hill, Co. Antrim. *Miner. Mag.* **23**, 607-615.

Trolard F., Génin J. M. R., Abdelmoula M., Bourrié G., Humbert B., and Gerbillon A. (1997) Identification of a green rust mineral in a reductomorphic soil by Mössbauer and Raman spectroscopies. *Geochim. Cosmochim. Acta* **61**, 1107-1111.

Turriziniani R. and Schippa G. (1955) Investigation of the quaternary solids CaO-Al_2O_3-$CaSO_4$-H_2O by the X-ray and DTA methods. *Ricerca Sci.* **24**, 2356-2363.

Turriziniani R. (1964) The calcium aluminate hydrates and related compounds. In *The Chemistry of Cements. Vol. 1*, Academic Press, London. pp. 233-286.

Uchikawa H. and Uchida S (1977) Influence of boric acid on hydration of ultra-rapid hardening cement. *Onoda Kenkyu Hokoku* **29 (98)**, 43-51.

Uchikawa H. (1986) Effect of character of glass phase in blending components on their reactivity in calcium hydroxide mixture. *Proc. 8th Intl. Congress on the Chemistry of Cements*, **I**, 245-250.

Van Aardt J. H. P. and Visser S. (1981) Synthesis of a calcium silicoaluminate hydrate at 5 °C. In *Proc. 7th Intl. Congress on the Chemistry of Cements* **IV**, 483-486.

van der Hoek E. E., Bonouvrie P. A., and Comans R. N. J. (1994) Sorption of As and Se on mineral components of fly ash: relevance for leaching processes. *Applied Geochem.* **9**, 403-412.

van der Hoek E. E. and Comans R. N. J. (1994) Speiciation of As and Se during leaching of fly ash. *Environmental Aspects of Construction with Waste Materials*, 467-476.

van der Pol A, Mojet B. L., van de Ven E., and de Boer E. (1994) Ordering of intercalated water and carbonate anions in hydrotalcite. An NMR study. *J. Phys. Chem.* **98**, 4050-4055.

van der Sloot H. A., Wijkstra J., van Stigt C. A., and Hoede D. (1985) Leaching of trace elements from coal ash and coal-ash products. In *Wastes in the ocean* **4**, John Wiley & Sons. pp. 468-497.

Vempati R. K., Rao A., Hess T. R., Cocke D. L., and Lauer H. V. Jr. (1994) Fraction and characterization of Texas lignite class 'F' fly ash by XRD, TGA, FTIR and SFM. *Cem. Concr. Res.* **24**, 1153-1164.

Voegeli P. T. Sr. and King R. U. (1969) Occurrence and distribution of molybdenum in the surface water of Colorado. *U. S. Geol. Survey Water-Supply Paper* **1535-N**, 1-32.

Warren C. J. (1992) Some limitations of sluiced fly ash as a liming material for acidic soils. *Waste Manag. Res.* **10**, 317-327.

Warren C. J. and Dudas M. J. (1984) Weathering processes in relation to leachate properties of alkaline fly ash. *J. Environ. Qual.* **13**, 530-538.

Warren C. J. and Reardon E. J. (1994) The solubility of ettringite. *Cem. Concr. Res.* **24**, 1515-1524.

Wedepohl K. H. (ed.) (1969) *Handbook of Geochemistry.* Springer-Verlag, Berlin.

Well L. S., Clarke W. F., and McMurdie H. F. (1943) Study of the system $CaO-Al_2O_3-H_2O$ at temperatures of 21° and 90° C. *J. Res. Nat. Bur. Std.* **30**, 367-409.

Wenda R. and Kuzel H. J. (1986) B^{3+} in calcium aluminate hydrates. *Proc. 8th. Intl. Congress on the Chemistry of Cements*, Brazil **III**, 307-314.

Wesche K (ed.) (1991) Fly ash in concrete: Properties and performance. Report of Technical Committee 67-FAB: Use of fly ash in building. E & FN Spon.

Zhou Z. and Dayal R. (1990) Characterization and leaching studies of FGD waste by products. *Waste Management* **10**, 53-59.

Appendix

Sample preparation and reaction times used for the Synthesis of B, Cr, Mo, Se, and S hydrocalumite solid solutions

Table A1. Actual quantities of reagents added to synthesize OH-hydrocalumite

Sample ID	$CaAl_2O_4$ (g)	CaO (g)	H_2O (g)	Reaction Time (day)
OH1	0.3161	0.3365	50.043	383
OH2	0.3161	0.3365	50.011	479

Table A2. Actual quantities of reagents added to synthesize (B, OH) solid solutions

Sample ID	$CaAl_2O_4$ (g)	B_2O_3 (g)	CaO (g)	H_2O (g)	Reaction Time (day)
B10	0.3161	0.0140	0.3365	50.022	276
B20	0.3161	0.0278	0.3365	50.015	276
B30	0.3161	0.0419	0.3365	50.029	381
B40	0.3161	0.0557	0.3365	50.037	269
B50	0.3161	0.0696	0.3365	50.009	383
B60	0.3161	0.0835	0.3365	50.013	381
B70	0.3161	0.0975	0.3365	50.027	271
B80	0.3161	0.1114	0.3365	49.996	271
B90	0.3161	0.1253	0.3365	49.996	381
B100	0.3161	0.1392	0.3365	50.002	383

Table A3. Actual quantities of reagents added to synthesize (Cr, OH) solid solutions

Sample ID	$CaAl_2O_4$ (g)	K_2CrO_4 (g)	CaO (g)	H_2O (g)	Reaction Time (day)
Cr20	0.3161	0.0777	0.3365	50.002	635
Cr40	0.3161	0.1554	0.3365	50.000	635
Cr50	0.3161	0.1942	0.3365	50.065	389
Cr60	0.3161	0.2330	0.3365	49.992	635
Cr80	0.3161	0.3107	0.3365	50.001	635
Cr100	0.3161	0.3884	0.3365	49.996	480

Table A4. Actual quantities of reagents added to synthesize (Cr, OH) solid solutions

Sample ID	$CaAl_2O_4$ (g)	$CaMoO_4$ (g)	CaO (g)	H_2O (g)	Reaction Time (day)
Mo10	0.3161	0.0400	0.3253	50.008	474
Mo20	0.3161	0.0800	0.3140	50.011	474
Mo30	0.3161	0.1200	0.3028	50.018	472
Mo40	0.3161	0.1600	0.2916	50.003	472
Mo50	0.3161	0.2000	0.2804	50.024	472
Mo60	0.3161	0.2400	0.2692	50.042	472
Mo70	0.3161	0.2800	0.2580	50.002	480
Mo80	0.3161	0.3200	0.2468	50.089	480
Mo90	0.3161	0.3600	0.2355	50.002	474
Mo100	0.3161	0.4000	0.2243	50.019	474

Table A5. Actual quantities of reagents added to synthesize (Se, OH) solid solutions

Sample ID	$CaAl_2O_4$ (g)	Na_2SeO_4 (g)	CaO (g)	H_2O (g)	Reaction Time (day)
Se10	0.3161	0.0378	0.3365	50.005	481
Se20	0.3161	0.0756	0.3365	50.038	481
Se30	0.3161	0.1134	0.3365	49.989	481
Se40	0.3161	0.1512	0.3365	50.000	514
Se50	0.3161	0.1889	0.3365	50.010	500
Se60	0.3161	0.2267	0.3365	50.096	514
Se70	0.3161	0.2645	0.3365	50.008	516
Se80	0.3161	0.3023	0.3365	50.013	500
Se90	0.3161	0.3401	0.3365	50.062	481
Se100	0.3161	0.3779	0.3365	49.998	523

Table A6. Actual quantities of reagents added to synthesize (S, OH) solid solutions

Sample ID	$CaAl_2O_4$ (g)	$CaSO_4 \cdot 2H_2O$ (g)	CaO (g)	H_2O (g)	Reaction Time (day)
S10	0.3161	0.0344	0.3253	50.005	558
S20	0.3161	0.0689	0.3140	50.036	521
S30	0.3161	0.1033	0.3028	49.993	521
S40	0.3161	0.1377	0.2916	50.027	558
S50	0.3161	0.1722	0.2804	49.999	558
S60	0.3161	0.2066	0.2692	50.035	558
S70	0.3161	0.2410	0.2580	50.014	558
S80	0.3161	0.2755	0.2468	50.001	558
S90	0.3161	0.3099	0.2355	50.046	558
S100	0.3161	0.3444	0.2243	50.023	516